Cranfield University

Athanasios Dimopoulos

Effect of carbon nanoparticle addition on epoxy cure

School of Applied Sciences

PhD Thesis

November 2007

Cranfield University
School of Applied Sciences
Materials Department

PhD Thesis
Academic Years 2004-2007

Athanasios Dimopoulos

Effect of carbon nanoparticle addition on epoxy cure

Supervisor: Professor Ivana K. Partridge

November 2007

ABSTRACT

The thesis reports studies of cure kinetics and the glass transition temperature advancements of three commercial epoxy resin systems: MY 750 / HY 5922 (Vantico), MTM 44 -1 (ACG) and 8552 (Hexcel Composites). This investigation was conducted with the utilisation of Differential Scanning Calorimetry (DSC) and Temperature Modulated DSC (TMDSC). Appropriate phenomenological cure kinetics models were built to predict the degree of cure as a function of temperature/time profile. The validity of superposition of dynamic and isothermal experimental data was established. Rheological measurements were performed in order to determine the gelation region under given cure conditions. The cure modelling methodology was validated against an international Round-Robin exercise led by the University of British Columbia (Canada).

The effects of carbon nanoparticle incorporation on the cure kinetics and the glass transition temperature advancement of two of the epoxy systems were also studied. Cure kinetics models were developed for the nanocomposites containing commercial multiwalled carbon nanotubes and a direct comparison was made with the models of the neat resin systems. The glass transition temperature advancement is shown to be affected in the early stages of the cure.

The state of the dispersion of the nanoparticles was studied in order to correlate it with the observed effects upon the cure and on the morphology of the cured samples. The presence of carbon nanotube clusters is shown to have an influence on the phase separation in the MTM 44-1 resin system.

As a potential industrial application of this study, optical fibre refractometers were utilised as an on-line cure monitoring technique. A good correlation was established between the measured refractive index changes during the cure and the degree of cure predicted by the above mentioned models, for the neat resin systems and their nanocomposites.

ACKNOWLEDGEMENTS

I would like to express my gratitude to my supervisor Professor Ivana K. Partridge for the support she provided over the three year period of this study, together with the continuous effort to improve the work.

I would like to thank Dr Alexandros A. Skordos for introducing me the world of data analysis and modelling. His crucial help on every aspect of this work and the continuous presence are gratefully acknowledged.

I would also like to thank Dr David Ayre for the help he provided on the TEM analysis and the valuable conversations we had covering several topics concerning this study. Many thanks to Mrs Christine Kimpton for the time spent on the SEM analysis and my colleagues Andrea Battisti and Mar Salinas Ruiz for the suggestions on critical aspects of this study. Many thanks also go to Mr Jim Hurley for the late conversations we had numerous times.

Many thanks go also to Mr Stephen J. Buggy, Dr Edmon Chehura and Professor Ralph P. Tatam from Shool of Engineering (Cranfield University) for the collaboration we had on the optical fibre project.

Finally a big thanks goes to my parents who provided encouragement over the three year period of this study.

This thesis is dedicated to my parents

LIST OF CONTENTS

LIST OF FIGURES

LIST OF TABLES

NOMENCLATURE

The symbols used are listed in the following order of appearance:

T_g	Glass Transition Temperature
α_t	Fraction of epoxide reacted at a given time t
α	Fractional conversion of reactive groups or degree of cure
m,n,k,l	Reaction exponents
da/dt	Reaction rate
k	Rate constant
A	Arrhenius pre-exponential factor
E	Activation energy
α_C	Critical attained conversion
α_{max}	Maximum attained conversion
T	Temperature
C	Diffusion factor
F,G,K,P	Fitting parameters
k_d	Diffusion region reaction rate
k_{r1}, k_{r2}	Chemical region reaction rates
α_p	Conversion at the peak of the curve
$g(T)$	Function of temperature
R	Universal Gas Constant
A_T	Amplitude of the imposed thermal modulation
∞	Infinite
C_p	Heat Capacity
c_p	Specific heat capacity
C_R	Reference heat capacity
C_S	Sample heat capacity
L	Length
D	Diameter
Q	Heat

r_o	Overall reaction order
t	Time
$tan\delta$	Loss factor
G'	Storage Modulus
G''	Complex Modulus
T_{go}	Glass Transition Temperature of uncured resin
$T_{g\infty}$	Glass Transition Temperature of fully cured resin
t_{gel}	Time at which gelation occurs
α_{gel}	Conversion at the gel point
β	Heating rate
η^*	Complex viscosity
η'	Real part of complex viscosity
λ	wavelength
λ_B	Bragg wavelength
B	Ratio of primary amines to epoxide groups
b	Fitting parameter
w	Fitting parameter
U	Fitting parameter
n_t	Refractive index at time t

ABBREVIATIONS

The abbreviations used are listed in the following order of appearance:

ABBREVIATION	EXPLANATION
CNTs	Carbon nanotubes
SWCNTS	Single walled carbon nanotubes
MWCNTs	Multi walled carbon nanotubes
DSC	Differential Scanning Calorimetry
DGEBA	Diglycidyl Ether of Bisphenol A
HY 5922	Polyoxypropylene diamine (curing agent)
MTM 44-1 resin	ACG one part resin system
8552 resin	Hexcel one part resin system
DGEBF	Diglycidyl Ether of Bispenol F
EN	Epoxy Novolac
PGE	Phenyl glycidyl ether
DGA	N,N diglycidyl aniline
TGMDA	N,N,N',N' tetraglicidyl-4,4'-methylene dianiline
TTT diagram	Time-Temperature-Transformation diagram
CTT diagram	Conversion-Temperature-Transformation diagram
NMR	Nuclear Magnetic Resonance
HPLC	High-Performance Liquid Chromatography
GPC	Gel Permeation Chromatography
FTIR	Fourier Transform Infrared Spectroscopy
RS	Raman Spectroscopy
DMA	Dynamic Mechanical Analysis

TBA	Torsional Braid Analysis
DEA	Dielectric Analysis
DR	Dynamic Rheometry
TMDSC	Temperature Modulated Differential Scanning Calorimetry
TMA	Thermomechanical Analysis
TEM	Transmission Electron Microscope
SEM	Scanning Electron Microscope
AFM	Atomic Force Microscope
OM	Optical Microscope
GA	Genetic Algorithms
VB	Visual Basic
CB	Carbon Black particles
TS	Thermoset
TP	Thermoplastic
RIPS	Reaction Induced Phase separation
RTM	Resin Transfer Moulding
RI	Refractive Index
OF	Optical fibres
LPG	Long Period grating
FBG	Fibre Bragg grating
TFBG	Tilted Fibre Bragg grating
CP	Cloud Point
LT	Light Transmission
LS	Light Scattering
SAXS	Small Angle X-ray Scattering
RCS	Refrigerated cooling system
TA	Thermal Analysis
HR	High Resolution

Chapter 1

1. Introduction

1.1 Background

The growth of demand for effective and weight reduced advanced materials which are used in structural applications has led to the evolution of the advanced materials industry. Metals and alloys were traditional materials used for many years. In recent years, advanced composite materials are rapidly becoming very important, with applications across a broad range of industries, especially in the aerospace and automotive sectors. These materials offer an attractive combination of properties, namely high stiffness and strength with low specific weight.

The process of the composite material fabrication is complex and involves heat transfer, along with chemical reactions in a system with time-temperature dependent properties. The irreversible chemical process which the materials undergo is called cure. The cure of thermosets is the process of crosslinking by which a reactive resin system passes through different stages, from liquid to rubber to solid, when a time/temperature profile is imposed. As the cure progresses, there is an increase in molecular weight accompanied by an increase in viscosity. This continues until eventually the system reaches ‘gelation’ and is no longer able to flow. An increase in the number and density of 3-D structural cross-links follows until finally the material achieves ‘vitrification’. At this point the material is usually a hard, glassy solid with a glass transition temperature higher than the cure temperature and no further cure reaction can be achieved at the chosen cure temperature. This marks the end of cure. At this point a particular degree of cure has been achieved,

defined as the percentage of unreacted species conversion as compared to a fully cured material. This basic process is shown schematically in figure 1.1.

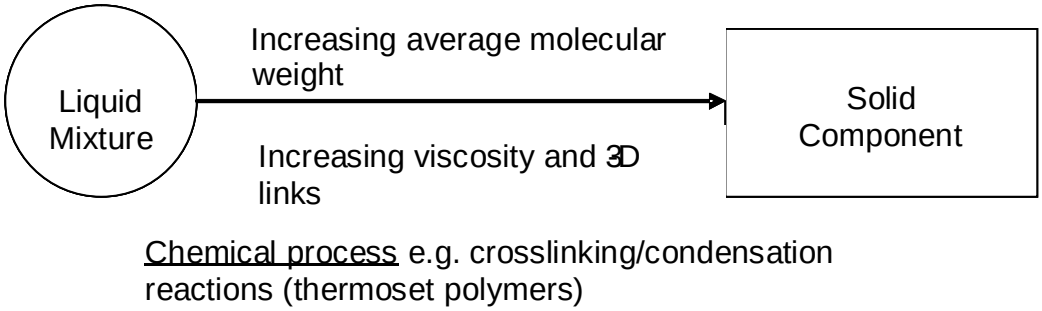

Figure 1.1: Fundamentals of the process of cure [1]

The nature of the manufacturing processes involved often creates expensive but unusable components due to significant component warpage from residual stresses developed during cure cycle or unacceptable level of voids created from poor impregnation of fibres by the polymer matrices. It is critical to reduce costs of manufacture and consistently create quality components by monitoring the resin cure process. The work reported in this thesis is situated within this context.

1.2 The value of cure kinetics modelling

A fully cured material has undergone as much reaction as possible such that further temperature increases or cure duration will not achieve further reaction. The latter affects the properties of the resin system and therefore imposes limitations on its processability. A detailed process model is required in order to analyse the properties of these materials and to understand the changes that take place during a 'cure process', such as the development of the glass transition temperature (T_g), the changes in the region of gelation and vitrification and the increase in the degree of cure. These are properties which characterise a resin system in any given stage of cure. The properties of the final products depend on the mechanism and the extent of the curing reaction. The knowledge of the cure kinetics becomes more apparent on industrial scale, because it enables the optimisation of the process in respect to the final

product properties. The optimisation of the cure process results in the reduction of the overall production time.

Moreover, the importance of the cure kinetics knowledge becomes valuable due to the implications on the production costs. In cases that the manufacturing process is not adequate to produce the desired products, and due to the non-reversible character of the reactions taking place, the final products will either be scrapped or used as fillers. The irreversible characteristics of the curing reactions do not allow for the recycling of the final products. A large volume of expensive scrap is produced annually by the industry. The knowledge of the cure profile of an epoxy resin allows, in principle, the reduction of the scrap volume.

1.3 Aims and objectives of present work

The programme of work reported in this thesis was firstly intended to characterise three different epoxy systems in terms of their cure kinetics, the glass transition temperature advancements and chemoviscosity profiles. Phenomenological models were to be developed and used to fit the experimental DSC data under both dynamic and isothermal heating conditions Diffusion limitations were to be taken into account so that the cure models may fit the experimental curves even at the later stages of the curing reactions. These models were required as independent 'calibration' of the instantaneous degree of cure for parallel work carried out by the Optics Group in the Cranfield University School of Engineering. This work concerns the potential use of optical fibre refractometers for on-line cure monitoring via real-time determination of the refractive index of the resin.

1.3.1 Fibre optic techniques for in-situ cure monitoring

Fibre optic techniques for cure monitoring are seen as a potential alternative to more established cure monitoring techniques, namely dielectric cure monitoring, for those situation where the latter cannot be used. Dielectric cure monitoring techniques have two main inherent disadvantages with respect to their usage [2-3,5-6]. Mould mounted sensors typically monitor the

surface resin close to the mould and hence do not accurately monitor the full component. Currently available embedded sensors, with dimensions typically 5 mm x 10 mm x 0.07 mm, have limited use due to their potential to create structural defects in the component. Thus, although the data from such sensors provide valuable information about the cure process, these types of sensors cannot be employed in structurally critical components. The relatively small dimensions of optical fibres, typically having a diameter of 125 μm, make them far more attractive for embedded sensor applications in composite materials. They may be readily incorporated into composite parts and have been shown to have a negligible effect on component strength. Fibre optic techniques are already used for in-situ monitoring [7,8]. However these techniques rely upon single parameter data to determine the degree of cure and often require special fibres. These issues may be solved by developing a new multi-parameter [9] sensor that will provide data about penetration of resin in the mould [10] and monitor the refractive index change of the resin which could be related to the degree of cure. The advantages of using these new embedded sensors within a composite structure is that this also allows the possibility of subsequent health usage monitoring of parameters such as strain and / or temperature.

1.3.2 Modelling the cure process

The cure kinetics modelling approach used in this study was evaluated in the context of a Round Robin program. For this purpose the T800/3900-2 prepreg system was tested and cure kinetics models were developed to simulate its curing. The purpose of the participation in this program was to compare the available modelling tools used from other groups and based on the same experimental data to test the reasons of the frequently observed deviations in the analysis of this data.

1.3.2.1 Effect of nanoparticle addition on the cure process

Having accomplished the initial objectives, further studies were carried out on the incorporation of carbon nanoparticles into two epoxy systems, namely

the MY 750 / HY 5922 and the MTM 44-1 resin systems. The main objective was to focus on achieving a good state of dispersion of the nanoparticles in the epoxy matrices and study how the achieved dispersion affects the cure kinetics mechanism and the glass transition temperature advancement.

Reinforced thermoset resins are produced commonly by incorporating reinforcing fillers into the polymeric matrix in order to improve selected material properties such as stiffness. The properties of such materials depend largely on the distribution of the filler in the matrix. The fillers are usually carbon or glass fibres, but in many cases additives such as chalk or surface-treated silicates have been used for this purpose.

In the last two decades, some studies have shown the potential improvement in properties and performance of fibre reinforced polymer matrix materials in which micro and nano-scale particles were incorporated, so that reinforced *nanocomposites* could be produced. A nanocomposite is defined as a composite where one of the components has a dimension in the nanometer range. The technology of micro and nano-scale particle reinforcement can be categorised into inorganic layered clay technology, single walled and multi-walled carbon nanotube, carbon nanofibre technology and metal particle technology [11].

Recently, much effort has been devoted to the synthesis and characterisation of carbon nanotubes, due to their very high aspect ratio and promising physical properties for many applications. They are fullerene-based structures that can be viewed as a single sheet of graphite rolled into a cylinder of several microns in length and 10-50 nm in diameter [12]. There are two main categories of carbon nanotubes (CNTs): 1) Single Walled Carbon Nanotubes (SWCNTs) and 2) Multi Walled Carbon Nanotubes (MWCNTs). A schematic of the two categories is depicted in figure 1.2:

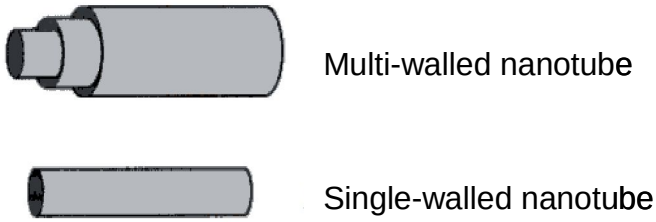

Figure 1.2: Multi-walled and single-walled nanotube structures [4]

Carbon nanotubes can be used as nanofillers in a polymer system to reinforce it. Still there is a considerable lack of understanding of the interfacial bonding between the reinforcements and the matrix material from both the analytical and experimental view. Uniform dispersion of nanoparticles and nanotubes overcoming their tendency to agglomerate due to the van der Waals bonding is the first step in the processing of nanocomposites. The separation of nanotubes is a prerequisite for aligning them. The lack of control of their orientation diminishes the effectiveness of nanotube reinforcement in composites, whether for structural or functional performance [4].

The effect of dispersed nanoparticles upon the chemical cure kinetics of thermosetting resins has also started to be studied [13-15]. The purpose of these studies focused not only on the cure kinetics, but also on aspects of processability and characterisation of the final composite products. It has been observed that the onset, breadth and total heat of the polymerisation reaction, as determined by Differential Scanning Calorimetry (DSC) can be altered by the presence of the nanoparticles [14,15]. Much work needs to be done in order to safely draw conclusions on the effect of nanoparticles upon the cure kinetics of the resins containing them.

1.4 Scope of the reported work

The work covers two main topics. It investigates:-

a) the cure kinetics and the glass transition temperature advancement of three epoxy resins, namely the two-part resin system MY 750 / HY

5922 and the one part MTM 44-1 and 8552 resin systems. This investigation is conducted with the utilisation of Differential Scanning Calorimetry (DSC) and Temperature Modulated DSC (TMDSC). Appropriate (phenomelogical) cure kinetics models are built to predict the degree of cure as a function of temperature/time profile.

b) the effect of carbon nanoparticle incorporation on the cure kinetics and the glass transition temperature advancement of the liquid MY 750 / HY 5922 resin and the toughened epoxy MTM 44-1. DSC and TMDSC are utilised for this purpose as well. Phenomenological cure kinetics models are built for the nanocomposites. A direct comparison is attempted with the models built for the neat systems. The glass transition temperature advancements are also studied and compared with the ones of the neat systems. The aim of these comparisons is to highlight the effect of the nanoparticle addition on the properties of the systems tested.

The state of dispersion of the carbon nanoparticles into the epoxy systems dispersed was studied with the utilisation of Transmission Electron Microscopy (TEM) and Scanning Electron Microscopy (SEM). The state of dispersion of the nanoparticles was studied in order to correlate it with the properties of the materials (cure kinetics in terms of DSC and glass transition temperature advancements).

As an industrial application of this study optical fibres were utilised as an online cure monitoring technique to monitor the refractive index change during the cure of the resin systems and their nanocomposites. In particular, refractive index measurements were conducted for the neat resins and their nanocomposites. A direct comparison was attempted in order to observe any differences due to the carbon nanoparticle incorporation. This utilisation was attempted in order to test the ability of optical fibres to monitor any changes in the formed nanocomposites.

1.5 Overview of the thesis structure

The thesis can be regarded as composed of six parts. The first part includes chapters 1 and 2, which contain the Introduction and the Literature Review. The second part contains the Materials and Methods utilised in this study (chapter 3). The third part, which comprises of chapters 4 to 6, presents the Results obtained by the experimental procedures developed. The fourth part consists of the Modelling Methodology development. Part five presents the industrial application of this study. The final part is an Overall Discussion on the results produced together with Suggestions for future work. In detail the thesis structure is as follows:

After chapter 1, where the importance of the fillers on the cure kinetics and the utilisation of optical fibres as a monitoring technique are presented, chapter 2 focuses on cure as a process and on reaction transformations. It is divided into two parts. In the first part a brief description of the cure kinetics models used to simulate the cure processes is presented. The second part focuses on the properties of carbon nanoparticles, i.e. structure, utilisation as fillers in composites and the properties of the formed materials.

Chapter 3 deals with the materials used and the sample preparation methods are also presented. It also focuses on the experimental techniques utilised in this study. Chapter 4 includes the microstructural characterisation of the epoxy systems and their nanocomposites containing carbon nanotubes and carbon black particles. The characterisation was carried out with the utilisation TEM and SEM imaging. Chapter 5 deals with the experimental resin data of dynamic and isothermal cure experiments of the systems tested. An analysis of the curing data is presented as well as the cure characterisation of the three systems and their nanocomposites. A comparison of the base resins and resins formed with the incorporation of the carbon nanoparticles is achieved in order to manifest the differences taking place. Some viscosity data of the base resin systems are also presented.

Chapter 6 deals with the glass transition temperature advancement of the base resin systems and their nanocomposites. A direct comparison is made.

The cure kinetics modelling methodology is analysed in chapter 7. A description of the methodology used is given and cure kinetics models are built for the resins and their nanocomposites. A comparison of the cure kinetics models is established and the differences are discussed.

Chapter 8 deals with the cure kinetics modelling and the characterisation of another epoxy resin. The second part deals with the results of the cure kinetics model analysis of the Round Robin study. The two systems tested are used for the validation of the cure kinetics modelling methodology developed in this study.

In chapter 9 the utilisation of optical fibres is presented and the correlation between the refractive index change during cure together with the cure kinetics data is analysed.

An overall discussion of the effect of carbon nanoparticle addition on the cure of the epoxy systems studied is presented in chapter 10, together with suggestions for future work. Chapter 11 deals with the general conclusions of this study.

Appendix A contains multiple photos of the RTM demonstration and the infusion test of the MY 750 / HY 5922 resin system, while appendix B contains the final report of the Round Robin participation.

Chapter 2

2. Literature Review

This chapter is divided into two sections. In the first section a brief description of the cure kinetics theory and the cure kinetics modelling methodology is presented. The accompanying phenomena are also analysed. The second section deals with the description of the preparation techniques of carbon nanoparticles, ie carbon nanotubes and carbon black particles. It also reviews the properties of the composites prepared by adding these nanoparticles.

2a. Theoretical background to cure kinetics modelling

2.1 Epoxy Reactions

The chemical reaction in which high molecular mass is formed from monomers is known as polymerisation. Cure is a polymerisation reaction where at least one of the monomers has a functionality greater than two. The curing reaction is referred to thermosetting systems. A subcategory of thermoset cure reactions contains the epoxy reactions. The epoxy or oxirane group is characterised by its reactivity toward both nucleophilic and electrophilic species and it is thus receptive to a wide range of reagents. Epoxy monomers polymerise through step-growth and chain-growth processes. The case of polyaddition (step-growth) polymerisation is mainly represented by epoxy-amine reactions [16].

The main commercial epoxy resins are illustrated in figure 2.1.

Epoxy monomer: 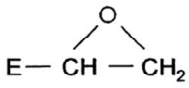 For E – :

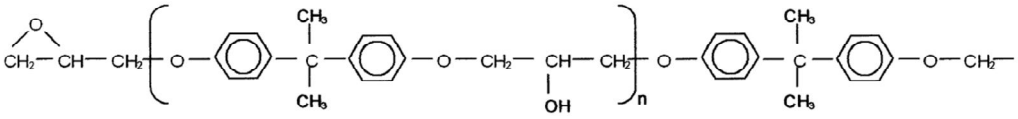

i) Diglycidyl ether of bisphenol A, DGEBA

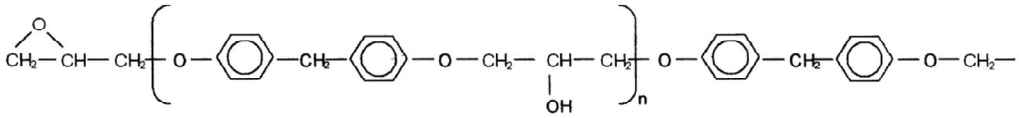

ii) Diglycidyl ether of bisphenol F, DGEBF

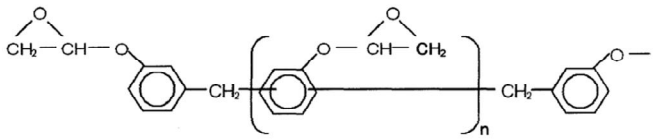

iii) Epoxy novolac, EN

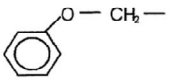

iv) Phenyl glycidyl ether, PGE

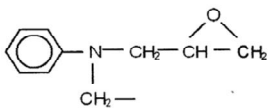

v) N,N diglycidyl aniline, DGA

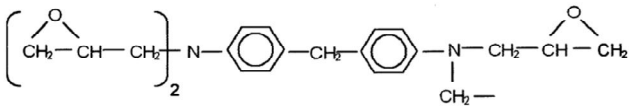

vi) N,N,N′,N′ tetraglycidyl -4,4′- methylene dianiline, TGMDA

Figure 2.1: Main commercial epoxy monomers (resins) [16]

Epoxy resins mostly react with hardeners or ‘curing agents’. A variety of hardeners have been produced for many purposes. Amines are the most common hardeners. A schematic of the main hardeners used is depicted in figure 2.2.

Aliphatic amines

$H_2N–(CH_2)_2 –[NH–(CH_2)_2]_i –NH_2$ (ethyleneamines)

Aromatic amines

i) 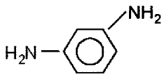 (m-Phenylene diamine)

ii) 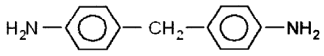 (4,4′Diaminodiphenylmethane)

iii) 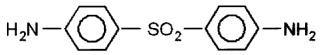 (4,4′Diaminodiphenylsulphone)

Dicyanodiamide (Dicy)

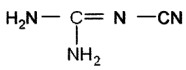

Figure 2.2: Main hardeners used in epoxy-based thermosetting systems [16]

The epoxy-amine cure involves three main reactions:

1) Primary amine addition
2) Secondary amine addition and
3) Etherification

Etherification occurs if there is excess of epoxy rings or if the reactivity of the secondary amines is low. The epoxy-amine reactions are represented in figure 2.3.

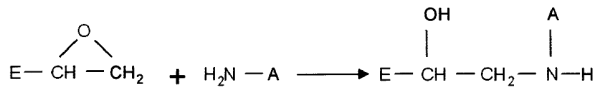

a. Primary amine addition

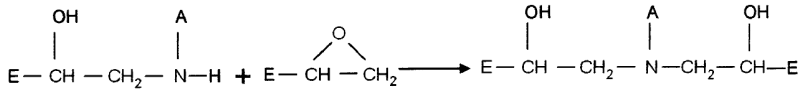

b. Secondary amine addition

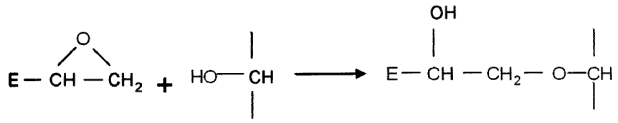

c. Etherification

A represents the remaining aliphatic or aromatic part of the hardener's monomer.

Figure 2.3: Step-growth copolymerisation of epoxy and amine monomers [17]

2.2 Curing reaction

Thermosetting resins are polymerised to form a three-dimensional network. During the curing reaction relatively low average molecular weight monomers are linked together by homopolymerisation or reaction with hardeners, resulting in an increase in molecular weight and complexity. The characteristic feature of thermosets is the formation of a complex three-dimensional crosslinking network. There are several phenomena that may occur during the curing process. The most important of these phenomena are phase separation, gelation, vitrification (devitrification) and degradation.

As the cure reaction progresses, the viscosity of the resin system increases up to a point where the thermoset does not behave as a liquid anymore. *Gelation* denotes the transition from the liquid to the rubbery state. A three-dimensional cross-linking molecular network is forming, which incorporates in its structure the entire material. *Vitrification* of the developing polymer network, occurring during a curing reaction of a thermosetting polymer system, occurs when the glass transition temperature, T_g, of the reacting system reaches the cure temperature due to the increase in molecular weight

or crosslink density. This transformation involves the change of the material from a *mobile* liquid or rubbery state to a *frozen* glassy state. Due to the attendant decrease of the chain segment mobility the reaction becomes *diffusion – controlled*. This eventually leads to a complete halt of the reaction, with residual reactive units as a consequence. As chemical, mechanical and electrical properties attain their ultimate value during the last stages of the cure process, the diffusion-controlled regime is a very important part [18].

Another phenomenon that may occur during a cure process is phase separation. In many resin systems, there are additives included, which enhance some properties of the systems. These additives together with the monomers form two or more distinct phases within the material. That is the case of heterogeneous materials. There are also many cases observed where initially homogeneous materials become heterogeneous due to the curing reaction. The reaction induced phase separation is caused by the solubility mismatch between the different chemical species, especially if modifiers such as rubbers or thermoplastics are present [19].

When the curing temperature is well above the glass transition temperature of a fully cured resin, the resin system may undergo degradation. This is a phenomenon where the covalent bonds that constitute the three-dimensional crosslinked polymer network start breaking down.

The phenomena described above may be illustrated using the popular transformation diagrams, such as the time-temperature-transformation (TTT) and the conversion-temperature-transformation (CTT) diagram, developed by Gillham [20]. A generic CTT diagram for a thermosetting resin system is depicted in figure 2.4.

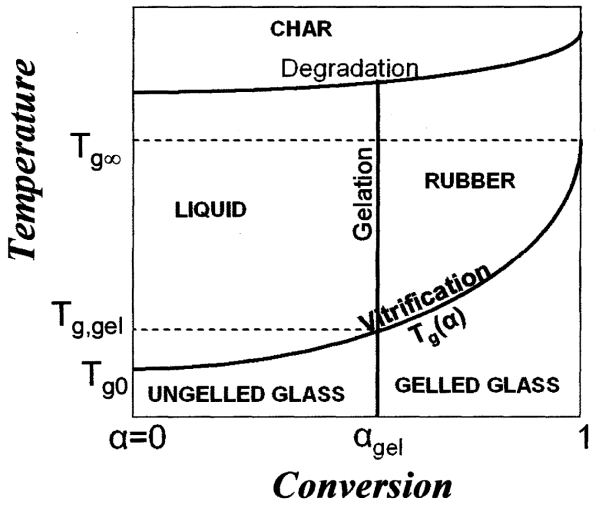

Figure 2.4: Conversion-Temperature-Transformation diagram for thermosetting resins under isothermal curing conditions (CTT diagram) [17]

2.3 Experimental techniques for cure monitoring

The process of the network formation in thermosetting polymers has been studied extensively in the past. Various techniques have been utilised for that purpose. They may be classified into two main categories: Direct techniques which follow the evolution of concentrations of the different reacting species, and indirect techniques which monitor the changes in the physical properties.

The direct techniques include the use of ^{13}C solid-state and liquid Nuclear Magnetic Resonance (NMR), High-Performance Liquid Chromatography (HPLC), Gel Permeation Chromatography (GPC), Fourier Transform Infrared Spectroscopy (FTIR) and Raman Spectroscopy. The indirect techniques include the techniques which characterise the chemorheological changes such as dynamic mechanical analysis [21,22] or torsional braid analysis [23], dielectric analysis [8-11], rheometry [24] and dynamic rheometry [25]. However, chemorheological techniques give no simultaneous quantitative information about the evolution of the conversion or rate of reaction with time and temperature.

Thermal analysis techniques are included in the indirect techniques. Thermal analysis techniques can be divided into calorimetric and thermomechanical. The calorimetric techniques are based on monitoring the heat exchanges, absorption or emission, of a material associated with physical transitions and chemical reactions. The thermomechanical techniques are either measuring dimensional changes or the complex modulus.

2.4 Cure Kinetics Modelling

Chemical cure kinetics models can be classified into two basic categories: a) mechanistic models and b) phenomenological models. Mechanistic models are built based on the balance of chemical species taking part in the chemical reaction. In many cases, it is not easy to derive a mechanistic model because the cure reaction is complex. Thus, phenomenological or empirical models are preferred in the study of the cure kinetics. Normally, phenomenological rate equations are suggested as suitable for analysing both isothermal and dynamic cure kinetics data [26].

2.4.1 Mechanistic models

Mechanistic models have some advantages over phenomenological models. For instance, without conducting time consuming experiments, it is easy to treat separately the influence of the types, concentration or number of initiators on the overall curing reaction rate. To date, much research has been conducted by many researchers in order to construct mechanistic models which adequately characterise the curing reaction of a system [27-35].

The main advantage of the mechanistic models is that they predict and interpret the mechanism of the curing reactions based on the ‘monitoring’ of the balances of the chemical species. In particular, in the case of epoxy-amine reactions, a full series of experiments is required so that the reactants concentrations are known at each step of the curing reactions. The experiments have to be based on a combination of different experimental techniques. Direct experimental monitoring of the reactants’ concentrations may not always provide the necessary data for the construction of an

analytical kinetic model. These ‘shortcomings’ usually lead to oversimplifying assumptions on which the kinetics equations are based on.

2.4.2 Phenomenological models

One of the most debatable problems of the epoxy-amine addition is how to decipher the paths followed in a curing reaction. Although several simultaneous reactions occur during the cure process, some simple models have been developed, assuming that only one reaction may represent the whole cure process. These expressions are empirical, ignoring the details of the curing mechanism, and are based on simulating the experimental observed curing behaviour. A review on the kinetic studies of thermosetting systems where phenomenological models are analysed is presented by Yousefi et al [36]. The present work relies on phenomenological models due to the fact that the composition of some of the resin systems used is not known (commercial resin systems).

2.4.3 Non-parametric techniques

A non-parametric procedure for modelling of the chemical cure kinetics was tested by Serra et al [37] on nonisothermal data of the thermal decomposition of dibenzoyl peroxide and the results when compared with those of the traditional methods showed very good agreement. The most significant feature of this method is its ability to provide a kinetic model that fits the experimental data, without any assumptions either about the functionality of the reaction rate with the degree of cure or the temperature. This technique was also utilised by Skordos and Partridge [38] in modelling the cure behaviour of a commercial epoxy system under isothermal and nonisothermal curing conditions. The procedure is entirely numerical and involves interpolation between experimentally determined values of cure reaction rates. The accuracy of the model is directly dependent on the accuracy of the experimental data. The important advantage of this technique, when compared with others, is that no information on the chemical nature of the process is required.

2.5 Incorporation of diffusion constraints into cure kinetics modelling

Thermosetting materials exhibit the vitrification phenomenon, which effectively stops the reaction before complete conversion is achieved (see paragraph 2.2). The cure process exhibits a diffusion controlled mechanism and as a consequence, the experimental conversion and the reaction rate are lower than predicted. In order to fulfil the condition that the reaction rate is equal to zero at the vitrification conversion, some reaction expressions were introduced such as the maximum attained conversion α_{max}. Gonzalez-Romero and Casillas [39] used the following expression to include the vitrification phenomenon:

$$\frac{d\alpha}{dt} = Ae^{-(E_a/RT)}(\alpha_{\max} - \alpha)^n e^{m\alpha} \qquad (2.1)$$

Where α is the degree of cure defined as the fraction of epoxide reacted at a given time t, $d\alpha/dt$ is the reaction rate defined as the difference of the degree of cure between two specific times $(\alpha_2-\alpha_1)/(t_2-t_1)$ or the differential of the fraction of epoxide reacted, E_α is the activation energy, A is the Arrhenius pre-exponential factor and m,n are fitting parameters

Batch and Macosko [31] used an existing model, developed on the variation of the glass transition temperatures with conversion, and extended it to the vitrification conversion:

$$\alpha_{\max} = \frac{1}{d}\left(\frac{1}{T_o} - \frac{1}{T_{cure}}\right) \qquad (2.2)$$

where d is a fitting parameter, T_{cure} is the cure temperature, and T_o is the theoretical temperature where no cure reactions could occur (α_{max} = 0). When high cure temperatures are used the upper bound for α_{max} is unity.

An alternative kinetics model was presented by Lam et al [40] for the curing reactions of styrene-based thermosetting systems. A similar technique was developed by Samaras [17] to model the curing reaction of a vinylester system. The overall reaction kinetics is a combination of chemically and diffusion–controlled reaction processes. The shift from a chemically to a diffusion-controlled reaction regime is progressive and does not occur exactly at a given time. To take into account the diffusion controlling step of the cure process, some attempts have been made to assign a more general form to the rate constants of the cure reactions. In this case phenomenological models are extended by including a diffusion rate k_d. An overall reaction rate constant k_{total} has been proposed by Rabinowitch [41] such as:

$$\frac{1}{k_{total}} = \frac{1}{k_c} + \frac{1}{k_d} \qquad (2.3)$$

where k_c is the chemical and k_d is the diffusion-controlled reaction constant.

Chern and Poehlein [42], suggested that diffusion becomes controlling when the degree of cure reaches a critical value α_c. Consequently the rate constant k_d was defined as:

$$k_d = k_c e^{-C(\alpha-\alpha_c)} \qquad (2.4)$$

where k_c is the rate constant for the chemical reaction and C is a constant.

Khanna and Chanda [43] defined a diffusion factor, $f(\alpha)$:

$$f(\alpha) = \frac{1}{1+e^{C(\alpha-\alpha_c)}} \qquad (2.5)$$

For $\alpha << \alpha_c$, $f(\alpha)$ approaches unity. The effective reaction rate at a given conversion was represented as the product of chemical reaction rate and $f(\alpha)$.

There are many kinetic expressions that are based on the well-known *Williams-Landel-Ferry* (WLF) equation [44]. It is an empirical equation which expresses the relaxation times, τ, of the polymer segments as a function of temperature:

$$\ln\left(\frac{\tau(T)}{\tau(T_o)}\right) = -\frac{C_1(T-T_o)}{C_2+(T-T_o)} \qquad (2.6)$$

where T_o is a reference temperature and C_1 and C_2 are constants.

Wisanrakkit and Gillham [33] modified the above equation by defining T_g as the reference temperature and using the diffusion control expressions k_d near the glass transition region, instead of the relaxation times τ, as follows

$$\ln\left(\frac{k_d(T)}{k_d(T_g)}\right) = \frac{C_1(T-T_g)}{C_2+(T-T_g)} \qquad (2.7)$$

Karkanas and Partridge [45-47] proposed a modification to account for the fact that the resin curing reaction proceeds only up to a certain degree. This expression included a modified WLF equation so that the constraints would be 'monitored' by the glass transition temperature development up to the *diffusion controlled* area.

2.6 General considerations of the modelling approaches used

The empirical models are based on the main assumption that the reaction rate of the curing reaction is a unique function of only two parameters, namely the temperature, T, and the degree of cure, $\alpha(t)$. This assumption should be valid when dynamic and isothermal curing experiments are conducted and combined in order to develop a cure kinetics model. Thermal history effects usually are not taken into account. The experimental data, when combined, reveal thermal history effects which become evident on the superposition of the dynamic and isothermal data, on a reaction rate versus degree of cure

diagram [38]. A unique value of the reaction rate may exist for every point in the temperature and conversion space, so that the curing mechanism may be independent of the thermal history. This prerequisite, when it is valid, the kinetics model is able to describe both the dynamic and isothermal curing conditions, using the same set of parameters.

The main advantage of phenomenological models is that they are based on a set of experiments, conducted under dynamic and isothermal curing conditions, so that no information on the chemical species is required. In some cases where the superposition effect is not valid, i.e. when phase separation occurs due to the presence of rubber or thermoplastic in a thermoset (toughened epoxy systems), mechanistic models seem to be more appropriate for the description of the complexity of the curing reaction. When that occurs and a phenomenological model is required to describe the cure process, a different approach is used. In this case the model is based on dynamic or isothermal curing experiments, leading to assumptions about the curing reactions, which are partially true [48-52]. Pascault et al [53-55] studied the kinetics of an epoxy-aromatic phase separating system. They also managed to monitor the appearance of the phase separation. A mechanistic model was built, which took into consideration the evolution of the two phases: i) starting from a homogeneous phase and ii) ending in a two phase heterogeneous. The model required monitoring of the mechanisms that take place in the whole conversion range. Swier and Van Mele [56] used a mechanistic model where the evolution of the curing reaction of a thermoset that contained two thermoplastics was monitored by terms of Temperature Modulated DSC (TMDSC).

In conclusion, mechanistic models are used to fit the experimental data when the concentrations of the reactants can be followed during the cure reaction. That requires the knowledge of the curing mechanism which is not the case for most commercial resins. Phenomenological models are based on a series of experiments under dynamic and isothermal curing conditions, whilst the knowledge of the curing reaction is not a prerequisite. Their use is more simplistic compared to the mechanistic ones.

2b. Theoretical background of polymer nanocomposites

2.7 Polymer nanocomposites based on carbon nanotubes

Polymer composites have been the mainstay of high-performance structural materials for aerospace, defense, marine, automotive, civil infrastructure, sporting goods, etc. for over a quarter of a century, offering high strength and stiffness, dimensional stability and good thermal properties. With the advent and application of nanotechnology, adaptations of polymer composites represent the promise of the next generation material systems for structural applications. Most of the work carried out in the polymer nanotechnology area concentrates on the improvement of electrical, thermal, mechanical, optical and barrier properties of polymer systems. Carbon nanoparticles and especially carbon nanotubes (CNTs) have extraordinary properties, which have attracted the attention of many researchers from diverse fields. The incorporation of carbon nanotubes into polymer systems has shown potential improvement in properties and performance, introducing one of the new generation of materials known as *polymer nanocomposites*.

Since their first observation nearly two decades ago by Iijima [57], carbon nanotubes have become the focus of considerable research. Numerous investigators have since reported remarkable physical and mechanical properties for this new form of carbon. In particular they exhibit characteristics that can be beneficial, as they can be used as:

- Reinforcement of polymer based composite materials, which can potentially improve properties such as stiffness, strength.
- Modifiers for high-temperature uses of polymers
- Conductive fillers in insulating polymer matrices to provide electrostatic discharge and electromagnetic radio interference protection and
- Doping of polymers to provide active materials for electronic applications.

The use of carbon nanotubes as reinforcing systems of polymer matrices may offer several advantages over conventional reinforcements. Carbon

nanotubes combine high aspect ratio, small size and greater strength and stiffness than the corresponding macroscopic forms. Furthermore, since they do not break as easily as carbon fibres during processing, they potentially have a substantial advantage in composite processing and manufacturing [4].

2.8 Carbon nanotube structures

Carbon nanotubes are fullerene-based structures that can be viewed as a single sheet of graphite rolled into a cylinder several microns in length and 10-50 nm in diameter [4]. In 1991, Iijima [57] discovered them while studying the material deposited on the cathode during the evaporation synthesis of fullerenes. Since the invention of a large-scale synthesis method by Ebbesen and Ajaian [58] in 1992, systematic investigations and attempts have been made to understand their chemical structure, to improve the synthesis techniques and to analyse the relationship between structure and properties.

A nanotube can be conceptualised as a tubular microcrystal of graphite. A graphitic sheet is a formation of trivalent carbon atoms forming a hexagonal network (see figure 2.5). By folding a graphite sheet, an open cylinder may be formed. The nanotube is typically closed at each end by hemispherical caps.

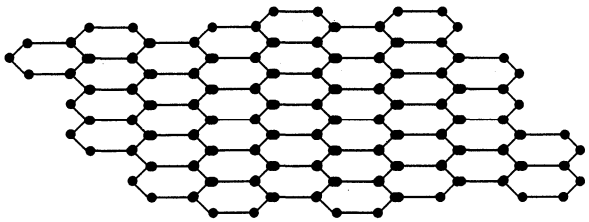

Figure 2.5: Schematic of the graphite sheet [4]

Due to symmetry of the carbon atoms in the graphitic sheet, different structures are possible, depending on how the sheet can be folded. Figure 2.6 shows the three different possible nanotube formations: arm-chair, zigzag and chiral. The characteristic of chirality formation of nanotubes has a great relevance, as it affects the physical properties. The latter also depend on the tube diameter.

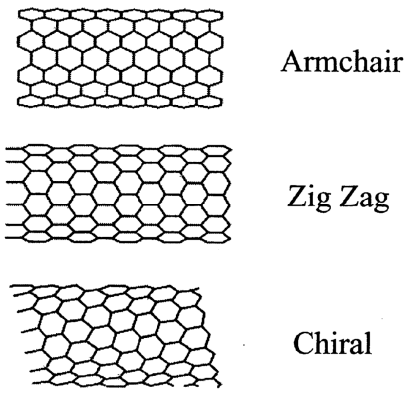

Figure 2.6: Schematic of the three different nanotube structures [4]

Carbon nanotubes can be categorised in two types, depending on their form: i) multi-walled and ii) single-walled carbon nanotubes (see figure 1.2). Multi-walled nanotubes were discovered first. This type of nanotube consists of concentric cylinders, which are placed around a common hollow cylinder with a specific separation between these layers. Each one of the cylinders has a diameter in the range of 2 to 25 nm and a length that can reach several microns.

The single-walled carbon nanotubes were synthesised later in mid 1990s. A single-walled nanotube has a structure similar to an ideal fullerene fibre.

2.9 Carbon nanotube preparation techniques

The characterisation of the nanotube properties are closely related to the production of relatively high quantities in the highest purity possible. For example, the first nanotubes that were produced using the carbon arc technique contained a high content of impurities, which made it difficult to predict the final properties of the nanotubes. The past few years a lot of effort has been devoted to the development of the production techniques so that high levels of purity may be reached, but the production techniques used still give relatively very small yields and degree of purification.

2.9.1 Multi-walled carbon nanotubes

Multi-walled carbon nanotubes are commonly produced by the carbon arc method. Figure 2.7 shows a schematic of the carbon arc apparatus:

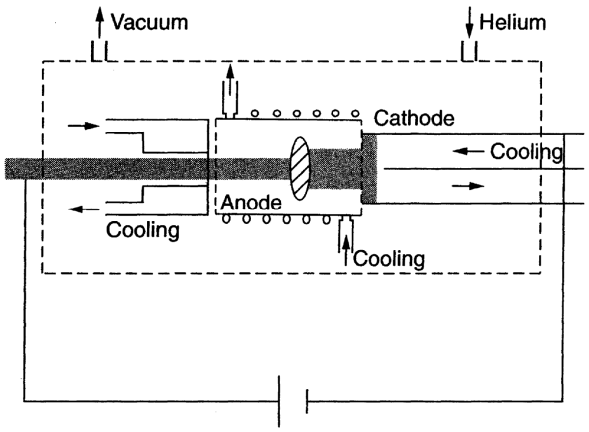

Figure 2.7: Schematic of the carbon arc apparatus [4]

The growth of multi-walled nanotubes on the cathode surface is obtained by generating a plasma arc in an inert atmosphere. This is done by applying a dc current and a voltage between two carbon rods. The deposit has the same shape as the positive electrode and is divided into two regions: the outer and the inner region. The outer region consists of nanotubes and nanoparticles, which are fused together, while the inner region consists of randomly oriented nanotubes, arranged into columns. The carbon arc allows the production of carbon nanotubes with better properties than those nanotubes produced by other techniques due to the high temperatures used. However, this method provides a limited quantity of material, which must be purified.

Another common technique is the chemical vapour deposition (CVD) which consists of the catalytic decomposition of either benzene or acetylene, over silica or graphite covered by metals or silica embedded with iron particles. The main disadvantage of this technique, when compared to carbon arc, is that the reactions are taking place at low temperatures. The final products are agglomerates, which contain catalyst particles and other carbon by-products.

Modifications of this technique include the microwave plasma-enhanced CVD and hot-filament plasma-enhanced CVD.

2.9.2 Single-walled carbon nanotubes

The techniques to produce single-walled carbon nanotubes are based on the vaporisation of graphite and catalyst mixing under an inert gas atmosphere.

The use of electric arc was the first technique to be exploited. The carbon arc apparatus was modified by drilling a hole in the anode and filling it with a mixture of metal catalyst and graphite powder. The nanotubes were produced in a weblike structure, consisting of tens of tubes in a chamber and not in the anode, as in the case of multi-walled nanotubes. Another technique is the laser ablation, where the nanotubes are formed in carbon plasma, under an inert atmosphere, usually argon. A very high yield is obtained.

2.9.3 Purification techniques

The nanotubes produced with most preparation methods contain a large amount of impurities. The most common technique to eliminate these impurities is to burn the material at a high temperature. Other purification methods have been developed recently based on 1) chemical oxidation, 2) filtration and 3) chromatography.

Chemical oxidation is a technique that is relatively cheap and easy to use. Very pure samples are obtained, but the yield is very low (~1 %). On the other hand, filtration and chromatography are non-destructive methods. However, filtration of single-walled nanotubes could become very slow due to the blocking of the filter pores.

2.10 Dispersion techniques

The study of the preparation methods of how nanotubes disperse in aqueous solution and their relative motion represents the first step in understanding their behaviour for application as fillers. Different solvents (ethanol, toluene, chloroform) and times were employed for the ultrasonication treatment. A list of the methods and the polymers used to disperse carbon nanotubes is shown in table 2.1.

Nanotubes	Polymer	Preparation method
Single-walled	Epoxy (Epon 828)	Ultrasonic dispersion
Single-walled; Multi-walled	PMMA	Mixing in ultrasonic bath and spin coating, ultrasonic dispersion, mixing followed by in situ polymerisation
Single-walled	Polypropylene	Electrochemical method, mixing and ultrasonic treatment
Single-walled;Multi-walled	Epoxy (Araldite LY 556)	Tube sonication followed by mixing with the polymer
Multi-walled	Epoxy (Epon 828)	Ultrasonic dispersion before the curing
Multi-walled	Polystyrene	Solution evaporation assisted by high-energy sonication
Multi-walled	Epoxy (Araldite LY 564)	Tube sonication, drying, and dispersion on a glass surface, spreading of the polymer by blade
Multi-walled	Poly(vinyl) alchohol	Mixing with the polymer, casting, and controlled water evaporation after chemical treatment of the tubes
Multi-walled	Polyhydroxyaminoether (PHAE)	Casting of nanotube suspension, polymer, and chloroform after sonication
Multi-walled	Urethane / diacrylate EBECRYL 4858	Tube sonication in ethanol, drying, and dispersion on a glass surface, polymer spreading by blade
Multi-walled	Epoxy (Epon 812)	Tube sonication and mixing with polymer
Multi-walled	p-Phenylenevinylene (PPV)	Chemical oxidation and spin coating
Multi-walled	Poly(m-phenylenevinylene)(PmPV)	Mixing and sonication

Table 2.1: Polymer-based carbon nanotube systems and corresponding dispersion method [4]

Multi-walled nanotube polystyrene composites were produced by a solution evaporation technique assisted by high-energy sonication [59]. The process consisted of separate dispersion and high-energy sonication of the polymer and the nanotubes in toluene, followed by mixing, casting into a culture dish, and solvent evaporation.

Melt processing is one of the most promising dispersion techniques. Lopez-Manchado et al [60] dispersed single-walled carbon nanotubes in isotactic polypropylene by shear mixing. Melt mixing was also used by Zhang et al [61], who studied the effect of this method on the interaction between multi-walled carbon nanotubes and a polystyrene matrix. When the pristine nanotubes and polystyrene were put in a solution, the interaction between them was not as good as expected. In contrast, when the melt mixing method was used, the interaction was significantly enhanced. Ghose et al [62,63] prepared a mixture of multi-walled carbon nanotubes with PETI-330 by dry mixing the components in a ball mill. Comparing again different methods to disperse the nanotubes, they reported a uniform dispersion when they used dry mixing.

Recently, Moniruzzaman et al [64] reported a new method for preparing single-walled nanotubes and epoxy nanocomposites, which involves high shear mixing and heating of the mixture prior to introducing the hardener. The glass transition temperature was noticed not to be affected by the use of this method, as in the cases of the aforementioned techniques.

The homogeneity of the composites and the nanotube dispersion are investigated by the utilisation of Transmission Electron Microscopy (TEM) and Scanning Electron Microscopy (SEM). Uniform distributions of carbon nanotubes into the polymer matrices are usually obtained at low concentrations of carbon nanotubes. In order to improve the nanotube dispersion in an epoxy matrix, a surfactant was used by Gong et al [65]. The surfactant addition was found to improve the state of dispersion.

2.11 Properties of polymer nanocomposites

2.11.1 Thermal stability

Early studies on the influence of the carbon nanotube addition into the polymeric matrix were an evaluation of multi-walled carbon nanotubes in the matrix of poly (vinyl alcohol) [66] and a study of multi-walled carbon nanotubes in an epoxy matrix [65]. These studies indicated that the nanotube addition moderately increases the glass transition temperature measured by dynamic mechanical analysis. However, in other cases, when a surfactant is used for the surface treatment of carbon nanotubes, it causes a decrease of the glass transition temperature [67,68]. In addition, the presence of nanotubes stiffened the polymer matrix, especially at high temperatures [68], and increased the temperature at which the onset of degradation initiates [69]. Cui et al [70] prepared carbon nanotubes by a classical CVD method, which were characterised and then used in a polymeric matrix. The results of the characterisation showed that a good dispersion was achieved without the use of a surfactant (Tergitol). The glass transition temperature increased as a function of nanotube content. On the other hand when a surfactant was used, it resulted in a better state of dispersion. However, the glass transition temperature decreased.

Another study by Gojny et at [71] on the addition of multi-walled nanotubes, which were treated with oxidising inorganic acids, showed that the functionalisation led to a reduced agglomeration and improved interaction between the nanotubes and the epoxy resin. The same group [67] studied the effect of the incorporation of functionalised multi-walled carbon nanotubes on the thermomechanical properties of epoxy resins. It was reported that samples containing functionalised nanotubes showed a stronger influence on the glass transition temperature in comparison to composites containing the same amount of non-functionalised nanotubes. The effect arises from the fact that the carbon nanotubes tend to reduce the mobility of the matrix by interfacial interactions. The chemical functionalisation of the nanotubes surface influences the interfacial adhesion between the nanotubes and the

epoxy resin. Similar results were also reported by Yaping et al [72], where a strong influence of the surface treatment of the nanotubes was found.

There are also other groups which have studied the mastering of the addition of functionalised nanotubes. This addition resulted in a reduced agglomeration and an improved interaction with the epoxy resin. However, by using different dispersion formulations and processing parameters [73], a reduction of the glass transition temperature was shown in some cases. For example Miyagawa et al [74,75] reported that when adding fluorinated single wall carbon nanotubes (FSWCNT) into an epoxy matrix, based on diglycidyl ether of Bisphenol F (DGEBF), the glass transition temperature decreased by approximately 30^{o}C. Continuing their work, but using vapor grown carbon fibres (VGCF) this time [74], they also reported that the glass transition temperature decreased by 30^{o}C. An explanation to this decrease might be that fluorination disrupts the van der Waals forces between the nanotubes and increases the solubility of the carbon nanotubes in solvents, such as alcohols and ketones, which leads to a greater degree of dispersion in these solutions. The decrease in T_g was attributed to the existence of the fluorine on single wall carbon nanotubes and in the case of the addition of the fibres to a chemical reaction between the hydroxyl groups on the VGCF surface and the curing agent, resulting in lower crosslink density. Valentini et al [76] modified single-walled nanotubes with amino groups, which were prepared via chemical addition of fluorine on the carbon nanotube surface by plasma treatment. This was combined with the use of a dc electric field to enhance the assembly of the modified carbon nanotubes into ordered films with rectifying diode behaviour. No significant change of the glass transition temperature was reported.

The thermo-mechanical properties of epoxy-based nanocomposites of randomly oriented single and multi-walled carbon nanotubes were examined based on the preparation methods, by Fidelus et al [77]. In this case, sodium dodecyl sulphate (SDS) surfactant was used so that the dispersion of the carbon nanotubes becomes better in the epoxy matrix. It was reported that there was a moderate improvement of Young's modulus, measured by

Dynamic Mechanical Thermal Analysis (DMTA). A significant enhancement of tensile impact toughness was also observed, although no significant change in the glass transition temperature of the epoxy nanocomposites compared to the neat epoxy matrix was noticed. The effects of different dispersion states of carbon nanotubes on epoxy nanocomposites were also studied by Song and Youn [78]. The dispersion states were altered depending upon whether a solvent was employed or not. This work was based on a previous report by Liao et al [79], which concluded that considerable improvements of the nanotube dispersion in single-walled carbon nanotube (SWNT) / SC-15 epoxy resin nanocomposites could be obtained through the use of tip sonication and the addition of acetone. As expected, when the solvent was employed in the CNTs dispersion process relatively well dispersed CNTs nanocomposites could be obtained. On the contrary, when the solvent was not employed in the sonication process, aggregates of pristine CNTs remained in the polymer matrix.

Recently, another study [80] focused on the effect of the modification of carbon nanotubes by acid treatment, plasma oxidation and amine treatment. The surface modified carbon nanotubes were well dispersed in the epoxy matrix and a strong interfacial bonding was developed with the polymer matrix. The most significant improvement was shown by the plasma oxidation. The result of the good dispersion was reflected on the higher storage and loss moduli of the nanocomposite. It was also found that improved tensile strength and elongation at break were achieved for the chemically treated nanocomposites.

2.11.2 Effect of fillers on composites

The change of the glass transition temperature and the reactivity of resins have been investigated by many researchers, when fillers such as carbon or glass fibres, carbon nanotubes or carbon black are added. In a report, published by Thostenson et al [81], it was mentioned that several groups concluded that the presence of a filler zeolite can accelerate effectively the curing reaction. This behaviour was attributed to a relatively high concentration of curing agents on the surface of the zeolite that provokes the

reaction. The glass transition temperature (T_g) of cured resin was slightly decreased with the addition of the zeolite filler. Wang et al [82] reported that carbon black particles can effectively absorb the amine hardener and work as a support to disperse the hardener during the curing of epoxy resin. Grenier and Grenier [83] compared with the effect of the addition of glass and carbon fibres to epoxy systems the utilisation of several techniques. The results of this study showed that the presence of glass or carbon fibres decreases the autocatalytic term by a considerable extent. Thus the kinetics is systematically slower in the presence of fibres. The same effect of the addition of the carbon nanotubes was observed by Liao et al [84] when 0.12 wt % SWNTs was added in an EPON 862 resin, containing 75 wt % of glass fibres, accompanied by an improvement in T_gs. In this case there is a possibility that these effects are a result of the synergistic effect between nanotube and fibre reinforcement. In other cases [85,86] the addition of glass and carbon fibres to epoxy systems does not appear to change the reaction mechanisms or the network structure.

2.11.3 Electrical properties

The addition of the carbon nanotubes to an epoxy matrix strongly affects the electrical properties of the formed nanocomposites. This effect can be used in many applications, including optoelectronics, electromagnetic shielding, electrostatic discharge, electroplating and membrane technologies. Table 2.2 reports some examples of carbon nanocomposites and the corresponding electrical conductivity.

Nanotube Content	Polymer	Composite Electrical Conductivity, S / m	Pure Polymer Electrical Conductivity, S / m
0.1 vol %	Epoxy	10^{-2}	5×10^{-8}
20 wt %	Polypyrrole	1.4×10^{-1}	2.6×10^{-2}
20 wt %	Poly(vinyl alchohol) (PVOH)	10^{-1}	2.9×10^{-9}
7-11 wt %	m-Phenylenevinylene (PMPV)	1.5×10^{-9} to 1×10^{-1}	2×10^{-10}

Table 2.2: Electrical conductivity of carbon nanocomposites [4]

These systems usually exhibit percolation behaviour. This phenomenon is characterised by the presence of a conductive path through the matrix, due to the formation of a three-dimensional network of conductive filler particles. A sharp drop in the electrical resistance characterises the percolation threshold.

A significant increase of the electrical conductivity was found for some polymer nacomposites. The polymer matrix, investigated by Sandler et al [87] is used in applications where high electrical conductivity is required. When carbon nanotubes were used, instead of carbon black particles, the overall conductivity increased. The same group studied the utilisation of multi-walled carbon nanotubes as conductive fillers in the same polymer matrix [88]. It was demonstrated that the specific bulk conductivity of these composites depends on the process parameters employed during the fabrication process. The resulting bulk composite conductivity ranged from dielectric behaviour to conductivities of 10^{-3} S m^{-1}.

Gojny et al [89] combined conventional fibres (e.g glass-, carbon-, aramid-fibres, etc.) and minute amounts of carbon nanotubes in an epoxy based composite system, which led to a significant increase of the electrical conductivity of the system. The same results were observed when a similar amount of carbon black was added to the epoxy matrix. The in-plane electrical

conductivity was more than one order of magnitude higher than in the z-direction. In another study, different nanoparticles such as fumed silica and carbon black were used to optimise the epoxy matrix system of a glass-fibre-reinforced composite [90]. In addition, an electrical field was applied during curing, in order to enhance the orientation of the nanofillers in the z-direction. The laminates that contained carbon nanotubes exhibited a relatively high electrical conductivity at very low filler contents.

The same group incorporated different types of carbon nanotubes (single-, double- and multi-walled nanotubes) using the same epoxy matrix [91,92] in order to evaluate the influence of the filler content on the electrical conductivity. The multi-walled nanotubes exhibited the highest potential for an efficient enhancement of the electrical conductivity due to their relatively low surface area.

The electrical properties of low-density polyethylene (LDPE), filled with multi-walled carbon nanotubes, were studied by Liang and Tjong [93]. The electrical properties were investigated as a function of CNT volume content, frequency and temperature. The results showed that the dielectric constant of nanocomposites increased slightly with increasing CNT content, up to a specific value. Thereafter, the dielectric constant increased sharply. It was found that the dielectric constant of LDPE / 3.6 vol % CNT nanocomposite was more than two orders of magnitude higher than that of the pure LDPE.

2.12 Cure kinetics of thermosetting nanocomposites

To date, the effects of the addition of carbon nanoparticles on the cure kinetics mechanisms have not been studied in depth. Some groups have studied these effects experimentally, using thermal analysis techniques.

The effects of the incorporation of single-walled carbon nanotubes (SWCNTs) on the cure reaction of a DGEBA epoxy resin with a diethylene triamine (DETA) hardener were investigated by means of thermal analysis and Raman Spectroscopy by Puglia et al [94]. The isothermal thermograms showed the typical ‘autocatalytic’ behaviour reported for DGEBA and its

composites. The results showed that carbon nanotubes act as a strong catalyst. However, no effects of the presence of SWCNTs on the maximum degree of cure of the epoxy were detected. In this study a shift of the exothermic reaction peak to lower temperatures was observed in the presence of carbon nanotubes at high heating rates, when dynamic cures were conducted.

Ton-That et al [95] analysed the results of DSC measurements when organo-nanoclays were incorporated into a DGEBA based resin system. The results were analysed with the Avrami approach, a method similar to the one developed by Ozawa [36], and it was observed that at the early stages of the dynamic DSC cure (i.e. at lower temperature), the activation energy of the epoxy nanocomposite is similar to that of the epoxy-amine system, but it gets substantially lower at the later stages (at higher temperatures). For the epoxy-amine mixture the presence of the nanoclays had little effect on the cure kinetics at the early stages, but it seems to affect the later stages.

Lu et al [96] used the same epoxy system (DGEBA) and a 4,4'-methylene dianiline (MDA) hardener to study the effect of zeolite addition on the cure behaviour. The experimental cure measurements indicated that the cure reaction can be accelerated effectively by the presence of the filler, but retarded at low temperatures because vitrification may be involved in the curing process. DGEBA and 2-ethyl-4-methylimidazole (EMI-2,4) resin system, when nanosilica particles were added, was studied by Zhou et al [97]. Two different curing kinetic methods were used to investigate the cure kinetics of that system. The first method assumes constant activation energy for the whole process, while the second one is based on a variable activation energy during cure. It was shown that the resin system obeys an autocatalytic behaviour and that the addition of nano-SiC particles does not alter the reaction mechanism.

Another study for the same epoxy system, when poly(oxypropylene)diamine was used as the curing agent and organically modified montmorillonite (OMMT) was incorporated into the system was

conducted by Ivankovic et al [98] by means of DSC under isothermal and dynamic heating conditions. Analysis of the DSC data indicated that the presence of the filler has a very small effect on the cure kinetics of the system. An autocatalytic phenomenological model was used to fit the experimental data. A similar effect was observed by Shi et al [99] when they studied the effect of the addition of montmorillonite based nanoclays into a polybenzoxazine thermosetting system.

The reduction in the reactivity of an epoxy system, when multi-walled carbon nanotubes were incorporated, was observed by Xie et al [100]. It was observed that the reaction kinetics is affected at higher heating temperatures for the isothermal cure of tetraglycidyl-4,4'-diaminodiphenylmethane (TGDDM) and 4,4'-diaminodiphenylsulfone (DDS) as the curing agent when carbon nanotubes were added. Despite that at the initial stages of the cure the presence of the nanotubes causes an accelerating effect on the epoxy reaction, at the later stages there seems to be a decrease of the reaction rates, when compared to those of the neat resin. This phenomenon is attributed to the large decrease in segment mobility at vitrification that hinders the reaction of MWNT/epoxy nanocomposites at higher temperatures. Another study by the same group [101] revealed that the presence of the fibres had only a negligible effect on the initial reaction rates and the time to maximum reaction rate when carbon nanofibres were used in the same system. An autocatalytic model was utilised, based on Kamal's equation [36] to simulate the cure process. The rate constant k_1 governs the early-stage autocatalytic reaction and k_2 affects the reaction after the initial autocatalytic stage. The results compared with those of the neat resin system suggested that the presence of the carbon nanofibres has only a very small accelerating effect on the reaction of the resin at the initial stage, whereas after the initial autocatalytic stage the filler hinders the reaction.

Most of these studies, conducted from the various groups mentioned were based on isothermal DSC experiments (except for the study of Ivankovic et al [98] which was based on both isothermal and dynamic DSC experiments),

which did not allow for a full characterisation of the materials' cure mechanism. This limits the temperature window on which the cure kinetics model is based, but also does not take into consideration any side reactions that may take place at higher temperatures. Limited data may also lead to misleading conclusions e.g. when the accelerating effect of the nanotube incorporation on the cure kinetics mechanism or the change in the reaction rates are studied. The conclusions also vary, depending on the analysis method, which 'allows' for a different evaluation of the kinetics parameters. For example there is a difference on the kinetics parameters evaluated by the isoconversional methods developed by Ozawa and Kissinger and the analysis methods which are based on phenomenological or mechanistic models when these are based on a full series of isothermal and dynamic cure experiments.

2.13 Industrial applications of carbon nanotubes

Carbon nanotubes have attracted a great deal of attention worldwide with their unique properties, which are leading to many promising applications. Potential practical applications have been reported such as chemical sensors, field emission materials, catalyst support, electronic devices, high sensitivity nanobalance for nanoscopic particles, nanotweezers, reinforcements in high performance composites, nanoprobes in metereology and biomedical and chemical investigations, anodes for lithium ion in batteries, nanoelectronic devices, supercapacitors and hydrogen storage [102].

Given the mechanical properties that have been reported on carbon nanotubes, an entire new class of composite materials arises with the utilisation of carbon nanotubes. The first commercially recognised use of milti-walled carbon nanotubes was electrically conducting components in polymer composites [103]. The electrical properties of the matrices used when carbon nanotubes are incorporated into can improve significantly. Then these composites may exhibit the same properties as metal or metal oxides. Carbon nanotube metal or metal oxide composites have been made to improve the electrical conductivity. For applications in polymer nanocomposites the elastic and fracture properties of carbon nanotubes must be understood along with interactions at the nanotube matrix interface. The mechanical performance of

carbon nanotubes in a polymer or ceramic matrix is believed to be superior when compared with traditional fillers, such as carbon black particles or ultra fine metal powders. The major difference from conventional fibre-reinforced composites is that the scale is narrowed down to nanometers instead of micrometers [104].

For industrial applications in nanocomposites, large quantities of nanotubes are required. It has been found that the best method for high quantity and low production cost of carbon nanotubes is the CVD method. Cost factors also lead more to the utilisation of multi-walled, rather than single-walled nanotubes [105]. Nanotube reinforced composites have already been successfully created. Experiments on a fully integrated nanocomposite using single-walled nanotubes demonstrated dramatic enhancement in some of the mechanical properties, such as the storage and tensile moduli, tensile strength, etc.

Rubber compounds reinforced with nanotubes have a range of potential applications in tire industry. By replacing the carbon black with carbon nanotubes, improved skid resistance and reduced abrasion of tires has been found in experimental studies [105]. The use of carbon nanotubes to improve materials will be investigated in the future as production increases and applicability in industrial settings becomes possible.

Chapter 3

3. Resins, Mixing Methods and Experimental Techniques

Three different epoxy-based resin systems were used in this study. All of them were commercially available epoxy / amine systems. A brief description of all the resin systems used is given in this chapter. The preparation methods when carbon nanoparticles were incorporated into these resin systems are presented. A description of the experimental techniques utilised in this study is also presented. These techniques include the cure monitoring techniques (DSC, Rheometry, Optical fibres) as well as the microscopic techniques (TEM, SEM).

3.1 Resins and Carbon Nanoparticles

3.1.1 MY 750 / HY 5922 Resin

The first commercial resin system used was supplied by Vantico Ltd under the trade name Araldite MY 750. It is a liquid, unmodified, solvent-free Bisphenol A based epoxy resin. It was supplied as a high viscosity liquid with a density of 1.15 – 1.20 g / cm^3 at 25^oC [106]. Its weight per epoxide (grams of resin containing one gram-equivalent of epoxide) is 185-192. According to the manufacturer the storage life of the base resin is 12 months when stored at -18^oC. A general schematic of its chemical structure is depicted in figure 3.1.

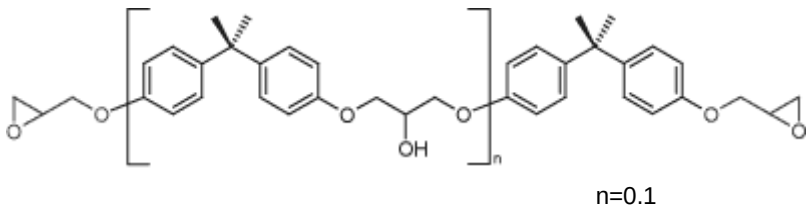

n=0.1

Figure 3.1: Schematic of the chemical structure of the DGEBA based system

Amine hardener HY 5922 (polyoxypropylene diamine)

The curing agent used is polyoxypropylene diamine with the commercial name HY 5922. It is a liquid, aliphatic diamine hardener, supplied by Vantico Ltd. It is a corrosive product with a density of 0.95 – 1.00 g / cm^3 at 25^oC [106]. A schematic of its chemical structure is presented in figure 3.2.

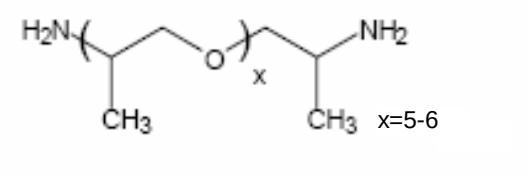

Figure 3.2: Schematic of the chemical structure of the HY 5922 (polyoxypropylene diamine) curing agent

The epoxy-amine system when fully cured exhibits a low glass transition temperature at 45^oC. The main applications are for the production of large coils for magnets and / or rotating machines and super-conductive magnets. It is mainly used in vacuum impregnation processes.

Manufacturer's cure process specification

- Cure at 40^oC for 6 hours and postcure at 80^oC for 3 hours.

Resin preparation

A single formulation of this resin system was used, namely the stoichiometric mixing ratio of 1 / 0.55 between the resin and the hardener, respectively. The resin and the hardener were originally stored at room temperature. The hardener was dissolved in the epoxy resin also at room temperature. The resin system was mixed until the temperature increased due to the exotherm of the reaction taking place. This indicated that the mixing was finished. The resin mixture batches produced were then placed in plastic containers and stored for further use and testing in the freezer at -18^oC, in order to prevent any further reaction taking place.

3.1.2 MTM 44-1 One Part Resin

MTM 44-1 is a dual cure temperature, high performance epoxy matrix, supplied by ACG, developed for both infusion and prepreg processing. It has been optimised for low pressure vacuum-bag processing and, in addition to resin film and prepreg formats, it may be supplied in partially or selective impregnated formats to reduce lay-up time, minimise surface defects and ensure very low internal void contents. After a freestanding postcure the system exhibits a high level of damage tolerance. This, together with its low density, makes the resin system a strong candidate for large aircraft primary structure, produced out of autoclave. It is a brown coloured tetrafunctional epoxy system that contains two aromatic polyamines as the curing agents and a thermoplastic as a toughening additive. The fully cured resin exhibits a density of 1.18 g/cm^3 [107].

The resin is available as resin film for vacuum infusion processes, in partially, selectively impregnated formats for vacuum processes and as full prepreg for autoclave processing.

According to the manufacturer the storage life of the resin is 12 months when stored at -18^{o}C or 21 days at room temperature.

Manufacturer's cure process specification

- Cure at 130^{o}C for 4 hours or at 180^{o}C for 2 hours.

3.1.3 8552 One Part Resin

This resin system is a high performance toughened epoxy matrix for use in primary aerospace structures. The neat resin is a dark yellow viscous material at room temperature, with a density of 1.301 g / cm^3 [108]. It is a tetrafunctional epoxy system, based on tetraglycidyl-p-aminophenol and tetraglycidyl methylene dianiline. The curing agent for this system is diamino diphenyl sulphone. It also contains a thermoplastic under the trade name Dapsone. The resin system was supplied by Hexcel Composites as a

commercial one part epoxy resin system. The resin exhibits a high glass transition temperature. According to the manufacturer the storage life of the resin is 12 months when stored at -18^{o}C or 10 days at room temperature.

Manufacturer's cure process specification

- Cure at 180^{o}C for 2 hours

This resin system was not used for the incorporation of carbon nanoparticles and it will be considered again in chapter 8, where the cure kinetics modelling and the glass transition temperature development are analysed.

3.1.4 Premix of EPON 828 and EPON 1009F resins containing Hyperion multi-walled carbon nanotubes

Nanotubes were predispersed into an EPON 828/1009 F resin system, supplied by Hyperion Catalysis International. EPON 828 is a DGEBA based resin system, while EPON 1009F is a high molecular weight solid epoxy resin derived from a liquid epoxy resin and bisphenol-A. The chemical name of the mixture is Phenol,4-4'-(1-methylethylidene)bis-, polymer with 2,2'[(2-methylethylidene)bis(4,1-phenyleneoxymethylene)]bis[oxirane] (batch number CP1204). The structural formula of the base resin (EPON 1009F) is depicted in figure 3.3.

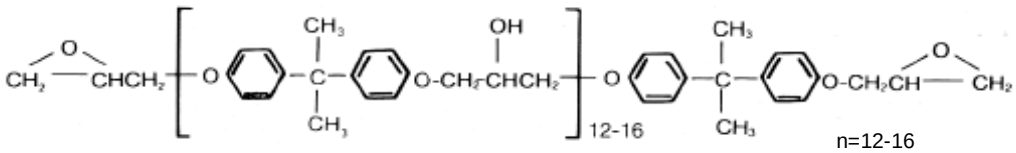

Figure 3.3: Schematic of the structural formula of EPON 1009F resin system [109]

The premix contained 3.06 wt % multi-walled carbon nanotubes predispersed in 79.7 wt % of EPON 828 and 17.3 wt % of EPON 1009F

resins. The mixture is black and odourless and has a density of 1.19 – 1.25 g/cm^3 in the uncured state [110]. It has a decomposition temperature of 300^{o}C.

3.1.5 Thomas Swan multi-walled carbon nanotubes (CNTs)

Multi-walled carbon nanotubes under the trade name ELICARB (product reference: SP7269, batch reference: K1005) were supplied by Thomas Swan Ltd. These are high-purity multi-wall carbon nanotubes delivered as a dry powder [111].

3.1.6 Monarch carbon black particles (CB)

Carbon black particles, under the code name Monarch 570, were supplied by Cabot. They were received in the form of a black powder. They are insoluble in water and have a density of 1.7 – 1.9 g/cm^3 at 20^{o}C [112].

3.2 Mixing Techniques

In this section, the mixing techniques of the carbon nanoparticle incorporation into the epoxy resin systems are described.

3.2.1 Shear mixing

A DISPERMAT® CN F2 model shear mixer was used to disperse the carbon nanoparticles in the liquid epoxy system. The compact drive unit contains a three phase motor and separately driven low noise ventilation. The central clamping system – part of the safety device – offers a safe and simple way of holding the dispersion container securely in position. The container is placed on the laboratory bench between the clamping arms and is automatically centered as the arms are tightened. The control panel has a digital display which allows the operator to switch between values for speed, torque or time. The safety device functions are also indicated on the digital display (see figure 3.4).

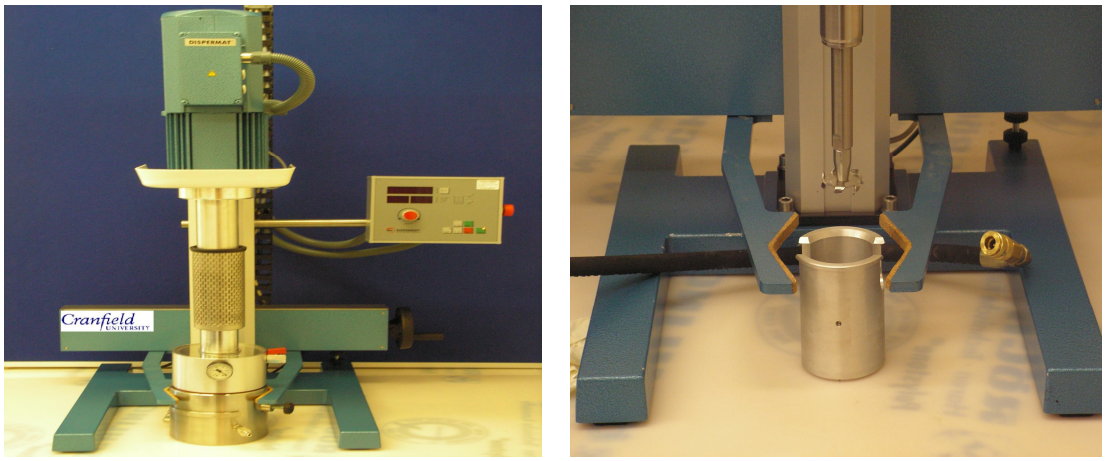

Figure 3.4: DISPERMAT® CN F2 high shear mixer used to disperse the Hyperion multi-walled carbon nanotubes and carbon black particles

The shear mixing process depends on the distance of the shear propeller from the surface of the liquid batch. The propeller is usually placed at a distance of almost 2/3 of the total height of the filled resin from the bottom of the batch. This specification allows for a better mixing and an even distribution of the carbon nanoparticles in the epoxy system. The mixing process takes

place with the incorporation of carbon nanoparticles in the resin, and then the addition of the curing agent.

The high shear mixer was utilised for the incorporation of Hyperion multi-walled carbon nanotubes and carbon black particles into the MY 750 / HY 5922 resin system.

3.2.2 Ultrasonic bath

An Elmasonic S 30 H series ultrasonic bath was used to disperse the Thomas Swan multi-walled carbon nanotubes and carbon black particles respectively in the MTM 44-1 resin system (figure 3.5). The bath is usually filled with distilled water up to 2/3 of its tank height. It can work in a broad range of temperatures and for unlimited periods of time. For the specific use the carbon nanoparticles were dispersed in a solvent (ethanol for the carbon nanotubes and distilled water in the case of carbon black) and sealed in a plastic container. The container was clamped at the surface of the water filled tank. The ultrasonication process lasted for one hour and was carried out at an elevated temperature. When the ultrasonication treatment finished, the container was removed from the bath and the tank was emptied.

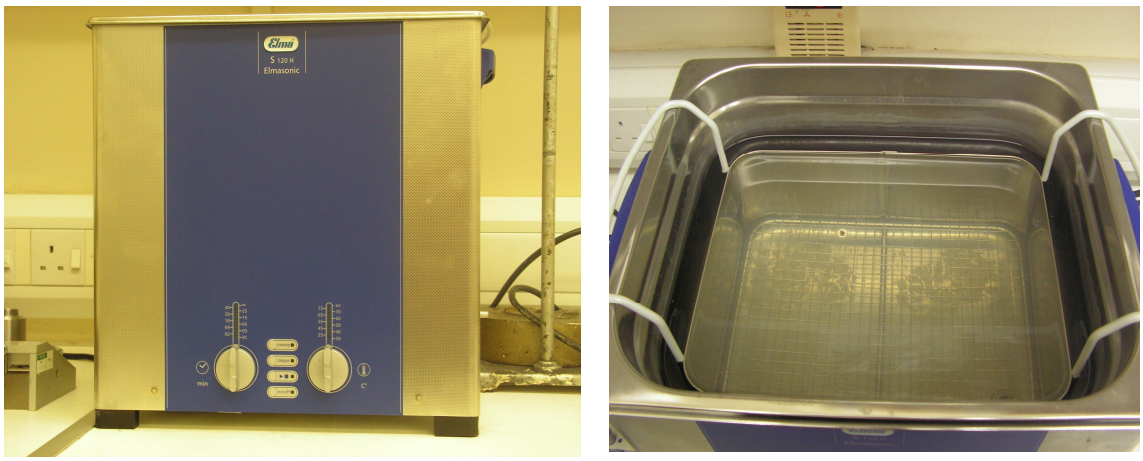

Figure 3.5: Elmasonic S 30 H series ultrasonic bath used to disperse the Thomas-Swan carbon nanotubes and carbon black particles

3.2.3 Ultrasonic horn

A Branson S-450D homogeniser, which consists of a disruptor horn and a digital power supply, was also used to achieve a good dispersion of the carbon nanotubes in the epoxy matrices (see figure 3.6). The ultrasonic probe transmits ultrasonic energy into the system. The dimensions of the horn and the output control determine the amplitude (tip movement) and degree of ultrasonic activity in the mixture. Generally, the smaller the tip diameter, the higher the amplitude is. The converter, which is part of the probe receives the electrical energy from the power supply and converts it to a 20 kHz mechanical vibration. The amplitude range may vary up to 240 Watt. The horn is inserted into the system tested. Locally, high temperatures may be reached. Predetermined values of the amplitude, temperature and total energy are required. These values should be sufficient to break the carbon nanotube clusters and not allow for re-aggregation, but at the same time protect the resin system from premature curing or decomposition.

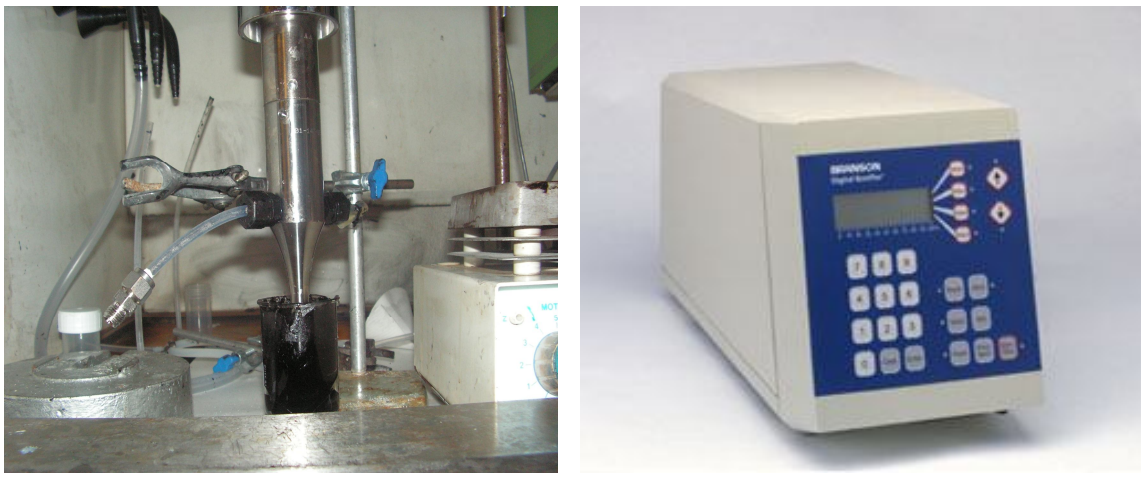

a) disruptor horn b) digital power supply

Figure 3.6: Branson S-450D homogeniser used for the ultrasonication treatment of the resin systems incorporating carbon nanotubes

This system was used for the MY 750 / HY 5922 and the MTM 44-1 resin systems to disperse the carbon nanotubes.

3.2.4 Mixing by hand

In some cases (especially with the MTM 44-1 resin system), due to the very viscous nature of the material**,** premixing by hand was necessary. This occurred when the carbon nanoparticles were to be incorporated in the system, before the ultrasonication treatment with the ultrasonic homogeniser or after the utilisation of the ultrasonic bath. The utilisation of the shear mixer or an electrical stirrer with such a viscous material was not possible in these cases at any temperatures below the onset of chemical reaction.

3.3 Carbon Nanocomposite Preparation Techniques

In this section, a brief analysis of the preparation processes used to disperse the carbon nanoparticles into the epoxy resin systems is given. These processes are a combination of the mixing techniques described in previous paragraphs. Different concentrations of carbon nanoparticles were incorporated into the resin systems. A summary of the sample compositions tested and the mixing techniques utilised is presented in table 3.1. The details of the sample preparation are analysed in the following paragraphs.

	Sample composition (wt %)			Mixing technique			
Batch / Epoxy system	Hyperion CNTs	Thomas Swan CNTs	Monarch CB	Shear mixing	Ultrasonic bath	Ultrasonic horn	Mixing by hand
1) MY 750-HY 5922	0.06	-	-	X	-	-	-
2) MY 750-HY 5922	0.12	-	-	X	-	-	-
3) MY 750-HY 5922	-	-	0.5	X	-	-	-
4) MY 750-HY 5922	-	-	1	X	-	-	-
5) MY 750-HY 5922	0.06	-	-	-	-	X	X
6) MTM 44-1	-	1	-	-	X	-	X
7) MTM 44-1	-	2	-	-	X	-	X
8) MTM 44-1	-	-	1	-	X	-	X
9) MTM 44-1	-	-	2	-	X	-	X
10) MTM 44-1	-	1	-	-	X	X	X

Table 3.1: Polymer-based carbon nanoparticle systems, sample compositions and the corresponding dispersion methods used

3.3.1 Mixing procedure of MY 750 / HY 5922 epoxy resin containing Hyperion carbon nanotubes (premix) and Monarch carbon black particles (batches 1-4)

The details of the dispersion process of the first four batches of the MY 750 / HY 5922 resin system (see table 3.1) that contain carbon nanotubes and carbon black, with the utilisation of shear mixing are as follows:

1) The MY 750 resin was heated in the oven at 70^{o}C for 20 minutes so that the viscosity decreased to a minimum.
2) The Hyperion carbon nanotube premix (similarly for the carbon black particles) was dispersed into the MY 750 resin, using the shear mixer (see figure 3.4) at 5000 rpm for 15 minutes. Then the amine hardener (HY 5922) was added at the ratio of 100 / 55. The whole mixing process lasted for a further 15 minutes and was stopped before any reaction would take place. Four different batches were prepared, containing 0.06 and 0.12 wt % of carbon nanotubes respectively (1 and 2 wt % concentration for carbon black). The batches were sealed in plastic containers and stored in the freezer at -18^{o}C for future use and testing.

3.3.2 Mixing procedure of MY 750 / HY 5922 epoxy resin containing Hyperion carbon nanotubes (premix) (batch 5)

The Hyperion carbon nanotube premix was mixed with the MY 750 / HY 5922 resin system by hand and further ultrasonication treatment (utilisation of ultrasonic horn). The difference in this procedure (compared to the one mentioned in paragraph 3.3.1) is that the additional step of the ultrasonication treatment was incorporated.

1) The MY 750 resin was heated in the oven at 70^{o}C for 20 minutes so that the viscosity decreased to a minimum.
2) The Hyperion premix was dispersed into the liquid resin. At first an initial mixing by hand was utilised. Then the product was put under the ultrasonic horn (see figure 3.6) to be sonicated for a total time of 10

minutes. The tip of the horn was set in contact with the surface of the resin and at the same time a magnetic stirrer was used in the bulk of the resin. The temperature range used was in the region of 50 to 70^{o}C, controlled by a hot plate. The ultrasonic pulses were introduced when the temperature of the resin system had dropped down to 50^{o}C. The ultrasonic pulses aimed to break the clusters of carbon nanotubes, but at the same time not let the carbon nanotubes re-aggregate. The production of the pulses causes a local heating of the resin. The maximum temperature was allowed to raise up to 70^{o}C. At that point the instrument stopped producing pulses, until the temperature dropped down to 50^{o}C again. The total time for the ultrasonication process lasted for 20 minutes with the time intervals (10 minutes of total ultrasonication). The time intervals and the power used were controlled from a Branson Digital Sonifier controller, depicted in figure 4.6b. The amplitude used was 100 % and the energy produced by the power supply was 34.6 kJ (peak power of 286 Watts measured).

3) After the ultrasonication treatment, the resin was allowed to cool to room temperature and then the amine hardener (HY 5922) was added at the ratio of 100 / 55. The batch was stirred by hand for a further of 20 minutes. Mixing by hand was chosen so that no curing would take place. One batch was prepared, containing 0.06 wt % of carbon nanotubes. The batch was sealed in a plastic container and stored in the freezer at -18 ^{o}C for future use and testing.

3.3.3 Mixing procedure of MTM 44-1 one part resin containing Thomas Swan carbon nanotubes and the Monarch carbon black particles (batches 6-9)

The MTM 44-1 resin system is a very viscous resin, due to the incorporation of a thermoplastic. In this case the utilisation of the shear mixer was not considered. The mixing was based on the utilisation of the ultrasonic bath (see figure 3.5) and stirring by hand, for the incorporation of carbon nanotubes and carbon black into the epoxy system.

1) Initially the carbon nanotubes were dispersed in ethanol (distilled water in the case of carbon black) in a plastic container. The container was sealed. The ultrasonic bath was filled up to 2/3 of the tank height with distilled water. Then the container was clamped at the surface of the water contained in the tank. The temperature was set to 60^{o}C and the total ultrasonication time was 60 minutes. After the ultrasonication treatment the container was opened and was placed in an oven at 80^{o}C for 20 minutes to evaporate ethanol (100^{o}C for 30 minutes in the case of carbon black). A carbon nanoparticle 'cake' was then produced.
2) Before any further action, the resin was heated on a hot plate at 80^{o}C for 10 minutes so that the viscosity decreased to a minimum. At that temperature no curing reaction was induced. Then the nanoparticle 'cake' was added and mixed by hand for a further 15 minutes. Four batches were prepared. The first one contained 1 wt % of carbon nanotubes and the second 2 wt % concentration (same concentration for the carbon black). The batches were sealed in plastic containers and stored in the freezer at -18 ^{o}C for future use and testing.

3.3.4 Mixing procedure of MTM 44-1 one part resin containing the Thomas Swan carbon nanotubes (batch 10)

This mixing process is similar to the one discussed in the previous paragraph. However in this process an extra step is added, that of the utilisation of the ultrasonic horn (see figure 3.6). After producing a batch that contained 1 wt % of carbon nanotubes by following the steps of the aforementioned process, the batch was tested under the ultrasonic horn. The tip of the horn was set in contact with the surface of the resin. In this case no hot plate, neither a stirrer was used. The temperature range used was 50 to 70^{o}C and was fully controlled from the power supply. The ultrasonic pulses were directed straight to the carbon nanotubes and the surface of the resin. The pulses provoked a local heating on the resin. The maximum temperature was allowed to raise up to 70^{o}C. At that point the instrument stopped producing pulses, until the temperature dropped down to 50^{o}C again. The

total time for the ultrasonication process lasted for 10 minutes with the time intervals (5 minutes of total ultrasonication). The batch produced was allowed to cool down to room temperature, it was sealed and stored at -18 ^{o}C for future use and testing.

3.4 Experimental Techniques for Cure Monitoring

In this section the experimental techniques utilised in this study are discussed. The first ones are Differential Scanning Calorimetry (DSC) and Rheometry, together with the utilisation of optical fibres as an online cure monitoring technique.

3.4.1 Differential Scanning Calorimetry (DSC)

DSC measures the amount of energy absorbed or released by a sample when it is heated or cooled, providing quantitative and qualitative data on endothermic (heat absorption) and exothermic (heat evolution) processes. The utilisation of DSC enables to:

a) measure the exothermic energy of polymer cure (as in epoxies), which allows to determine the degree of cure
b) measure glass transition temperatures and
c) determine melting points in polymers and the energy associated with the transition.

A typical DSC apparatus is shown in figure 3.7.

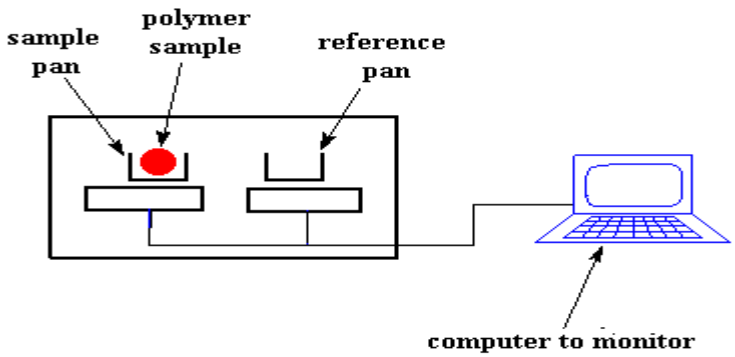

Figure 3.7: Schematic representation of a typical DSC cell [113]

The calorimeter consists of a sample holder and a reference. Under each holder there is a temperature sensor. The reference sample should have a well-defined heat capacity over the range of temperatures to be scanned. The

basic principle underlying this technique is that, when the sample undergoes a physical transformation more (or less) heat will need to flow to it than the reference to maintain both at the same temperature. Observation of the difference in heat flow between the sample and reference, the amount of heat absorbed or released during such transitions is measured. A flow of nitrogen gas is maintained over the samples to create a reproducible and dry atmosphere. The sample is sealed into small aluminium pans.

3.4.1.1 Theory of DSC

Differential Scanning Calorimetry is used to estimate the heat flow signal, between the sample and a reference, which is usually an empty pan. This signal can be expressed by the following equation:

$$\frac{dH}{dt} = C_R \frac{d\Delta T}{dt} + (C_S - C_R)\frac{dT_S}{dt} + \frac{dQ}{dt} \qquad (3.1)$$

where C_S is the sample heat capacity, C_R is the reference heat capacity and Q is the heat, emitted by the sample. When conventional DSC is utilised, the temperature program applied is an expression of the form:

$$T_S = T_o + \beta T \qquad (3.2)$$

where T_o is the initial temperature in the DSC cell, T_s is the sample temperature and β is the heating rate. Usually an empty pan is used as a reference. When such a case occurs, the combination of equations 3.1 and 3.2 yields the following expression:

$$\frac{dH}{dt} = C_R \frac{d\Delta T}{dt} + C_S \beta + \frac{dQ}{dt} \qquad (3.3)$$

From the general equation 3.3, it follows that the resultant heat flow is composed of three components [114]: the signal of the instrument itself $Cd\Delta T/dt$, the signal of the heat capacity of the sample $C_s\beta$, and the signal corresponding to the transformations of the sample.

In order to extract the necessary information about the chemical cure kinetics from the DSC signal, two assumptions have to be valid:

1) A baseline to the raw heat flux signal of the DSC has to be defined as a function of time and
2) The reaction rate of the reaction undergone has to be proportional to the heat flow signal.

The role of the baseline is to define the area below the DSC signal, so that by integrating this area, the ΔH_{total} may be calculated under dynamic and isothermal curing conditions. The second assumption correlates the estimated heat with the degree of the curing reaction.

An evolution of conventional DSC is Temperature Modulated Differential Scanning Calorimetry (TMDSC), which overcomes these limitations and therefore provides a new insight into the material properties. In this case a sinusoidal perturbation on the dynamic heating conditions, which are used in standard DSC experiments, is superimposed [115]. The resulting modulated signal is expressed by equation 3.4.

$$T_S = T_o + \beta T + A_T \sin(\omega_T t) \qquad (3.4)$$

where A_T is the amplitude and ω_T is the angular frequency. The advantage of TMDSC is the capability to use the modulation in order to calculate the heat capacity of the sample as a function of temperature or time. It has been used in many cases [115,116] to measure the glass transition temperatures of epoxy systems, however, some complications may arise. These complications are caused by the speed of the curing reactions and the resulting exotherms which in many cases violate the main requirement of its use, which is a steady state material throughout a single measurement.

3.4.1.2 TA Instruments 2920 TMDSC

Experiments were conducted on a TA Instruments TMDSC 2920 apparatus which was fitted with a cooling unit, to achieve measurements in sub-ambient temperatures. The specific DSC cell comprises of a constantan disk enclosed in a silver block. The constantan disc constitutes the platform where the sample and the reference are placed, being inside special pans supplied by the manufacturer. Two symmetric raised positions on the surface of the constantan disc designate the exact place for the sample and the reference pan. Thermocouples are placed in these positions which are connected in series to monitor the temperature difference between the sample and the reference. The temperature inside the cell is controlled by a heating element encased in the surrounding metal block.

Nitrogen purge gas is used to avoid any oxidation of the samples during the experiments. The nitrogen flow rate is 30 cm^3 / min. Further temperature control is achieved in the specific DSC by the use of an external attached refrigerated cooling system, RCS, based on the supply of nitrogen gas around the cell.

Instrument calibration was performed before the beginning of any set of experiments. This procedure included calibration for:

1) the measured temperature
2) the estimated heat flow and
3) the instrument baseline.

The temperature and the heat flow calibration are achieved simultaneously by measuring the characteristic temperature and the enthalpy associated with a phase transition of a standard reference material. High-purity indium was used as a reference material with its melting point being the phase transition of interest. Indium was exposed to a constant heating rate of 5^oC/min. The melting temperature or enthalpy was compared with the actual values for indium and a temperature offset and heat flow calibration was calculated and

stored in the instrument for use in subsequent experiments. The instrument baseline calibration was performed by imposing the temperature profile of the actual experiment on the cell without placing any pans inside.

3.4.2 Rheometry

In addition to the DSC tests conducted, rheological measurements were made to detect the approximate gelation time. These tests were conducted on a Bohlin Instruments rheometer, model CVO, system which was used in the oscillation mode. The geometry used was a 40 mm parallel plate system with the bottom plate fixed and the top plate oscillating at a fixed frequency. The measurements were made by controlling the applied stress, so that the corresponding strain never exceeded predetermined limits. Prior to each experiment, frequency and stress sweeps were made, in order to determine the appropriate frequency and stress ranges.

All experiments were conducted under isothermal curing conditions in the temperature range of 80-200^{o}C. After preheating the plates at the desired temperature, the sample was placed on the lower plate, while the upper plate was lowered to make contact with the resin. The test was stopped when the viscosity had exceeded the value of 15-20 kPas.

3.4.3 In-situ cure monitoring using optical techniques

Cure monitoring is performed by measuring some physical quantity, which corresponds directly or indirectly to the material state. In the case of optical methods, a characteristic of the material tested is required so that the cure reaction may be studied. This characteristic can be the absorption of radiation by the molecular groups or the change in the refractive index. The change in the refractive index can be monitored by optical fibres, which are embedded in the system tested. Here, a brief discussion about the basic principle of their utilisation as a cure monitoring technique is given.

3.4.3.1 Cure monitoring using optical techniques

Significant amount of research has been conducted on developing on-line cure monitoring techniques. The problem of real-time determination of the state of cure of composite materials, particularly large structures being cured in autoclaves, is of considerable importance in industry. One of the most promising methods is the use of optical fibre-based sensor systems. The past few years Fibre Bragg Grating (FBG) Sensors (fibres with intra-core gratings) have been used extensively in research, because they are very well suited for measuring temperature and strain variations. Significant information is directly related to the absolute wavelength change [117,118]. During the cure process, the refractive index of epoxy resin systems varies in the region of 1.48-1.60, mainly due to the increase in density. By monitoring the change in the refractive index during cure, it is possible to measure the conversion during cure.

A Fibre Bragg Grating sensor's regulation is based on the formation of a modulation of the core of an optical fibre. The refractive index modulation forms a volume hologram that reflects a narrow band of optical wavelengths back along the optical fibre. The wavelength reflected (λ_β) by the FBG depends on the refractive index of the fibre for the guided mode (n_{eff}) and the periodicity of the refractive index modulation (Λ) of the FBG as follows:

$$\lambda_B = 2n_{eff}\Lambda \qquad (3.5)$$

Monitoring shifts in the Bragg wavelength corresponds to monitoring changes in the period of the FBG. Strain and temperature effects on the FBG will alter the period, hence its use as a strain and temperature sensor. A schematic diagram of an FBG sensor and the simplified spectrum is depicted in figures 3.8 and 3.9.

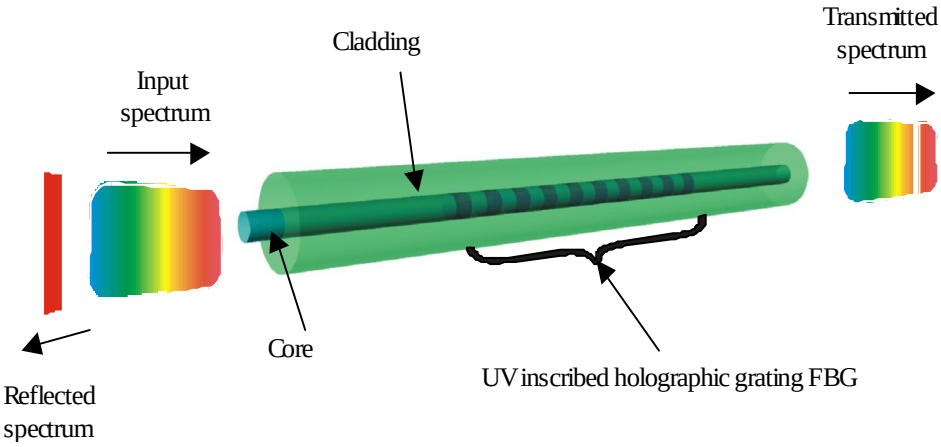

Figure 3.8: Schematic diagram of Fibre Bragg Grating sensor [119]

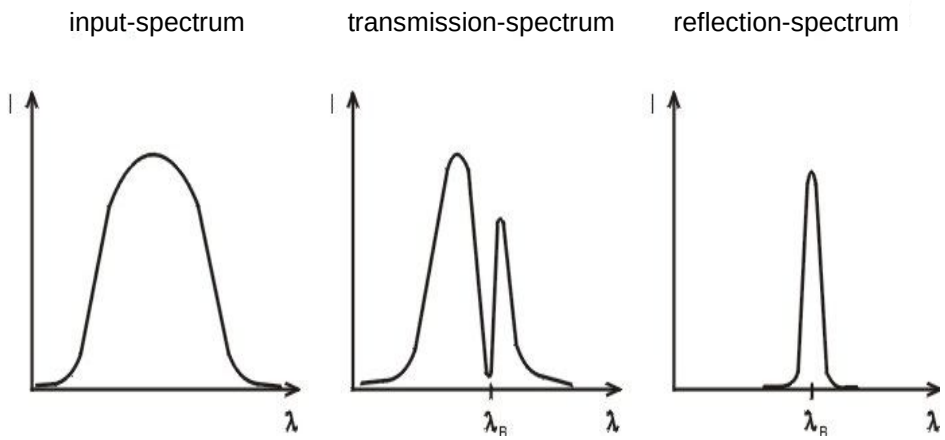

Figure 3.9: Simplified spectrum acquired by the use of FBGs [119]

Here, a brief description of the basic principles of the optical fibres (FBG sensors in particular) was given. The incorporation of optical fibres into the resin systems and their nanocomposites is going to be discussed in chapter 9, where the Fresnel technique is utilised.

3.5 Microstructural characterisation techniques

3.5.1 Transmission Electron Microscopy (TEM)

A Philips CM20 STEM electron microscope was used in bright field mode to analyse microtomed sections of material under analysis. An accelerating voltage of 120kV was used and the TEM was fitted with a LaB6 filament (condensor aperture 200 µm and objective aperture 100 µm). TEM photographs were obtained on 3¼ x 4 inch microscope film using nominal exposure time of 4 seconds.

Transmission electron microscopy (TEM) requires very thin specimens for analysis, generally 60 to 100 nm in thickness. Such specimens are cut from a bulk sample using a diamond knife mounted in an ultramicrotome. A typical procedure is as follows:

A rectangular block sample measuring approximately 3 mm x 3 mm x 8 mm is taken from the bulk specimen and mounted in the ultramicrotome (Reichert-Jung Ultracut E ultramicrotome). The initial preparation to produce the correct geometry from which to take an ultra-thin section is carried out using a glass knife to produce a pyramid at the end of the mounted block (figure 3.10a). A cutting angle of 30° is used for the microtome knife. The glass knife is then replaced with a diamond knife (Diatome diamond knife, cryo 45°, 3 mm with boat) and the boat of the diamond knife is filled with water. The top of the pyramid section of the specimen is removed with the diamond knife to give a surface approximately 0.2 mm x 0.2 mm. Then the ultramicrotome is used in automatic mode to finally take sections nominally 80 nm thick from the prepared specimen. Sections cut are manipulated on the surface of the water in the boat attached to the knife and removed on a copper support grid (300 thin bar, copper 3.05 mm grid). All specimens analysed to date were microtomed at room temperature.

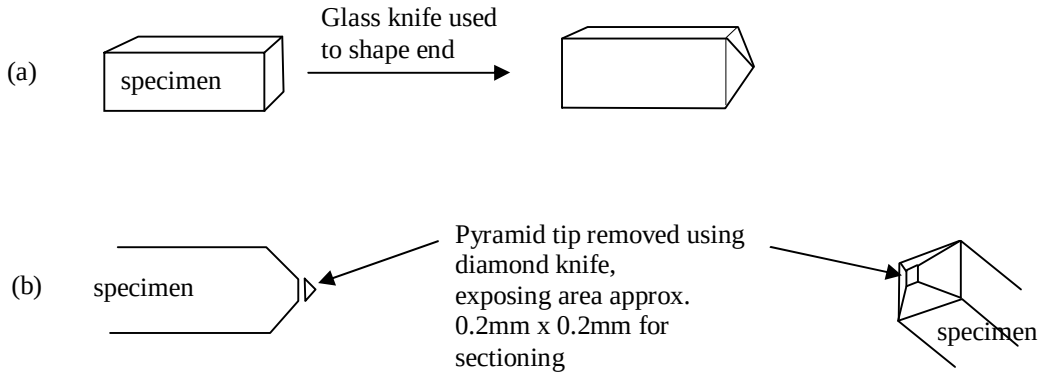

Figure 3.10: Schematic showing specimen preparation prior to taking ultra-thin sections for TEM analysis: a) glass knife used to shape end of specimen block and b) diamond knife used to remove tip of pyramid on end of specimen block, leaving an area approximately 0.2 mm x 0.2 mm for microtoming

3.5.2 Scanning Electron Microscopy (SEM)

Detailed examination of surface nanostructures was carried out with a high resolution Philips FEI XL30 SFEG analytical SEM. This scanning electron microscope is capable of producing high-resolution images of a sample surface. SEM images have a characteristic three-dimensional appearance and are useful for judging the surface structure of the sample. The spatial resolution of the SEM depends on the size of the electron spot which in turn depends on the magnetic electron-optical system which produces the scanning beam. The resolution is also limited by the size of the interaction volume, or the extent to which the material interacts with the electron beam. The SEM has compensating advantages, including the ability to image a comparatively large area of the specimen; the ability to image bulk materials and the variety of analytical modes available for measuring the composition and nature of the specimen.

Scanning electron microscopy images of the fracture surface requires specimens with typical dimensions of 2 cm x 1 cm x 1 cm. Such specimens are prepared by curing in an oven, covered by an aluminium foil layer. After curing the layer is taken out. The sample is put in liquid nitrogen (at -180^{o}C) and notched. Then it is hit. The fractured specimen is then coated in order to

obtain a conductive surface. Carbon is a very cheap coating material, but in most cases gold or gold-palladium is preferred. Both coatings are usually applied at a thickness of 20-30 nm, which is too thin to interfere with dimensions of surface features.

Chapter 4

4. Microstructural Characterisation of the Carbon Nanoparticle Addition to the Epoxy Resin Systems

In this chapter, the state of the dispersion of carbon nanotubes and carbon black particles into the epoxy systems was studied with the utilisation of Transmission Electron Microscopy (TEM) and Scanning Electron Microscopy (SEM). The TEM and SEM images acquired are analysed in order to evaluate the state of dispersion of the incorporated carbon nanoparticles.

4.1 Microstructural characterisation of the addition of carbon nanoparticles into the MY 750 / HY 5922 resin system

Transmission Electron Microscopy (TEM) was utilised to characterise the surface of the epoxy system when carbon nanoparticles were added. Two different concentrations were used: 0.06 and 0.12 wt % for the Hyperion carbon nanotubes (batches 1,2 and 5) and 0.5 and 1 wt % for the Monarch carbon black particles (batches 3 and 4). The samples were cured in the oven at 120^{o}C for 2 hours. Under these conditions the curing of the samples was considered complete. Figure 4.1 shows the dispersion of carbon nanotubes achieved by shear mixing (batches 1 and 2). In figure 4.1a there are some agglomerates, but it can be seen that there are some nanoparticles which have not formed clusters. In figure 4.1b, where the double concentration was used, the state of dispersion does not show significant differences, except for the fact that the size of the cluster seems to be higher (compared with the lower concentration used). However, in figure 4.2 it is observed that the process based on mixing by hand and the utilisation of the ultrasonic homogeniser for the 0.06 wt % concentration of carbon nanotubes led to a good dispersion (batch 5). Individual carbon nanotubes may be observed.

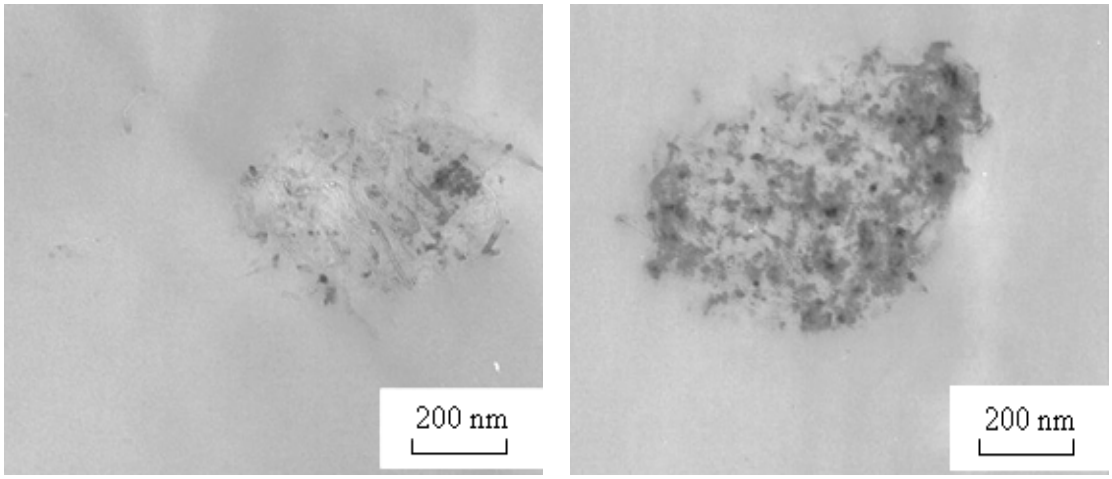

a) b)

Figure 4.1: TEM images of a) 0.06 % and b) 0.12 wt % of Hyperion carbon nanotubes dispersed into the MY 750 / HY 5922 resin system (batches 1 and 2)

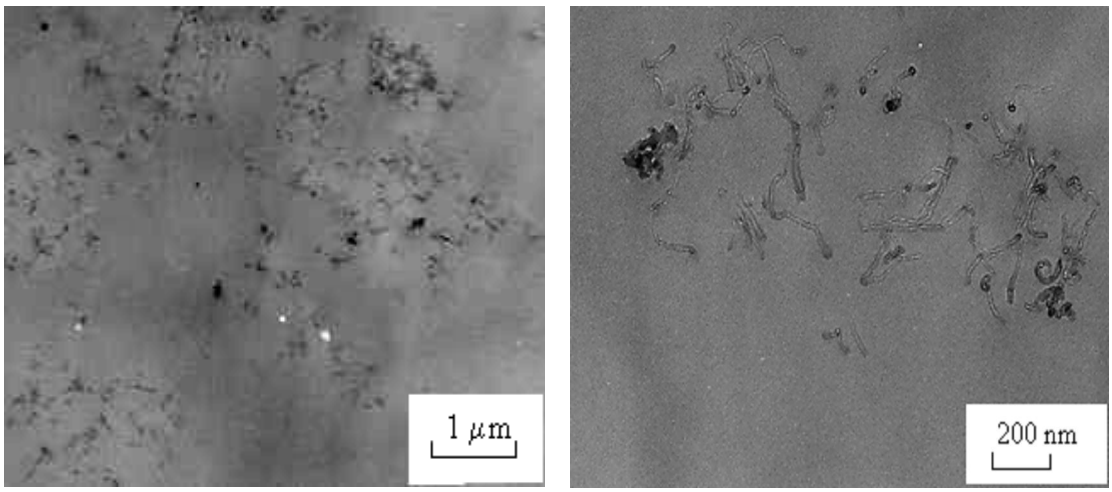

a) b)

Figure 4.2: TEM images of 0.06 wt % of Hyperion carbon nanotubes dispersed into the MY 750 / HY 5922 resin system a) low magnification and b) high magnification (batch 5)

Figure 4.3 depicts the dispersion of the 0.5 and 1 wt % concentration of carbon black particles (batches 3 and 4). CB tend to agglomerate, especially when the concentration increases. This becomes obvious when figure 4.3a is compared with figure 4.3b. Carbon black particles are spheres that have a lower surface / volume ratio which means that they are easier than carbon nanotubes to disperse. Carbon nanotubes due to Van der Waals forces and the higher surface / volume ratio tend to agglomerate more easily. This is

easily understood by the fact that only 0.06 wt % concentration of carbon nanotubes can be compared with the 1 wt % concentration of carbon black, in terms of the surface / volume ratio. The carbon black state of dispersion is better when compared to the state of dispersion of carbon nanotubes, having used the shear mixing technique in both cases.

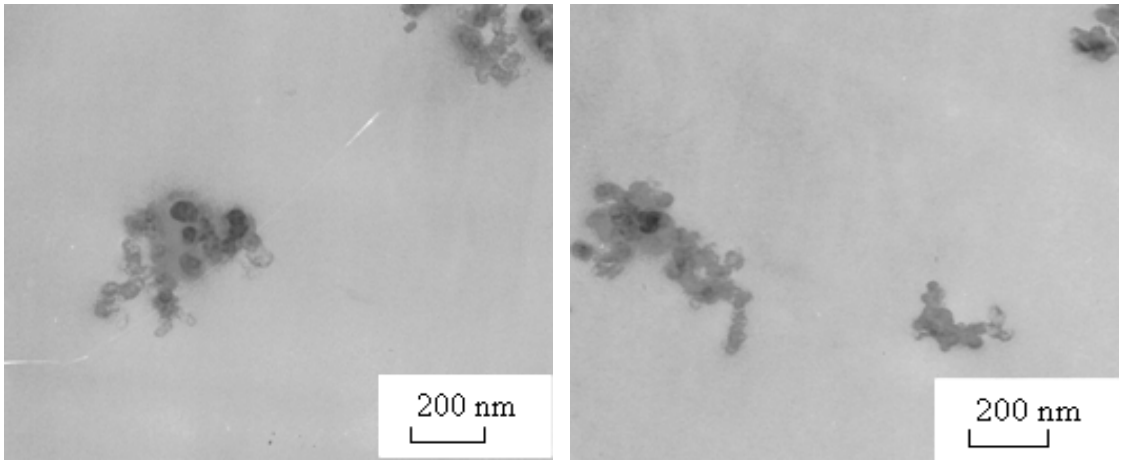

a) b)

Figure 4.3: TEM images of a) 0.5 % and b) 1 wt % of carbon black particles dispersed by into the MY 750 / HY 5922 resin system (batches 3 and 4)

The 0.06 wt % concentration of carbon nanotubes (1 and 5) and the 1 wt % of carbon black particles (batch 3) were used for SEM imaging. The SEM images of the fracture surfaces of the epoxy resin incorporating carbon nanoparticles are illustrated in figures 4.4 to 4.6. Figure 4.4 shows the fracture surface of the epoxy resin system when carbon nanotubes were incorporated (without the ultrasonication treatment utilised). Some clusters of the carbon nanotubes are seen in the 4.4a image and an individual one in figure 4.4b. Some cracks are observed on the surface of the epoxy matrix. These cracks are probably cracks of the coated surface of the samples. The same effect is seen in figures 4.6a and 4.6b, where the carbon black particles were incorporated into the epoxy matrix. The incorporation of carbon nanotubes after the ultrasonication treatment resulted in a very good dispersion (see figure 4.5).

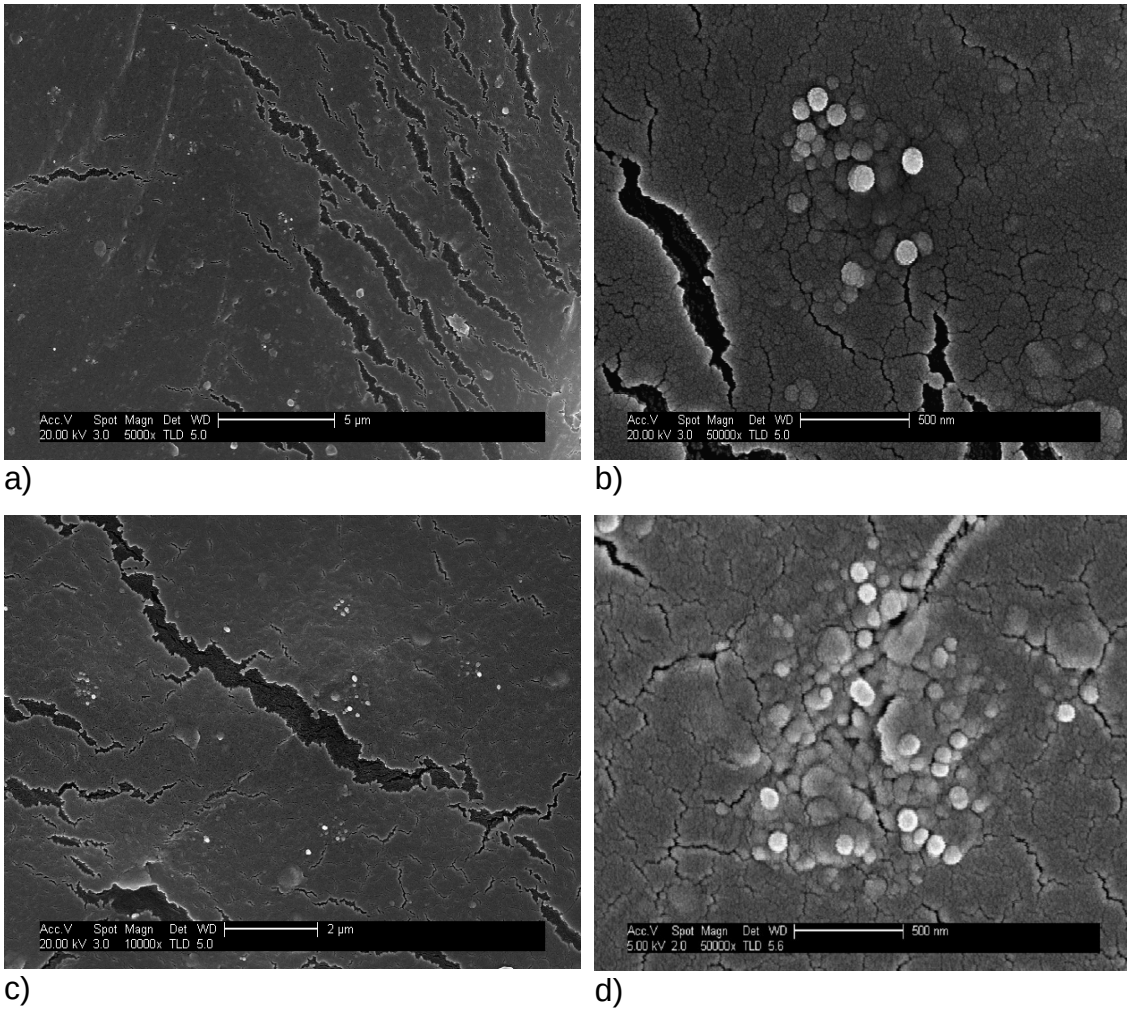

a) b)

c) d)

Figure 4.4: SEM images of the fracture surface of the MY 750 / HY 5922 resin system containing 0.06 (a and b) and 0.12 wt % of Hyperion carbon nanotubes (c and d) (batches 1 and 2)

Here, are presented two different concentrations of carbon nanotubes dispersed in the epoxy, as an indication of the state of dispersion. The 0.06 wt % concentration seems to be better dispersed than the 0.12 wt % one. However, it is seen in figure 4.4a that there are agglomerates dispersed throughout the whole area. The ultrasonication process resulted in small clusters, but also in the separation of carbon nanotubes (individual carbon nanotubes observed, figure 4.5b).

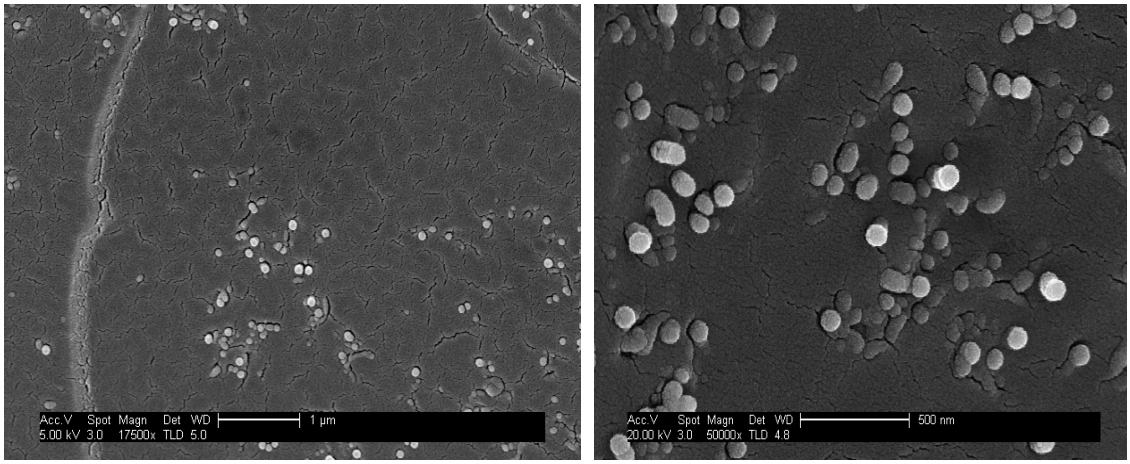

a) b)

Figure 4.5: SEM images of the fracture surface of the MY 750 / HY 5922 resin containing 0.06 wt % of Hyperion carbon nanotubes a) low magnification and b) high magnification (batch 5)

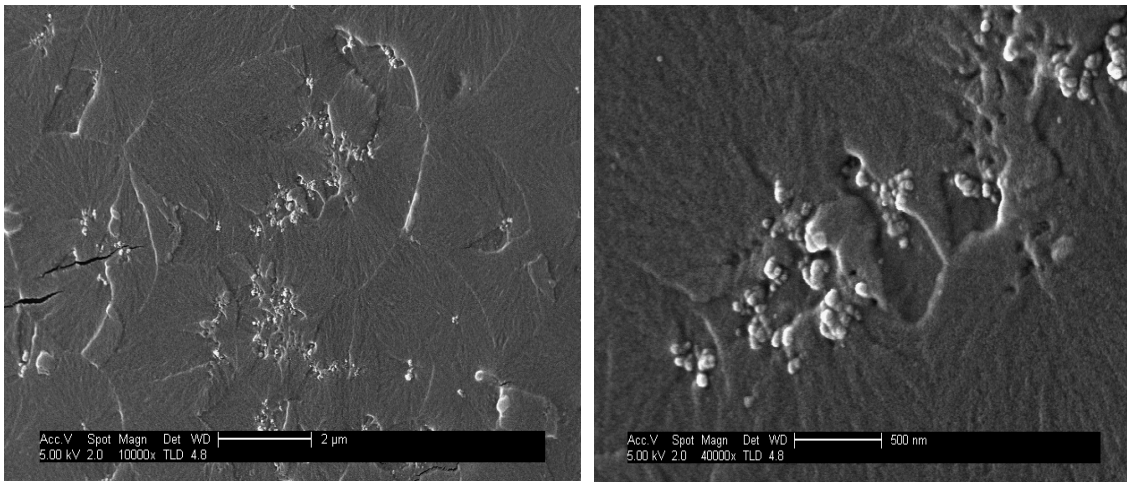

a) b)

Figure 4.6: SEM images of the fracture surface of the MY 750 / HY 5922 resin containing 1 wt % carbon black particles a) low magnification and b) high magnification (batch 4)

These micrographs show that there is an increase in the roughness of the fracture surfaces due to the addition of the carbon nanoparticles. Comparison between figures 4.4 and 4.6 shows that the apparent roughness of the fracture surfaces varies significantly from one nanocomposite to another. This also suggests that this difference depends upon the type of the nanoparticles incorporated. Similar effects were observed in the work of Kinloch and Taylor [120], in which different types of silicates were incorporated in the same epoxy matrix. The apparent roughness of the fracture surfaces examined was found

to be a function of the local concentration of nanoparticles in the epoxy system.

Both of the figures suggest that the nanoparticles were embedded and held to the matrix, and that they were broken instead of being pulled-out. Similar results were reported by Shen et al in the incorporation of multi-walled carbon nanotubes in an epoxy matrix [121].

4.2 Microstructural characterisation of the addition of carbon nanoparticles into the MTM 44-1 resin system

TEM was also utilised to characterise the state of the dispersion of incorporated carbon nanoparticles into the commercial MTM 44-1 system. Two different concentrations were used: 1 and 2 wt % for the Thomas Swan carbon nanotubes (batches 6,7 and 10) and the Monarch carbon black particles (batches 8,9), respectively. The samples were cured in the oven at 190^{o}C for 2 hours. Under these conditions the curing of the samples was considered complete.

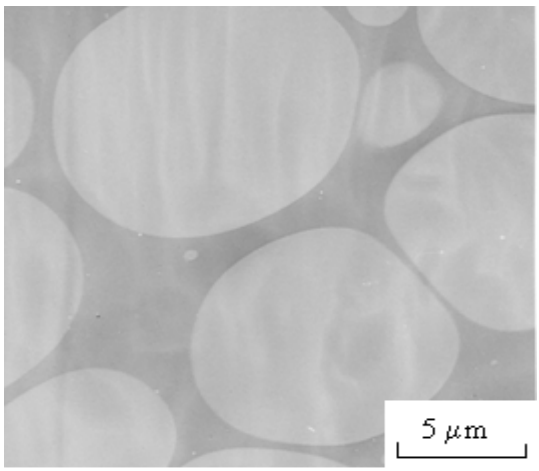

Figure 4.7: TEM image of the fully cured neat MTM 44-1 resin system

Figure 4.7 represents the microstructure of the fully cured neat resin system. This resin system is a toughened epoxy that contains a thermoplastic as the toughening additive. The image shows that the fully cured resin is separated into two regions: a thermoset-rich phase which is shown as the formation of particles that have 3-13 μm diameters and a thermoplastic-rich

phase, which is the continuous phase formed between the epoxy particles (The determination of which phase is which is analysed in the next paragraph-differential etching test). This is a phenomenon, called phase separation, which is common in toughened thermosetting systems. The initial mixture is homogeneous and due to the molar mass increase of the thermoplastic precursor, phase separation occurs at a given conversion [122]. The beginning of phase separation can be determined by Light Transmission (LT), where the cloud point is characterised, Light Scattering (LS), Small Angle X-ray Scattering (SAXS) [58] or Dielectric Spectroscopy [123] and TMDSC [124]. At that point a heterogeneous system forms, which contains the epoxy-rich phase and the thermoplastic-rich phase. However, a small percentage of each of the components may be left in the other phase. In this paragraph the carbon black particles will be presented before the carbon nanotubes, due to the chemical treatment undergone and the results produced.

4.2.1 Microstructural characterisation of the addition of Monarch carbon black particles into the MTM 44-1 resin system (TEM imaging)

Carbon black particles, when incorporated to the initial homogeneous mixture, are evenly dispersed. At the point of phase separation and when thermoset particles start forming in the continuous thermoplastic phase, carbon black seem to prefer the thermoset-rich phase. This localisation effect is illustrated in figures 4.8a and 4.8b. They are formed in clusters in the periphery of the particles. As the curing reaction progresses, the growth of the thermoset-rich phase particles depresses the preferability of CB for this phase and makes them move to the interface. Nevertheless, there are some remaining CB clusters in the thermoset-rich phase, but only a small percentage when compared with the initial concentration at the beginning of the phase separation.

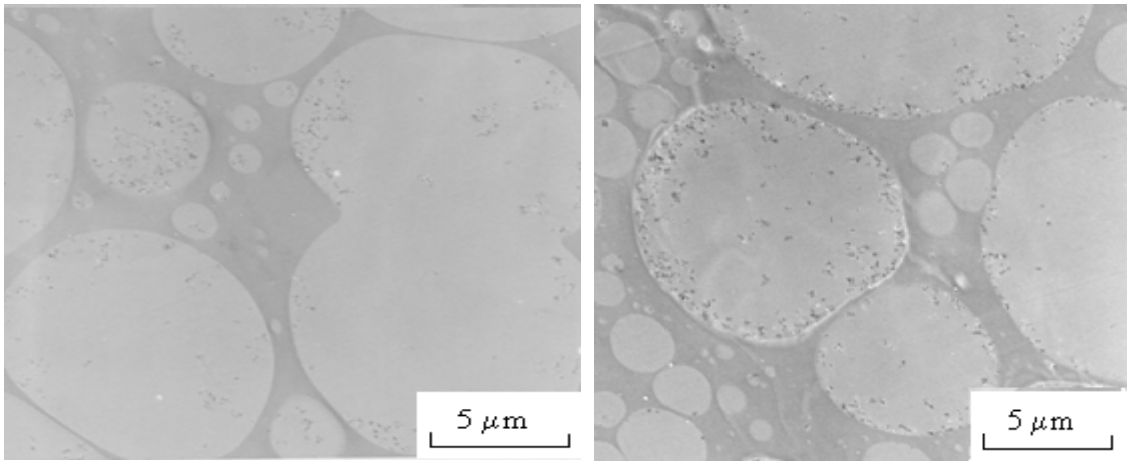

a) b)

Figure 4.8: TEM images of the fully cured MTM 44-1 system containing a) 1 and b) 2 wt % of Monarch carbon black particles (batches 8 and 9)

Figure 4.8a is the image of the nanocomposite containing 1 wt % CB. The carbon black particles are localised at the interface, especially in the bigger thermoset domains. In the smaller domains, there are some residues left in the inner region of the thermoset-rich phase. In figure 4.8b it is easy to observe that most of the carbon black particles prefer the interface. This localisation phenomenon has been studied by some researchers. Gubbels et al [125] incorporated carbon black particles in blends of polyethylene / polystyrene in order to study the electrical properties of the formed nanocomposite. It was observed that during the initial stages of phase separation, the nanoparticles were localised in the polystyrene-rich phase, but later on, at the final stages of the reaction they seemed to prefer the interface of the polyethylene/polystryrene-rich phases. In another study of the same group [126], it was observed that the choice of the processing conditions play a significant role on the 'immobilisation' of the carbon black particles at the polymer interface. When carbon black particles were dispersed in a blend of polystyrene / polyisoprene [127] it was observed that the selective localisation of CB at the interface of the co-continuous polymer blend resulted from the thermodynamics of the polystyrene / polyisoprene / carbon black ternary system. Zaikin et al [128] reported that the redistribution of carbon black particles at the interface of an heterogeneous polymer blend and their partial localisation at this interface take place, when the interfacial tension of the

polymer-polymer system is sufficiently high and in the case when the polymer components of the blend differ significantly in the energies of the absorption interaction with the carbon black surface. Sumita et al [129] also observed that CB particles were localised at the interface of a poly(methyl) methacrylate / polypropylene blend.

Figure 4.9 illustrates the TEM images of the epoxy system when 1 and 2 wt % of carbon black particles was incorporated. These images are a higher magnification of the ones presented in figure 4.8.

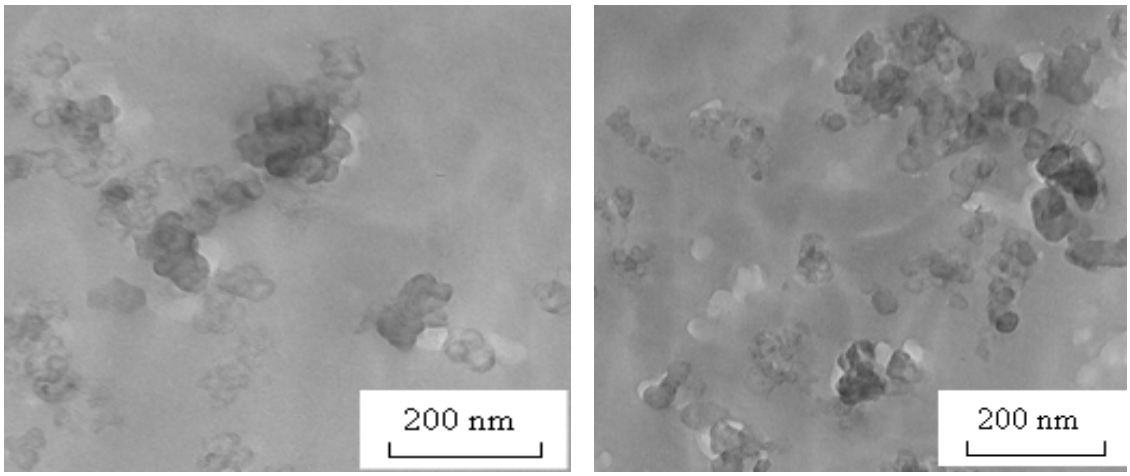

a) b)

Figure 4.9: Magnified TEM images of the fully cured MTM 44-1 resin system containing a) 1 and b) 2 wt % of carbon black particles (batches 8 and 9)

It can be observed in figure 4.9 that the carbon black particles tend to agglomerate. The size of the clusters, when compared with the carbon black particles incorporated in the MY 750 / HY 5922 resin system is smaller. An explanation of this observation is that the ultrasonication treatment (ultilisation of the ultrasonic bath) helps the nanoparticles to disperse evenly in the epoxy matrix. Despite the fact that the dispersion is not excellent, it is still adequate enough to help the interaction of the carbon black particles with the epoxy matrix.

4.2.2 Microstructural characterisation of the addition of Thomas Swan carbon nanotubes into the MTM 44-1 resin system (TEM imaging)

So far the studies were concentrated on the addition of carbon black particles in heterogeneous polymer blends in order to increase the electrical conductivity of the formed products. The selective localisation effect of the addition of Thomas Swan carbon nanotubes in the MTM 44-1 resin is also presented. In this case the carbon nanotubes were dispersed and sonicated in ethanol in the ultrasonic bath, instead of distilled water. Figure 4.10 illustrates the TEM images of the epoxy resin when 1 and 2 wt % of Thomas Swan carbon nanotubes were incorporated after ultrasonication in the ultrasonic bath and mixed by hand.

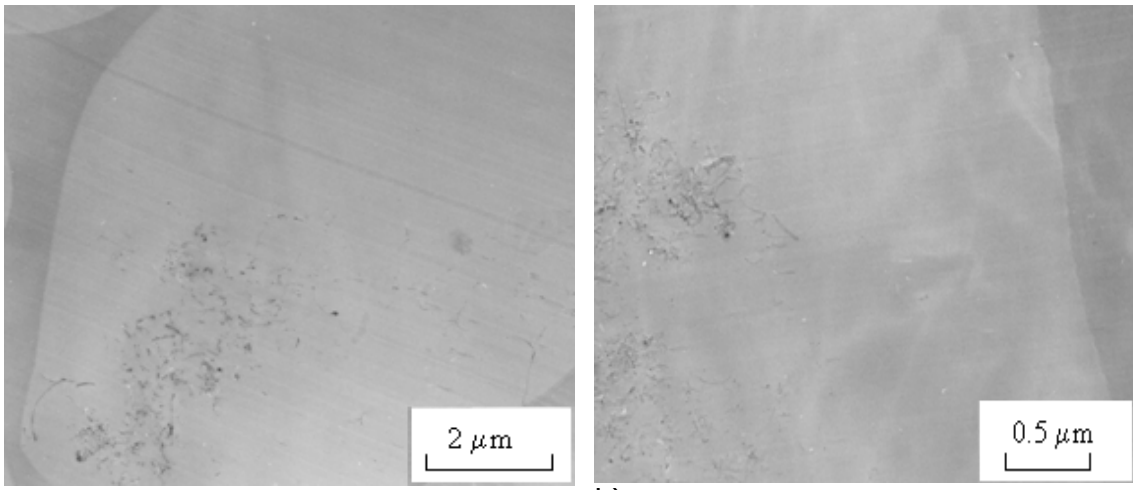

a) b)

Figure 4.10: TEM images of the fully cured MTM 44-1 resin system containing a) 1 and b) 2 wt % of Thomas Swan carbon nanotubes (batches 6 and 7)

The images show that the carbon nanotubes are localised in the thermoset-rich phase and not at the interface. Image 4.10a shows that part of the dispersed carbon nanotubes are accumulated towards the interface, with most of them localised in the thermoset-rich region. In figure 4.10b, where the concentration is higher almost all the nanotubes are localised in the inner region of the thermoset-rich phase. The ultrasonication treatment plays a significant role. As the initial agglomerates of carbon nanotubes are dispersed, they still have a tendency to re-aggregate after the ultrasonication

treatment. This tendency is not as strong as before, though. The results of the treatment are presented in figures 4.11a and 4.11b for the two concentrations of carbon nanotubes used. Although some clusters still exist, the majority of CNTs tend to be isolated from each other.

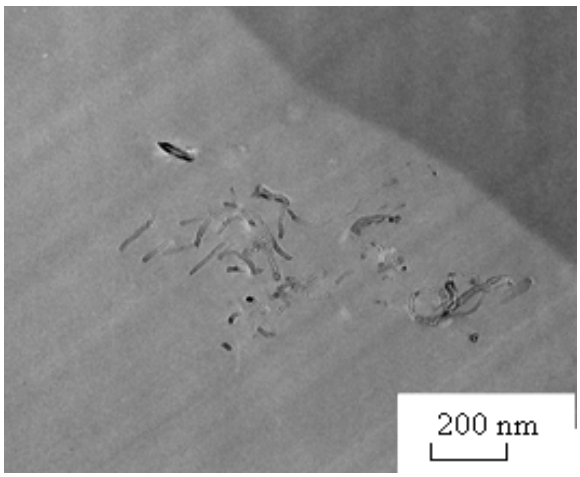

a)

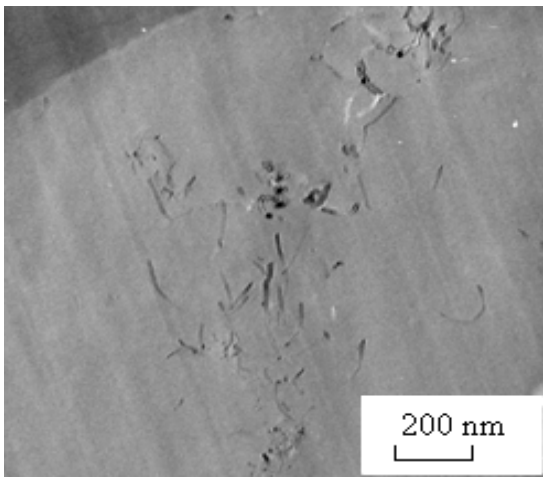

b)

Figure 4.11: Magnified TEM images of the fully cured MTM 44-1 resin system containing a) 1 and b) 2 wt % of Thomas Swan carbon nanotubes (batches 6 and 7)

4.2.3 Microstructural characterisation of the addition of Thomas Swan carbon nanotubes and Monarch carbon black particles into the MTM 44-1 resin system (SEM imaging)

The first step was to test the assumption that the spheres observed in the SEM images are thermoset-rich phase particles, occluded by thermoplastic-rich continuous phase. A cryo-fracture surface of a cured specimen of the neat resin system was etched in methylene chloride for 20 minutes. Methylene chloride was chosen as it is a good solvent for thermoplastics. After this time the specimen was washed with acetone and left to dry at room temperature. For comparison the images of etched and non-etched samples are presented together. Figures 4.12a and b present the non-etched specimens, while figures 4.12c and d show the surfaces after the etching process. The non-etched samples exhibit classical brittle fracture in the occluded phase, cooroborative of the suggestion that this is the thermoset phase. On the etched surfaces, the continuous phase has been swollen rather

than dissolved in the methylene chloride, which makes it difficult to estimate the volume fraction of the solvent-susceptible (thermoplastic) phase present.

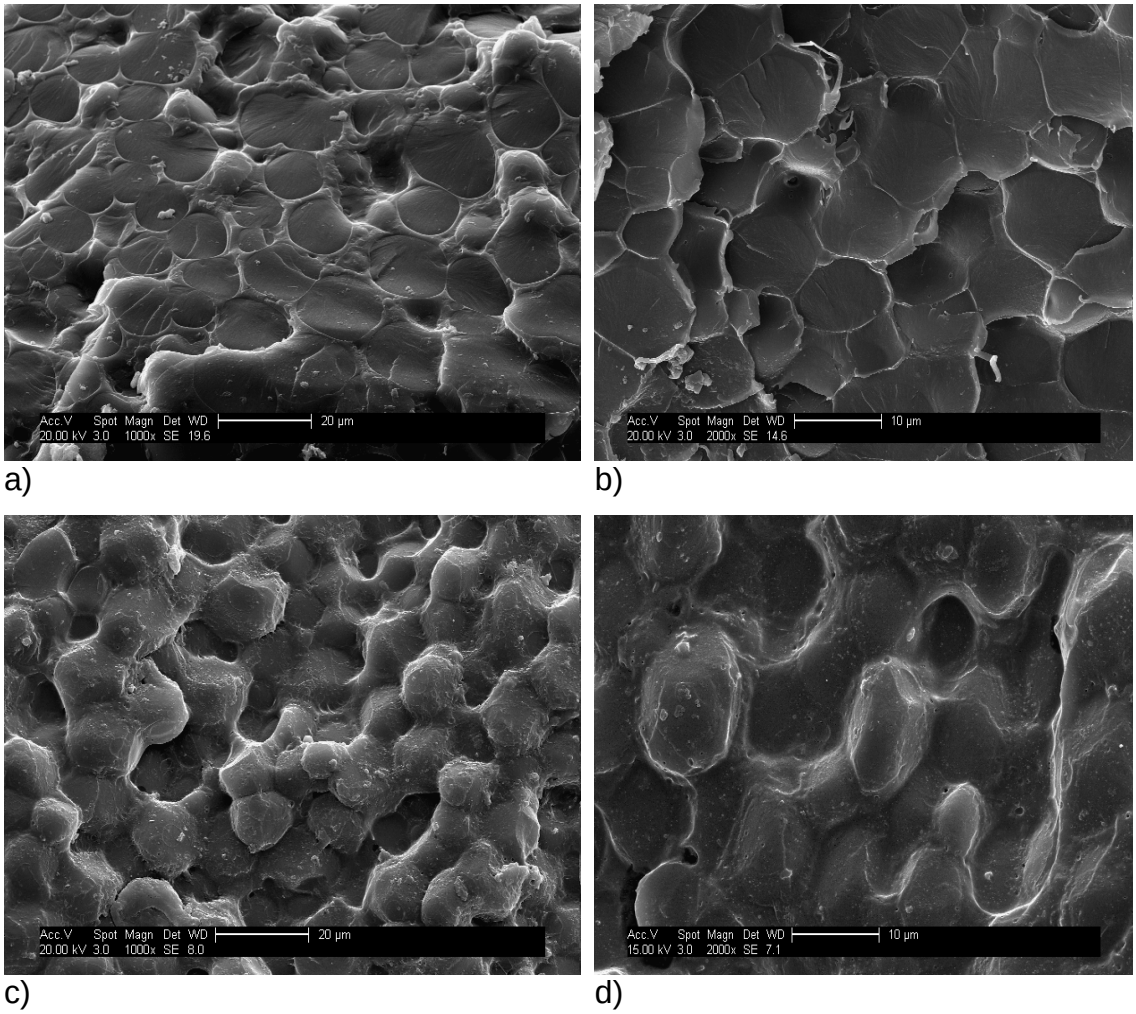

a) b)

c) d)

Figure 4.12: Low magnification SEM images of the MTM 44-1 resin system (a and b) non-etched and (c and d) after the etching treatment in methylene chloride for 20 minutes

The 1 wt % concentration of Thomas Swan carbon nanotubes (batch 6) and the 2 wt % of carbon black particles (batch 9) were used for SEM imaging. Figures 4.13 to 4.15 show the SEM images of the topography of the MTM 44-1 resin with the addition of 1 wt % carbon nanotubes and 2 wt % carbon black particles respectively, dispersed with the utilisation of the ultrasonic bath and mixed by hand. In figures 4.13a and b, 4.14a and b, but also 4.15a and b it is seen that the carbon nanoparticles are localised either at the epoxy-rich phase (carbon nanotubes) or at the interface (carbon black particles), confirming the observation from TEM images. In figure 4.13c, a

network of carbon nanotubes is depicted. This image indicates that carbon nanotubes have a good interface with the epoxy matrix. It is clear in figure 4.13d (magnified image of figure 4.13c), where it is seen that most of the carbon nanotubes were broken, although some of them were pulled-out during the fracture preparation. A very similar result was reported from Ci and Bai [130,131].

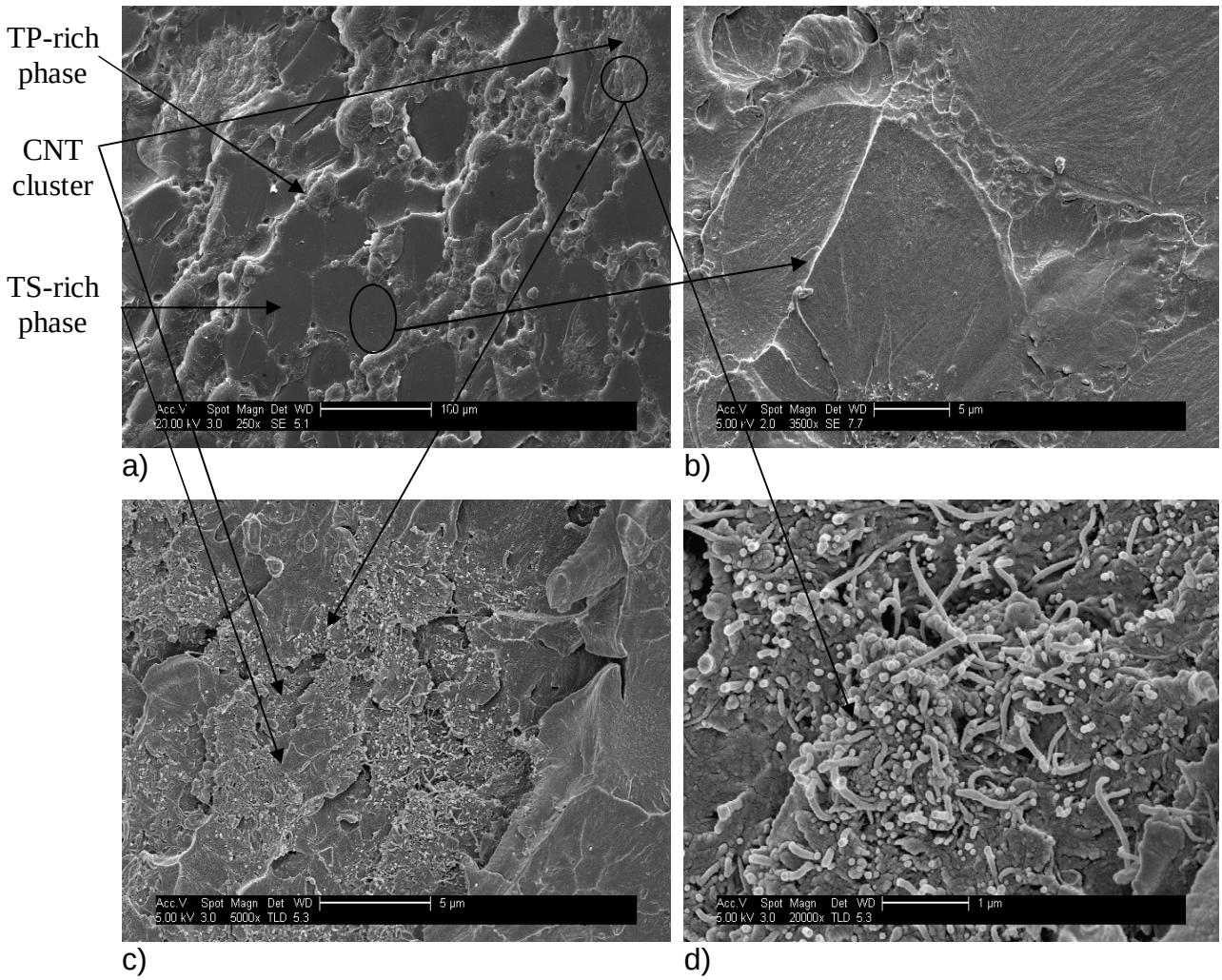

Figure 4.13: SEM images of the fracture surface of the MTM 44-1 resin system containing 1 wt % of the Thomas Swan carbon nanotubes (batch 6) (images c and d represent a cluster of carbon nanotubes formed in the epoxy-rich phase)

The batch that was produced with the utilisation of the ultrasonic bath, mixed by hand and then sonicated with the use of the ultrasonic probe (see table 3.1) and contained 1 wt % carbon nanotubes concentration (batch 10), did not show significant differences. The main difference was based on the

fact that except for the formation of the big clusters, some individual carbon nanotubes could be spotted as well. This is attributed to the occurence of phase separation, but also to the viscous nature of the material, which did not allow for an improvement of the processing conditions. The SEM images of this masterbatch are presented in figure 4.14. Figures 4.14a and b represent low magnification images of the two-phase material. Especially in image 4.14a, it is seen that the epoxy-rich phase domains form a big ‘superparticle’, in the shape of a big circle with a width exceeding 50 μm (mean diameter calculated from the TEM images ~ 8 μm). However, smaller epoxy-rich particles still exist. This is attributed to the fact that with the utilisation of TEM a small area of the epoxy matrix is observed, while on SEM a bigger area is captured. Figure 4.14b shows an even distribution of carbon nanotubes in the epoxy matrix. This means that the majority of carbon nanotubes were dispersed in the epoxy-rich phase forming big clusters (higher magnification images in figures 4.14c and d), but also in the thermoplastic-rich phase where smaller agglomerates or even individual nanotubes could be observed (figures 4.14e and f).

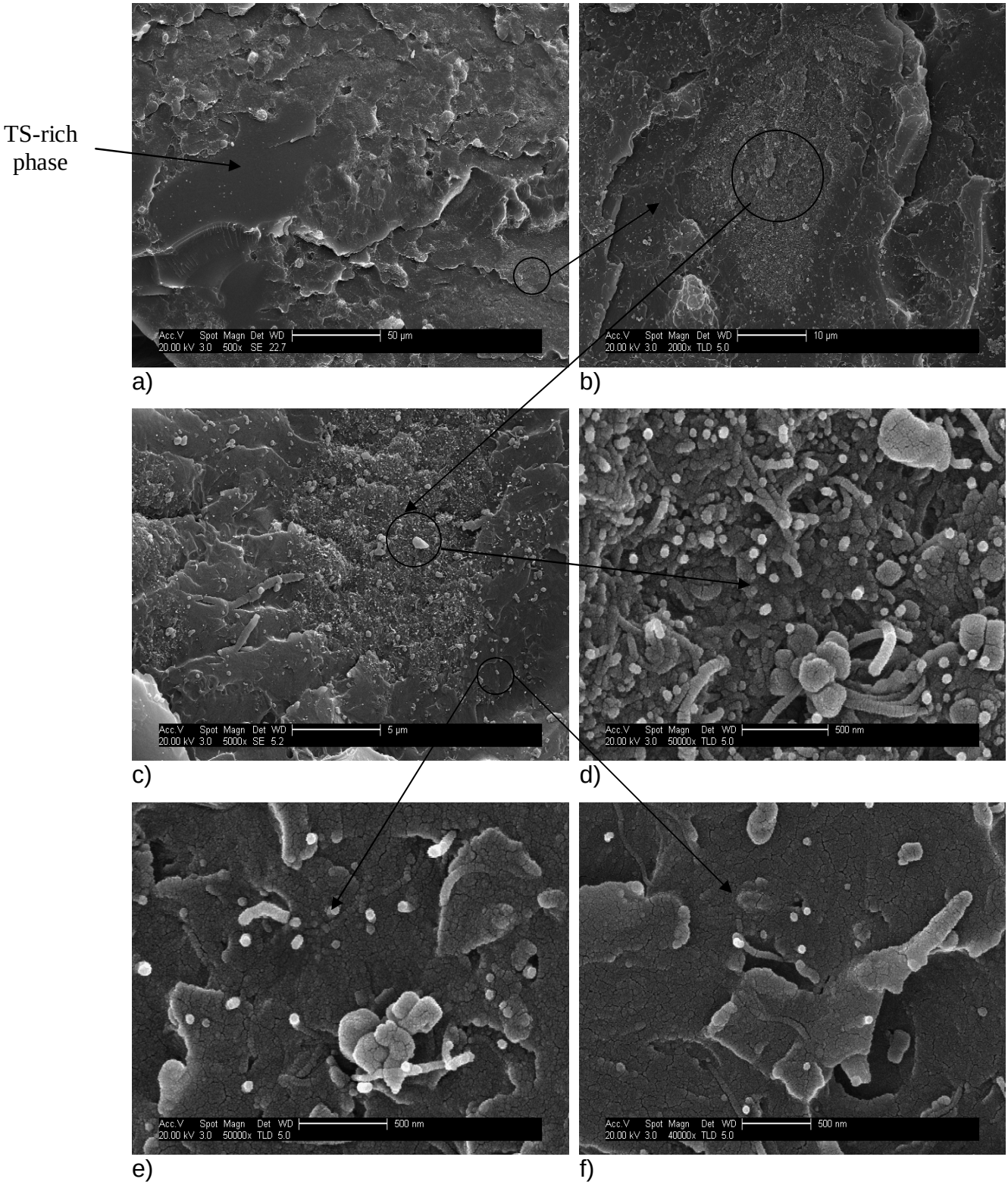

Figure 4.14: SEM images of the fracture surface of the MTM 44-1 resin system containing 1 wt % of the Thomas Swan carbon nanotubes (batch 10)

Figures 4.15a and b illustrate the formation of the two-phases (after phase separation) for the batch that contains carbon black particles dispersed with the utilisation of the ultrasonic bath and mixed by hand (batch 9). The epoxy-rich phase forms spherical domains, while the thermoplastic-rich phase fills in the gap between domains (continuous phase).

Figure 4.15c shows the localisation of the carbon black particles at the interface of the thermoset / thermoplastic-rich phases. Figure 4.15d shows the magnification of a carbon black cluster. However, in figure 4.15e, it is seen that big clusters form in the epoxy-rich phase, similar to the clusters of carbon nanotubes (viewed in figure 4.14). Figure 4.15f is a high magnification of the cluster imaged in figure 4.15e, showing the density of the carbon black spheres.

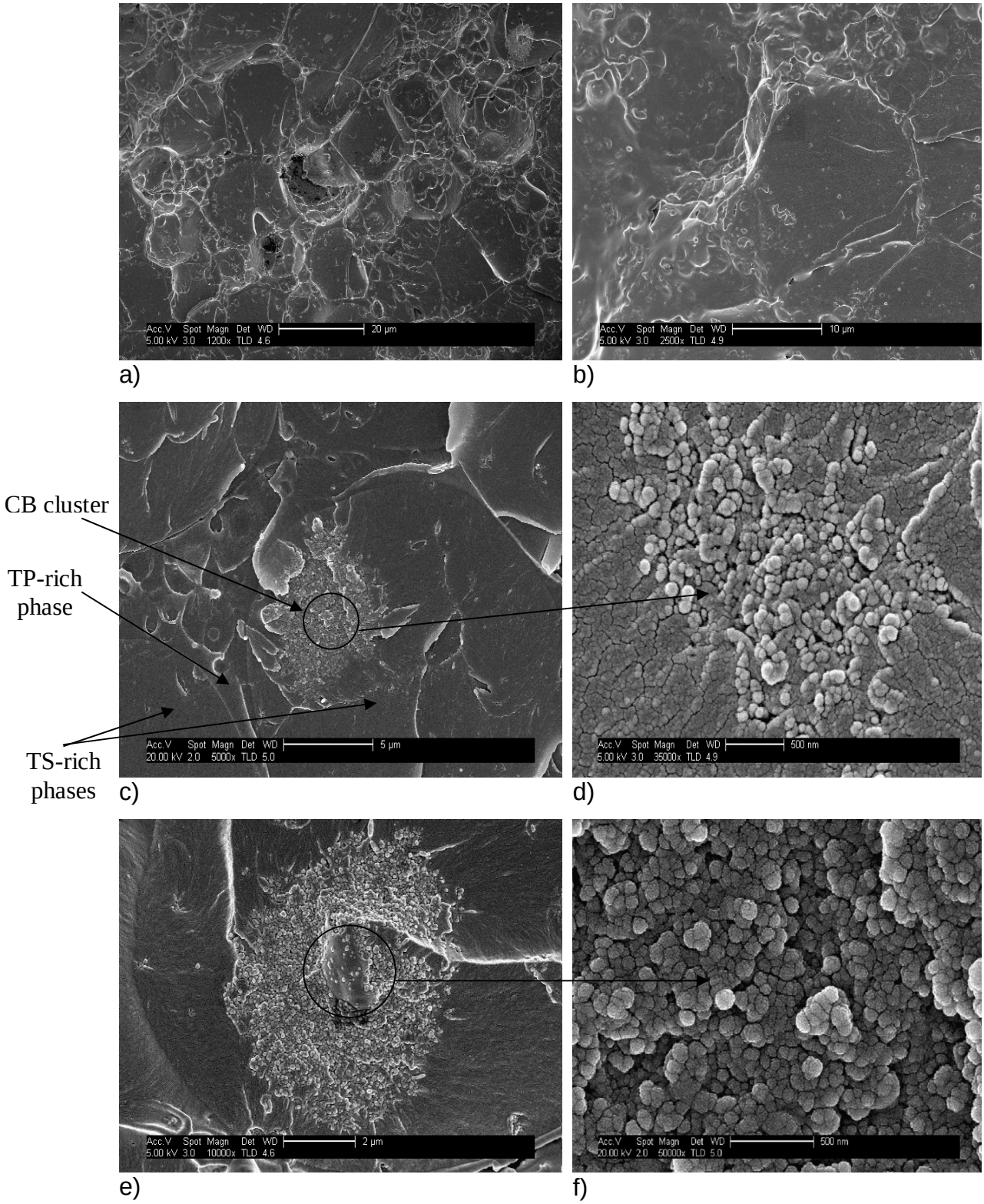

Figure 4.15: SEM images of the fracture surface of the MTM 44-1 resin system containing 2 wt % carbon black particles (batch 9)

Chapter 5

5. Thermal Analysis and Cure Characterisation of the Epoxy Systems and their Nanocomposites

In this chapter, the analysis of the collected DSC data as far as the cure kinetics and the advancement of the glass transition temperatures are concerned is presented. It also deals with the cure kinetics behaviour of the thermosetting systems and their nanocomposites, under dynamic and isothermal curing conditions. The collected data are analysed and discussed. The incorporation of carbon nanoparticles led to nanocomposites with different properties from the initial materials. A direct comparison between experimental DSC data under isothermal and dynamic heating conditions is presented.

5.1 Thermal Analysis Experiments

In chapter 3 it was mentioned that DSC was utilised as the main experimental technique to study the cure kinetics of the epoxy systems and their nanocomposites. When using DSC, the two main assumptions that were mentioned in paragraph 3.4.1.1 (see page 55) have to be valid. Especially the reaction rate of the reaction undergone, which is calculated from the DSC data, has to be proportional to the heat flow signal. In a DSC experiment the heat flow measured is the overall heat of the reactions taking place. The methodology of the analysis of the DSC data for the base resin systems and their nanocomposites is presented in the following paragraphs. The preparation of the batches and the samples were analysed in chapter 3.

5.1.1 Dynamic Cure Experiments

Several dynamic runs at constant heating rates were made in order to determine the conversion profiles for all the resin systems and their

nanocomposites. The amount of resin used for each experiment was 8-10 mg, encapsulated in aluminum pans and placed in the instrument cell at ambient temperatures. All the experiments were repeated at least two times each, depending on the reproducibility of the heat flow curves.

Dynamic experiments were conducted by imposing a constant heating rate on the sample up to the point where it was fully cured. The heat evolution was monitored from 20^{o}C to 320^{o}C using the following heating rates: 0.5, 1, 2.5, 5, 7.5 and 10^{o}C/min. A typical thermogram of a dynamic cure run of MY 750 / HY 5922 resin system is shown in figure 5.1.

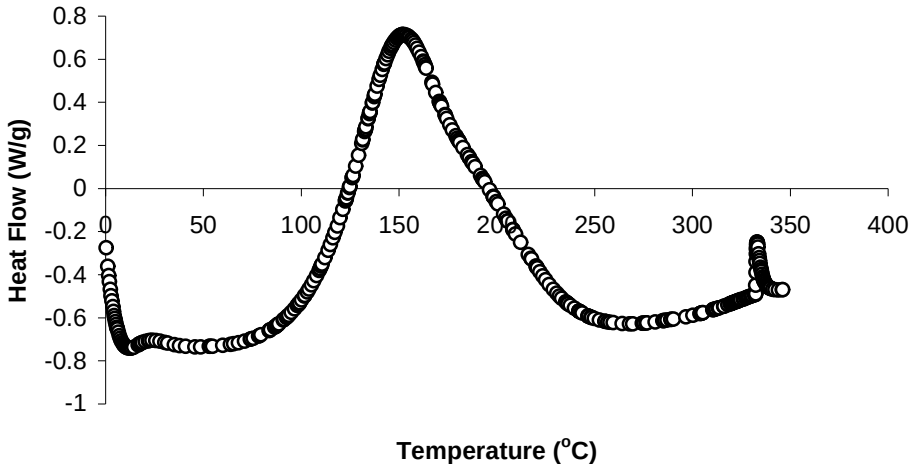

Figure 5.1: Raw data of heat flow versus temperature for a dynamic heating experiment of MY 750 / HY 5922 resin system at 20^{o}C/min

The analysis of the data was conducted by using an analysis routine developed by Dr Skordos. This routine translates the raw DSC data (heat flow, time and temperature) into reaction rate and degree of cure. The reaction rate is proportional to the heat flow signal measured. The routine operates as follows:

1) First of all the initial and final time and temperature are chosen (begin and end of the reaction).
2) This step defines the area that will be integrated. A sigmoidal baseline was utilised for all the dynamic DSC experiments.

3) The integration of the area chosen automatically calculated the total heat of the reaction, the degree of cure and the reaction rate.

An example of the integration is given for the raw data presented in figure 5.1:

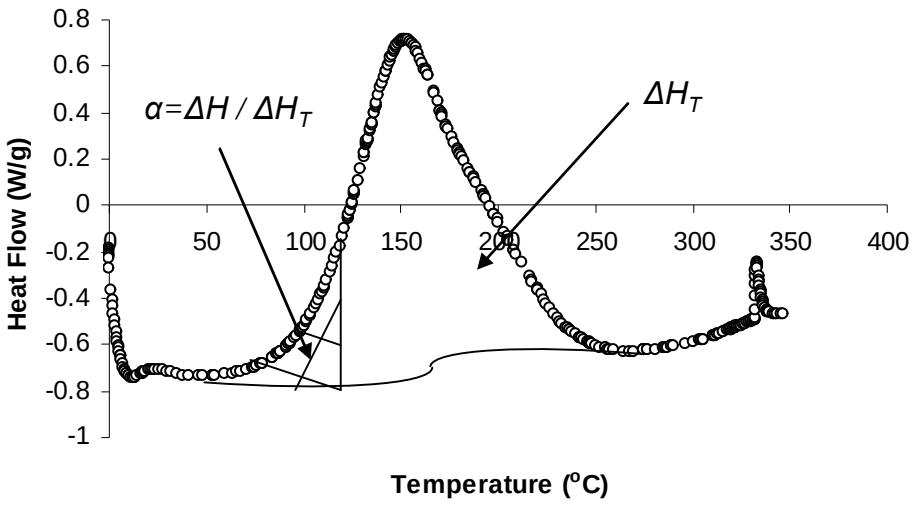

Figure 5.2: Integration of the raw data of heat flow versus temperature for a dynamic heating experiment of MY 750 / HY 5922 resin system at 20°C/min, presented in figure 5.1

The lowest bound of the integration is T_o, which is the lowest temperature at which reaction begins and T_f is the final temperature at which reaction is terminated. Integration of the total area under the diagram results in the calculation of the total heat of reaction, ΔH_T. The degree of cure α is calculated by using equation 5.1:

$$\alpha = \Delta H / \Delta H_T \qquad (5.1)$$

where ΔH is the heat of reaction calculated for the portion of the reaction highlighted in figure 5.2. The reaction rate da/dt is then calculated by the using equation 5.2:

$$\frac{d\alpha}{dt} = \frac{\alpha_2 - \alpha_1}{t_2 - t_1} \qquad (5.2)$$

where α_1 and a_2 are the degrees of cure that correspond to the time intervals t_1 and t_2 of the curing reaction respectively.

The degree of cure is the same as the one defined as the fraction of epoxide reacted at a given time t. The reaction rate calculated from this relationship is proportional to the heat flow signal measured by DSC. It is the overall reaction rate of the curing reactions monitored by DSC, and not the reaction rate calculated for each separate reaction that takes place.

5.1.2 Isothermal Cure Experiments

Isothermal experiments were conducted in a temperature window of 40-200^{o}C depending on the resin system. The isothermal experimental procedure comprised of three segments: A constant heating rate of 20^{o}C/min was imposed on the sample to heat it up to the desired temperature. A specific period of time was required for the sample to equilibrate thermally after the dynamic segment to the temperature the experiment was conducted. The required time was usually around one minute. After thermal equilibrimium was achieved, the sample was left to cure isothermally at that temperature. Figure 5.3 shows an example of the isothermal cure of 8552 resin.

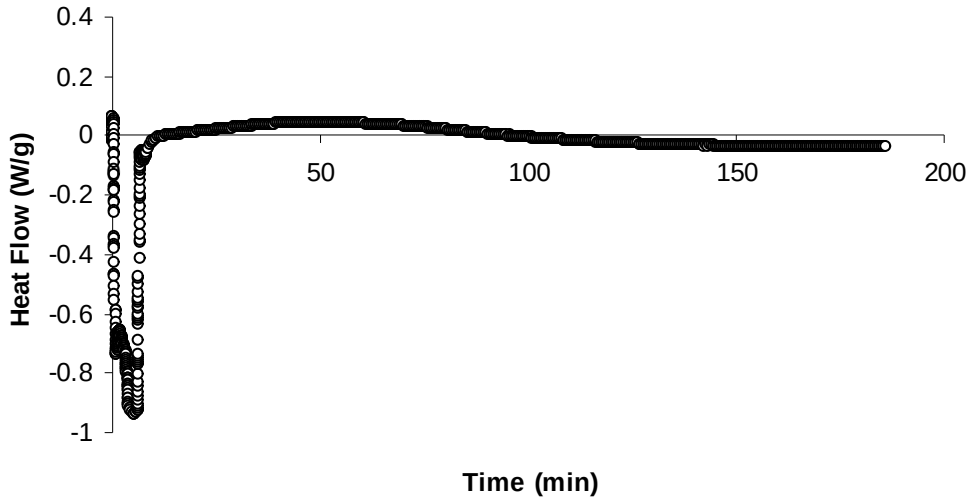

Figure 5.3: Raw calorimetric data for the isothermal cure of 8552 resin at 140^{o}C

The baseline for the integration was estimated by drawing a horizontal line from the end of the curing experiment to the beginning of the test. This line was considered to start at the moment when the thermal equilibrium has been established. An example of the analysis of figure 5.3 is presented in figure 5.4.

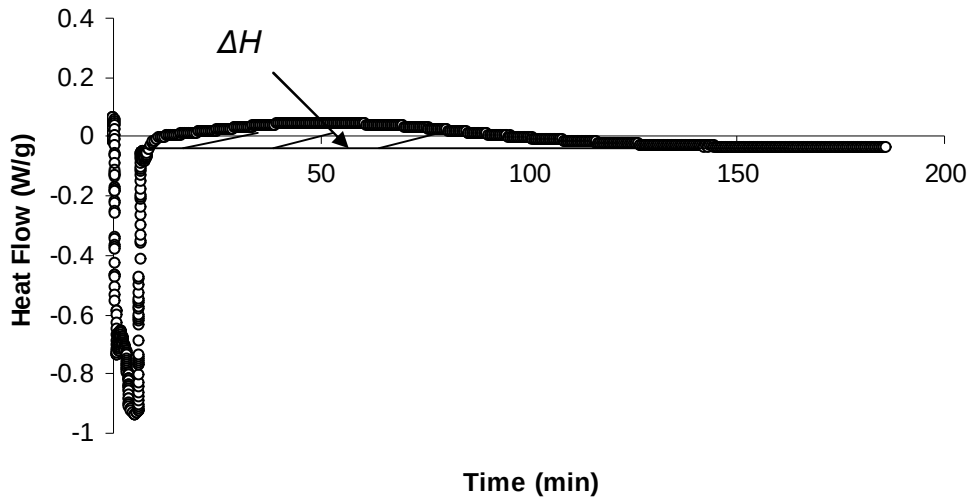

Figure 5.4: Integration of the raw calorimetric data for the isothermal cure of 8552 resin at 140^{o}C, presented in figure 5.3

The three segments of the isothermal cure are presented in figure 5.5.

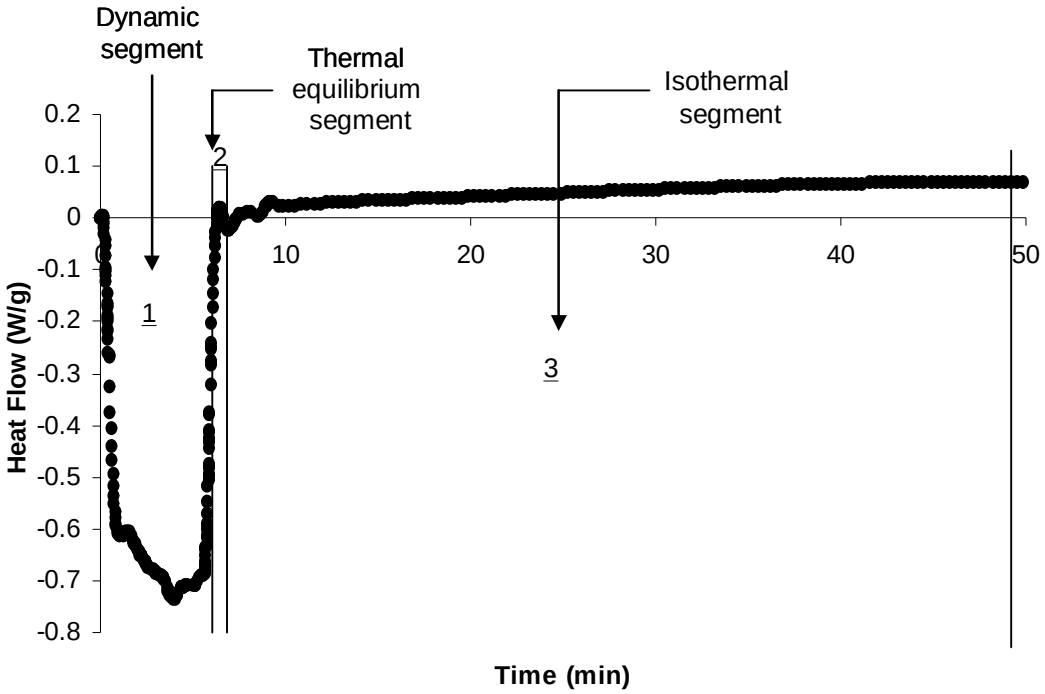

Figure 5.5: Magnification of the data presented in figure 5.3. The test consists of three segments: 1) dynamic segment, 2) thermal equilibrium segment and 3) isothermal segment

The same routine that was utilised for the analysis of the dynamic DSC data was used here. The routine this time used the total heat of reaction, $\Delta H_{T,}$ measured from dynamic DSC data to calculate the degree of cure and the reaction rate. The experiments were conducted at least twice, so that a good reproducibility of the results could be obtained.

5.1.3 Glass Transition Temperature Measurements

Temperature Modulated Differential Scanning Calorimetry (TMSDC) was utilised to measure the glass transition temperature (T_g) advancement as a function of the degree of cure of each resin system and its nanocomposites. Experimental T_g was defined in this study as the inflection point of the observed step in the heat capacity (C_p) versus temperature curves. An example of that definition is given in figure 5.6, where a heat hapacity versus temperature curve is illustrated for the cure of MY 750 / HY 5922 resin system.

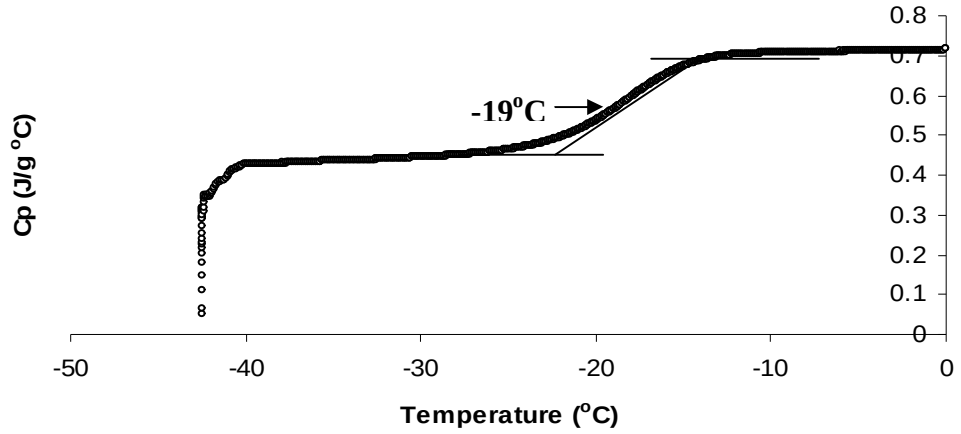

Figure 5.6: TMDSC approach of the glass transition temperature (T_g) determination for the case of the MY 750 / HY 5922 sample partially cured up to 20 % conversion. The step in the heat capacity versus temperature curve is well defined (T_g is considered to be the inflection point)

A number of experiments were performed using DSC for the identification of glass transition and its advancement during cure. The whole conversion range was covered, focusing particularly in the high conversion region. 8-10 mg of resin was encapsulated in aluminum pans and was partially cured under dynamic heating conditions (usually using a heating rate of 1°C /min) up to the predefined conversion, where the experiment was stopped and the sample was rapidly cooled. At that point the curing reaction was assumed to be terminated. The degree of cure to partially cure the samples was calculated from the dynamic DSC data using the analysis routine described earlier. For example, in order to partially cure the specimen presented in figure 5.6, a dynamic run at 1°C/min was tested up to a specific temperature. That temperature, calculated from the DSC analysis routine corresponded to the specific conversion (20 %). The samples were moved and stored to the freezer at -18°C. Then TMDSC was applied to the partially cured specimen of the resin for the evaluation of the T_g values. Initially the sample was left to equilibrate in the cell at a specific temperature, depending on the system tested. Then a heating rate of 0.5 to 1°C /min was imposed accompanied by a

temperature modulation with 60 seconds period and 1°C amplitude. The experiments were conducted at least three times each so that a good reproducibility of the results could be achieved.

5.1.4 Reproducibility of the Experiments

The experiments were conducted using samples from the same batches of the materials for the whole series of dynamic, isothermal and temperature modulated experiments. Figure 5.7 presents three dynamic tests of the MY 750 / HY 5922 resin system as a check on sampling error. The total heats of reaction for the three samples, presented in table 5.1, show variation of +/- 7 J/g from the mean, corresponding to a 2 % error.

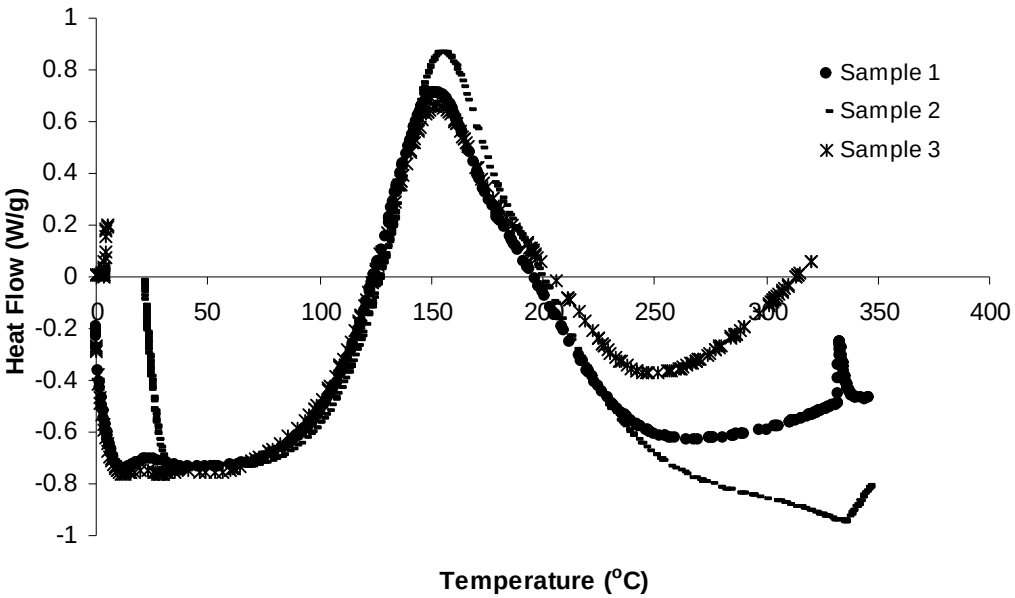

Figure 5.7: Dynamic DSC data of the MY 750 / HY 5922 resin system cured at 20°C/min, all samples taken from the same batch

Similarly reproducible results were found for the isothermal and temperature modulated tests conducted (±1°C, see section 6.2), even between different batches of the same material and unaffected by the presence of nanoparticles. In the case of the MY 750/ HY 5922 system additional precautions had to be taken to ensure that the sample batch had not progressed in cure within frozen storage . All measurements were carried

out within 10 days of mixing and checks on the total heat of reaction were performed thoughout. If the total heat of reaction was found to have dropped by more than 5%, a fresh sample was prepared.

Rate (20^{o}C/min)	Sample 1	Sample 2	Sample 3	Difference from the mean
ΔH_T (J/g)	337	352	348	7

Table 5.1: Total heats of the reaction for the dynamic cure of three samples of the MY 750 / HY 5922 resin system

The analysis of the DSC data is presented in the next part of the chapter.

5.2 Cure characterisation of the epoxy systems and their nanocomposites

This part of the chapter deals with the cure kinetics behaviour of the thermosetting systems and their nanocomposites, under dynamic and isothermal curing conditions. The collected data are analysed following the the methodology described in paragraph 5.1. A direct comparison between experimental DSC data under isothermal and dynamic heating conditions is presented. This comparison is valuable for the comparison between the cure kinetics models that will be presented in chapter 6.

5.2.1 Cure characterisation of the MY 750 / HY 5922 resin system and its nanocomposites containing Hyperion carbon nanotubes and Monarch carbon black particles (batches 1-5)

DSC experiments were performed for the MY 750 / HY 5922 resin system under isothermal and dynamic heating conditions, using the methodology that was discussed in paragraphs 5.1.1 to 5.1.3. The diagrams that represent the reaction rate refer to the overall reaction rate calculated from the DSC data and defined in paragraph 5.1. The main assumption that the reaction rate is proportional to the heat flow signal has to be valid. Based on this assumption,

an autocatalytic reaction mechanism is followed when the reaction rate peak is exhibited at time $t \neq 0$ [36]. Consequently an n^{th} order reaction mechanism is when the reaction rate peak is exhibited at time $t=0$ [36].

The temperature range for the isothermal tests was between 40-90^{o}C. The reaction rate data are presented in figures 5.8 and 5.9. The isothermal data in figure 5.8 indicate an autocatalytic reaction mechanism, as the maximum of the reaction rate signal is exhibited after the beginning of the reaction (inset in figure 5.8).

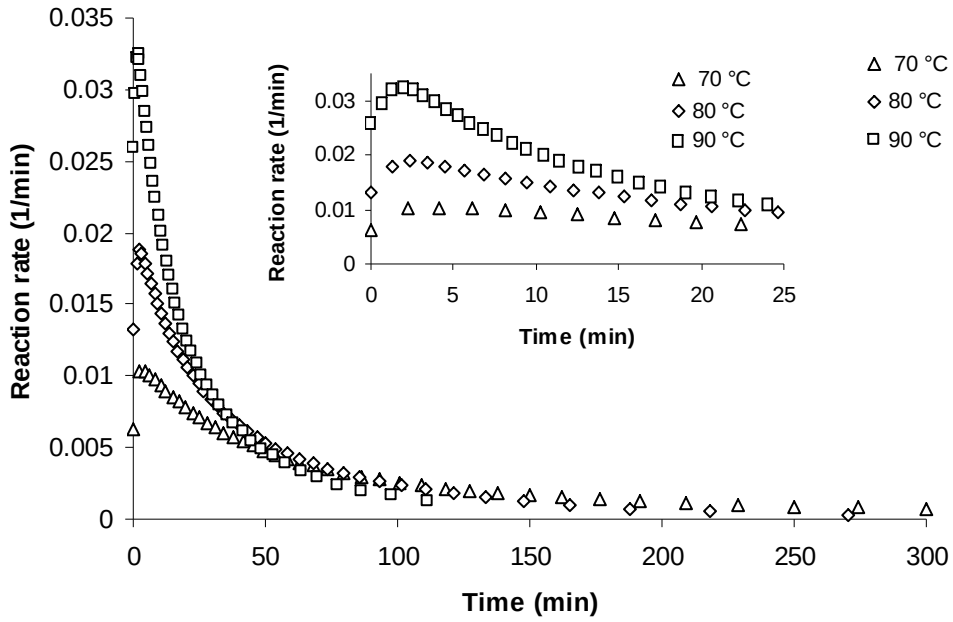

Figure 5.8: Reaction rate versus time for the isothermal cure of the MY 750 / HY 5922 resin system at different temperatures

For example for the isothermal cure of the resin at 70^{o}C, the maximum reaction rate peak is exhibited at t=3.5 minutes. Dynamic experiments were conducted for different heating rates, between 0.5 and 10^{o}C/min. A single exothermic peak was observed in the reaction rate curves during the cure under constant heating conditions. The maximum value of the reaction rate was observed at the highest heating rate used (see figure 5.9).

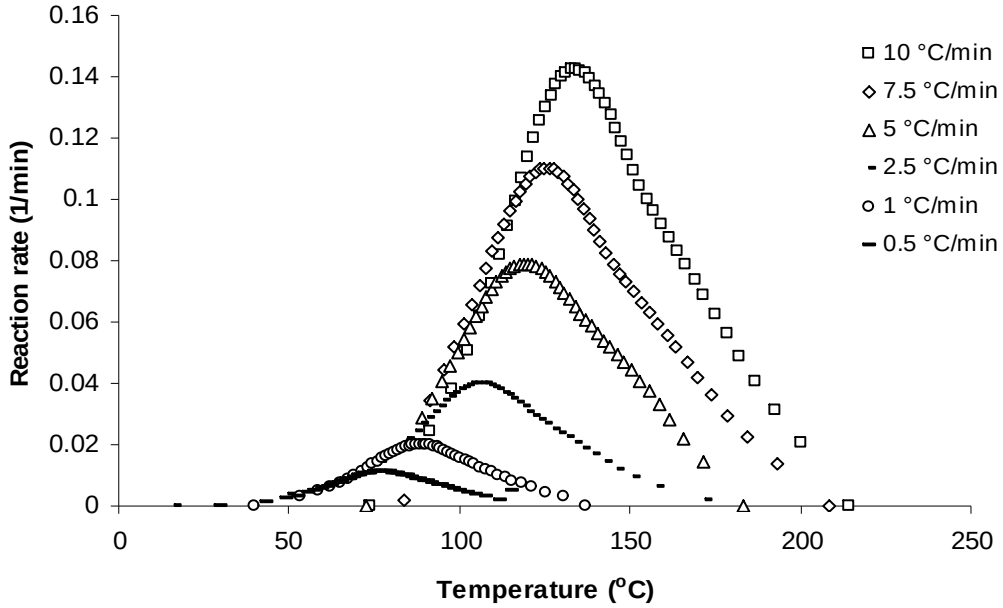

Figure 5.9: Reaction rate versus temperature for the dynamic cure of the MY 750 / HY 5922 resin system at constant heating rates

Figure 5.10 presents the reaction rate versus degree of cure curves under isothermal heating conditions.

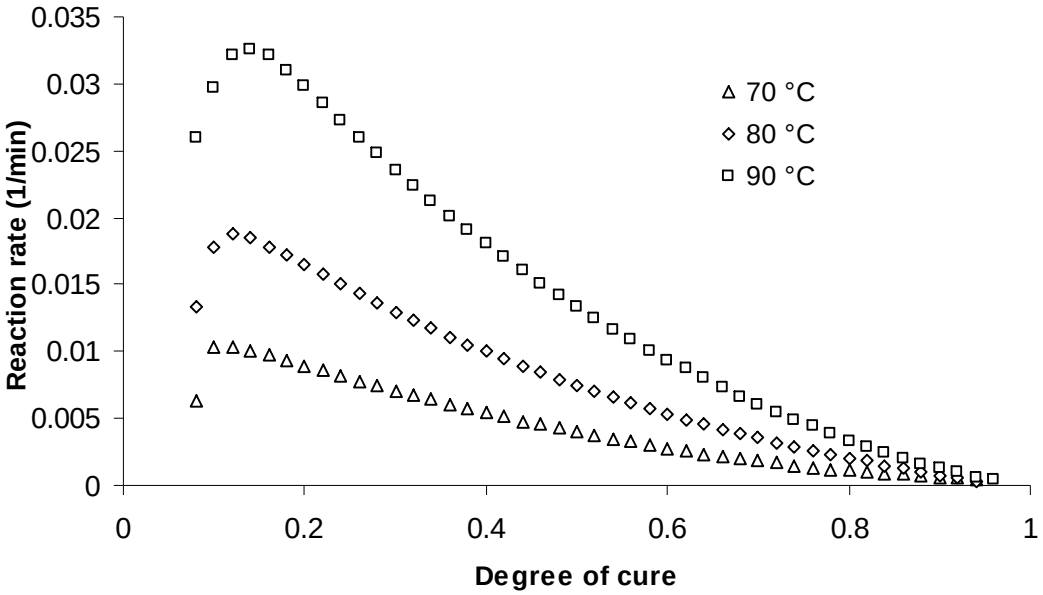

Figure 5.10: Reaction rate versus degree of cure for the isothermal cure of the MY 750 / HY 5922 resin system at different temperatures

Figure 5.10 is produced by plotting the reaction rate versus the degree of cure calculated after the analysis of the isothermal cure data. The curves in figure 5.10 start at an initial conversion of 8 %. It was observed that during the mixing process of the epoxy resin with the amine hardener (stirring by hand) the system became warm. That means that during the mixing part of the reaction has already started. In order to measure the loss in the total heat of reaction because of the initial mixing, the resin was put in an aluminum pan and then an excess of the hardener was added without mixing. That occurred so that the reaction would not initiate. The pan was placed directly in the DSC cell and a dynamic run was conducted in order to measure the total heat of reaction. It was found that the total heat was ~ 370 J/g. The same applied in the case of the Hyperion carbon nanotube and Monarch carbon black particle incorporation. Again the same value was measured. In order to prepare the nanocomposites, the shear mixer or mixing by hand and the use of the ultrasonic horn were utilised. These preparation techniques led also to an initial loss of total heat, because of the mixing process. When combining the values of total heats of reaction, summarised in table 5.2 with the total heat measured without any mixing, it was estimated that the initial conversion for the Hyperion carbon nanotube incorporation was ~ 4.2 % (in either method used to disperse them in the epoxy resin) and ~ 3.8 % for the Monarch carbon black particles.

The total heat of the reaction was estimated when the dynamic curves were integrated. The total heat of reaction, ΔH_T, was evaluated for the neat epoxy resin system, and its nanocomposites, when carbon nanoparticles were incorporated. For convenience from now on the nanocomposites with Hyperion carbon nanotubes that were dispersed by hand and then ultrasonicated (utilisation of the ultrasonic horn-batch 5) will be mentioned as ultrasonicated, while the ones that were prepared by shear mixing (the same applies for the dispersion of carbon black particles-batches 1-4) will be called just nanocomposites. These results are summarised in table 5.2.

Rate (^{o}C/min)	10	7.5	5	2.5	1	0.5	Average ΔH_T (J/g)	Standard Deviation
MY 750/HY 5922	333	334	348	340	335	353	344	16
MY 750/HY 5922 0.06 wt % CNTs (batch 1)	298	305	310	306	324	355	318	18
MY 750/HY 5922 0.06 wt % CNTs (ultrasonicated-batch 5)	360	365	367	364	335	374	361	13
MY 750/HY 5922 1 wt % CB (batch 4)	306	296	296	345	307	-	310	20

Table 5.2: Total heats of reaction under dynamic heating conditions for the neat MY 750 / HY 5922 resin and its nanocomposites, containing the Hyperion carbon nanotubes (with and without ultrasonication treatment) and Monarch carbon black particles, respectively

The total heats of reaction do not vary significantly as a function of the heating rates. There is an increase in the total heats of reaction when the carbon nanotubes undergo ultrasonication treatment. However, according to the standard deviations measured, no significant difference was observed in the total heats of the reaction when carbon nanoparticles were incorporated into the resin systems. The resin system produced, when carbon nanotubes were incorporated (batches 1 and 5) was tested under dynamic and isothermal heating conditions. The system that contained carbon black particles (batch 4) was tested only under dynamic heating conditions. The temperature range for the isothermal tests was between 40-100^{o}C (60-100^{o}C for the ultrasonicated batch). Figures 5.11 to 5.16 illustrate the results for the system containing carbon nanotubes and carbon black particles. The insets in figures 5.11 and 5.12 show the reaction rate maxima at the beginning of the reaction. The isothermal data in figures 5.11 and 512 indicate that the same autocatalytic reaction mechanism is followed as in the case of the neat

system (insets in figures 5.11 and 5.12). Dynamic experiments were conducted for different heating rates, between 0.5 and 10^{o}C/min. A single exothermic peak is also observed in the reaction rate curves during the cure under constant heating conditions (figures 5.13 to 5.15). Figure 5.15 illustrates the reaction rate curves for the dynamic cure of the resin system containing carbon black particles.

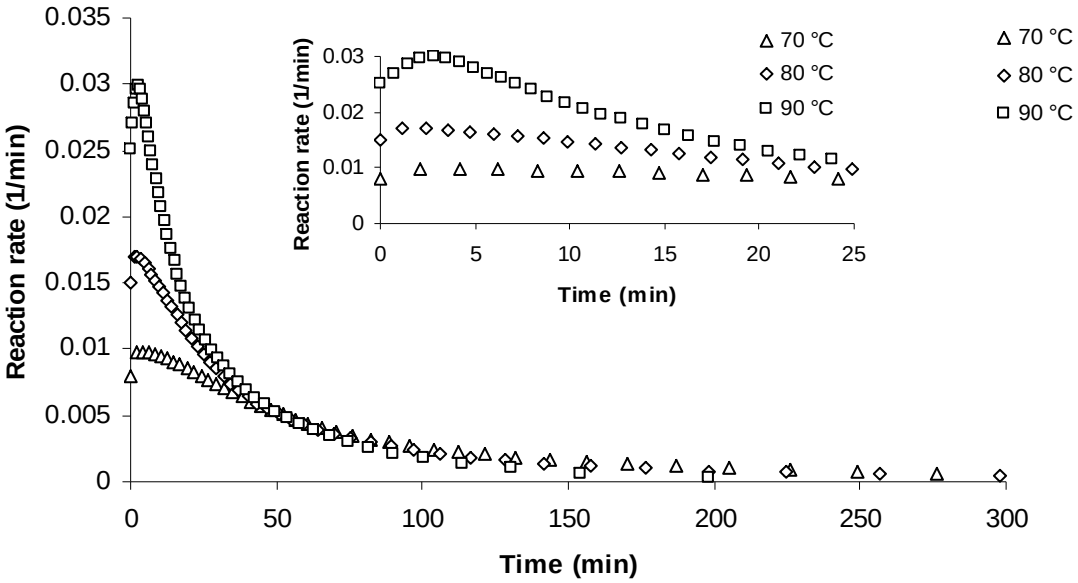

Figure 5.11: Reaction rate versus time for the isothermal cure of MY 750 / HY 5922 resin system containing 0.06 wt % of Hyperion carbon nanotubes at different temperatures (batch 1)

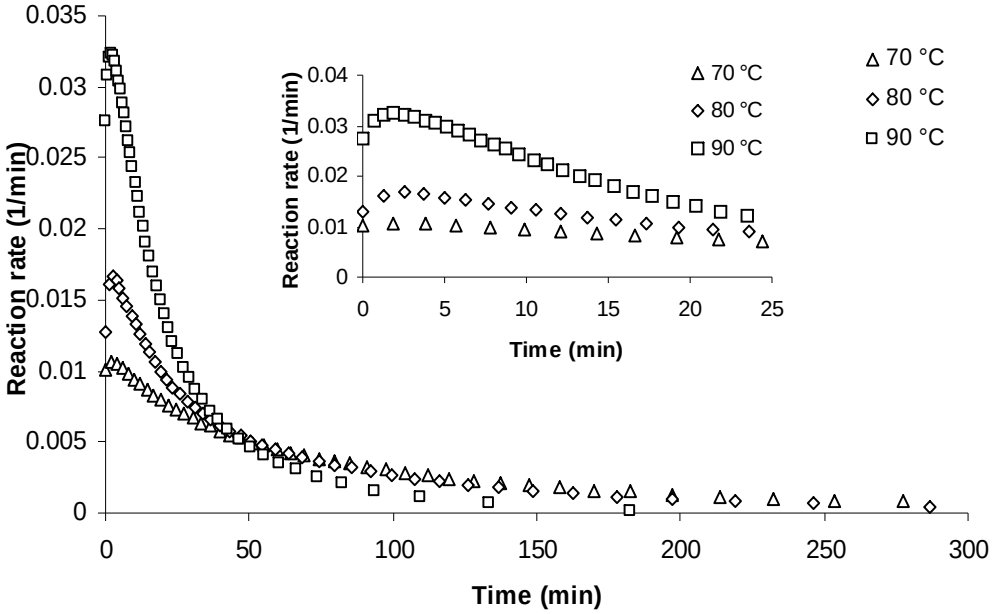

Figure 5.12: Reaction rate versus time for the isothermal cure of MY 750 / HY 5922 resin system containing 0.06 wt % of Hyperion carbon nanotubes at different temperatures (batch 5)

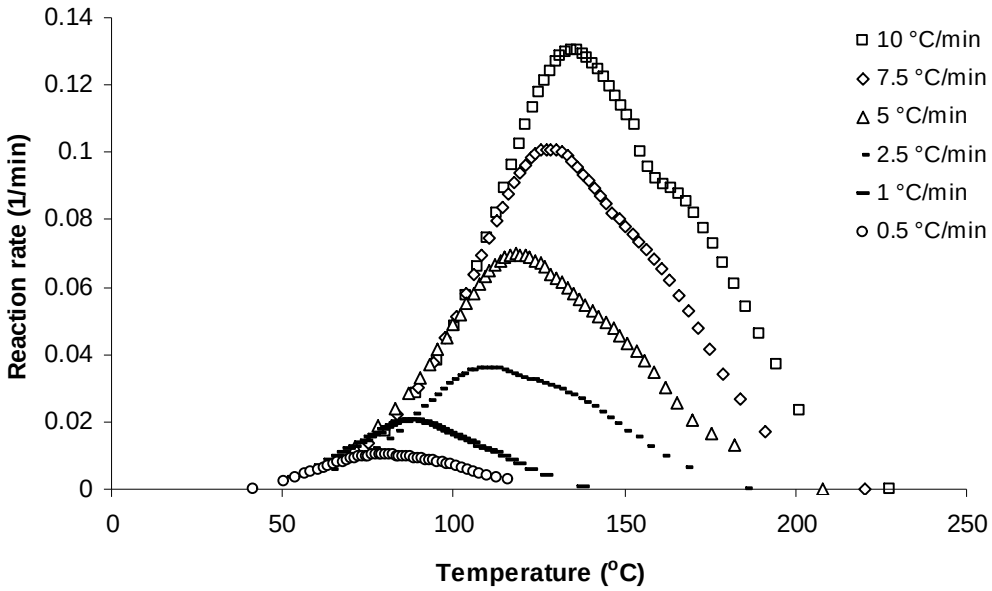

Figure 5.13: Reaction rate versus temperature for the dynamic cure of the MY 750 / HY 5922 resin system containing 0.06 wt % of Hyperion carbon nanotubes at constant heating rates (batch 1)

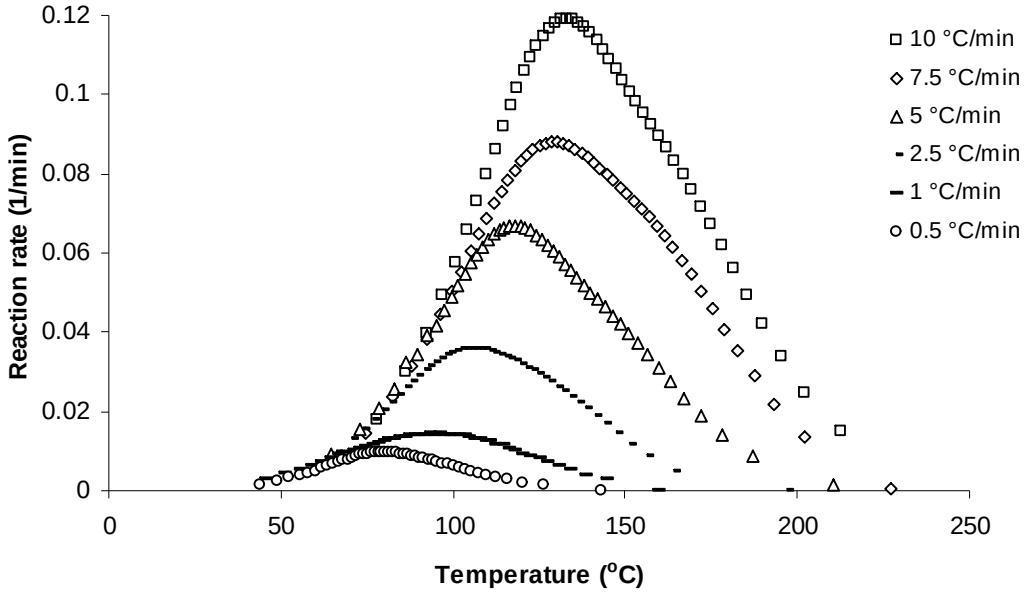

Figure 5.14: Reaction rate versus temperature for the dynamic cure of the MY 750 / HY 5922 resin system containing 0.06 wt % of Hyperion carbon nanotubes at constant heating rates (batch 5)

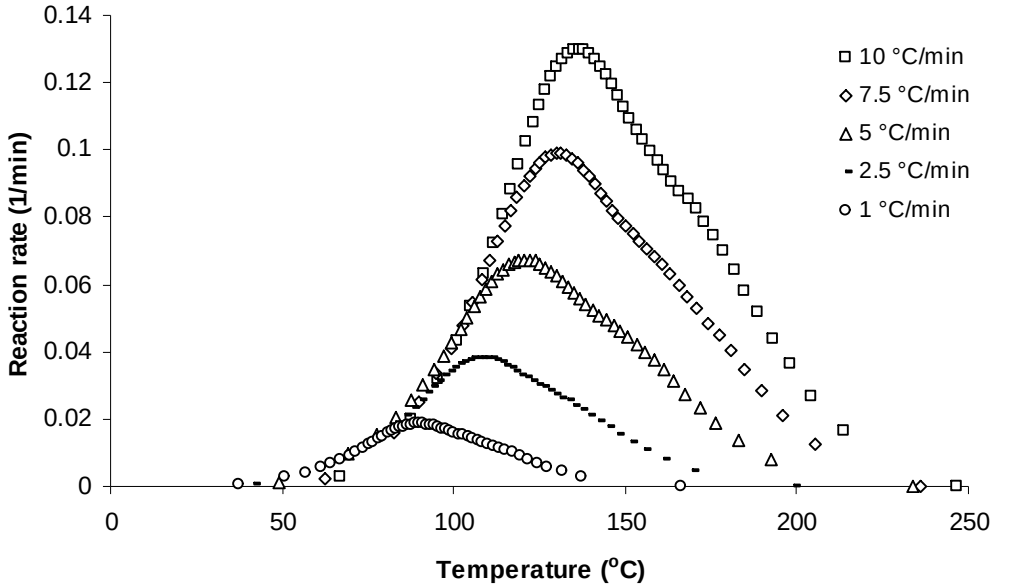

Figure 5.15: Reaction rate versus temperature for the dynamic cure of the MY 750 / HY 5922 resin system containing 1 wt % of Monarch carbon black particles at constant heating rates (batch 3)

Figures 5.16 and 5.17 illustrate the reaction rate versus degree of cure curves under isothermal heating conditions. The curves start at a conversion of ~ 4 %.

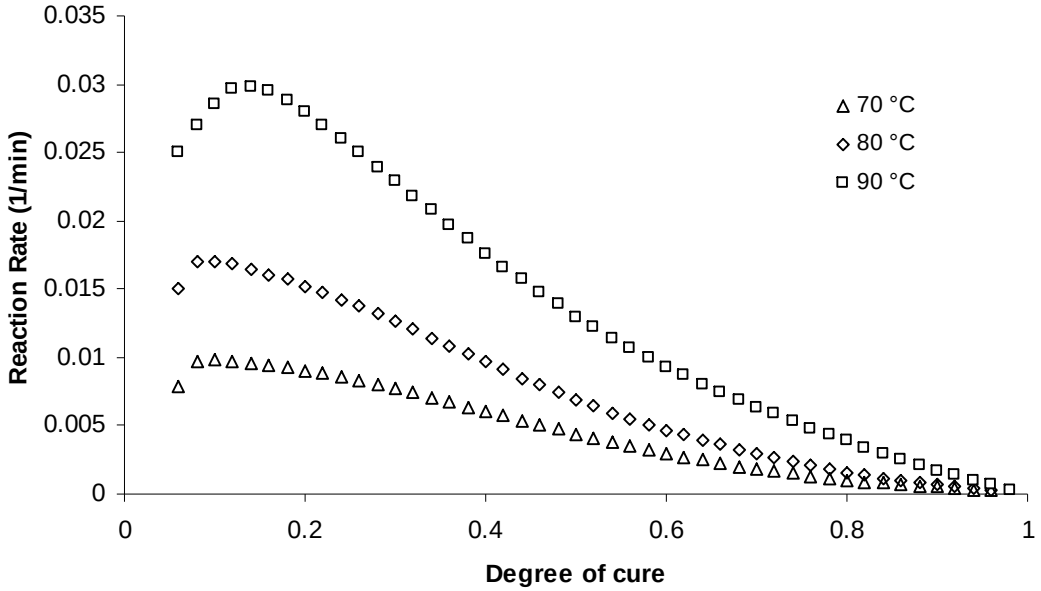

Figure 5.16: Reaction rate versus degree of cure for the isothermal cure of the MY 750 / HY 5922 resin system containing 0.06 wt % of Hyperion carbon nanotubes at different temperatures (batch 1)

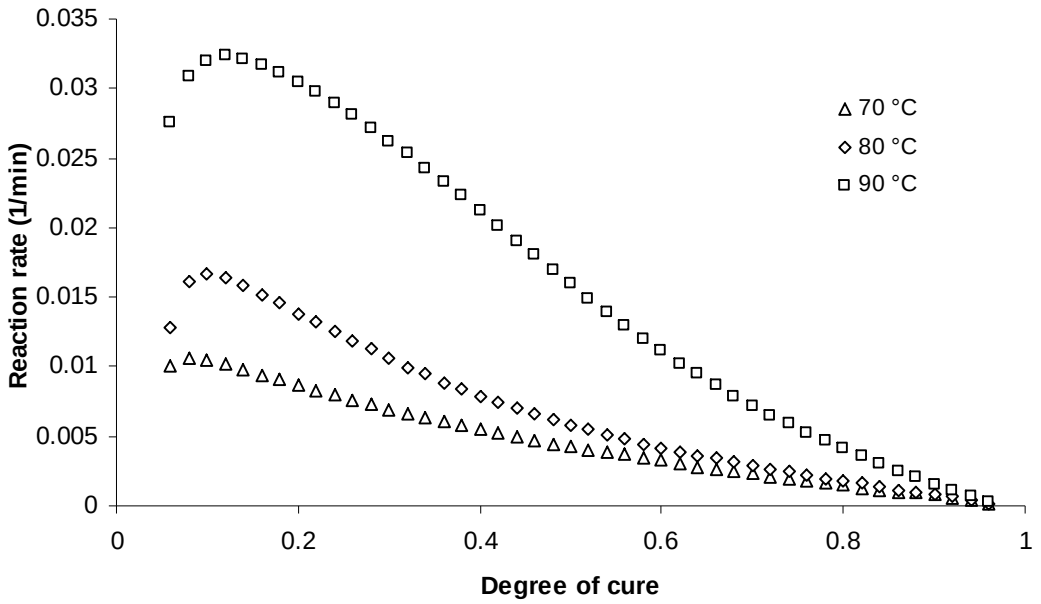

Figure 5.17: Reaction rate versus degree of cure for the isothermal cure of the MY 750 / HY 5922 resin system containing 0.06 wt % of Hyperion carbon nanotubes at different temperatures (batch 5)

Comparison between figures 5.9 and 5.13 leads into two main observations:

a) the curves shift to higher temperatures and become broader when carbon nanoparticles are incorporated
b) the values of the reaction rates of the systems decrease slightly when carbon nanoparticles are incorporated (see figure 5.18). However the overall total heats of the reaction measured are almost the same (see table 5.2)

The first observation is depicted by comparing the dynamic tests at all the heating rates tested, for the neat resin system and its nanocomposites, which is summarised in table 5.3. The illustration of the dynamic curves is also shown in figure 5.18. For convenience, a single heating rate was used (10^{o}C/min). The errors indicated by the bars are 2 %.

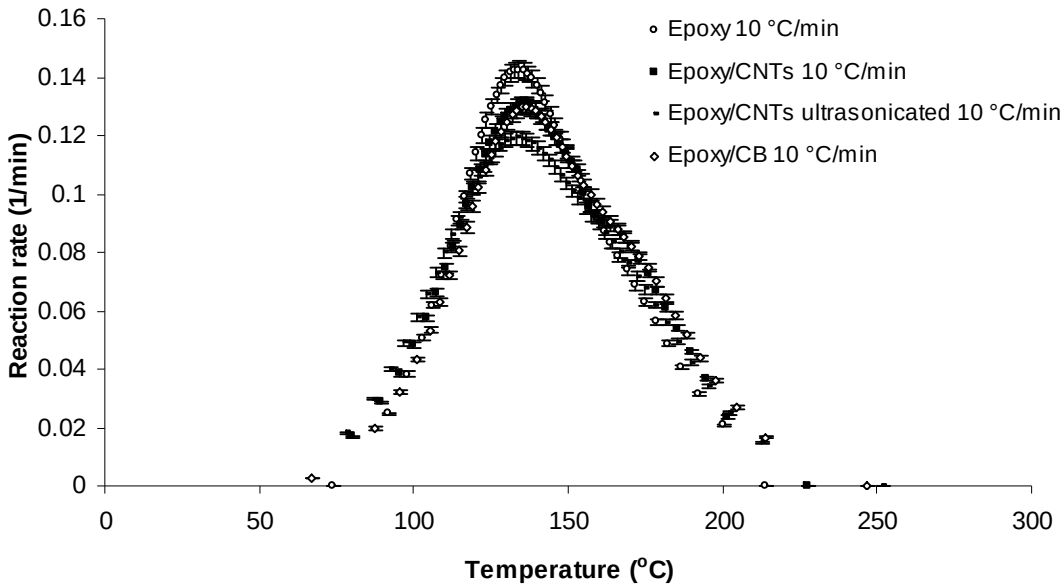

Figure 5.18: Dynamic DSC tests at 10^{o}C/min for the MY 750 / HY 5922 resin system and its nanocomposites containing 0.06 wt % of Hyperion carbon nanotubes (with and without ultrasonication treatment) and 1 wt % of Monarch carbon black particles (including the experimental errors)

Rate (^{o}C/min)	10	7.5	5	2.5	1	0.5
T_{max} (^{o}C) MY 750 / HY 5922	135	126	120	106	89	78
T_{max} (^{o}C) MY 750 / HY 5922 0.06 wt % CNTs	136	129	121	108	90	82
T_{max} (^{o}C) MY 750 / HY 5922 0.06 wt % CNTs (ultrasonicated)	134	129	122	109	93	79
T_{max} (^{o}C) MY 750 / HY 5922 1 wt % CB	137	132	122	110	91	-

Table 5.3: Temperature of reaction maxima under dynamic heating conditions for the neat MY 750 / HY 5922 resin system and its nanocomposites containing 0.06 wt % of Hyperion carbon nanotubes (with and without ultrasonication treatment) and 1 wt % of Monarch carbon black particles, respectively

It could be observed that there is a shift of 1-3^{o}C of the temperatures of the reaction rate maxima when the carbon nanoparticles are incorporated into the resin system. The maximum reaction rates with the addition of carbon nanoparticles are lower from the ones of the neat resin. In order to see this change with the incorporation of carbon nanoparticles, a direct comparison of the reaction rates under isothermal heating conditions was established. The reaction rates under isothermal curing conditions follow a similar trend. Figure 5.19 presents the comparison of the reaction rates of the epoxy system and its nanocomposite containing 0.06 wt % of Hyperion carbon nanotubes, dispersed with the utilisation of the ultrasonic horn and mixed by hand, for the isothermal cure at different temperatures (70 to 90^{o}C).

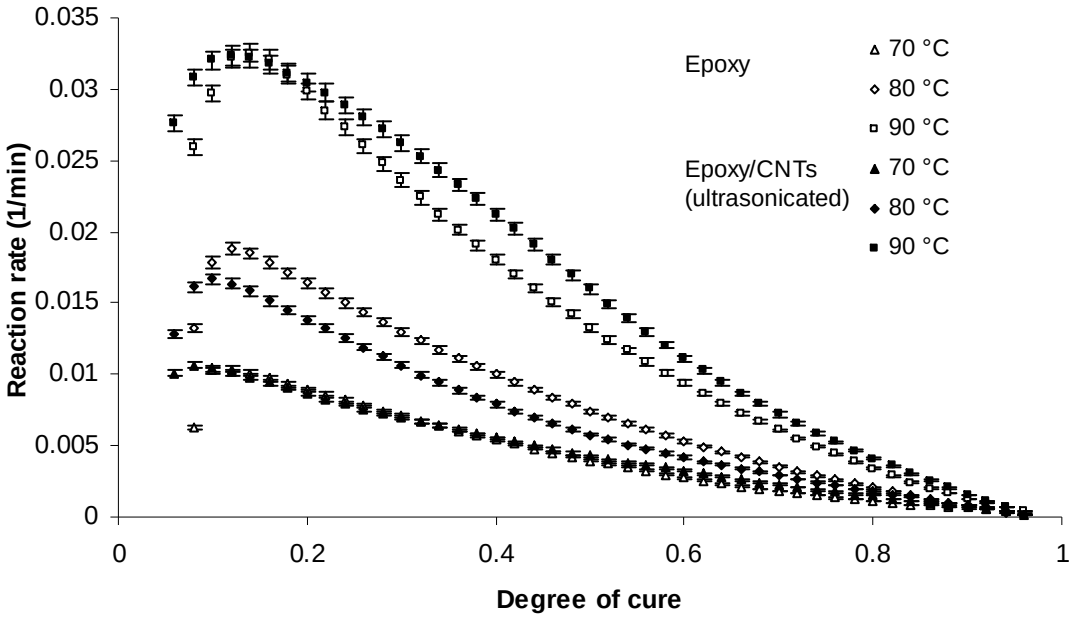

Figure 5.19: Reaction rates versus degree of cure (including experimental errors) for the MY 750 / HY 5922 resin system and its nanocomposite containing 0.06 wt % of Hyperion carbon nanotubes (batch 5) under isothermal curing conitions at different temperatures

In figure 5.19 there is a slight difference in the reaction rates of the epoxy system with the incorporation of carbon nanotubes. The same difference is also shown in figure 5.20 presents a comparison of the reaction rates of the epoxy system and its nanocomposite containing 0.06 wt % of Hyperion carbon nanotubes (prepared by shear mixing) for the isothermal cure at different temperatures (70 to 90^{o}C). The errors indicated by the bars are 2 %.

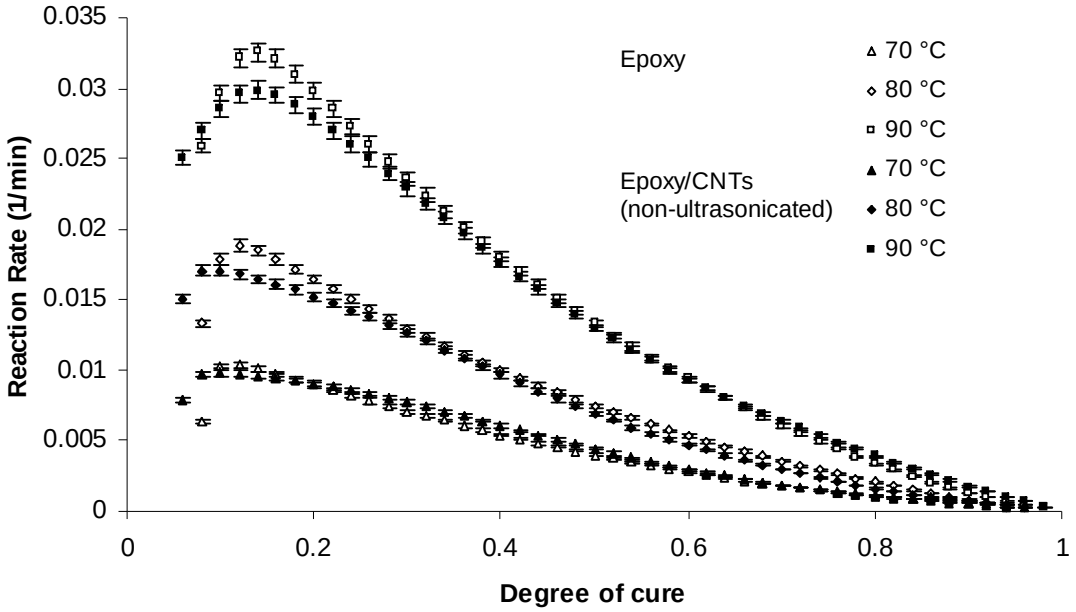

Figure 5.20: Reaction rates versus degree of cure (including experimental errors) for the MY 750 / HY 5922 resin system and its nanocomposite containing 0.06 wt % of Hyperion carbon nanotubes (batch 1) under isothermal cure at different temperatures

Figures 5.21 and 5.22 represent the reaction rate peaks that shift to lower times.

The results presented in figures 5.18 to 5.22 suggest that there is a slight difference in the reaction mechanism. However, if the errors in table 5.2 are considered, the conclusion would be that the incorporation of carbon nanoparticles into this resin system does not show any difference in the curing mechanism.

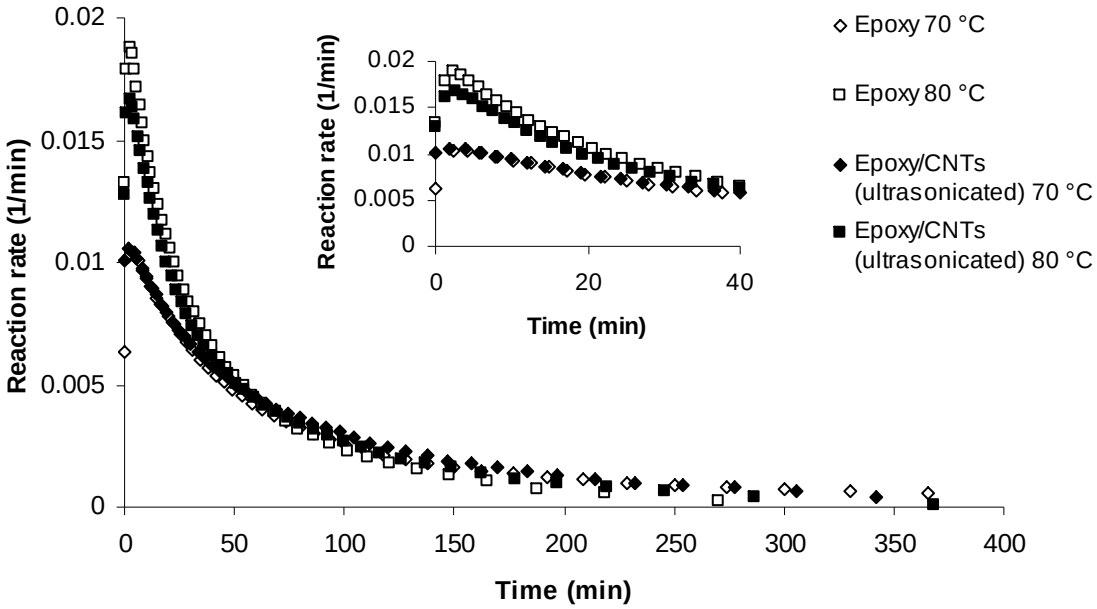

Figure 5.21: Reaction rates time for the MY 750 / HY 5922 resin system and its nanocomposite containing 0.06 wt % of Hyperion carbon nanotubes (batch 5) under isothermal curing conitions at different temperatures

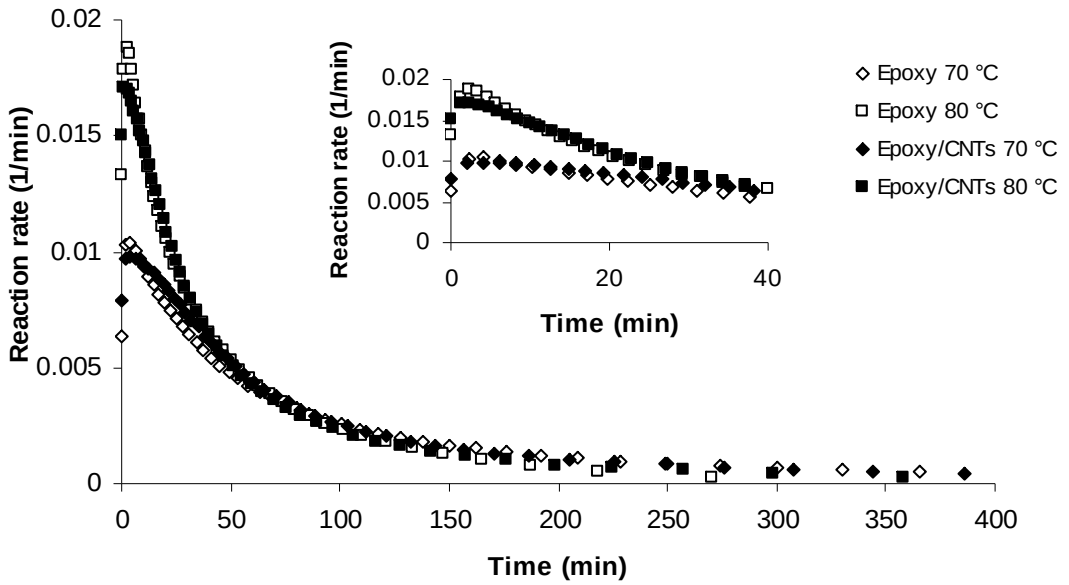

Figure 5.22: Reaction rates versus time for the MY 750 / HY 5922 resin system and its nanocomposite containing 0.06 wt % of Hyperion carbon nanotubes (batch 1) under isothermal cure at different temperatures

5.2.2 Cure characterisation of the MTM 44-1 resin system and its nanocomposites containing Thomas Swan carbon nanotubes and Monarch carbon black particles (batches 6-10)

Calorimetric experiments were performed for the MTM 44-1 resin system under isothermal and dynamic heating conditions. The temperature range for the isothermal tests was between 130-190^{o}C. The reaction rate data are presented in figures 5.23 to 5.25. The isothermal data in figure 5.23 indicate an autocatalytic reaction mechanism (the maximum reaction rates are exhibited at times $t \neq 0$). The dynamic data presented in figure 5.24 show that there are more than one distinct peaks observed. It is thus indicated that the cure kinetics is complicated and contains more than one reaction schemes.

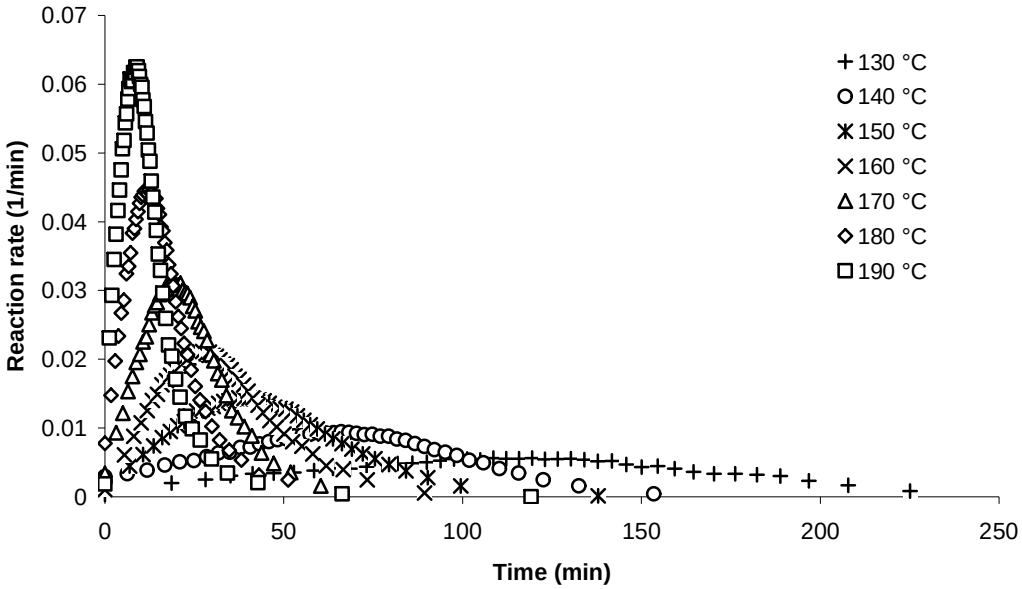

Figure 5.23: Reaction rate versus time for the isothermal cure of the MTM 44-1 resin system at different temperatures

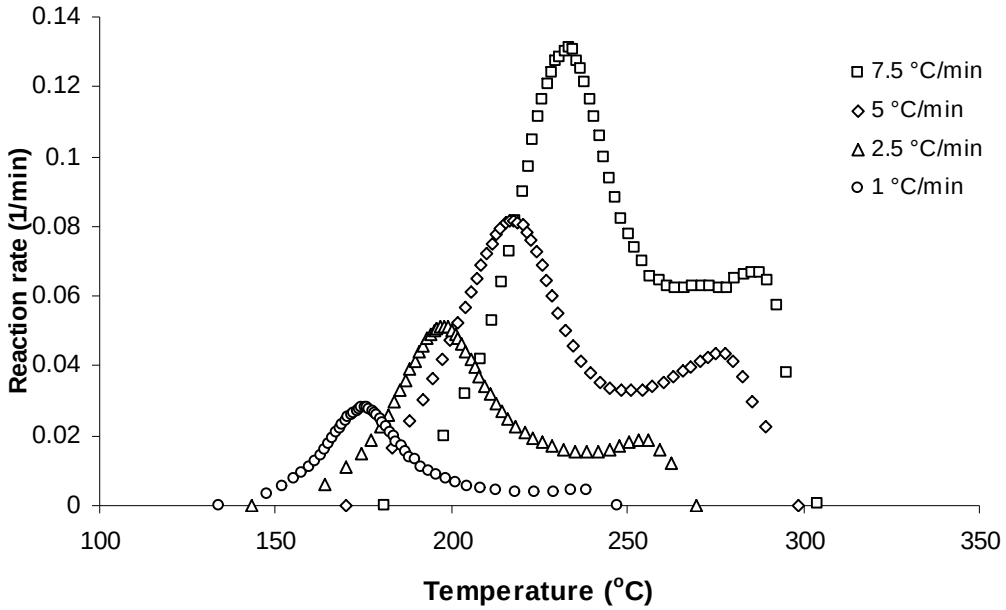

Figure 5.24: Reaction rate versus temperature for the dynamic cure of the MTM 44-1 resin system at constant heating rates

The utilisation of equation 5.1 leads to the estimation of the degree of cure and the reaction rates. Figure 5.25 illustrates the reaction rate versus degree of cure curves for the isothermal cure of the resin system at different temperatures.

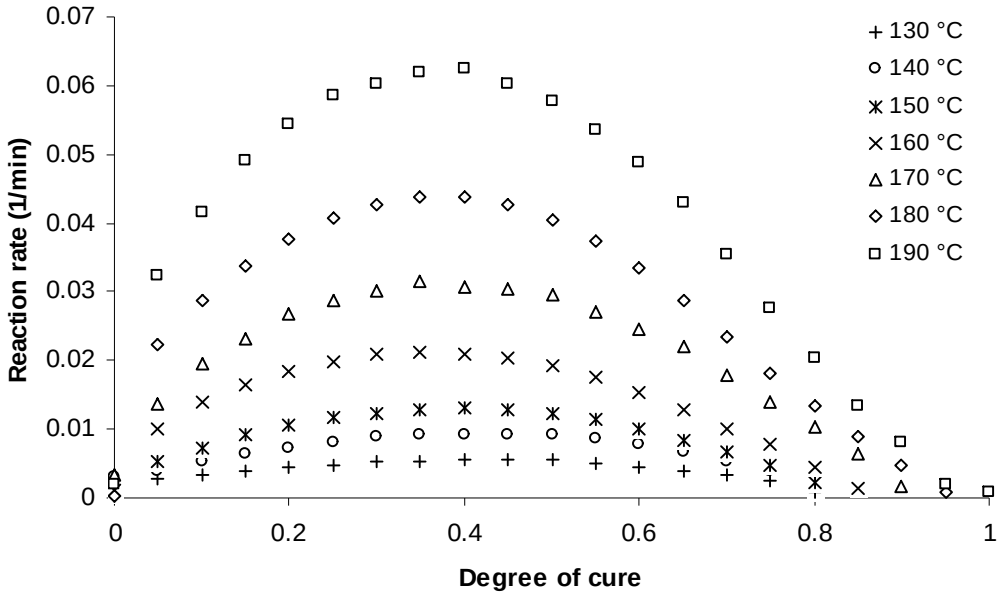

Figure 5.25: Reaction rate versus degree of cure for the isothermal cure of the MTM 44-1 resin system at different temperatures

In figure 5.25 it can be observed that the isothermal tests do not lead to a fully cured material, due to the occurrence of vitrification. This is the reason for the premature termination of the reaction. This phenomenon is controlled by the increase in the glass transition temperature during curing, so when it reaches values around the curing temperature, diffusion limitations occur.

The total heat of reaction, ΔH_T, was evaluated for the neat epoxy resin system, and its nanocomposites, when carbon nanoparticles were incorporated. The results are summarised in table 5.4.

Rate (^{o}C/min)	10	7.5	5	2.5	1	0.5	Average ΔH_T (J/g)	Standard Deviation
MTM 44-1	-	-	484	478	467	457	472	12
MTM 44-1 / 1 wt % CNTs	451	441	446	434	438	-	442	7
MTM 44-1 / 2 wt % CB resin	421	-	442	424	423	-	428	15

Table 5.4: Total heats of reaction under dynamic heating conditions for the neat MTM 44-1 resin and its nanocomposites, containing the Thomas Swan carbon nanotubes and the Monarch carbon black particles (masterbatches 4 and 5) respectively

The average values of the total heats of reaction suggest that the addition of carbon nanoparticles induces a decrease in the total heat of reaction. The errors are not so high for these values of the total heats of the reactions measured. That means that there is a decrease measured in the total heats of reaction when the nanoparticles are incorporated into the resin system. The resin system produced, when the Thomas Swan carbon nanotubes were incorporated was tested under isothermal heating conditions. Some dynamic tests were also conducted in order to measure the total heat of reaction. The nanocomposite that contained carbon black particles was tested only under dynamic heating conditions and was used for comparison.

The isothermal data in figure 5.26 suggest that an autocatalytic reaction mechanism is followed, in the case of the nanocomposite. The dynamic experiments were conducted for heating rates, between 1 and 7.5^{o}C/min. Two reaction rate peaks were observed. These results are presented in figure 5.27. Figure 5.28 illustrates the reaction rate versus degree of cure curves for the addition of carbon nanotubes, while figure 5.29 represents the reaction rate curves for the dynamic cure at different heating rates, when Monarch carbon black particles were incorporated into the epoxy system.

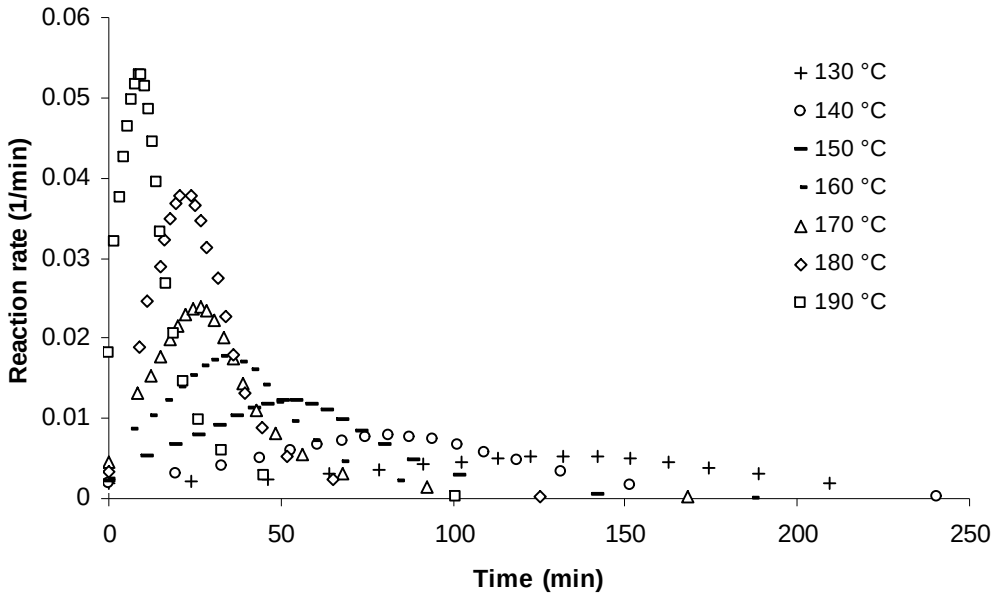

Figure 5.26: Reaction rate versus time for the isothermal cure of the MTM 44-1 resin system containing 1 wt % of Thomas Swan carbon nanotubes (batch 6) at different temperatures

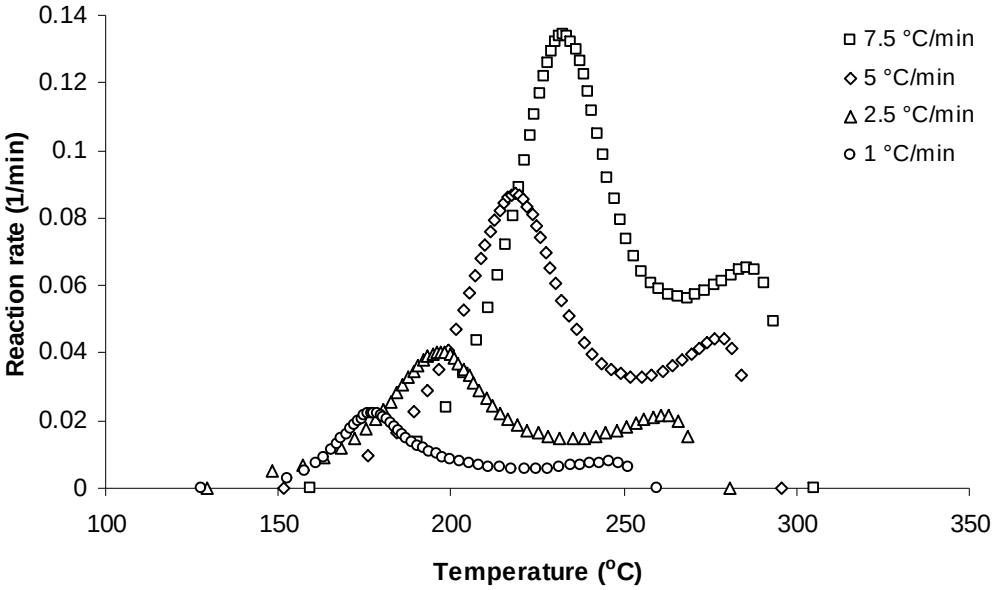

Figure 5.27: Reaction rate versus temperature for the dynamic cure of the MTM 44-1 resin system containing 1 wt % of Thomas Swan carbon nanotubes (batch 6), at constant heating rates

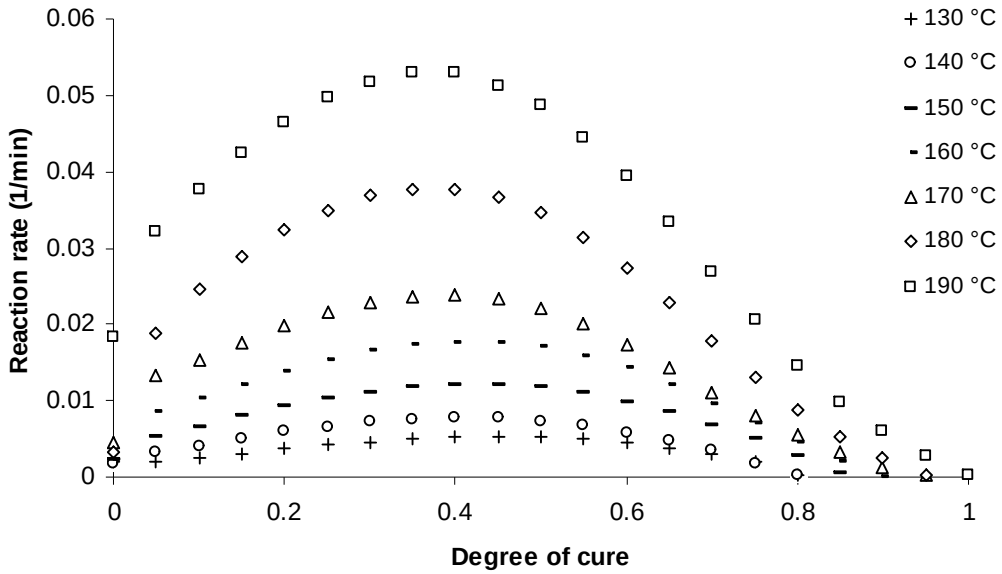

Figure 5.28: Reaction rate versus degree of cure for the isothermal cure of the MTM 44-1 resin system containing 1 wt % of Thomas Swan carbon nanotubes (batch 6) at different temperatures

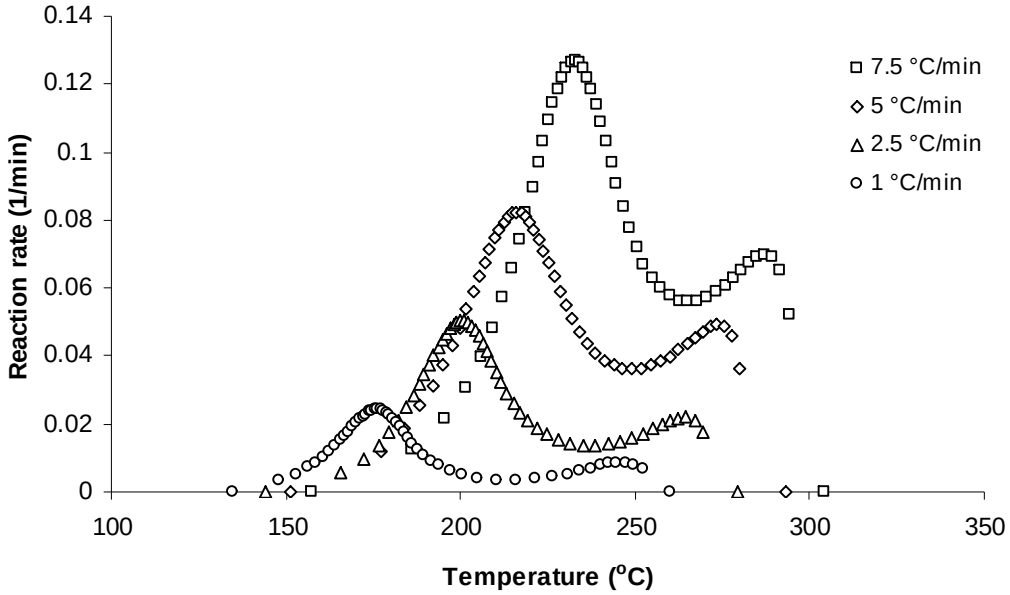

Figure 5.29: Reaction rate versus temperature for the dynamic cure of the MTM 44-1 resin system containing 2 wt % of Monarch carbon black particles (batch 9) at constant heating rates

The dynamic data for the epoxy resin and its nanocomposites when combined provide valuable information about the differences in the reaction mechanism followed. It can be observed from the dynamic experiments that the incorporation of nanoparticles causes a decrease in the reaction rates. There is also a shift of the reaction maxima leading to either slightly higher or lower temperature maxima. Data for the dynamic cure of the resin system and its nanocomposites under dynamic heating conditions are illustrated in figure 5.30. One heating rate was used for convenience (7.5^{o}C/min). The results are also summarised in table 5.5. The experimental errors are 2 %.

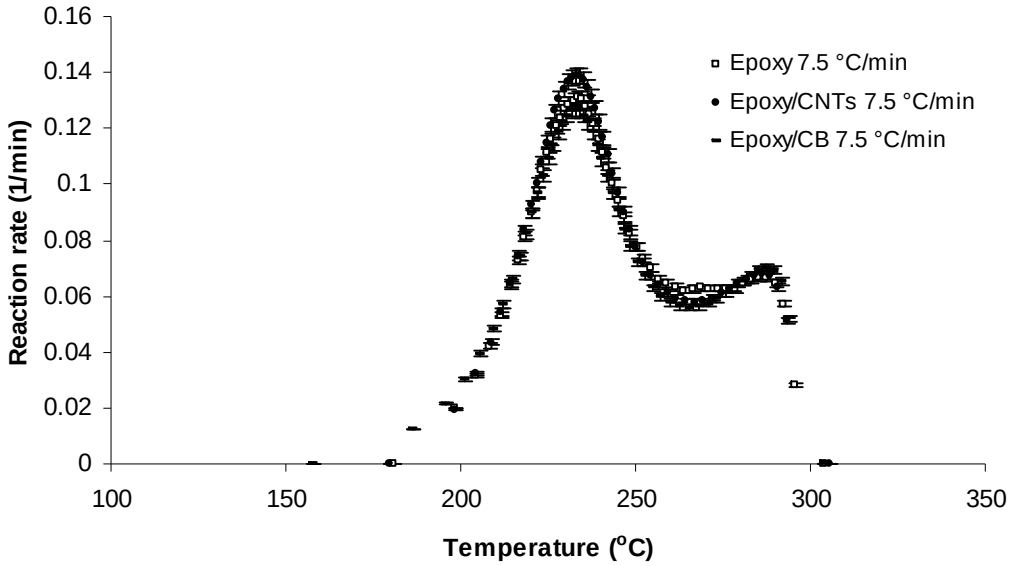

Figure 5.30: Dynamic DSC tests at 7.5°C/min (including experimental errors) for the MTM 44-1 resin system and its nanocomposites containing 1 wt % of Thomas Swan carbon nanotubes and 2 wt % of Monarch carbon black particles (batches 6 and 9)

Rate (°C/min)	7.5	5	2.5	1
T_{max} (°C) MTM 44-1	234	218	199	176
T_{max} (°C) MTM 44-1 / 1 wt % CNTs	234	219	197	177
T_{max} (°C) MTM 44-1 / 2 wt % CB	232	217	199	177

Table 5.5: Temperature maxima of reaction under dynamic heating conditions for the neat MTM 44-1 resin and its nanocomposites, containing carbon nanotubes and carbon black particles (batches 6 and 9), respectively

The decreased reactivity when carbon nanotubes are incorporated into the system is observed by the comparison of the reaction rates under isothermal heating conditions, presented in figure 5.31. The experimental errors are 2 %.

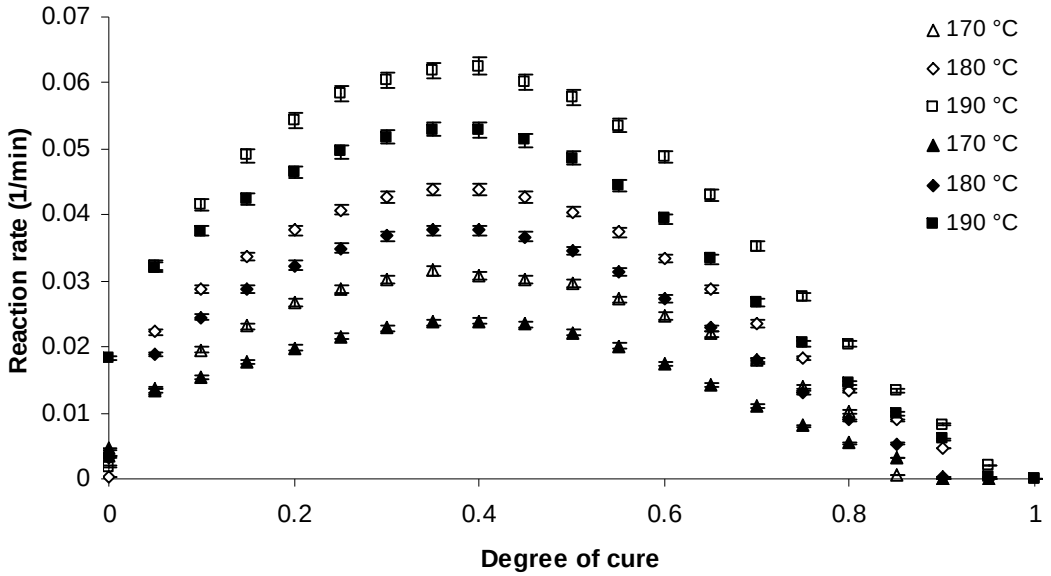

Figure 5.31: Reaction rates versus degree of cure (including the experimental errors) for the MTM 44-1 resin system and its nanocomposite containing 1 wt % of Thomas Swan carbon nanotubes (batch 6) under the isothermal cure at different temperatures

The reaction rates (see figure 5.31) show a decrease with the addition of carbon nanotubes. This is also observed in the results illustrated in figure 5.32 (experimental errors 2 %). It can be observed that the incorporation of carbon nanotubes causes a decelerating effect on the cure reaction. For example, it takes 19 minutes to reach the peak of the curve for the isothermal cure at 160^{o}C in the case of the neat MTM 44-1 resin system. This time is increased to 24 minutes with the incorporation of carbon nanotubes. The trapping effect of the hardener surrounding the carbon nanotubes may be responsible for the drop in the reaction rates [6].

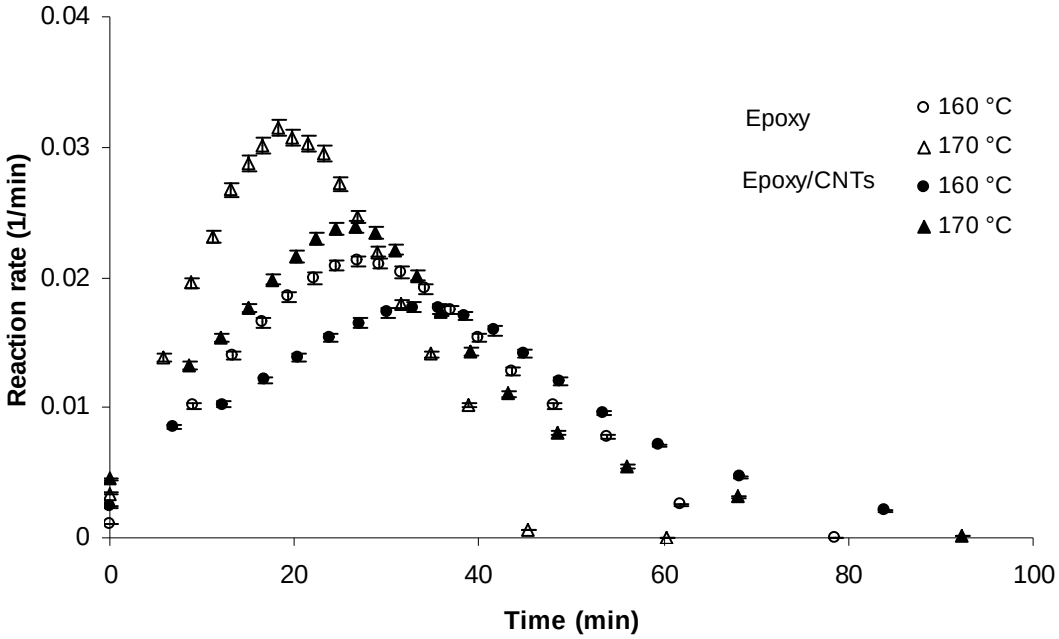

Figure 5.32: Reaction rates versus time (including the experimental errors) for the isothermal cure of the MTM 44-1 resin system and its nanocomposite containing 1 wt % of Thomas Swan carbon nanotubes (batch 6) at different temperatures

It is observed in figure 5.31 that the existence of vitrification is the possible reason for the premature ending of the reaction at the tested temperatures. In order to verify this assumption different isothermal modulated DSC experiments were conducted. When the T_g is found to be in the region of the experimental temperature, that means that vitrification occurs. This is easily observed in figures 5.33 and 5.34. The results are also summarised in table 5.6

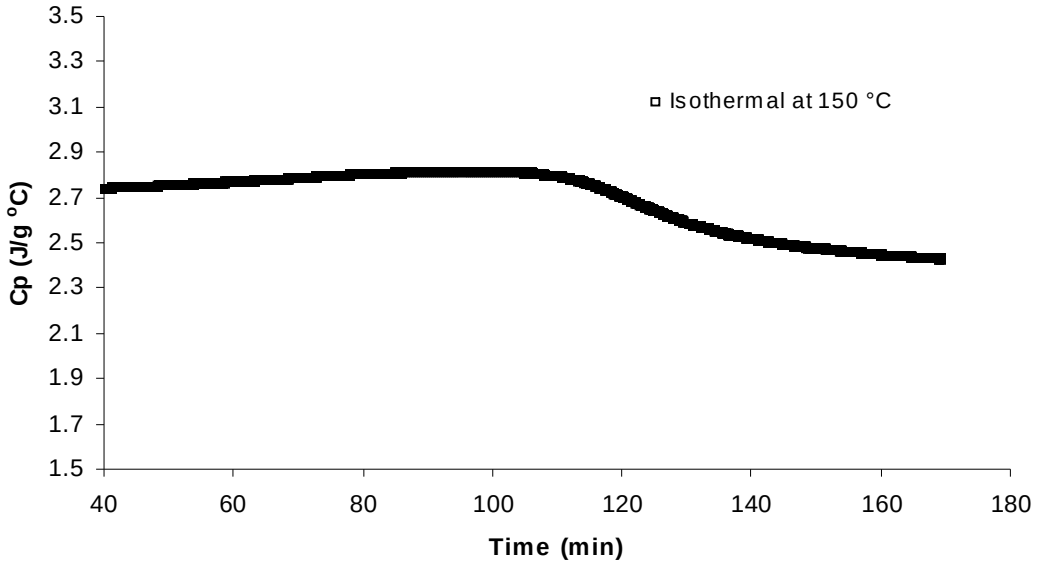

Figure 5.33: Isothermal modulated DSC test at 150°C showing the advancement of vitrification as a function of the curing temperature for the MTM 44-1 resin system (vitrification occurs at 124 minutes)

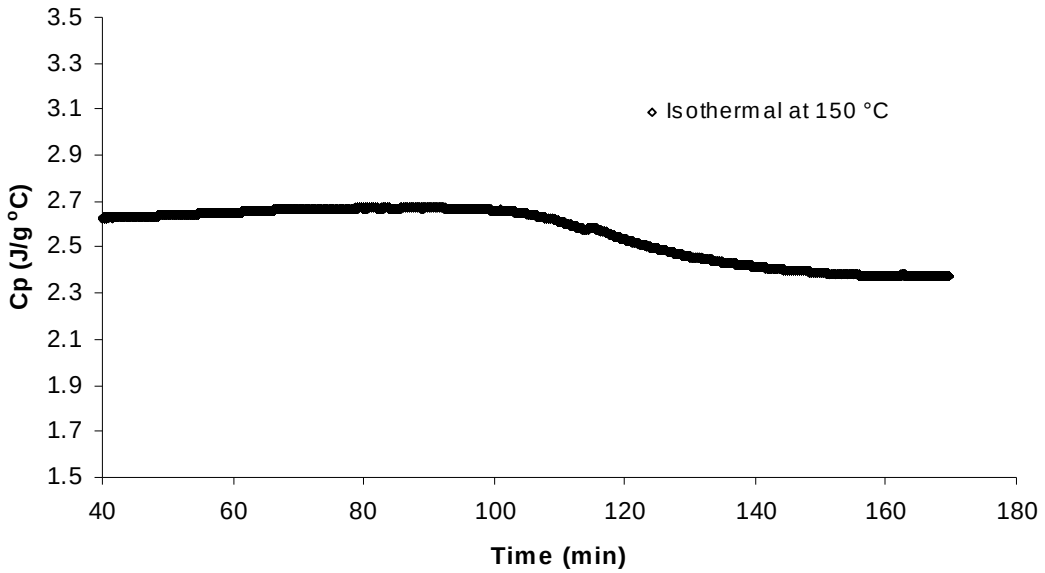

Figure 5.34: Isothermal modulated DSC test at 150°C showing the advancement of vitrification as a function of the curing temperature for the MTM 44-1 resin system containing 1 wt % of Thomas Swan carbon nanotubes (vitrification occurs at 118 minutes)

System / Vitrification time (min)	130°C	150°C	170°C	190°C
MTM 44-1 resin	227	124	79	64
MTM 44-1 / 1 % wt CNTs resin	225	118	77	63

Table 5.6 Vitrification times for the MTM 44-1 resin system and its nanocomposite containing 1 wt % of Thomas Swan carbon nanotubes acquired from a number of isothermal modulated DSC experiments at different cure temperatures

The vitrification times that are summarised in table 5.6 can be combined with the isothermal data of figures 5.33 and 5.34. It is observed from this comparison that at the time that vitrification occurs, the degree of cure at that specific temperature becomes the maximum achieved. For example, the isothermal test at 150°C for the neat resin showed that vitrification occurred at 124 minutes cure time. If a comparison is made between that time and the cure time in figure 5.33, it is seen that the maximum degree of cure is reached at about 123 minutes. This leads to the conclusion that vitrification occurs and terminates the curing reaction at a specific time (prematurely), before a fully cured state of the material can be reached.

5.2.3 Cure characterisation of the 8552 resin system

The 8552 resin exhibits a single peak when cured under dynamic heating conditions. The heating rates tested for the dynamic cure of the resin system were in the range of 1 to 10°C/min. The reaction rate versus time curves show a bell shape, which is common for the autocatalytic reaction mechanism (figure 5.36). Isothermal tests were conducted in the temperature range of 140–200°C (figure 5.35)

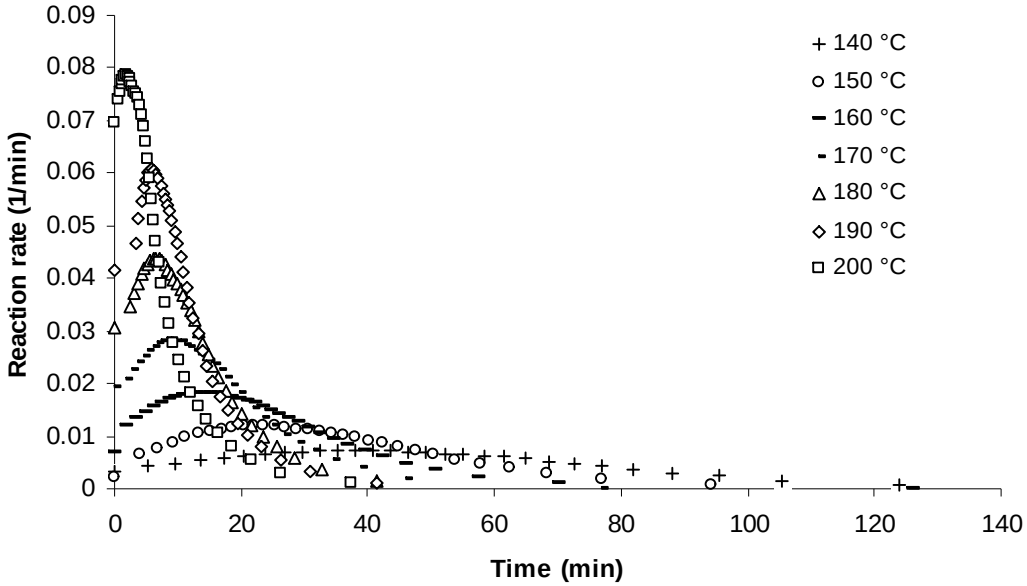

Figure 5.35: Reaction rate versus time for the isothermal cure of the 8552 resin system at different temperatures

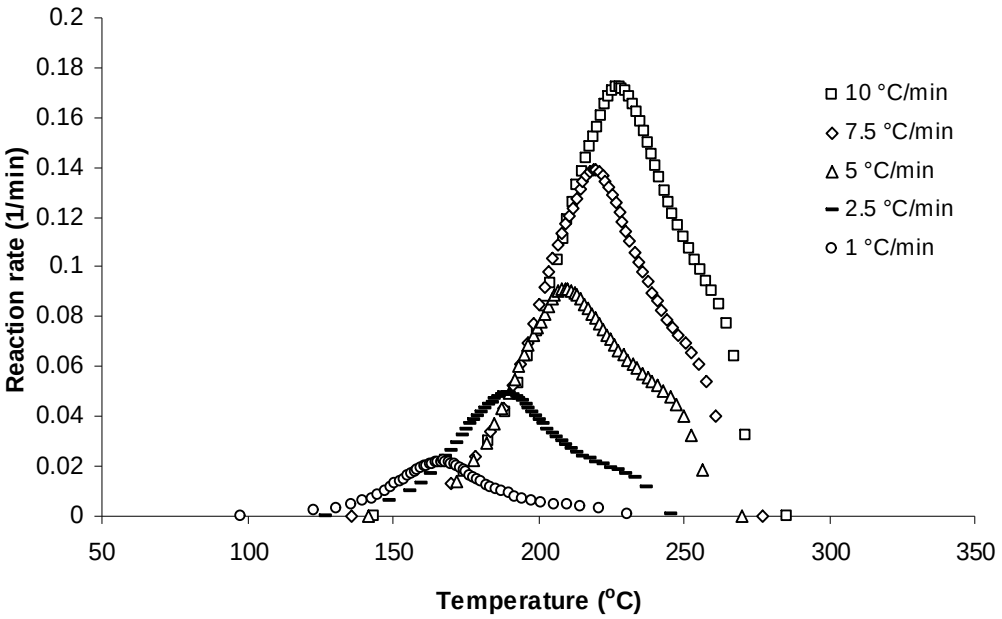

Figure 5.36: Reaction rate versus temperature for the dynamic cure of the 8552 resin system at constant heating rates

The total heat of reaction, ΔH_T, was evaluated for the epoxy resin system by integrating the DSC heat flow versus time curves. The results are summarised in table 5.7.

Rate (^{o}C/min)	10	7.5	5	2.5	1	0.75	Average ΔH_T (J/g)	Standard Deviation
8552 resin	653	640	676	671	639	657	656	15

Table 5.7: Total heats of reaction under dynamic curing experiments for the 8552 resin system

After the calculation of the total heats of the reaction, the degree of cure and subsequently the reaction rates as a function of conversion were estimated. The reaction rate versus degree of cure curves for the isothermal cure of the resin system in the temperature range of 140-200^{o}C are illustrated in figure 5.37.

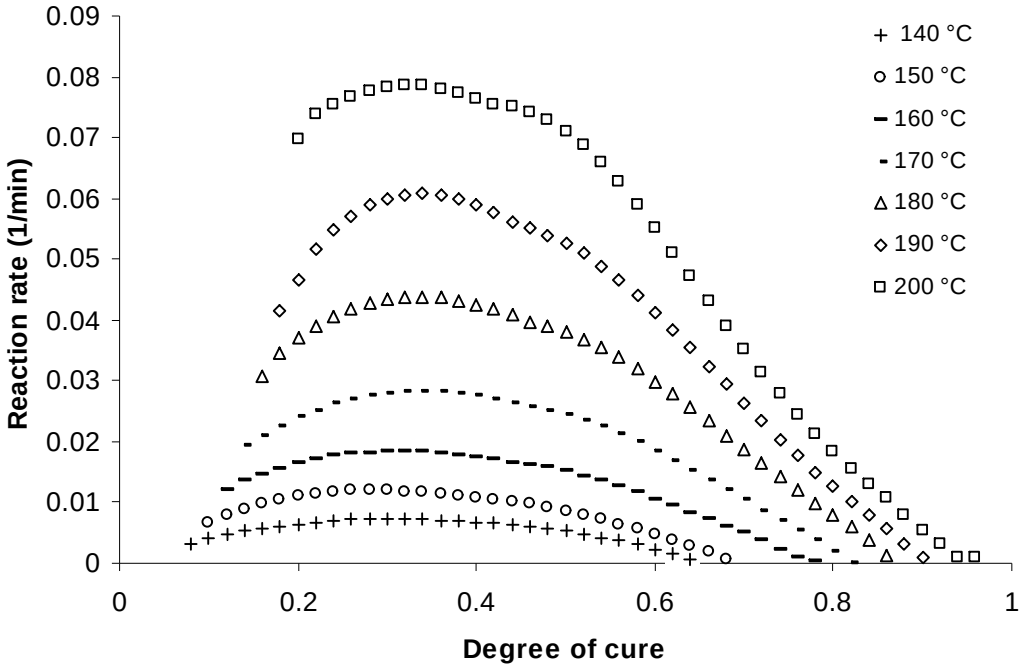

Figure 5.37: Reaction rate versus degree of cure for the isothermal cure of the 8552 resin system at different temperatures

It is observed in figure 5.37 that the reaction starts at a conversion that is higher that 0. That is the case for this system because of the fact that by the time the isothermal temperature is reached, the reaction has already started

(see also analysis of figure 5.5). The initial conversion was calculated from the combination of dynamic and isothermal segments using the analysis presented in paragraph 5.1.

The isothermal cure does not lead to a fully cured material. Vitrification occurs, which imposes mobility limitations and the reaction is terminated prematurely.

5.3 Rheological Experiments of the resin systems

In this part, some rheological measurements of the base systems are presented as a means to calculate the processing window of the systems. The analysis of the experimental method was presented in chapter 3.

5.3.1 Rheological Experiments of MY 750 / HY 5922 resin system

Tests were conducted under isothermal conditions for a range of temperatures. Gelation was considered to have occured when the value of the viscosity reached 10 kPa s [17,47]. The results of the rheological measurements of the MY 750 / HY 5922 resin system for the curing in the temperature range of 80-110^{o}C are presented in figure 5.38 and the gelation times are summarised in table 5.8.

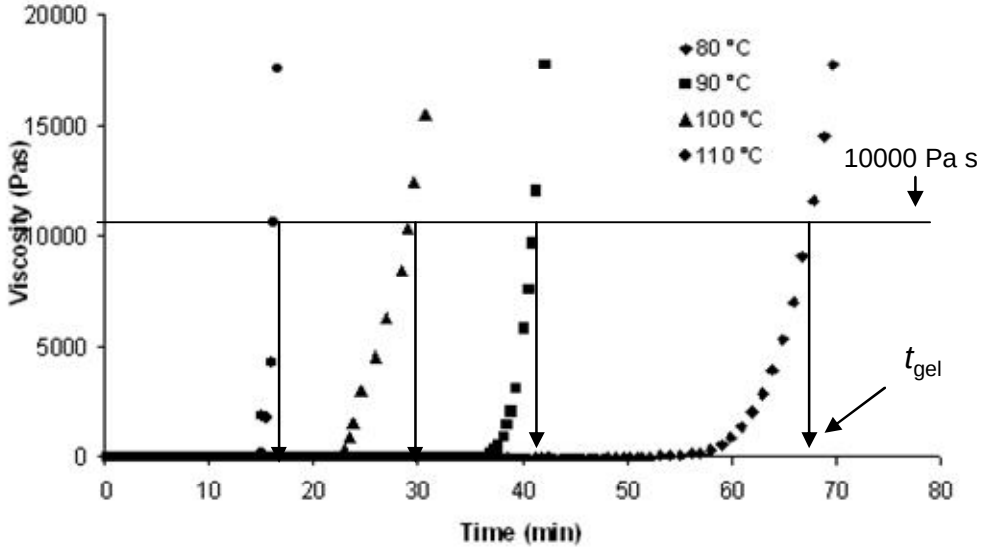

Figure 5.38: Viscosity advancement with cure time for the isothermal cure of MY 750 / HY 5922 resin in the temperature range of 80-110°C

Curing temperature (°C)	80	90	100	110
Gelation times (min)	68	41	28	16

Table 5.8: Gelation times for the isothermal curing of MY 750 / HY 5922 resin in the temperature range of 80-110°C

The evolution of viscosity during the isothermal cure tests shows initially a stable signal up to a specific point where a rapid increase occurs. This rapid increase signifies the gelation region where a significant build up of the crosslinked network occurs. Higher curing temperatures lead to the reduction of the time required for the phenomenon to take place as the reaction progresses much faster. The cure cycle for this resin system suggests that the temperature range for the rheological experiments should be between 40-80°C (see page 40). At 40°C isothermal, it requires up to 7 hours time for the system to gel. Some measurements tested in this temperature failed, due the very slow nature of the reaction, which resulted in a very noisy instrumental signal. It was then considered to test the system to higher temperatures that require less time for gelation to occur.

Based on the results of table 5.8 and the isothermal cure kinetics tests (presented in chapter 7), it was estimated that the average gel conversion of the MY 750 / HY 5922 resin system is 72 % with a standard deviation of 3 %.

5.3.2 Rheological Experiments of MTM 44-1 resin system

The same procedure as in the case of the MY 750 / HY 5922 resin system was followed for the investigation of the MTM 44-1 system. The rheological measurements were conducted isothermally in the temperature range of 140-180^{o}C. The results are presented in figure 5.39 and the gelation times are summarised in table 5.9. The material was first put on the plate and while the temperature of the instrument increased up to the desired value for the isothermal test to start, its viscosity decreased to a minimum. The upper plate was then easily embedded on the surface of the specimen. The same critirion as in the case of the MY 750 / HY 5922 resin system was applied for the determination of the gel point (gelation was considered to occur when viscosity reached the value of 10 kPa s [17,47]). The gelation time t_{gel} is defined as the time that gelation ocuurs (the time that it takes for the viscosity to reach the value of 10 kPas).

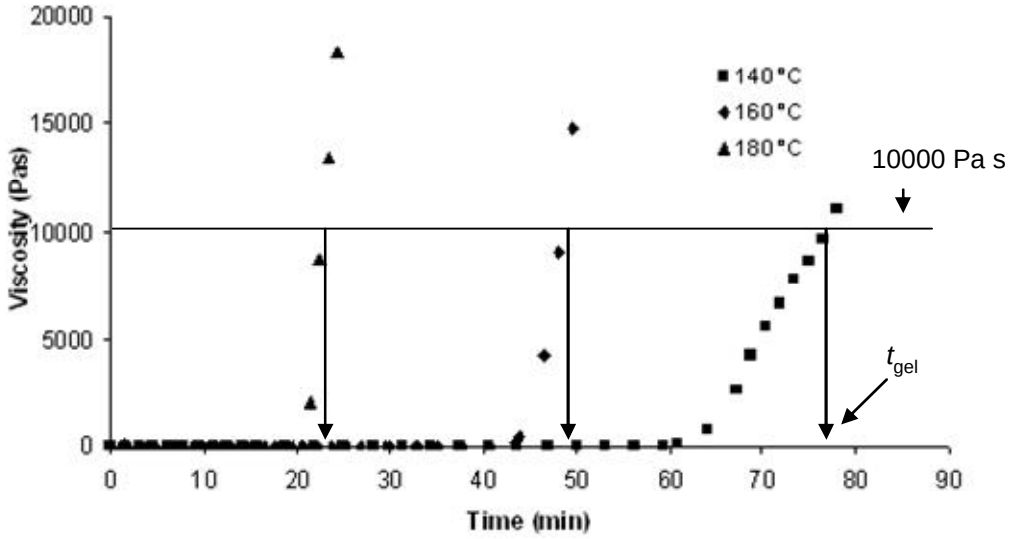

Figure 5.39: Viscosity advancement with cure time for the isothermal cure of the MTM 44-1 resin in the temperature range of 140-180°C

Curing temperature (°C)	140	160	180
Gelation times (min)	80	45	22

Table 5.9: Gelation times for the isothermal curing of MTM 44-1 resin in the temperature range of 140-180°C

Based on the results of table 5.9 and the isothermal cure kinetics data, presented in chapter 7, it was estimated that the average gel conversion of this resin system is 62 % with a standard deviation of 4 %. Available technical data for this resin system, reported from ACG indicate resin gelation time to occur at 150 minutes for the isothermal cure at 130°C [107], which corresponds to a gel conversion value of 60 % according to the cure kinetics model.

5.3.3 Rheological Experiments of 8552 resin system

The rheological measurements for the 8552 resin system were conducted isothermally in the temperature range of 160-190°C. The results are presented in figure 5.40 and the gelation times are summarised in table 5.10.

The same process as in the case of the MTM 44-1 resin was followed to conduct the experiments. Again gelation was considered to occur when viscosity reached the value of 10 kPa s.

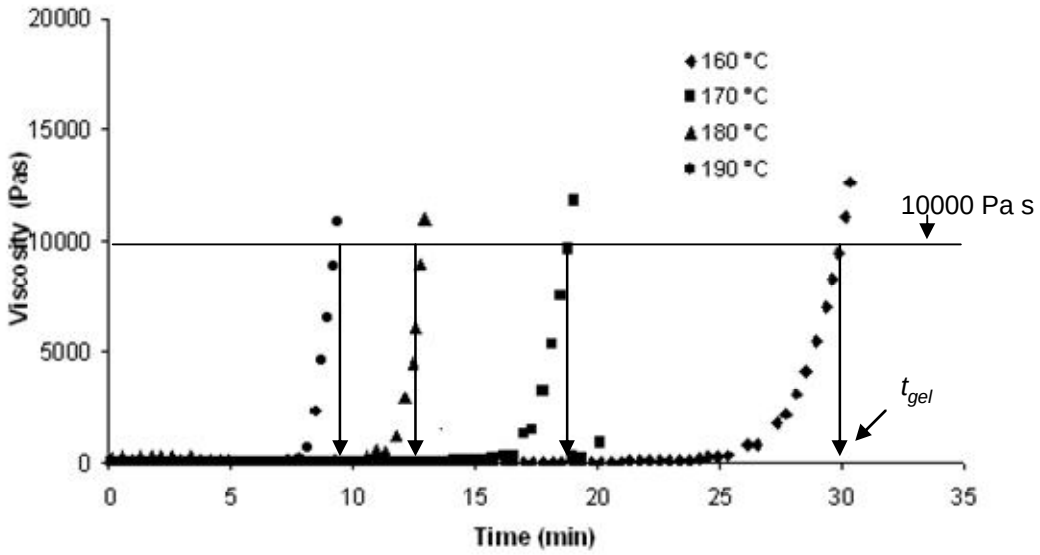

Figure 5.40: Viscosity advancement with cure time for the isothermal cure of the 8552 resin in the temperature range of 160-190^{o}C

Curing temperature (^{o}C)	160	170	180	190
Gelation times (min)	29	19	13	10

Table 5.10: Gelation times for the isothermal curing of 8552 resin in the temperature range of 160-190^{o}C

The results illustrated in table 5.10 when combined with the isothermal cure kinetics data, presented in chapter 7, allowed for the estimation of the average gel conversion, which was found to be 64 % with a standard deviation of 2 %. Available technical data about this resin system, reported from Hexcel Composites indicate resin gelation time to occur at 12 minutes for the isothermal cure at 180^{o}C [108], which corresponds to a gel conversion value of 65 % according to the cure kinetics model.

Chapter 6

6. Glass Transition Temperature Advancements of the Resin Systems and their Nanocomposites

In this chapter the glass transition temperature advancement of the resin systems and their nanocomposites is presented. A direct comparison is attempted and the differences observed are discussed.

6.1 Glass transition temperature advancements of the MY 750 / HY 5922 resin system and its nanocomposites containing Hyperion carbon nanotubes and Monarch carbon black particles (batches 1-5)

Initially, two equations were established to simulate the glass transition temperature (T_g) advancement during the cure of epoxy-amine systems. These are the DiBenedetto equation [132], which is based on thermodynamic considerations and the Havlicek-Dusek equation [16,132], which is purely empirical. The analytical form of the DiBenedetto equation is presented below:

$$Tg(\alpha) = Tgo + \frac{w\alpha(Tg\infty - Tgo)}{1 + (1-w)\alpha} \qquad (6.1)$$

where T_{go} is the glass transition temperature of the uncured sample, $T_{g\infty}$ the glass transition temperature of the fully cured sample, α the specific conversion and w a fitting parameter. The empirical Havlicek-Dusek equation has the following form:

$$\frac{1}{Tg(\alpha)} = \frac{1-\alpha}{Tgo} + \frac{\alpha}{Tg\infty} + U\alpha(1-\alpha) \qquad (6.2)$$

where U is a fitting parameter. In the case of the neat epoxy system none of these models can predict with accuracy the advancement of the glass transition temperature. The T_g evolution as a function of degree of cure for the MY 750 / HY 5922 resin system is illustrated in figure 6.1.

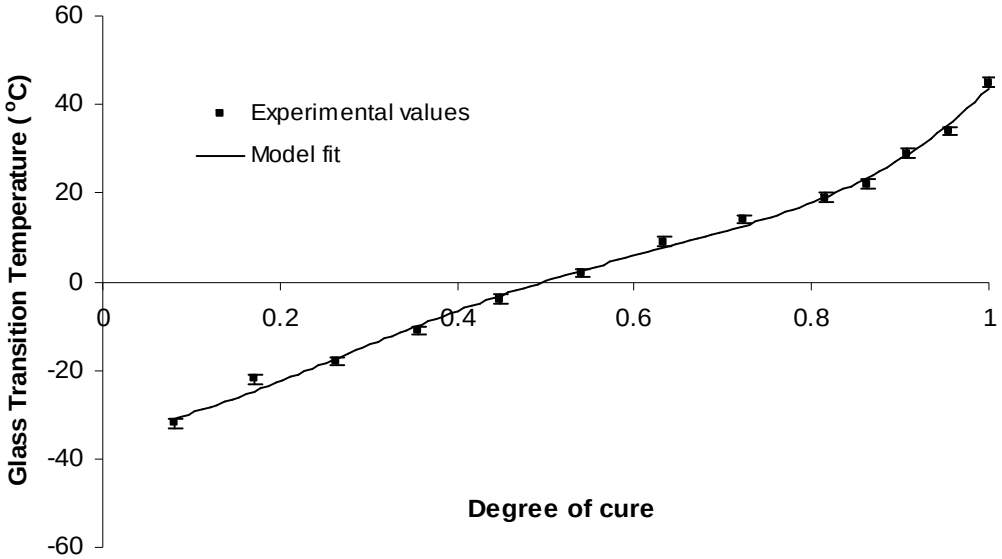

Figure 6.1: Superposition of experimental glass transition temperature values (including experimental errors) and predicted values utilising the empirical polynomial equation 6.3 for the MY 750 / HY 5922 resin system

The glass transition temperature evolution is well predicted by using a polynomial fourth order equation of the form:

$$T_g(\alpha) = 291.6\alpha^4 - 519.3\alpha^3 + 288.1\alpha^2 + 17.1\alpha - 33.8 \quad (6.3)$$

This equation simulates the T_g evolution very well in accordance to the experimental data. It is noticed in figure 6.1 that the value of the uncured resin T_{go} is -32°C and the one of the fully cured, T_{goo} is 45°C. The same procedure was followed to identify vitrification and its advancement during cure when carbon nanotubes (with and without ultrasonication treatment) and carbon black particles were incorporated into the epoxy system. The total heats of reaction and the values of the glass transition temperatures that correspond to the uncured and the fully cured specimens, together with the standard deviations are summarised in table 6.1. The nanocomposite that incorporated the Hyperion carbon nanotubes and was prepared with the utilisation of the ultrasonic horn and mixed by hand is named ultrasonicated. All the other specimes were prepared by shear mixing.

Ratios	ΔH_T (J/g)	T_{go} (^{o}C)	T_{goo} (^{o}C)
MY 750 / HY 5922	344±16	-32±1	45±1
MY 750 / HY 5922 0.06 wt % CNTs resin	318±18	-43±1	40±1
MY 750 / HY 5922 0.06 wt % CNTs (ultrasonicated)	360±13	-45±1	51±1
MY 750 / HY 5922 0.12 wt % CNTs	284±20	-46±1	45±1
MY 750 / HY 5922 0.5 wt % CB	324±15	-28±1	42±1
MY 750 / HY 5922 1 wt % CB	310±20	-34±1	41±1

Table 6.1: Total heats of reactions and glass transition temperature values corresponding to the MY 750 / HY 5922 resin system and its nanocomposites dispersed with the Hyperion carbon nanotubes (ultrasonicated and non-ultrasonicated) and the Monarch carbon black particles respectively (batches 1-5)

The results in table 6.1 show that the reproducibility of the measurements (±1^{o}C) is very good. That suggests that the values of the glass transition temperature measurements are valid for a direct comparison. The glass transition temperature advancements as a function of the degree of cure for the epoxy resin and its nanocomposites, when carbon nanotubes and carbon black particles are incorporated, are presented in figures 6.2 to 6.4. The values start at a value of the degree of cure which is greater than 0 % (see page 91).

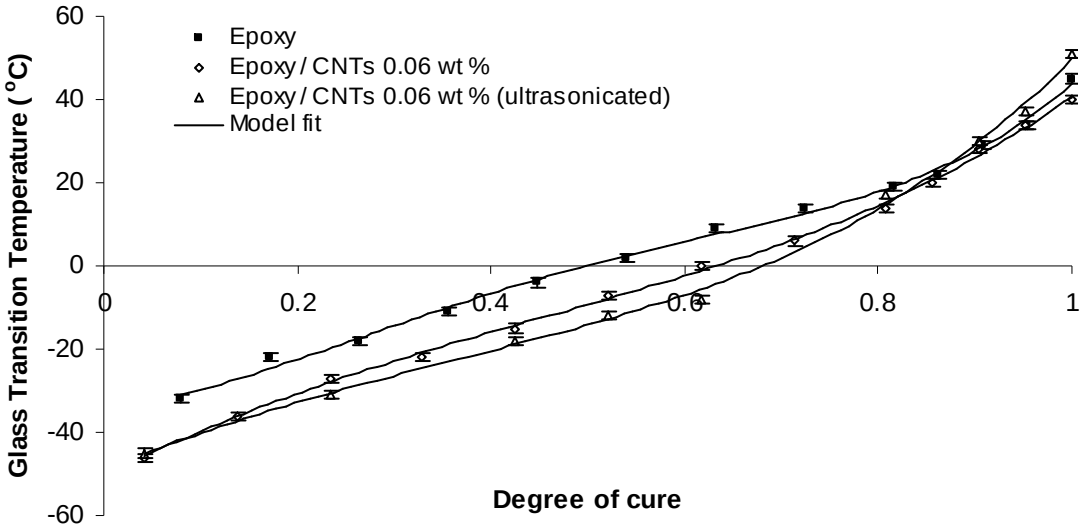

Figure 6.2: Superposition of experimental (including experimental errors) and simulated values of glass transition temperatures as a function of the degree of cure for the MY 750 / HY 5922 resin system and its nanocomposites containing 0.06 wt % of Hyperion carbon nanotubes (batches 1 and 5)

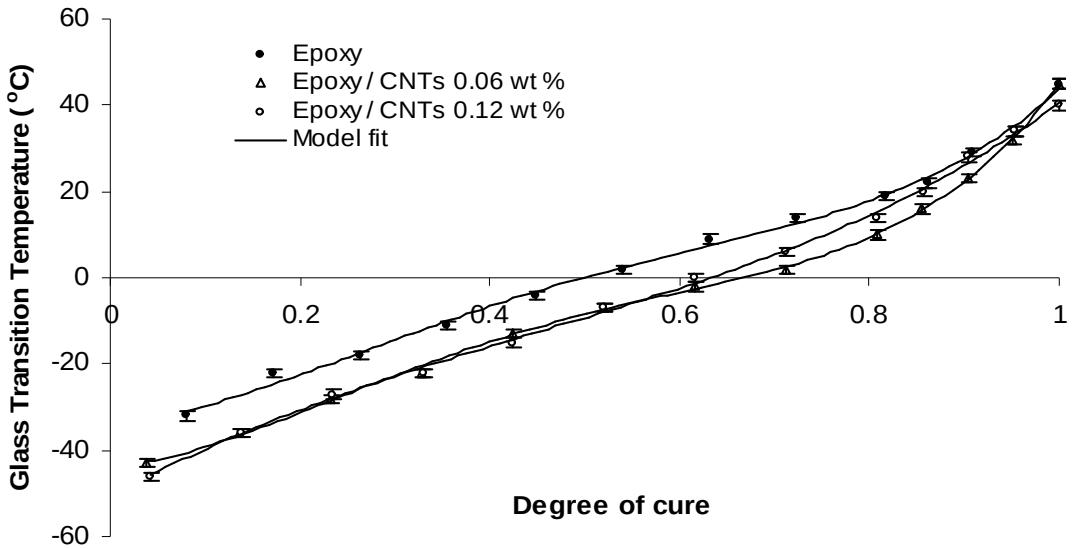

Figure 6.3: Superposition of experimental (including experimental errors) and simulated values of glass transition temperatures as a function of the degree of cure for the MY 750 / HY 5922 resin system and its nanocomposites containing 0.06 and 0.12 wt % of Hyperion carbon nanotubes (batches 1 and 2)

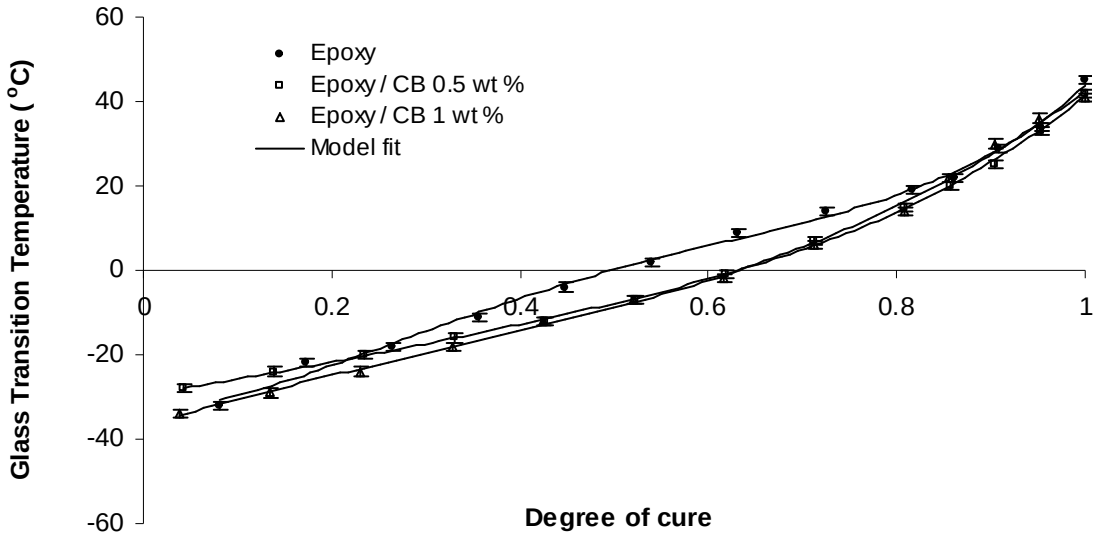

Figure 6.4: Superposition of experimental (including experimental errors) and simulated values of glass transition temperatures as a function of the degree of cure for the MY 750 / HY 5922 resin system and its nanocomposites containing 0.5 and 1 wt % of Monarch carbon black particles (batches 3 and 4)

The models utilised to simulate the glass transition temperature advancement are empirical fourth order polynomial equations. Their parameter values are summarised in table 6.2.

Ratios	α^4	α^3	α^2	α	Intercept
MY 750 / HY 5922	291.6	-519.3	288.1	17.1	-33.8
MY 750 / HY 5922 0.06 wt % CNTs	25.4	48.2	-99.5	117.1	-50.5
MY 750 / HY 5922 0.06 wt % (ultrasonicated) CNTs	46.7	39.5	-82.5	95.1	-48.9
MY 750 / HY 5922 0.12 wt % CNTs	392	-653.8	330.4	20	-43.9
MY 750 / HY 5922 0.5 wt % CB	82.6	-94.4	52.5	29.9	-29.2
MY 750 / HY 5922 1 wt % CB	16.8	46.66	-53	69.3	-37

Table 6.2: Fitting parameters of the empirical polynomial relationships simulating the glass transition temperature advancements

Figure 6.2 illustrates the glass transition temperature advancement of the MY 750 / HY 5922 resin system and the nanocomposites that contain 0.06 wt % of Hyperion carbon nanotubes, prepared by 1) shear mixing and 2) with the utilisation of the ultrasonic horn and mixed by hand (ultrasonicated). The incorporation of carbon nanotubes leads to lower initial values of T_{go} (see also table 6.1) which are almost the same (-45 to -46^{o}C in both cases, -32^{o}C for the neat system). This trend is followed up to 80 % conversion. At this specific conversion, there is a divergence. The nanocomposite that was prepared by shear mixing ends up in a value of T_{goo}= 40^{o}C, while the one which underwent ultrasonication treatment increased at 51^{o}C (45^{o}C for the neat system). The ultrasonication treatment increased the final glass transition temperature by 6^{o}C, compared with the T_g of the bulk system and by 11^{o}C compared to the

nanocomposite prepared by shear mixing. This increase is attributed to the better state of the dispersion of the nanotubes as the result of the ultrasonication treatment. On the other hand, the decrease in the final glass transition temperature is based on the fact that inferior dispersion is achieved (formation of clusters).

Figure 6.3 illustrates the results of the incorporation of different concentrations of Hyperion carbon nanotubes prepared by shear mixing. The evolution of the glass transition temperature is the same with the 0.06 wt % concentration (also presented in figure 6.2) up to 60 % conversion. After that specific conversion, where a divergence is noticed, the nanocomposite containing 0.12 wt % CNTs resulted in a final T_{goo} value of 45^{o}C (see also table 6.1). The same applies for the two concentrations of carbon black particles incorporated (figure 6.4) that resulted at fully cured T_{goo} of 41 and 42^{o}C respectively. Their initial values of T_{go} were almost the same with those of the neat system.

In order to understand the mechanism that affects the evolution of the glass transition temperatures, different ratios of the neat resin with the amine hardener were tested. That was based on the observations of Vanlandingham et al [133], who reported that when the ratio of the epoxy resin to the amine hardener increased, a reduction in the values of the glass transition temperatures of the fully cured resin were noticed. The uncured T_g values, the fully cured and the total heat of the reaction were measured for different ratios. A first scan of the neat epoxy resin (without any amine hardener) revealed a T_g of -16^{o}C. When the epoxy resin and the amine hardener are mixed together, they end up in an initial value of the glass transition temperature of -32^{o}C, which is attributed to the mixing process (T_g of amine hardener -80^{o}C). The epoxy to amine content ratios tested and the values measured that correspond to the uncured T_{go}, the fully cured T_{goo} and the respective total heats of the reaction are presented in table 6.3.

Ratios (epoxy to amine)	ΔH_T (J/g)	T_{go} (^{o}C)	T_{goo} (^{o}C)
100 / 55	344	-32±1	45±1
100 / 53.5	-	-34±1	-
100 / 49.5	325	-36±1	31±1
100 / 44	285	-39±1	21±1
100 / 22	-	-45±1	-

Table 6.3: Total heats of reaction and glass transition temperature values corresponding to the neat resin at different ratios tested

It is interesting to note that when the amine hardener is reduced by 10 % (ratio 100 / 49.5) a reduction in the total heat of reaction by 10 % is observed. Also the T_{go} decreases 4^{o}C and the $T_{g\infty}$ value decreases by 14^{o}C. When an additional 10 % of the amine hardener is reduced, another 10 % reduction to the total heat of the reaction is observed. The theory suggests that when carbon nanoparticles are incorporated into a resin system two main phenomena take place [129,130]:

1) Consumption of the amine hardener, which results in a reduction of the reactivity and consequently a reduction of T_g
2) Mobility limitations which do not allow the chain groups to move freely, which results in an increase of the T_g

As far as the T_{go} is concerned the addition of the carbon nanotubes leads to a reduction of 10-13^{o}C (this reduction of the glass transition temperature is going to be discussed in chapter 10 in details). The same effect is observed when the ratio of the resin and the hardener is reduced (see table 6.3). During the curing reaction the hardener is consumed. The carbon nanotubes (and the carbon black particles) release some hardener resulting in a smaller amount attached to them as the curing reaction comes to an end. At that point the consumption of the hardener results in the reduction of the final $T_{g\infty}$, but at the same time mobility limitations do not allow the chain groups to move freely, which results in an increase of the T_g. In the case of the 0.06 wt % concentration of incorporated carbon nanotubes (by shear mixing) there is a reduction in the T_{goo} of the fully cured resin, compared to the neat system,

which means that the effect of the reduction of the reactivity prevails to the effect of the mobility limitations. The mobility limitations, however, prevail in the case of a good dispersion achieved (for the same concentration of carbon nanotubes, after the ultrasonication process), which results in an increased glass transition temperature [74]. The 0.12 wt % concentration of carbon nanotubes incorporated by shear mixing, lead to the same value of $T_{g\infty}$ with the neat resin (45^{o}C) due to the fact that none of the above mentioned phenomena prevails over another. In the two concentrations of carbon black particles tested, the T_{goo} values were 3 and 4^{o}C lower, respectively, than that of the neat resin. In this case the effect of the reduction of the reactivity prevails to the effect of the mobility limitations, a reduction in the final value of the glass transition temperature is observed. Similar results are reported in [12,74,94].

6.2 Glass transition temperature advancements of the MTM 44-1 resin system and its nanocomposites containing Thomas Swan carbon nanotubes and Monarch carbon black particles (batches 6-10)

The glass transition temperature advancement as a function of the degree of cure for the MTM 44-1 resin system is illustrated in figure 6.5.

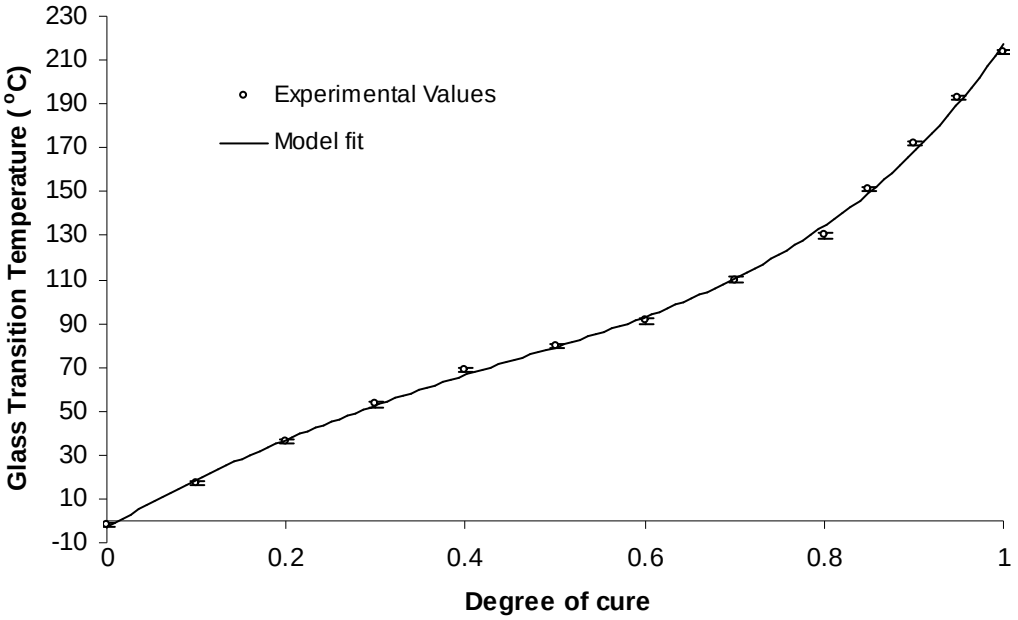

Figure 6.5: Superposition of experimental glass transition temperature values (including experimental errors) and predicted values for the MTM 44-1 resin system, utilising the empirical polynomial equation 6.4

The glass transition temperature advancement can be modelled by a polynomial fourth order equation:

$$T_g(\alpha) = 249.1\alpha^4 - 135.9\alpha^3 - 120.5\alpha^2 + 227.3\alpha - 3 \qquad (6.4)$$

The glass transition temperature of the uncured resin T_{go} is -2 ^{o}C and of the fully cured, T_{goo}, 214 ^{o}C. The same procedure, as this used for the MY 750 / HY 5922 resin system was followed to identify the glass transition temperature advancement for the resin when carbon nanotubes and carbon black particles were incorporated. Table 6.4 illustrates the total heats of reaction and the values of glass transition temperatures that correspond to the uncured and the fully cured systems.

Ratios	ΔH_T (J/g)	T_{go} (^{o}C)	T_{goo} (^{o}C)
MTM 44-1 resin	472±12	2±1	214±1
MTM 44-1 / 1 wt % CNTs resin (*)	442±17	-2±1	202±1
MTM 44-1 / 2 wt % CNTs resin	428±13	-1±1	207±1
MTM 44-1 / 1 wt % CB resin	459±11	2±1	212±1
MTM 44-1 / 2 wt % CB resin	441±15	-1±1	215±1

(*) the 1 wt % concentration of Thomas Swan carbon nanotubes was also dispersed in the MTM 44-1 resin system with the utilisation of the ultrasonic bath, mixing by hand and use of the ultrasonic horn (batch 10). It showed an initial T_{go} of 8^{o}C (final T_{goo}=204^{o}C) and the total heat of reaction measured was 427 J/g. This indicated that the specimen had already started curing and it was not further tested.

Table 6.4: Total heats of reactions and glass transition temperature values corresponding to the MTM 44-1 resin system and its nanocomposites containing Thomas Swan carbon nanotubes and Monarch carbon black particles, respectively (batches 6-10)

The values of the glass transition temperatures measured are reproducible, showing an error of ±1^{o}C. The values of the total heats of reactions statistically show a variation, which is within the experimental error. That means that there is difference in the values, leading to a reduction of the total heats of reaction when the carbon nanoparticles are incorporated into the system.

The glass transition temperature advancement as a function of the degree of cure for the epoxy system and its nanocomposites containing carbon nanotubes and carbon black particles are presented in figures 6.6 and 6.7, respectively. In order to illustrate the differences, the model fits are shown in different figures (figures 6.8 and 6.9).

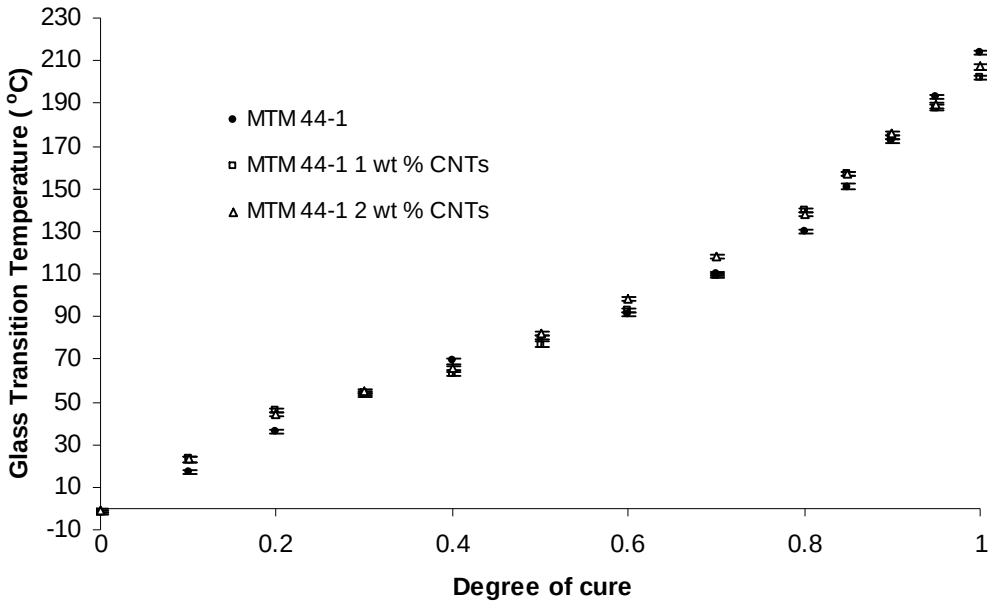

Figure 6.6: Glass transition temperatures (including the experimental errors) as a function of the degree of cure for the MTM 44-1 resin system and the MTM 44-1 nanocomposites containing 1 and 2 wt % Thomas Swan carbon nanotubes (batches 6,7)

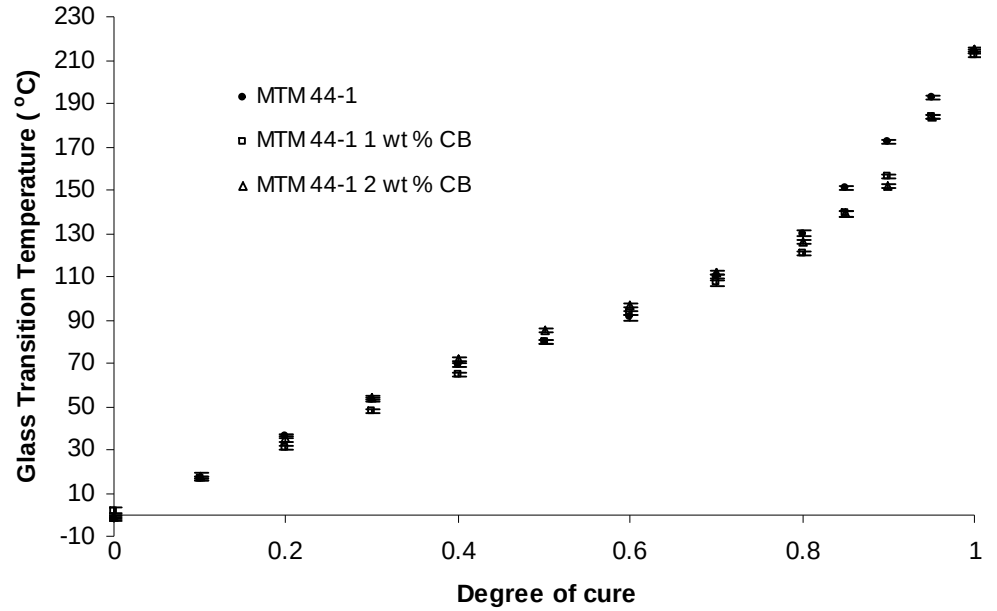

Figure 6.7: Glass transition temperatures (including the experimental errors) as a function of the degree of cure for the MTM 44-1 resin system and the MTM 44-1 nanocomposites containing 1 and 2 wt % Monarch carbon black particles (batches 8,9)

Based on the results summarised in table 6.4 and presented in figures 6.6 and 6.7, it is observed that the addition of carbon nanotubes decreases the T_g of the fully cured specimens by 12^{o}C for the 1 wt % concentration and by 7^{o}C for the 2 wt % concentration of carbon nanotubes, respectively. Similarly to the MY 750 / HY 5922 nanocomposites, there are two phenomena that take place during the later stages of the curing reaction; trapping effect of the amine hardener and the immobilisation of the polymer chains due to the presence of carbon nanotubes. In this case the trapping effect of the hardener is the phenomenon that prevails, resulting in decreased values of the final glass transition temperatures [129,130]. However, this is not the case for the carbon black particle incorporation, where similar values to the neat epoxy resin were obtained (only the 1 wt % concentration of carbon black particles showed a decrease of 3^{o}C). The initial T_{go} values decrease by 4^{o}C with the addition of carbon nanoparticles, except for the 1 wt % carbon black particle concentration. For the carbon black particle addition, the trapping effect caused is counterbalanced by the immobilisation of the polymer chains, leading to similar T_g values as the neat resin system [74]. Further treatment of the nanocomposite containing 1 wt % of Thomas Swan carbon nanotubes (ultrasonication treatment, similar to that of the MY 750 / HY 5922 nanocomposites – also see table 6.4) could not be achieved due to the very viscous nature of the resin. The achievement of a better state of dispersion might lead to increased final glass transition temperatures, but limitations occur due to phase separation. For this case though, it seems that the carbon nanoparticles consume some of the curing agent, leading to a reduction in the final T_g [12,94]. This immobilisation effect of the polymer chains that results in the further enhancement of the glass transition temperatures is not able to prevail over the previous phenomenon.

The model values of the fourth order polynomial equations utilised to simulate the glass transition temperature advancements are summarised in table 6.5 and presented in figures 6.8 and 6.9.

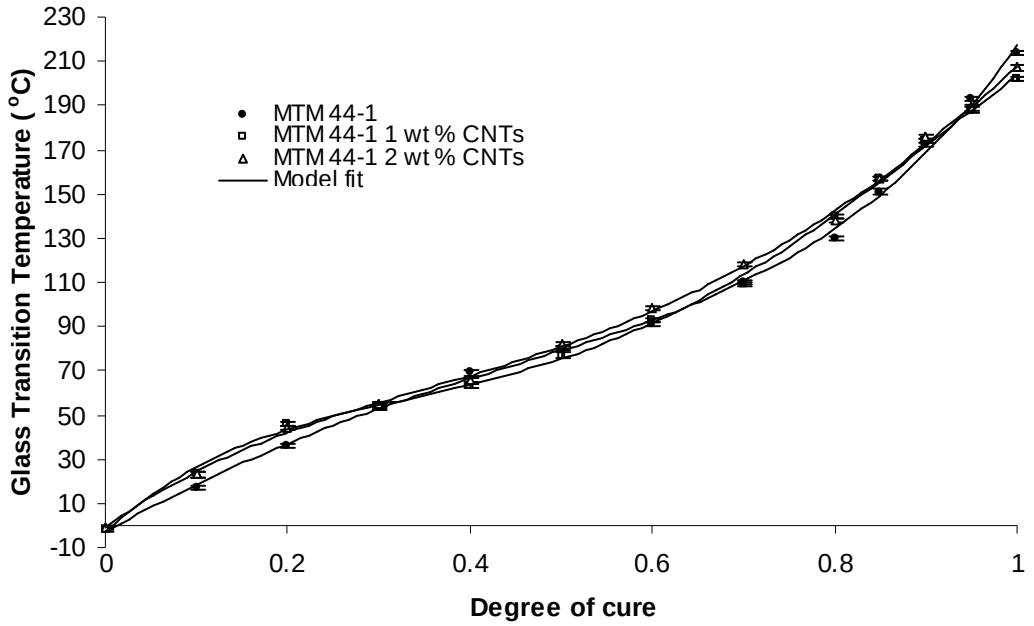

Figure 6.8: Superposition of experimental and simulated values of glass transition temperatures (including the experimental errors) as a function of the degree of cure for the MTM 44-1 resin system and and the concentrations of Thomas Swan carbon nanotubes tested (batches 6,7)

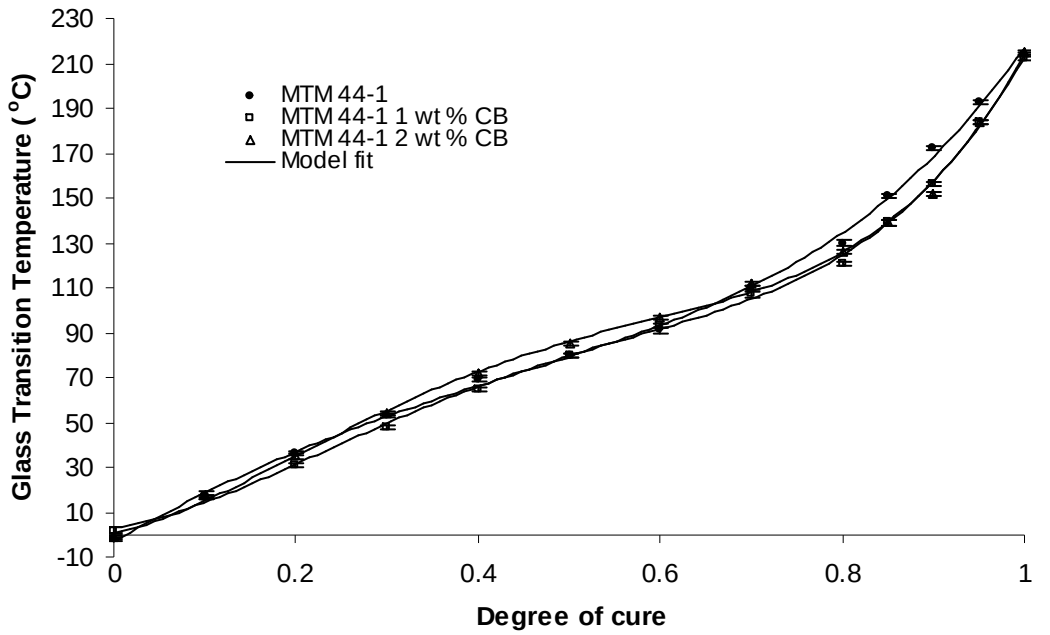

Figure 6.9: Superposition of experimental and simulated values of glass transition temperatures as a function of the degree of cure for the MTM 44-1 resin system and the concentrations of Monarch carbon black particles tested (batches 8,9)

Ratios	α^4	α^3	α^2	α	Intercept
MTM 44-1	249.1	-135.8	-120.5	227.3	-3.0
MTM 44-1 1 wt % CNTs	-537.7	1355.8	-993.7	382.3	-3.2
MTM 44-1 2 wt % CNTs	-221.1	704.0	-580.1	306.1	-1.3
MTM 44-1 1 wt % CB	826.7	-1313.0	635.3	60.1	3.2
MTM 44-1 2 wt % CB	920.5	-1450.0	648.2	94.7	0.4

Table 6.5: Fitting parameters of the empirical polynomial relationships simulating the glass transition temperature advancements

In the description of the process of the incorporation of the carbon nanoparticles, it was mentioned that elevated temperatures had to be used in order for the viscosity to drop down to a minimum so that the dispersion process would become easier. At the temperatures used, no initial reaction took place. The dynamic experiments revealed a complex cure reaction, consisting of two peaks. Based on the work done by Bonnet et al [54,55] Temperature Modulated DSC was utilised in order to pinpoint the point of phase separation, which leads to a two-phase system. That was not possible here, due to the fact that the thermoplastic possibly diluted into the thermoset at a specific conversion. The results presented here are a function of the glass transition temperature advancements of the two phases formed, as will be discussed later on in the overall discussion part.

6.3 Glass transition temperature advancement of the 8552 resin system

The glass transition temperature advancement of the neat resin system was studied by the utilisation of TMDSC, following the methodology described in paragraph 5.1.3. The glass transition temperature (T_g) evolution as a

function of degree of cure for the 8552 resin system is illustrated in figure 6.10.

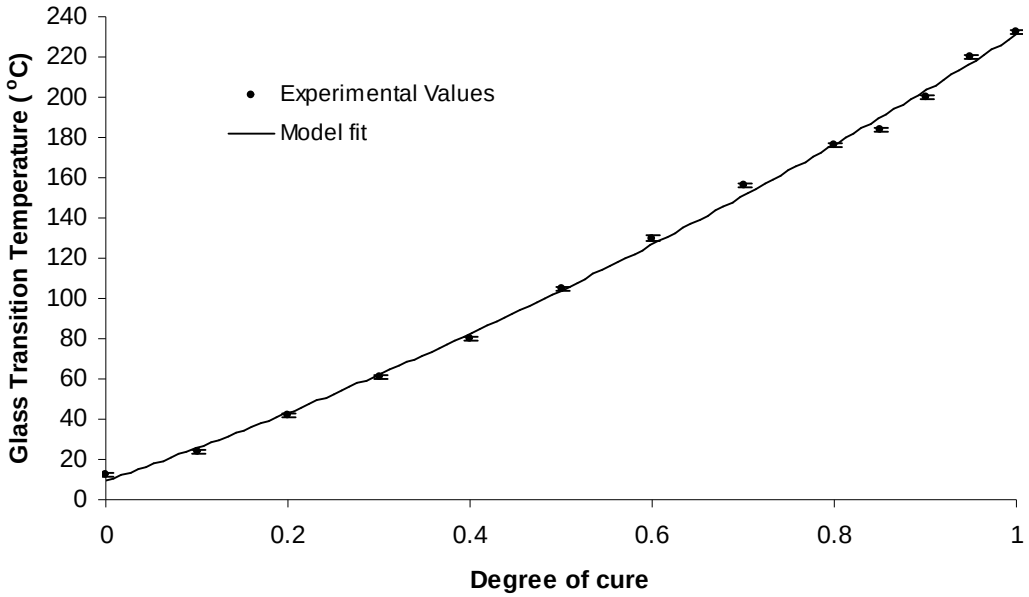

Figure 6.10: Superposition of experimental glass transition temperature values (including the experimental errors) and predicted values utilising the empirical polynomial equation 6.5

The glass transition temperature advancemet is modelled by using a polynomial second order equation of the form:

$$T_g(\alpha) = 65.5\alpha^2 + 156.3\alpha + 9.41 \qquad (6.5)$$

The value of the glass transition temperature, T_{go}, corresponding to the uncured resin is 15±1°C and that of the fully cured, $T_{g\infty}$, is 232±1°C. Roylance et al [134] illustrated the glass transition temperature advancement of the 8552 resin, using ultrasonic processing. It was observed that the fully cured material exhibits a T_{goo} value of around 200°C, which is lower than the case here. This difference may be justified by the fact that with the utilisation of TMDSC the inflection point is measured, while with the use of DMTA [134], the onset of $tan\delta$ is measured.

Chapter 7

7. Cure Kinetics Modelling of the Resin Systems and their Nanocomposites

The chapter deals with the development of the cure kinetics modelling methology. The two resin systems presented here are the MY 750 / HY 5922 together with the commercial one part MTM 44-1 resin and their nanocomposites. The modelling procedure is based on the utilisation of Genetic Algorithms as a parameter estimation technique. The diffusion constraints at the end of the curing reaction were taken into account and the glass transition temperature advancement was incorporated in one of the cases (MY 750 / HY 5922 resin). A comparison between the cure kinetics models developed for the neat resin systems and their nanocomposites produced with the addition of carbon nanotubes is also presented.

7.1 Cure Kinetics Modelling Methodology

In this part of the chapter the superposition principle is analysed together with the cure kinetics modelling methodology. The superposition principle is an essential assumption in order to fit both dynamic and isothermal DSC data.

7.1.1 The Superposition Principle

The main assumption in order to build a cure kinetics model, based on dynamic and isothermal heating experiments, is that the reaction rate is a unique function of temperature and conversion. The validity of this assumption may be tested when non-isothermal experimental data are superimposed with isothermal experiments in a reaction rate versus degree of cure diagram. The comparison between the isothermal and dynamic data is qualified by the relative error, which is an indication of the validity of superposition. The relative error is calculated as the sum of the relative differences between the dynamic reaction rates and the isothermal ones, as indicated by equation 7.1.

$$RE = \frac{1}{n}\sum_{1}^{n}\frac{\left[\left(d\alpha/dt\right)_{iso} - \left(d\alpha/dt\right)_{dyn}\right]}{\left(d\alpha/dt\right)_{iso}} \qquad (7.1)$$

where n denotes the number of points. Figures 7.1 to 7.4 illustrate the superposition for the MY 750 / HY 5922 resin system and its nanocomposites containing 0.06 wt % of Hyperion carbon nanotubes (batches 1 and 5) and the MTM 44-1 resin system respectively.

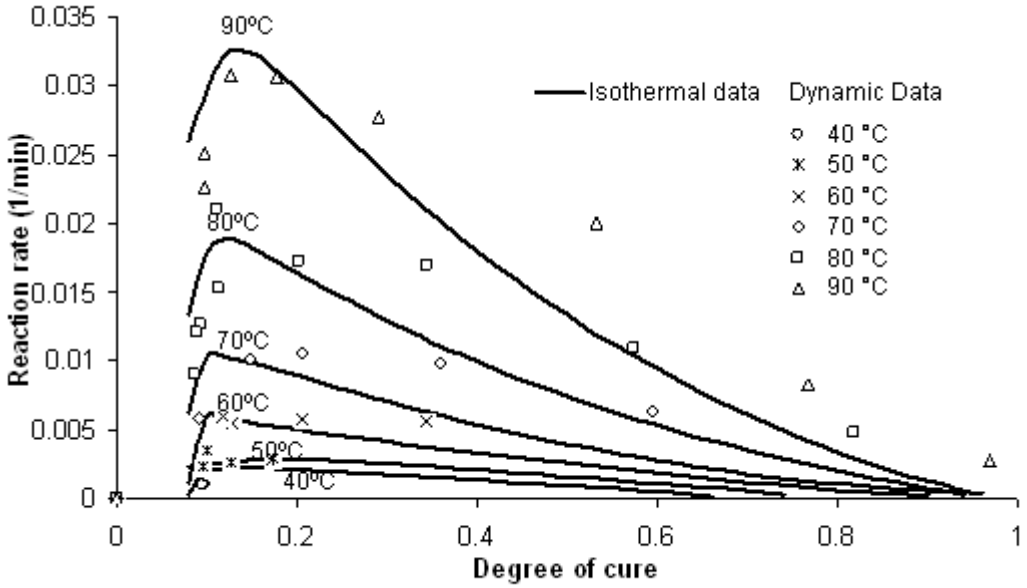

Figure 7.1: Superposition of dynamic and isothermal DSC reaction rate-degree of cure data for the MY 750 / HY 5922 resin system

The different heating rates used for the dynamic cure cause variations in the total heats of reaction measured. This variation causes extra discrepancies when the isothermal data are superpositioned with the dynamic. Discrepancies that do not exceed 10 % lead to a model fitting which is acceptable. Further increase causes less accurate fitting and minimises the time-temperature window where superposition is valid. The discrepancy between the equivalent dynamic and isothermal curing experiments for the MY 750 / HY 5922 resin system is 13 %. This value was calculated with the utilisation of equation 7.1. For example, the reacton rate that corresponds to the isothermal cure at 50^{o}C is 0.0033 and the one that corresponds to the dynamic cure at 50^{o}C is 0.0029. The relative error for these values is 13%.

When all the values are added, the discrepancy for the resin system is calculated. Figure 7.2 and 7.3 present the superposition of the nanocomposites that contain 0.06 wt % Hyperion carbon nanotubes.

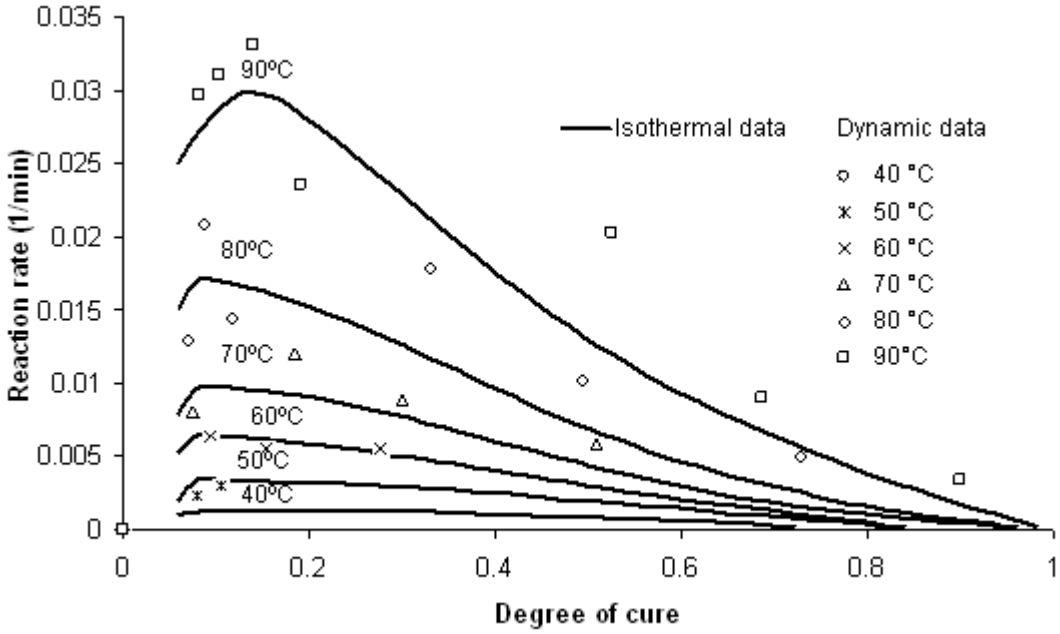

Figure 7.2: Superposition of dynamic and isothermal DSC reaction rate-degree of cure data for the MY 750 / HY 5922 resin system containing 0.06 wt % of Hyperion carbon nanotubes (batch 1)

The MY 750 / HY 5922 resin system which contains 0.06 wt % CNTs (batch 1-non ultrasonicated) shows almost the same discrepancy as the neat resin (see figure 7.2). In this case the average relative error does not exceed 12 %. The nanocomposite that was prepared with the utilisation of the ultrasonic horn and mixing by hand (batch 5-ultrasonicated) exhibited an average relative error that did not exceed 12 % (see figure 7.3). The isothermal tests for the neat resin and the non-ultrasonicated nanocomposite were conducted in the temperature window of 40-100^{o}C, while for the ultrasonicated nanocomposite the temperature window was 60-100^{o}C. The superposition of the experimental curves in all of the above mentioned cases is valid in a 'narrower' time-temperature window, which still allows the construction of a cure kinetics model. That is the result of the discrepancies that exceed the 10 % value. This window is limited in this case to the temperature window of 50-100^{o}C.

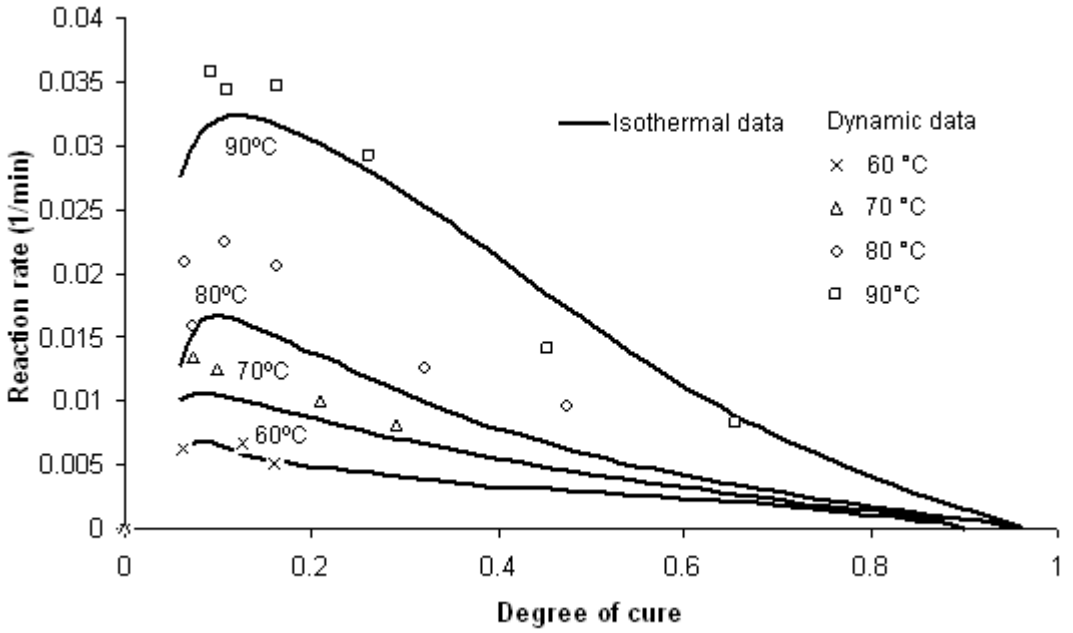

Figure 7.3: Superposition of dynamic and isothermal DSC reaction rate-degree of cure data for the MY 750 / HY 5922 0.06 % wt carbon nanotubes (batch 5) resin system

Based on the same principle, the superposition of the dynamic and isothermal cure data of the MTM 44-1 resin system is illustrated in Figure 7.4.

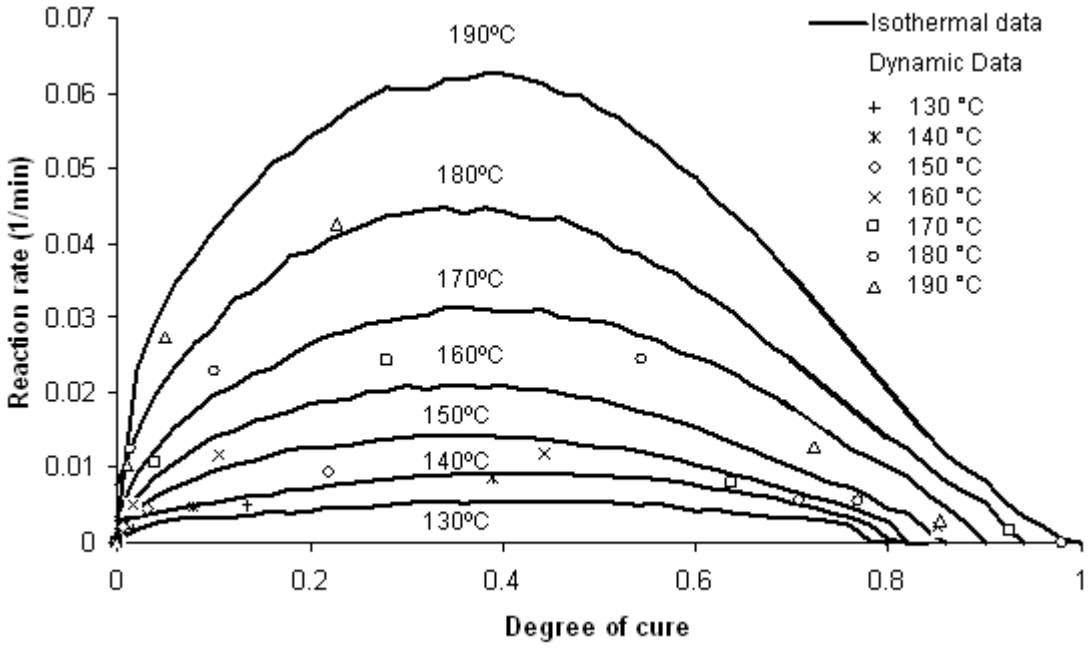

Figure 7.4: Superposition of dynamic and isothermal DSC reaction rate-degree of cure data for the MTM 44-1 resin system

The MTM 44-1 resin system shows a relative incostistency between the isothermal and dynamic heating conditions which was estimated to be 26 %. For example, during the dynamic cure of the MTM 44-1 resin at 5^{o}C/min the reaction rate is 0.011 min^{-1} at 11 % conversion when the curing temperature is 160^{o}C, while during the isothermal cure at 160^{o}C the reaction rate is 0.014 at the same conversion, showing a discrepancy of 26 %. This discrepancy is the result of the phase separation effect [54]. The resin system contains a thermoplastic which phase separates from the thermoset at a specific conversion. The assumption for the existence of superposition between the isothermal and dynamic heating experiments is not valid in this case. The model, however, used to study the curing reaction of the resin system will be based on isothermal experiments. The same trend of the superposition was observed with the incorporation of the Thomas Swan carbon nanotubes into the system as well. Again the superposition showed a discrepancy that exceeded 26 %. The respective superposition graph of the resin, under isothermal and dynamic heating conditions is similar to that presented in figure 7.4.

7.1.2 Genetic Algorithms

Genetic Algorithms [135] belong to a family of evolutionary optimisation methods, which involve a population of individual values and the search of the best parameters. The members of the population (individuals) are usually encoded in bit strings and the algorithm is iterated until some convergence cretiria are met. The initial population of parameters, which belong to the first generation is chosen randomly and it is then transformed into a new population, with the utilisation of operators. Such operators are selection, crossover and mutation. Selection is the operator that regenerates some of the individual values in the given population. Crossover is based on the exchange of digits between two selected individuals and producing new ones for the next series of parameters. Mutation randomly changes digits of the individuals with a very low probability. When the operators are iterating, they produce a new generation of parameters from the initial population. The fitness of this new generation of parameters is re-evaluated. In case that it

does not meet the convergence criteria the procedure is iterated producing another generation with better fitness.

Genetic Algorithms can be used for the estimation of the parameters of an equation used to fit a curve, by defining the relative error between the points of the curve and the equivalent points that are estimated for the equation. The relative error is introduced as the convergence criterion of the algorithm. These curve fitting capabilities are used to estimate the fitting parameters of the kinetics models. The genetic algorithm used in this study was developed by Skordos and Partridge [136]. The experimental data were fed into the algorithm and for every set of parameters the kinetics model estimated the reaction rate for a given temperature and conversion. Then the code calculated the relative errors of these simulated values from the experimental data. The iterations continued until the minimisation of the relative error was achieved.

7.1.3 Cure Kinetics Modelling Methodology

The cure kinetics modelling methodology consists of the following steps:

1) Testing of the superposition of isothermal and dynamic DSC data (section 7.1)
2) Choosing the appropriate cure kinetics model to fit the experimental data (that depends on the cure mechanism ie n^{th}order-autocatalytic). Empirical phenomenological models are utilised that incorporate a function that deals with the diffusion limitations (see section 2.5)
3) Utilisation of the Genetic Algorithms to estimate the model parameters. Depending on the relative error of the fitting, the parameters are estimated. Fitting with relative error around 10 % is a very good fitting (similar to the superposition discrepancies). Fitting that exhibits relative errors more than 10 % is a good fitting that is applied in a narrow ‘time-temperature window, while errors less than 10 % lead to overfitting.

In the next part the cure kinetics models developed for the two resin systems and their nanocomposites are presented.

7.2 Cure kinetics modelling

7.2.1 Cure kinetics modelling of the MY 750 / HY 5922 and its nanocomposites containing 0.06 wt % of Hyperion carbon nanotubes (batches 1 and 5)

The validity of the superposition between the isothermal and the dynamic cure data allows for the construction of a cure kinetics model (figures 7.1 to 7.3). The incorporation of the T_g models into the cure kinetics models is essential, in order to achieve an accurate fit. In the case of the MY 750 / HY 5922 resin system and its nanocomposites, the proposed model used to fit the kinetic data is a double autocatalytic model, based on Karkanas et al [46]:

$$\frac{d\alpha}{dt} = k_1\alpha^k(1-\alpha)^l + k_2\alpha^m(1-\alpha)^n \qquad (7.2)$$

where $k_1 = \frac{k_{r1}k_d}{k_{r1}+k_d}$, $k_2 = \frac{k_{r2}k_d}{k_{r2}+k_d}$, $k_{r1} = A_1e^{-E_1/RT}$, $k_{r2} = A_2e^{-E_2/RT}$

$$k_d = A_d e^{-E_d/RT} e^{-\frac{(FT-G)}{K(T-T_g)}+P}, \; T_g(\alpha) = f(\alpha)$$

α is the degree of cure

T is the temperature in Kelvin

A is the pre-exponential factor (min^{-1})

E is the activation energy (J/mole)

A_d is the diffusion controlled pre-exponential factor (min^{-1})

k_{r1}, k_{r2} are the chemical region reaction rates

k_d is the diffusion region reaction rate

k, l, m and n are fitting parameters

F, G, K, P are fitting parameters and

T_g is the glass transition temperature as a function of the degree of cure.

The model is a modification of the original empirical model suggested by Kamal and Sourour [29]. The modification lies on the fact that glass transition

temperature evolution was included so that the diffusion controlled are could be fitted with accuracy. The form of the glass transition temperature as a function of the degree of cure for the resin system and its nanocomposites is given by equation 7.4 and the polynomial equations presented in table 6.2. The T_g model in incorporated into the cure kinetics model so that the latter recognises where the maximum conversion is achieved, especially for the isothermal experiments. It also deals with the diffusion limitations (included in k_d function). This model consists of fourteen parameters, namely, $A_1, E_1, A_2, E_2, k, l, m, n, F, G, K, P$. These parameters were estimated in order to succeed the best fit to the experimental data by using genetic algorithms. Both isothermal and dynamic data were fed into the GA routine. The parameters were estimated with an average relative error of 14 % for all of the cases tested. This error is very close to the error of the superposition, stating that a very accurate fit was achieved. This error was calculated with the utilisation of equation 7.3 (similar to equation 7.1)

$$RE = \frac{1}{n}\sum \frac{\left[\left(da/dt\right)_{\exp} - \left(da/dt\right)_{est}\right]}{\left(da/dt\right)_{\exp}} \qquad (7.3)$$

where n is the number of experimental points,

exp are the experimental (isothermal and dynamic) reaction rates and

est are the estimated reaction rates with the utilisation of the model.

The GA routine calculated the parameters of the model. This estimation is summarised in table 7.1. The fitting under isothermal and dynamic heating conditions for the neat resin and its nanocomposites is presented in figures 7.5 to 7.10

PARAMETERS	MY 750/HY 5922	MY 750/HY 5922 0.06 wt % CNTs (non-ultrasonicated)	MY 750/HY 5922 0.06 wt % CNTs (ultrasonicated)
A_1 (min^{-1})	$1.79x10^6$	$1.09x10^6$	$1.82x10^6$
E_1 (kJ/mol)	56.85	50.59	51.7
A_2 (min^{-1})	$5.06x10^6$	$1.48x10^6$	$6.1x10^5$
E_2 (kJ/mol)	59.11	51.7	51.85
k	0.59	0.36	0.37
l	2.74	2.33	2.82
m	0.57	0.11	0.27
n	0.97	0.94	1.13
A_d (min^{-1})	$8.39x10^{19}$	$8.54x10^{18}$	$2.33x10^{19}$
E_d (kJ/mol)	4.66	2.48	7.76
F	0.006	0.0019	0.002
G	0.019	0.0046	0.032
K	0.0015	0.00033	0.00048
P	0.0975	0.0097	0.015

Table 7.1: Estimated parameters for the fitting of data obtained from isothermal and dynamic cure experiments for the MY 750 / HY 5922 resin system and its nanocomposites containing 0.06 wt % carbon nanotubes (batches 1 and 5)

The fitting shows that the models follow the experimental curves including the diffusion controlled area with high accuracy. There is only a deviation in the dynamic experiments at higher heating rates for the epoxy resin (e.g. 10^oC/min) where the model prediction is lower that the experimental data. This discrepancy is expected as it is observed at temperatures higher than 170^oC, where the superposition of isothermal and dynamic data is not valid (see figure 7.8). The same observation applies to the higher dynamic heating rates of the nanocomposite containing the non-ultrasonicated carbon nanotubes (see figure 7.2).

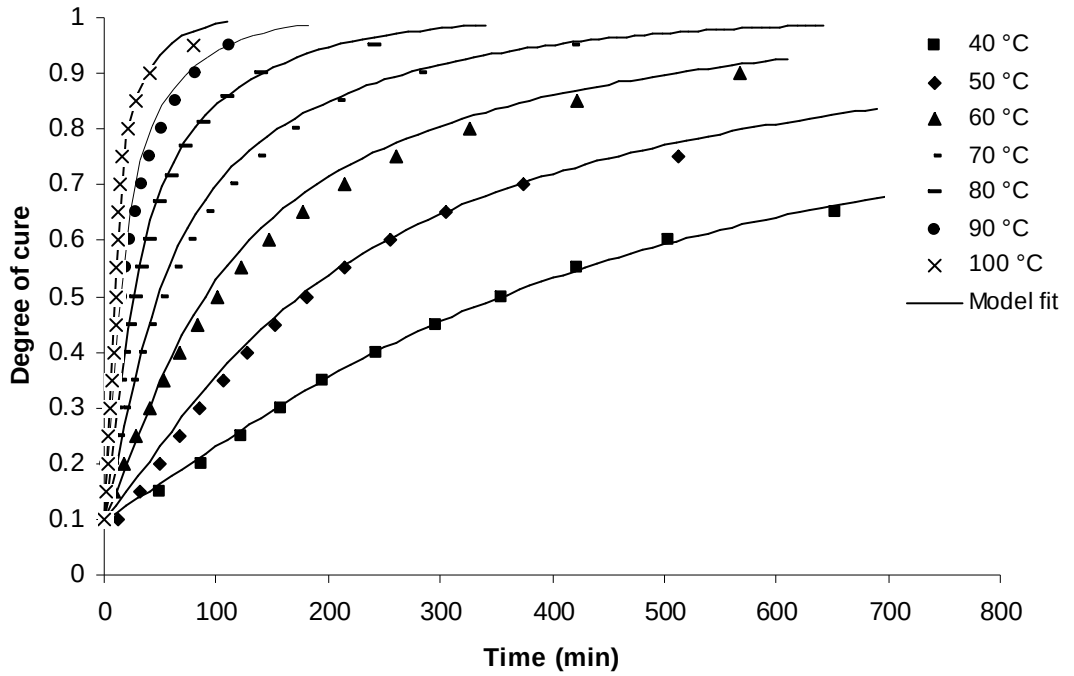

Figure 7.5: Comparison between experimental and simulated values of degree of cure versus time for isothermal experiments for the MY 750 / HY 5922 resin system

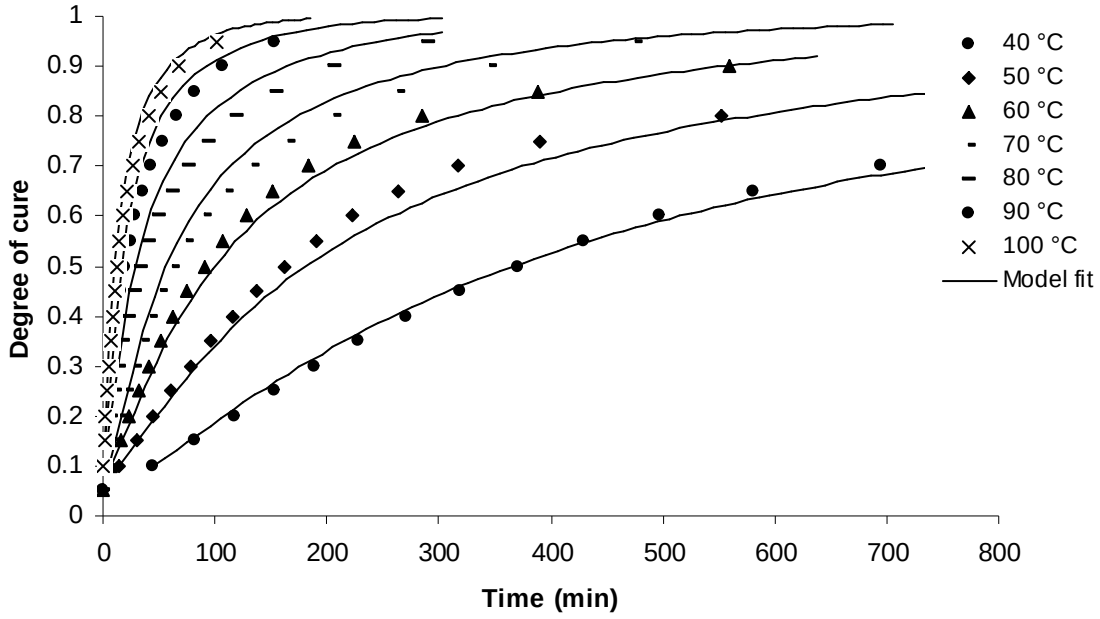

Figure 7.6: Comparison between experimental and simulated values of degree of cure versus time for isothermal experiments for the MY 750 / HY 5922 resin system containing 0.06 wt % of Hyperion carbon nanotubes (non-ultrasonicated)

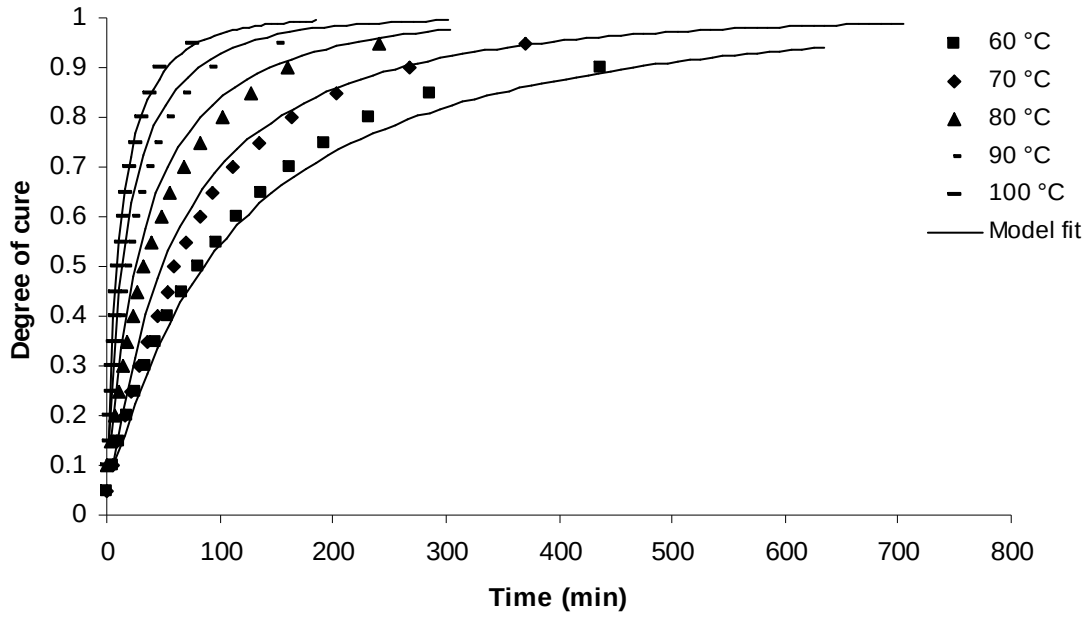

Figure 7.7: Comparison between experimental and simulated values of degree of cure versus time for isothermal experiments for the MY 750 / HY 5922 resin system containing 0.06 wt % of Hyperion carbon nanotubes (ultrasonicated)

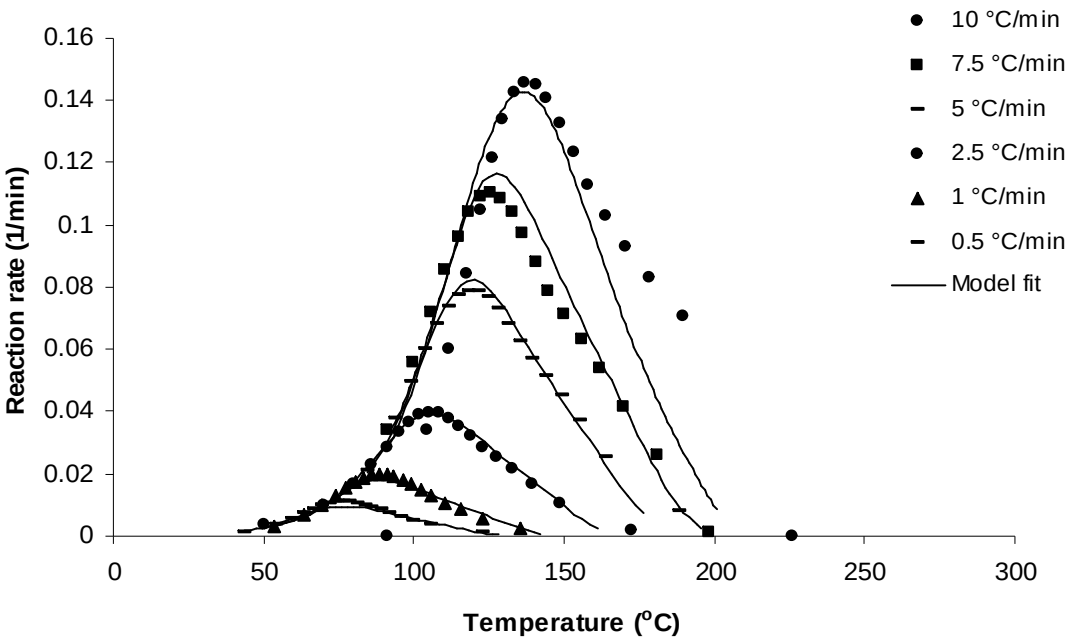

Figure 7.8: Comparison between experimental and simulated values of reaction rate versus temperature for a number of dynamic experiments for the MY 750 / HY 5922 resin system

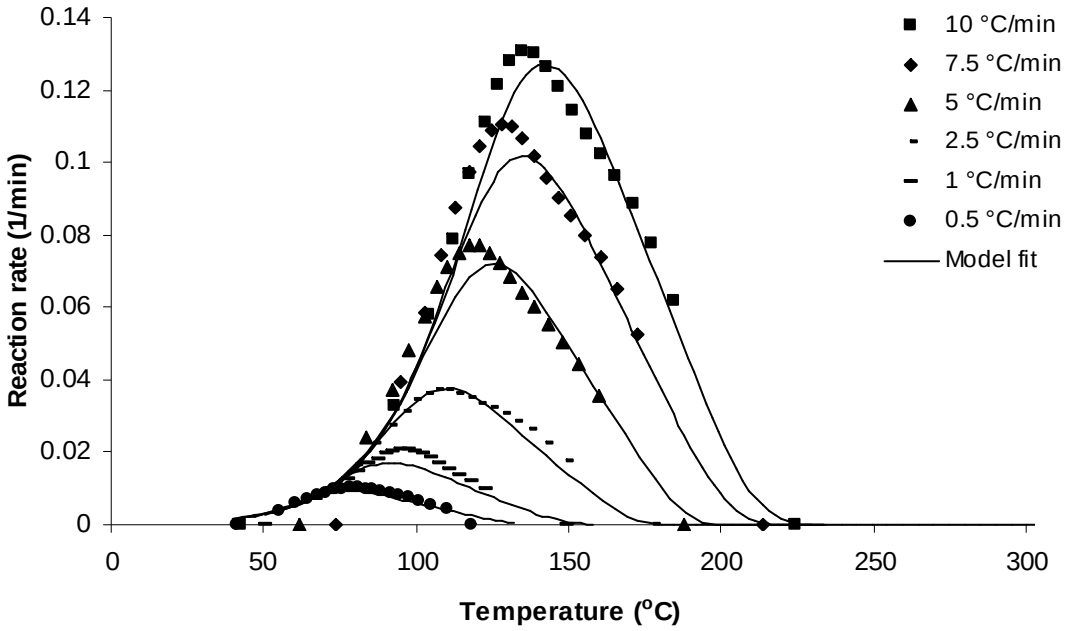

Figure 7.9: Comparison between experimental and simulated values of reaction rate versus temperature for a number of dynamic experiments for the MY 750 / HY 5922 resin system containing 0.06 wt % of Hyperion carbon nanotubes (non-ultrasonicated)

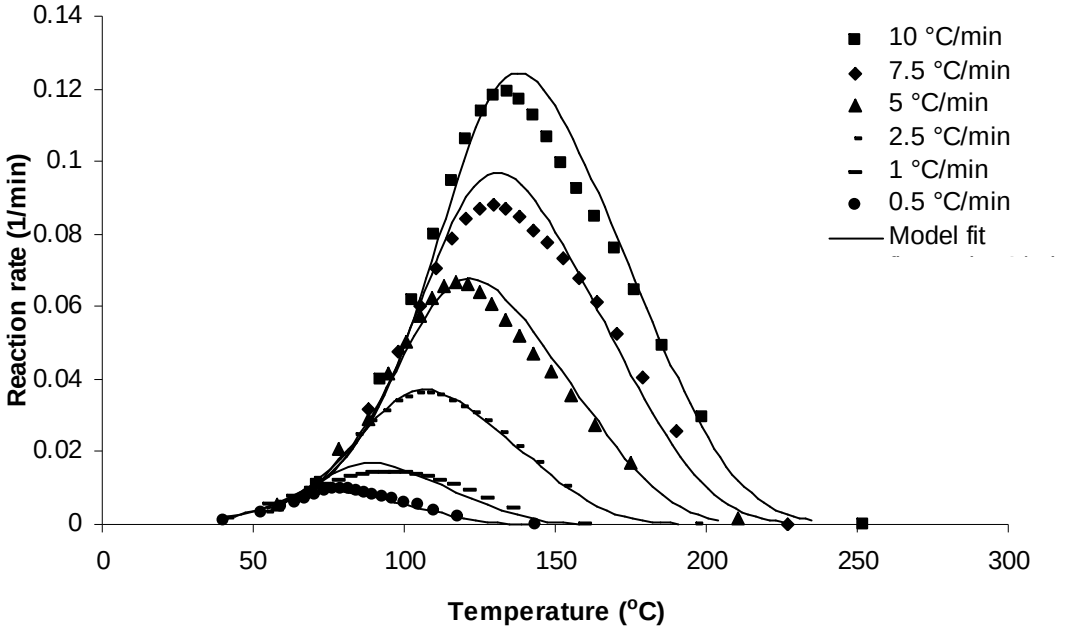

Figure 7.10: Comparison between experimental and simulated values of reaction rate versus temperature for a number of dynamic experiments for the MY 750 / HY 5922 resin system containing containing 0.06 wt % of Hyperion carbon nanotubes (ultrasonicated)

If a comparison is attempted between the kinetic parameters of the models presented in table 7.1, it is observed that the pre-exponential factors A_1 and A_2 of the nanocomposite containing the non-ultrasonicated carbon nanotubes are lower from that corresponding to the neat system, while those of the ultrasonicated nanocomposite are greater. The pre-exponential factors A_d of the diffusion term are in both cases lower for the nanocomposites compared to the neat resin. Especially for the non-ultrasonicated nanocomposite it is about an order of magnitude lower than the other two cases. The activation energies E_1 and E_2 show a decrease, following the order: neat resin > ultrasonicated nanocomposite > non-ultrasonicated nanocomposite. A possible explanation for this is that the incorporation of carbon nanotubes causes a decrease of the reaction rates at the initial stages of the curing reaction. Puglia et al [94] observed similar effects in a carbon nanotube filled DGEBA / DETA resin system. It was observed that there was a shift of the exothermic reaction peak to lower temperatures, suggesting an accelerating role of the carbon nanotube incorporation. This effect was also observed in the work of Xie et al [100,101], especially at the initial stages of the curing reaction. In the later stages, where diffusion limitations occur, the carbon nanotubes cause a further immobilisation of the polymer chains, in the network already formed. This may also be verified when the activation energies of the diffusion term, E_d, are compared. A higher value is observed for the ultrasonicated nanocomposite and a lower value in the case of the material with inferior dispersion. This observation, combined with the increased glass transition temperatures suggest improved dispersion intensifies immobilisation effects caused by carbon nanoparticles towards the final stages of the curing reaction. Ton-That et al [95] observed in their study that the activation energy of an epoxy nanocomposite, incorporating nanoclays, had the same value as the epoxy-amine system at the early stages of dynamic DSC cure. At the later stages, though it was substantially lower. They used the Avrami approach, which indicated a steric effect of the clays on the cure of the nanocomposite.

Figure 7.11 presents a comparison of the degrees of cure versus time under isothermal curing conditions for the two batches that incorporated carbon nanotubes. The experimental errors are 2 %.

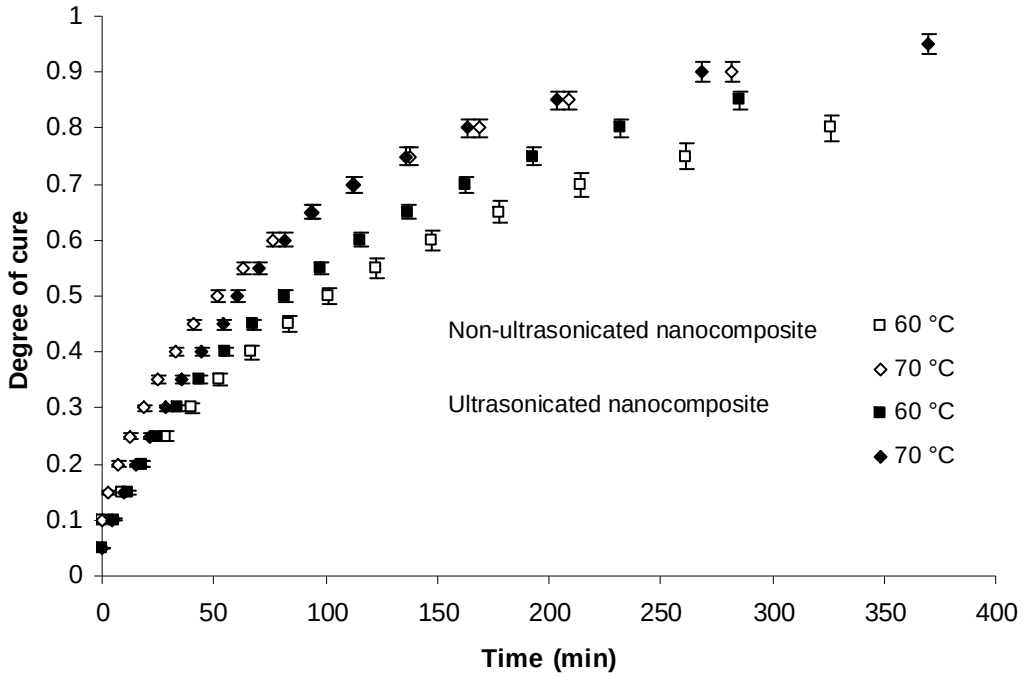

Figure 7.11: Comparison of degrees of cure versus time curves (including the experimental errors) for the isothermal cure of the MY 750 / HY 5922 nanocomposites containing 0.06 wt % of Hyperion carbon nanotubes a) non-ultrasonicated nanocomposite and b) ultrasonicated nanocomposite (batches 1 and 5, respectively)

At 60^{o}C it is observed that the reaction reaches a higher conversion at less time for the ultrasonicated nanocomposite compared to the non-ultrasonicated material. At 70^{o}C this trend vanishes as the two nanocomposites reach almost the same final conversion at the same time. Figure 7.11 suggests that the ultrasonication treatment affects the final properties of the product.

7.2.2 Cure kinetics models of the MTM 44-1 resin system and its nanocomposite containing Thomas Swan carbon nanotubes (batch 6)

The experimental data presented at the beginning of this chapter allowed for the determination of the methodology to use in order to simulate the cure

kinetics. Figures 5.25 and 5.28 presented in chapter 5 indicated that an autocatalytic reaction mechanism is followed for the cure of the resin system and its nanocomposite. The addition of the thermoplastic in the thermoset and the occurrence of phase separation limit the validity of superposition between the dynamic and isothermal curing data (figure 7.4). In this case, the cure kinetics models utilised to simulate the cure kinetics of the materials were based only on isothermal cure experiments, in the region where superposition holds.

The proposed model used to fit the kinetic data is a modification of the double autocatalytic model, based on Karkanas et al [46] equation. The difference here, compared with the model used for the MY 750 / HY 5922 resin system and its nanocomposites (equation 7.2) is that the glass transition temperature advancement is not incorporated into the model. Instead of that, a diffusion factor was utilised in order to take the diffusion limitations into account.

$$\frac{d\alpha}{dt} = \left(k_1 \alpha^k (1-\alpha)^l + k_2 \alpha^m (1-\alpha)^n\right) f(\alpha) \qquad (7.4)$$

where $k_1 = A_1 e^{-E_1/RT}$, $k_2 = A_2 e^{-E_2/RT}$, $f(\alpha) = \frac{1}{1+e^{C(\alpha-\alpha c)}}$, $\alpha_C = f(T)$

α is the degree of cure

T is the temperature in Kelvin

A is the pre-exponential factor (min^{-1})

E is the activation energy (J/mol)

k, l, m and n are fitting parameters

α_c is the maximum conversion attained at each isothermal temperature used which is a function of temperature

$f(\alpha)$ is the diffusion function, which takes into account the diffusion limitations at the later stages of the curing reaction. This factor was adopted by Khanna and Chanda [43].

The maximum degrees of cure α_c, as a function of temperature for the isothermal cure of the resin system at the different temperatures tested, are presented in figures 7.12 and 7.13. The fit was achieved by the utilisation of the first order polynomial equations 7.5 and 7.6:

$$\alpha_c = 0.0036T - 0.675 \qquad (7.5)$$

$$\alpha_c = 0.0036T - 0.654 \qquad (7.6)$$

where T is the absolute temperature, expressed in Kelvin. This expression was incorporated into the diffusion term of the kinetics model.

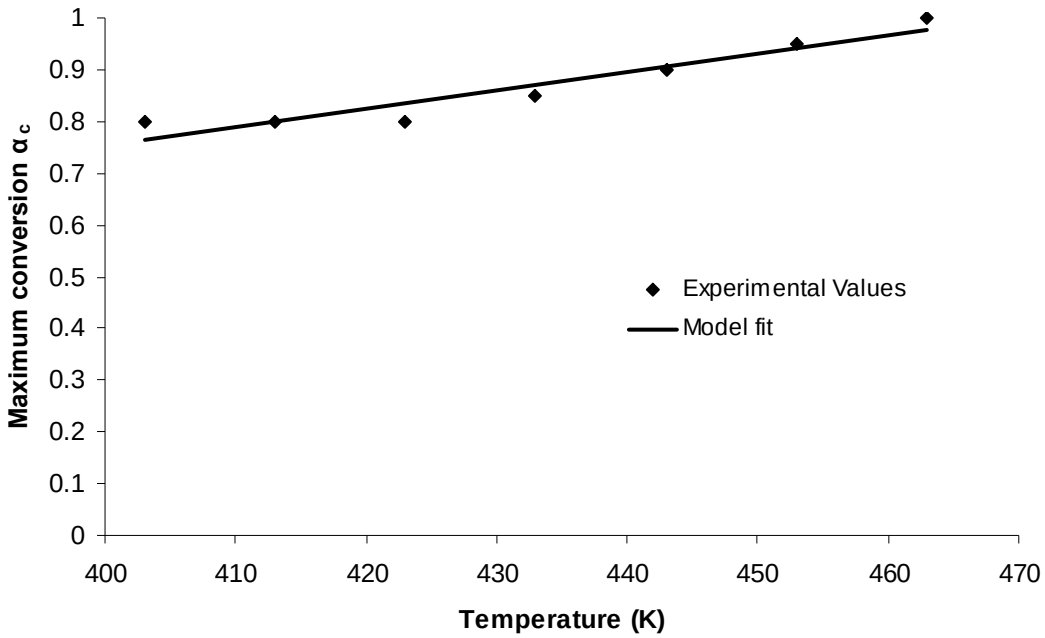

Figure 7.12: Plot of the attained maximum degree of cure as a function of temperature for the isothermal cure of the MTM 44-1 resin system at different temperatures

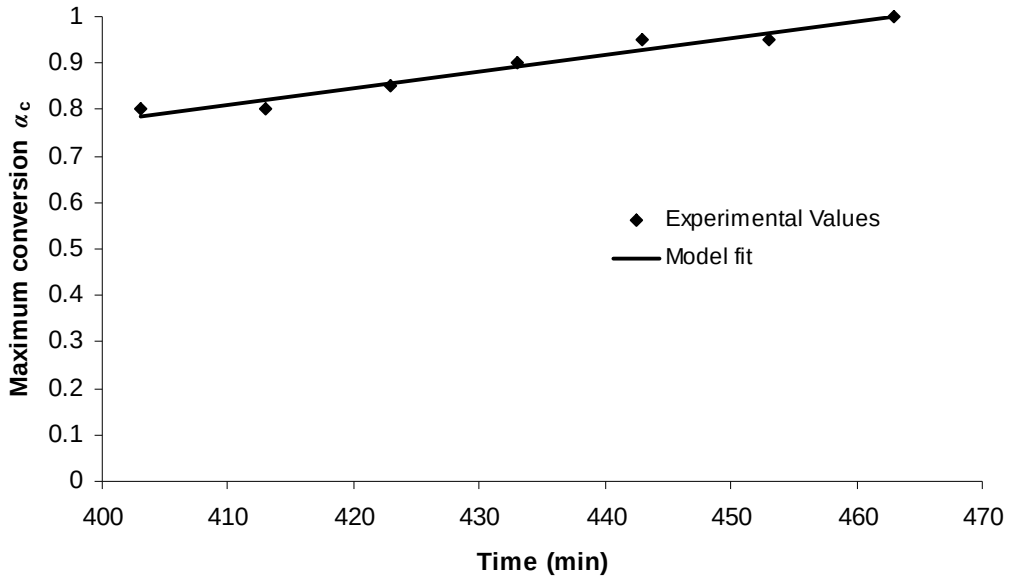

Figure 7.13: Plot of the attained maximum degree of cure as a function of temperature for the isothermal cure of the MTM 44-1 resin system containing 1 wt % of Thomas Swan carbon nanotubes, at different temperatures

If the diffusion function is replaced by a diffusion factor C and equations 7.5 and 7.6 are incorporated into the proposed model, nine parameters have to be estimated, namely, $A_1, E_1, A_2, E_2, k, l, m, n, C$. These parameters were estimated in order to achieve the best fit to the experimental data by using the Genetic Algorithm routine. Both isothermal and dynamic data were fed into the GA routine resulting in the values presented in table 7.2. The utilisation of equation 7.3 led to the estimation of the relative errors of the fitting for both of the cases of the resin system and its nanocomposite. They were found to be around 11 %. These values allow for an accurate fit of the isothermal DSC data.

PARAMETERS	MTM 44-1 resin	MTM 44-1 1 wt % CNTs resin
A_1 (min^{-1})	$1.97x10^6$	$1.73x10^6$
E_1 (kJ/mol)	60.82	66.75
A_2 (min^{-1})	$1.96x10^6$	$1.97x10^6$
E_2 (kJ/mol)	56.29	56.88
k	0.49	0.05
l	2.02	1.67
m	1.84	1.4
n	2	1.94
C	0.101	0.011

Table 7.2: Estimated parameters for the fitting of data obtained from isothermal and dynamic experiments for the MTM 44-1 resin system and its nanocomposite containing 1 wt % of Thomas Swan carbon nanotubes (batch 6)

The model fit for the isothermal cure of the epoxy resin and the resin containing carbon nanotubes are presented in figures 7.14 and 7.15. The fitting shows that the models follow the experimental curves with high accuracy, though that there is a deviation in the case of the nanocomposite at the higher isothermal experiments (e.g. 170 and 180^oC).

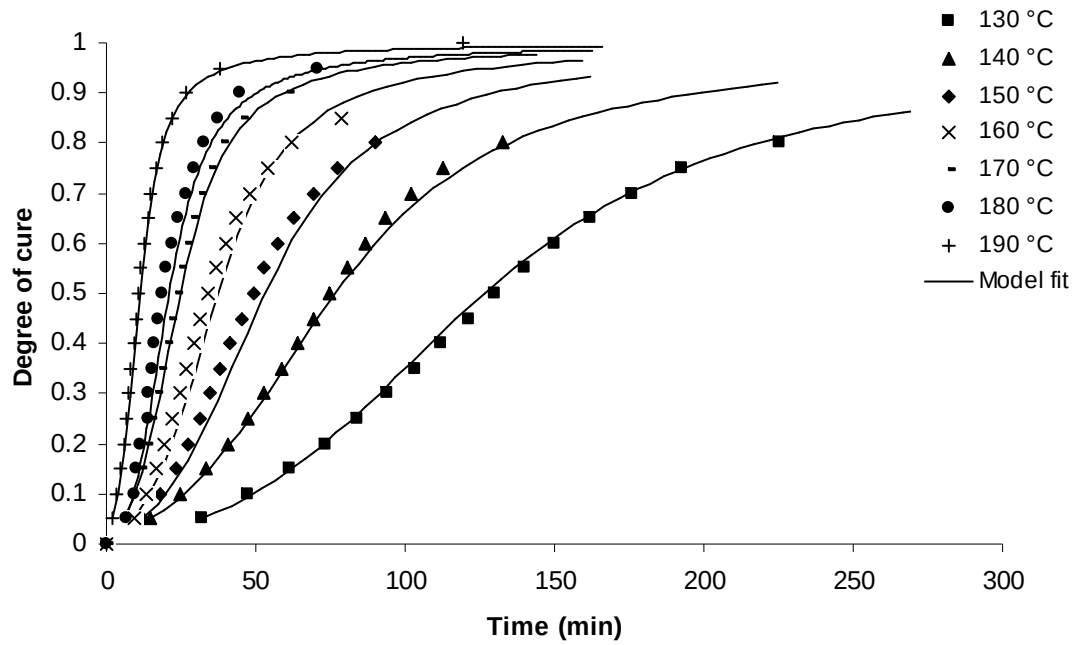

Figure 7.14: Comparison between experimental and simulated values of degree of cure versus time for a number of isothermal experiments for the MTM 44-1 resin system at different temperatures

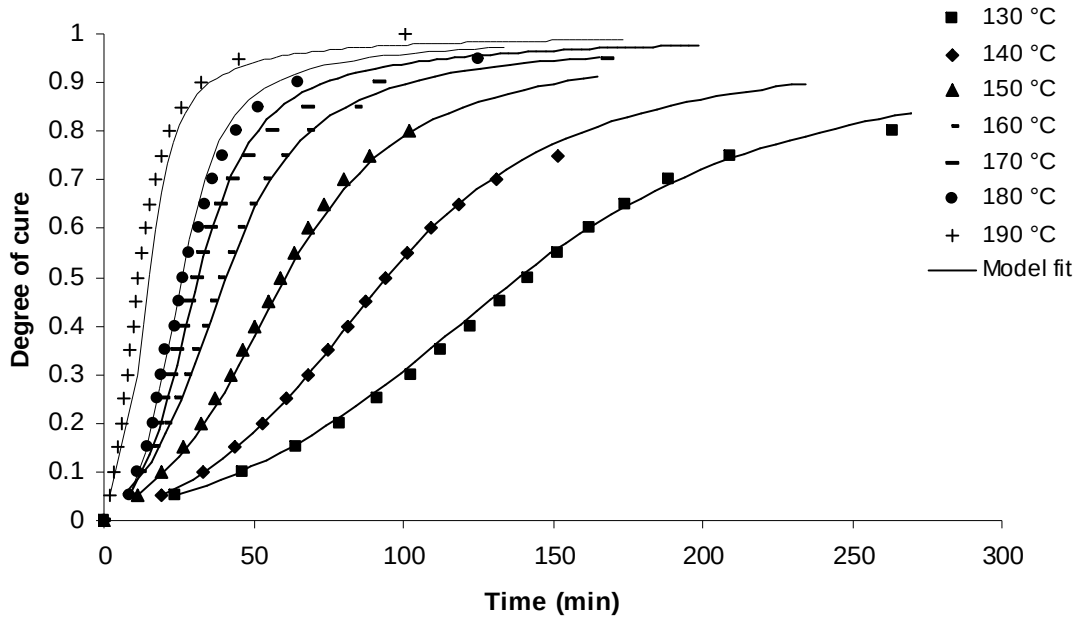

Figure 7.15: Comparison between experimental and simulated values of degree of cure versus time for a number of isothermal experiments for the MTM 44-1 resin system containing 1 wt % of Thomas Swan carbon nanotubes, at different temperatures

A direct comparison of the kinetic parameters for both the cases, which are summarised in table 7.2, allows for the following observations. The pre-exponential factor A_2 is almost identical for the two systems. A difference is observed for the pre-exponential factor A_1, where a decrease is noted with the incorporation of carbon nanotubes. The activation energy E_1 shows an increase, while E_2 decreases for the nanocomposite, respectively. A possible explanation to this effect is that the incorporation of carbon nanotubes causes a decrease of the reaction rates at the initial stages of the curing reaction. The diffusion factor C is almost ten times greater for the neat resin. This difference was also observed for the MY 750 / HY 5922 resin and its non-ultrasonicated nanocomposite. This observation, combined with the reduced glass transition temperatures of the nanocomposite, suggests that the immobilisation effects are not strong when carbon nanotubes are incorporated into the system. However, it becomes more complicated due to the fact that vitrification ceases the reaction prematurely. The decelerating effect caused by the incorporation of carbon nanotubes into the resin system is illustrated in figure 7.16. For convenience the temperatures used are limited to 130 and 140^{o}C. The experimental errors are 2 %.

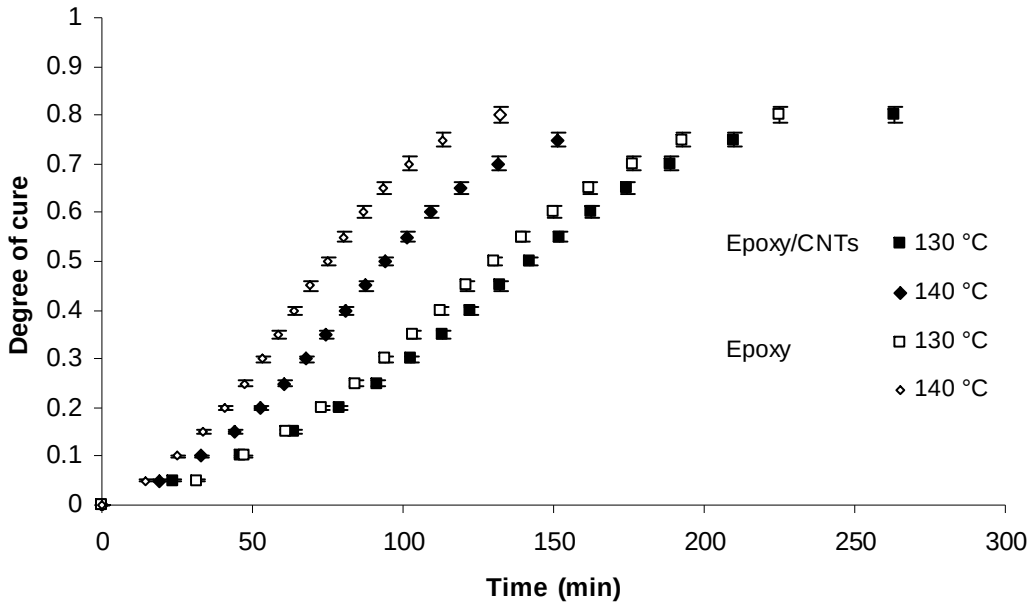

Figure 7.16: Comparison of degrees of cure versus time (including the experimental errors) for the isothermal cure of the MTM 44-1 resin system and its nanocomposite containing 1 wt % of Thomas Swan carbon nanotubes (batch 6) at different temperatures

It is observed that at 130^{o}C the nanocomposite reaches the same conversion as the neat system (around 80 %), but it takes more time (225 minutes for the neat system and 270 minutes for the nanocomposite). This trend is different for the 140^{o}C cure, where the conversion is lower, but it also takes more time for the nanocomposite to reach the same degree of cure. This decelerating effect, observed when carbon nanotubes are incorporated into the resin system was also seen in figure 5.32, chapter 5. A reduction of the reaction rates was observed, leading to the conclusion that the nanocomposite exhibits a slower reaction when compared to the neat epoxy system.

The next chapter contains the cure kinetics modelling of the 8552 resin system and the T800/3900-2 composite and it constitutes the validation of the cure kinetics modelling methodology presented in this chapter.

Chapter 8

8. Cure Kinetics Modelling of the 8552 Resin System / T800/3900-2 Cure Composite (Round Robin Participation) – Methodology Validation

This chapter constitutes the validation of the cure kinetics modelling methodology analysed in the previous chapter. The first part of this chapter deals with the cure kinetics modelling of the thermosetting system tested, namely 8552 resin system, under dynamic and isothermal curing conditions. The modelling procedure is based on the utilisation of Genetic Algorithms, described in the previous chapter. The diffusion constraints at the end of the curing reaction were taken into consideration. In the second part of the chapter the cure kinetics modelling analysis of the T800/3900-2 prepreg is presented, based on the experimental data provided from the participation in a Round Robin program, organised by the UBC Composites group from the University of British Columbia, Canada. The aim of this participation was to compare the techniques used in order to build a cure kinetics model based on the same experimental data and analysis (provided by the coordinator). For this purpose the utilisation of Genetic Algorithms was also a prerequisite. The analysis of all the stages of Round Robin participaton is presented in the appendix (appendix B). A sensitivity analysis of the models utilised in this study is also presented in this chapter.

8a. Cure kinetics modelling of the 8552 resin system

8.1 The superposition principle

The experimental data, presented in paragraph 5.2.3, showed that the 8552 resin system follows an autocatalytic reaction mechanism (figure 5.35) and exhibits vitrification at the later stages of the curing reaction. That was evidenced from the fact that during the isothermal curing experiments the reaction does not reach full conversion. The validity of the superposition

principle that was analysed in paragraph 7.1.1 is an essential assumption that needs to be tested so that a cure kinetics model may be constructed. Figure 8.1 illustrates the superposition of isothermal and dynamic reaction rate (presented in figures 5.36 and 5.37) versus degree of cure curves for the 8552 resin system.

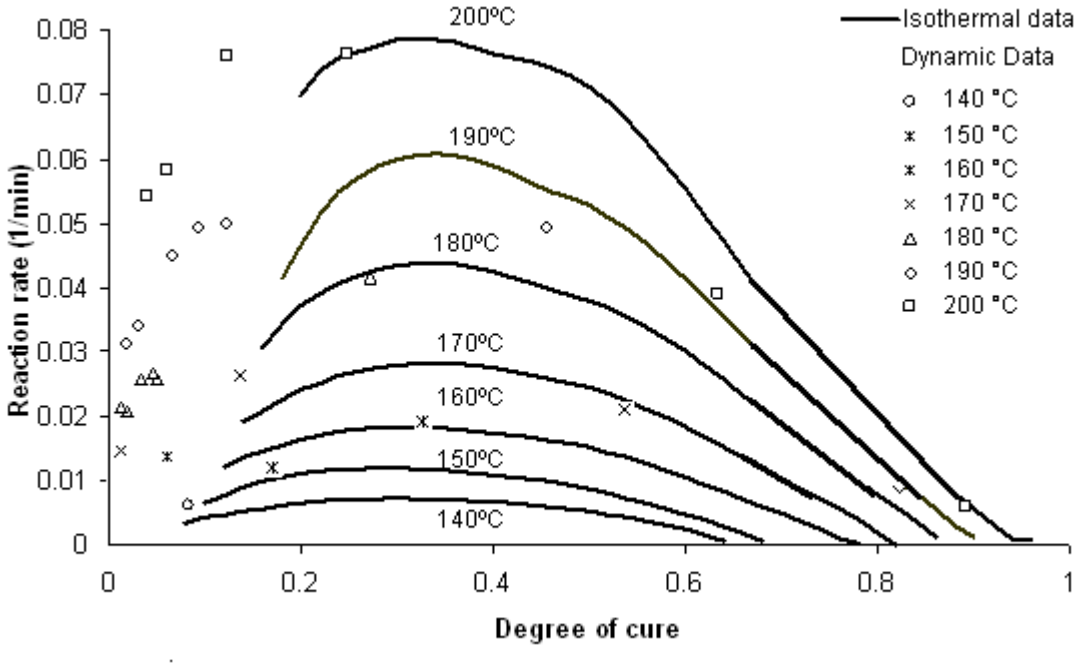

Figure 8.1: Superposition of dynamic and isothermal DSC reaction rate-degree of cure data for the 8552 resin system

For the 8552 resin system, the superposition of the isothermal experiments is in very good agreement with the dynamic ones. Utilisation of equation 7.1 revealed that the relative error between the isothermal and dynamic DSC data is 11 %. This discrepancy allows for the construction of a cure kinetics models, which is valid for the temperature range of 140-200^{o}C (the isothermal DSC test range). However, the model may be valid to a time-temperature window which exceeds the aforementioned temperatures.

8.2 Cure kinetics modelling of the 8552 resin system

The proposed model to be used here is the same model utilised in the case of the MTM 44-1 resin system. In order to take into account any diffusion limitations, a function of the degree of cure was incorporated.

$$\frac{d\alpha}{dt} = \left(k_1 \alpha^k (1-\alpha)^l + k_2 \alpha^m (1-\alpha)^n\right) f(\alpha) \qquad (8.1)$$

where $k_1 = A_1 e^{-E_1/RT}$, $k_2 = A_2 e^{-E_2/RT}$, $f(\alpha) = \frac{1}{1+e^{C(\alpha-\alpha_c)}}$ and

α is the degree of cure

T is the temperature in Kelvin

A is the pre-exponential factor (min^{-1})

E is the activation energy (J/mol)

k, l, m and n are exponents showing the reaction order and

$f(\alpha)$ is the diffusion function, taking into account the diffusion limitations at the later stages of the curing reaction, adopted by Khanna and Chanda [43]. In this expression α_c is the critical or maximum conversion reached at each isothermal temperature used. For $\alpha << \alpha_c$, $f(\alpha)$ approaches unity. When α becomes almost equal to α_c, at the later stages of the curing reaction, the diffusion factor becomes almost zero.

In the case of the 8552 resin system, a similar model was utlised [137] in order to fit the experimental data. It was demonstrated that the reaction rates decrease significantly if at any point the resin undergoes vitrification. The result is that a limiting degree of cure is reached after glass transition occurs, expressed by the term α_c. The critical degree of cure as a function of temperature for the isothermal cure of the resin system at different temperatures is presented in figure 8.2. The fit was achieved with the utilisation of a linear expression, which is

$$\alpha_c = 0.0045T - 1.1634 \qquad (8.2)$$

where T is the absolute temperature, expressed in Kelvin. This expression was then incorporated into the diffusion factor.

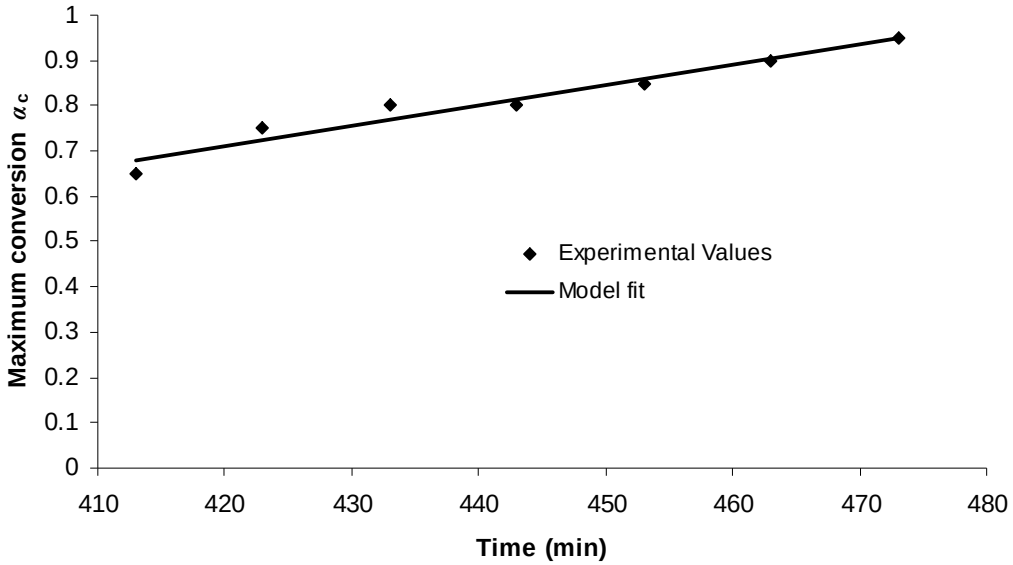

Figure 8.2: Plot of maximum attained degree of cure as a function of temperature of the isothermal cure of the 8552 resin system at different temperatures

If the diffusion factor is named C and equation 8.2 is incorporated in this factor, then the proposed model consists of nine parameters, namely, $A_1, E_1, A_2, E_2, k, l, m, n, C$. These parameters were calculated with the utilisation of the Genetic Algorithms routine. Both isothermal and dynamic data were fed into the GA routine resulting in the values presented in table 8.1. Utilisation of equation 7.3 led to the estimation of the fitting error. It was calculated to be 14 %. It is a bit higher than the superposition error, however it still allows for an accurate fit in the temperature window of the conducted isothermal tests.

PARAMETERS	8552 resin system
A_1 (min^{-1})	$1.81x10^6$
E_1 (kJ/mol)	61.94
A_2 (min^{-1})	$1.92x10^6$
E_2 (kJ/mol)	61.84
k	2.22
l	1.99
m	0.56
n	1.81
C	10.59

Table 8.1: Estimated parameters for the fitting of data obtained from isothermal and dynamic experiments

The fitting shows that the model follows the experimental curves with high accuracy. The model fit for the isothermal and dynamic heating tests is presented in figures 8.3 and 8.4. In figure 8.3, it is observed that there is a deviation at the isothermal cure experiment conducted at 140^{o}C, where the model predicts a higher degree of cure, but also at 180^{o}C, where the predicted degree of cure is slightly lower than the experimental value. The model fit presented in figure 8.3, also shows that the model follows the experimental curves for the 1 and 2.5^{o}C/min heating rates; this does not apply for the 5-10^{o}C/min. At these high heating rates, the model is able to predict the curve up to a specific conversion. The model fails to follow the later stages of the cure reaction due to the fact that the superposition was tested and it was found to be valid for the temperature window of 140-200^{o}C. The model values calculated are underestimating the reaction rates above 200^{o}C.

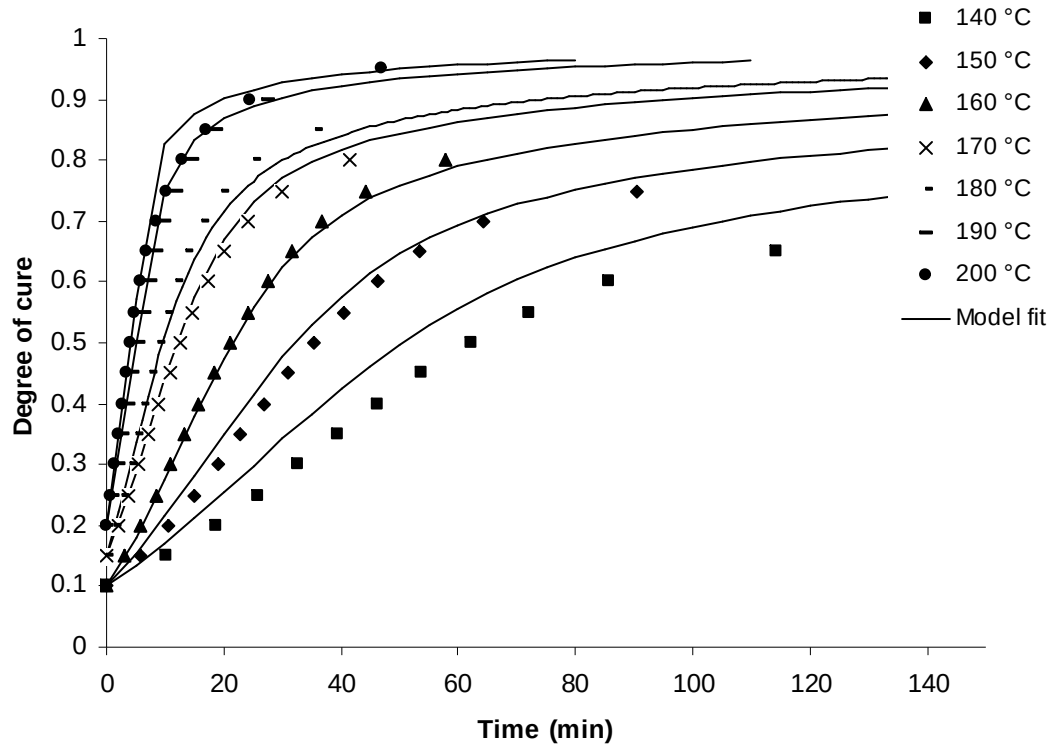

Figure 8.3: Comparison between experimental and simulated values of degree of cure versus time for a number of isothermal experiments for the 8552 resin system

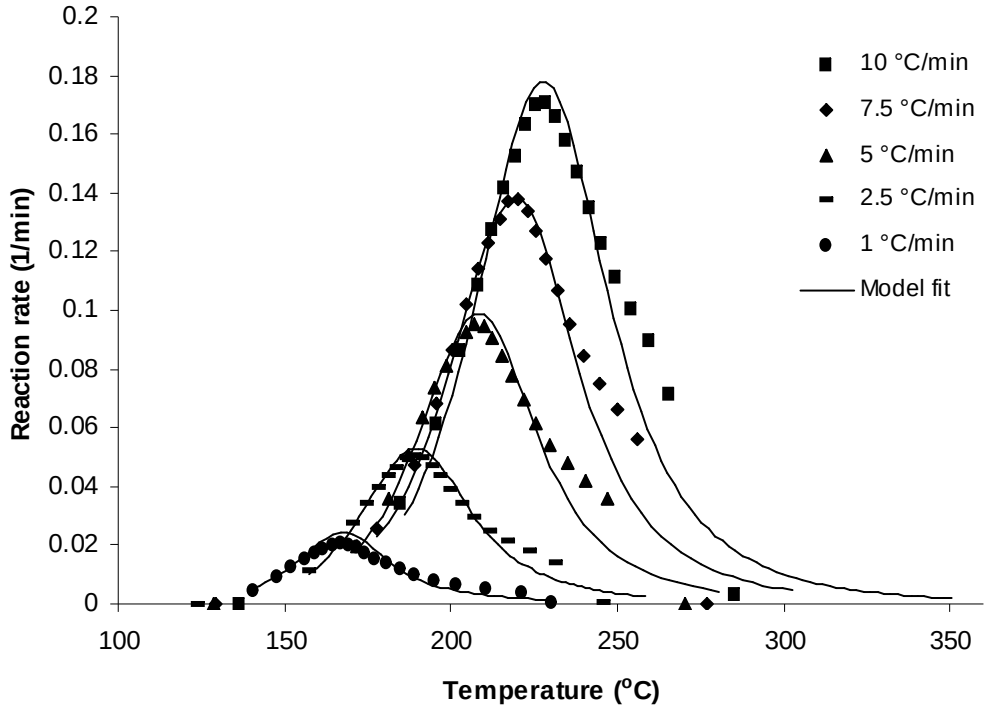

Figure 8.4: Comparison between experimental and simulated values of reaction rate versus temperature for a number of dynamic experiments for the 8552 resin system

As it was reported in chapter 5, the total heat of reaction was estimated to be 657 J/g. Other researchers who investigated the same epoxy system calculated total heats in the range of 483 to 560 J/g. This was attributed to the fact that they studied the 8552 prepregs. In these cases different cure kinetics models were utilised to fit the experimental data. For example Sun et al [138] used a similar phenomenological model to describe the cure kinetics of the 8552 prepreg, which contained 33 % carbon fibres. Their experiments were conducted in the region of 110 to 220^{o}C. While the activation energy of the first Arrhenius factor, E_1 was found to be 57.3 kJ/mol, similar to the one presented in table 8.1, on the other hand the activation energy E_2 was found to be 19.6 kJ/mol (61.84 here). This difference may be attributed to the fact that the prepreg contained carbon fibres and that this model did not take into account any dynamic heating experiments. The same group [139] used on the same epoxy prepreg a 'dynamic phenomenological model' which utilises a combination of area under peak calculations and peak temperatures to formulate the cure kinetics model. This model assumed two reaction peaks. Player et al [140] utilised an empirical phenomenological equation to describe the curing reaction of 8552 resin, without incorporating factors that take into account any diffusion limitations. The total heat of reaction measured was 483 J/g and the activation energy was found to be 63.4 kJ/mol, as in this case.

8b. Cure kinetics modelling of the T800/3900-2 prepreg system (Round Robin Participation)

The purpose of the participation in the Round Robin study was to isolate the sources of variability between cure kinetics models developed by different laboratories for the same material. It progressed through a number of stages using a prepreg material. The sources of model variability tested were: sample preparation, experimental method, data reduction, data analysis and model selection. At each stage the participants were given a set of DSC data to analyse, based on the fact that the same starting point prior to data reduction and model fitting would apply. At the final stage the data used was already analysed and the same cure kinetics model was applied from each

participant. The only difference was the technique used to calculate the fitting parameters of the model [141]. Here the results of the final stage are presented. The participation in this program helped in terms of comparing the different techniques. The final results are summarised in appendix B.

8.3 The superposition principle

Dynamic heating experiments were conducted in the range of 1 to 15^{o}C/min, while the isothermal cure kinetics data cover the temperature range of 130^{o}C up to 200^{o}C, with a 10^{o}C interval between successive experiments. The isothermal and dynamic data are presented in figures 8.5 and 8.6.

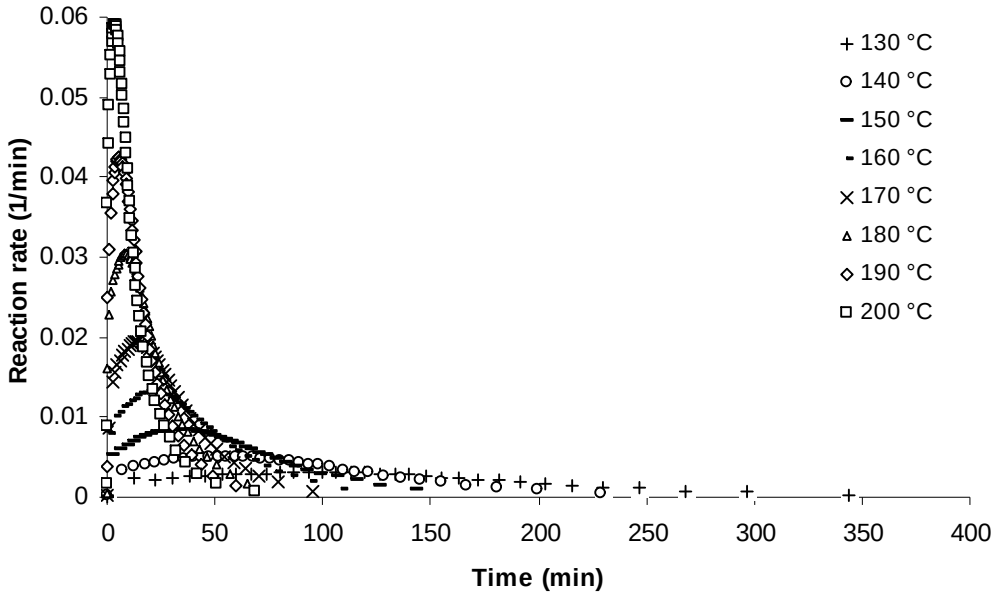

Figure 8.5: Reaction rate versus time for the isothermal cure of the T800/3900-2 prepreg at different temperatures

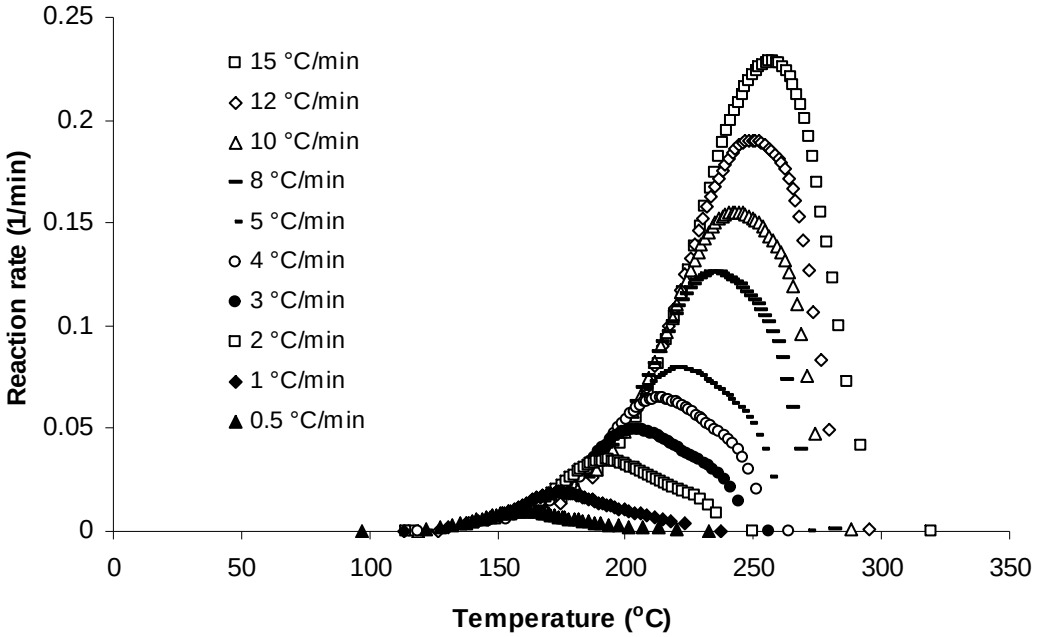

Figure 8.6: Reaction rate versus temperature for the dynamic cure of the T800/3900-2 prepreg at constant heating rates

The average total heat of reaction obtained for the prepreg system, based on the experimental data provided was 134.46 J/g. The validity of the superposition principle tested between the isothermal and the dynamic experimental data is illustrated in figure 8.7.

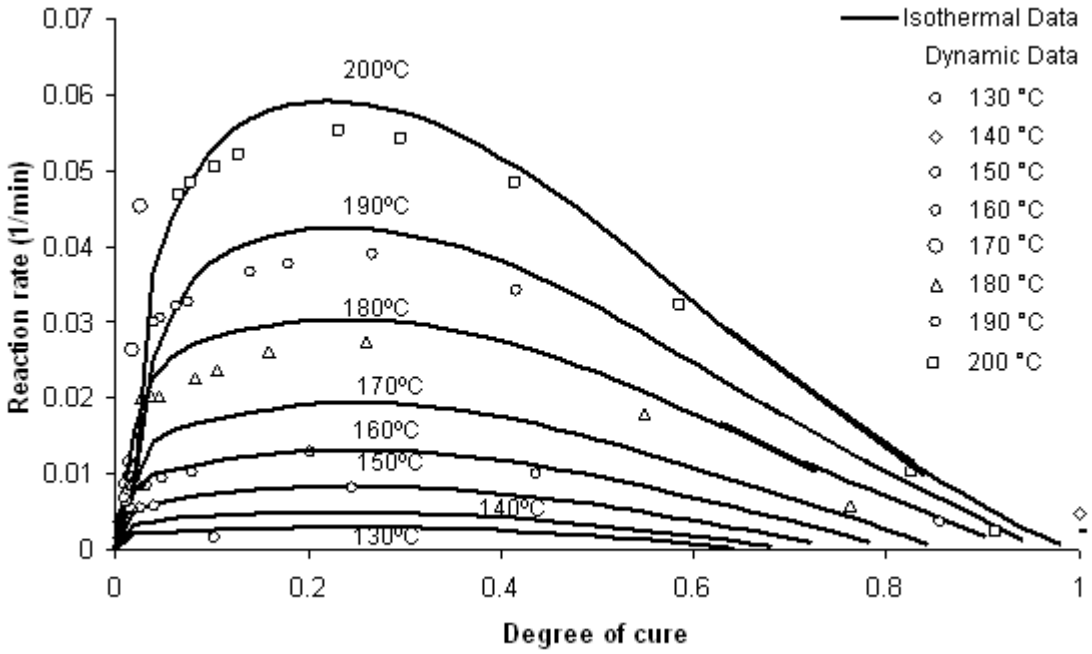

Figure 8.7: Superposition of dynamic and isothermal DSC reaction rate-degree of cure data for the T800/3900-2 prepreg

It can be observed that superposition of the isothermal is in very good agreement with the dynamic tests, showing an overall average relative error of 11 %. This low value of experimental error allows for the development of a cure kinetics model that is based on both isothermal and dynamic DSC data.

8.4 Cure kinetics modelling of the T800/3900-2 prepreg system

The bell shape of the dynamic data indicate an autocatalytic reaction mechanism. The proposed model to be used is a combination of a mechanistic and a phenomenological model that contains diffusion constrains to allow adequate fitting of the later stages of the curing reaction.

$$\frac{d\alpha}{dt} = \frac{k_{eff}(1-\alpha)(B-\alpha)(b+\alpha)}{1+\exp(C(\alpha-(\alpha_C T-\alpha_{C_0})))} + k_3\alpha^m(1-\alpha)^n \qquad (8.3)$$

where $k_{eff} = A_{eff}e^{-E_{eff1}/RT}$, $k_3 = A_3 e^{-E_3/RT}$, and

a is the degree of cure

T is the temperature in Kelvin

A is the pre-exponential factor (min^{-1})

E is the activation energy (J/mol)

B is the ratio of primary amines to epoxide groups (=1 / r), described by Cole et al [142]

b is a fitting parameter

m , n are fitting parameters,

α_c is the maximum degree of cure reached at each isothermal test,

α_{co} is the critical degree of cure at T=0 K (a fitting parameter) and

C is the diffusion factor, taking into account the diffusion limitations at the later stages of the curing reaction, adopted by Khanna and Chanda [43].

The above model consists of eleven parameters; A_{eff}, E_{ff}, A_3, E_3, m, n, B, b, C, α_c and α_{co}. In order to achieve an accurate fit, it was crucial to decrease the number of the parameters, so that the maximum degree of cure was calculated as a function of the absolute temperature from the maximum reached conversions under isothermal curing conditions. The maximum degree of cure as a function of temperature for the isothermal cure of the resin system at different temperatures is presented in figure 8.8. The fit was achieved with the utilisation of a first order polynomial expression, which is the following:

$$\alpha_c = 0.0055T - 1.611 \qquad (8.4)$$

where T is the absolute temperature, expressed in degrees Kelvin. This expression was incorporated into the diffusion factor. After this estimation, the number of parameters was reduced to nine; A_{eff}, E_{ff}, A_3, E_3, m, n, B, b and C. These parameters were estimated by using a genetic algorithm. Both isothermal and dynamic data were fed into the GA routine resulting in the values presented in table 8.2.

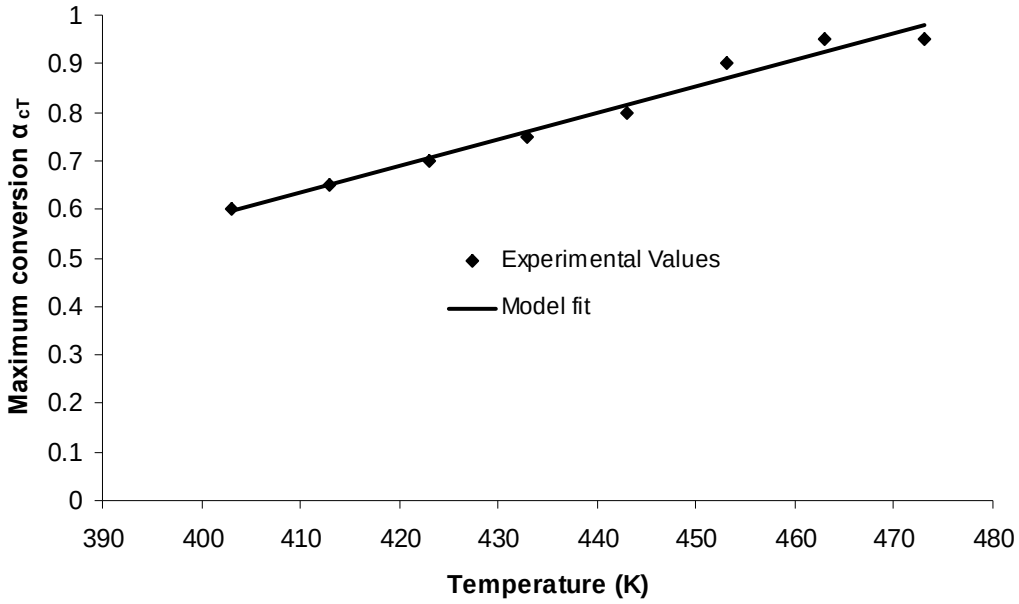

Figure 8.8: Plot of maximum attained degree of cure as a function of temperature of the isothermal cure of the T800/3900-2 prepreg at different temperatures

PARAMETERS	T800/3900-2 prepreg
A_{eff} (min^{-1})	4.16×10^6
E_{eff} (kJ/mol)	66.36
A_3 (min^{-1})	1.49×10^6
E_3 (kJ/mol)	66.29
B	1.289
b	0.01
m	0.204
n	3.849
C	15.049

Table 8.2: Estimated parameters for the fitting of data obtained from isothermal and dynamic experiments

According to Cole et al [142], the amine-to-epoxide ratio (r) should be between 0.77 and 1 for this material, and B should be between 1 and 1.3. The model predicted a value for B=1.289, (r=0.776), which is within the

proposed range. This model can predict the degree of cure with high accuracy, without the need of incorporating the glass transition temperature evolution, which requires further testing.

Comparison between experimental and simulated data for the same thermal profiles showed that the model results deviate less than 11 % from the experimental ones for isothermal and dynamic conditions as can be seen in figures 8.9 to 8.11.

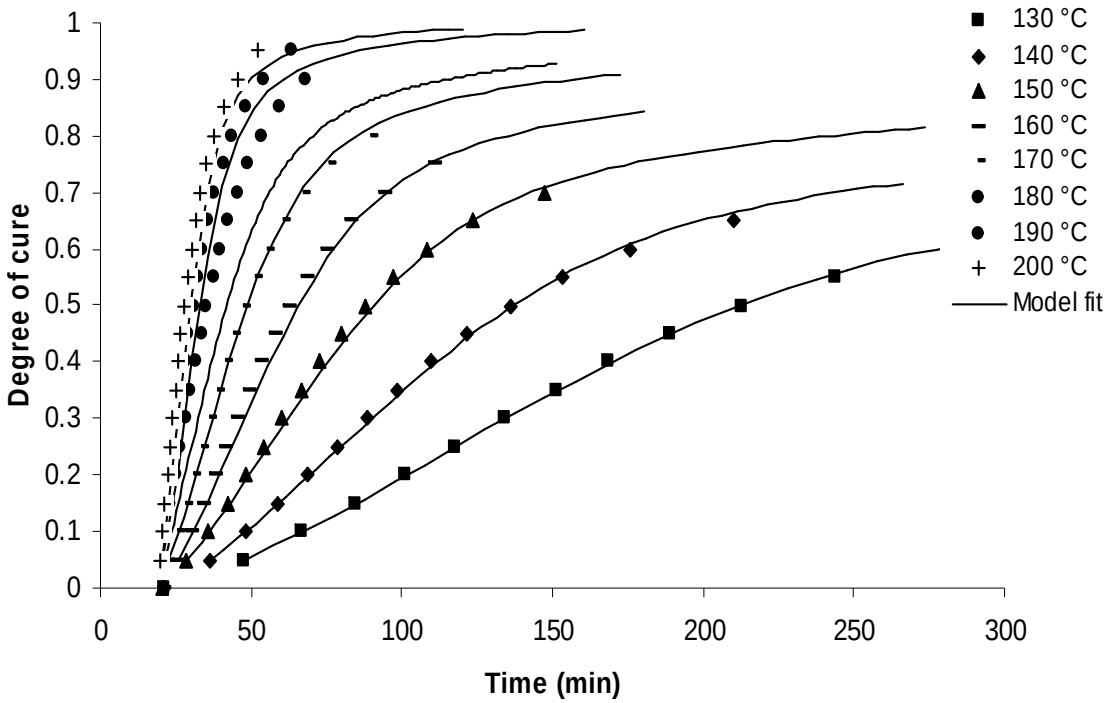

Figure 8.9: Comparison between experimental and simulated values of degree of cure versus time for a number for isothermal experiments for the T800/3900-2 prepreg

The model simulates the experimental curves with high accuracy, even at the later stages of the curing reaction. A discrepancy is observed for the 180^{o}C isothermal test due to incomplete cure (more time was required for this isothermal test so to be considered complete). A deviation is also observed in the case of the higher heating rates, especially after the 250^{o}C (see figure 8.10). This deviation may be justified by the fact that the superposition is valid up to 200^{o}C, where data is available. However, the model seems to fit well the experimental data even beyond that temperature.

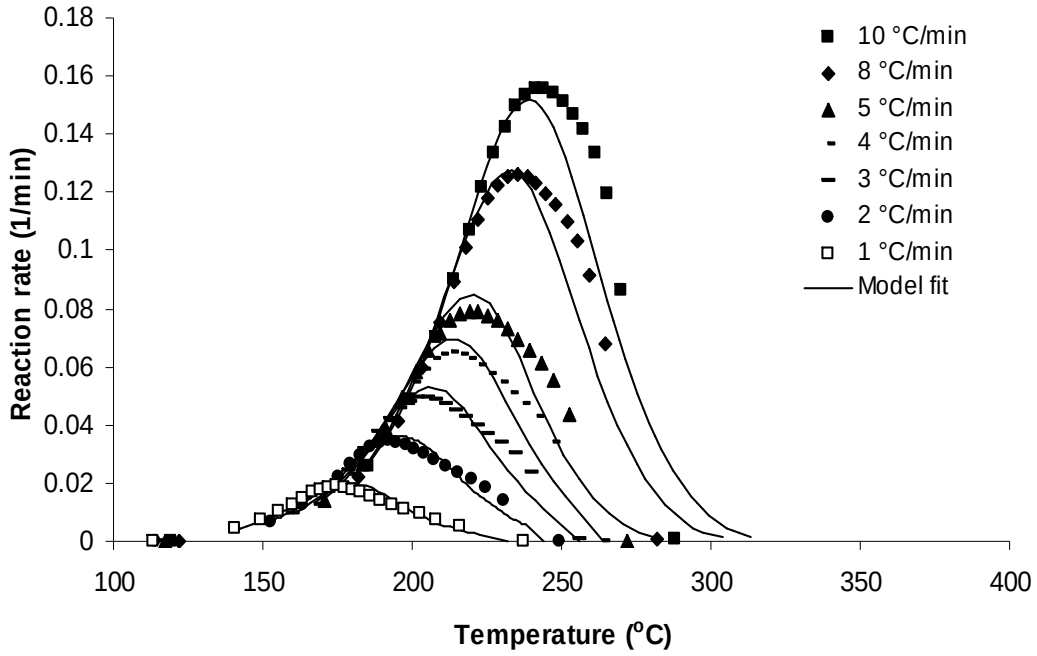

Figure 8.10: Comparison between experimental and simulated values of reaction rate versus temperature for a number of dynamic experiments for the T800/3900-2 prepreg

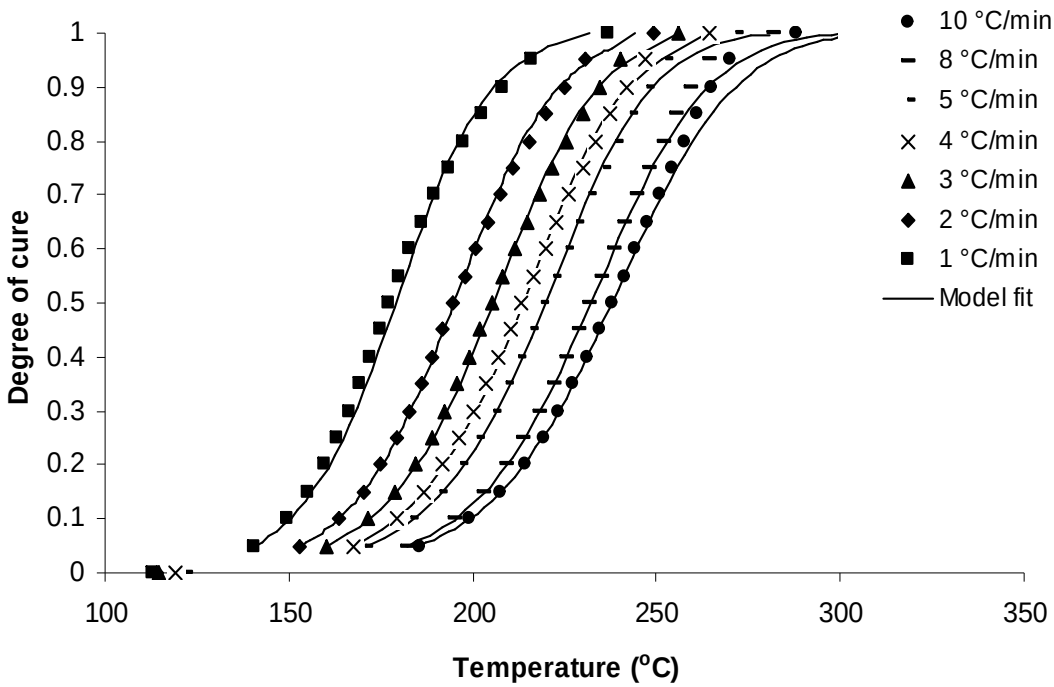

Figure 8.11: Comparison between experimental and simulated values of degree of cure versus temperature for a number of dynamic experiments for the T800/3900-2 prepreg

8.5 Sensitivity analysis of the models utilised

The sensitivity of the model fit was investigated by incorporating a fixed ±2.5 % error on the estimated model parameters. For demonstration purposes, the kinetic model used for the isothermal cure of the MTM 44-1 resin system, described by equation 7.4, was utilised for the investigation of its sensitivity. The estimated parameters are given in table 7.2. For convenience a fixed error of ±2.5 % was incorporated into the model for each parameter and the kinetic simulation was repeated for the isothermal cure at 160^{o}C. The initial fitting parameters as well as the parameters estimated from the sensitivity analysis are presented in table 8.3.

PARAMETERS	MTM 44-1 resin	-2.5%	+2.5%
A_1 (min^{-1})	1.97x10^{6}	1.92x10^{6}	2.02x10^{6}
E_1 (kJ/mole)	60.82	59.30	62.34
A_2 (min^{-1})	1.96x10^{6}	1.91x10^{6}	2.01x10^{6}
E_2 (kJ/mole)	56.29	54.88	57.69
k	0.49	0.48	0.50
l	2.02	1.97	2.07
m	1.84	1.79	1.89
n	2	1.95	2.05
C	0.101	0.098	0.104

Table 8.3: Fitting parameters used in the model sensitivity analysis of the cure kinetics model (equation 7.4) describing the isothermal cure for the MTM 44-1 resin system at 160^{o}C

The effect of each parameter on the simulated kinetic model is shown in figures 8.12 to 8.20. The model fitting starts at a conversion of 5 %.

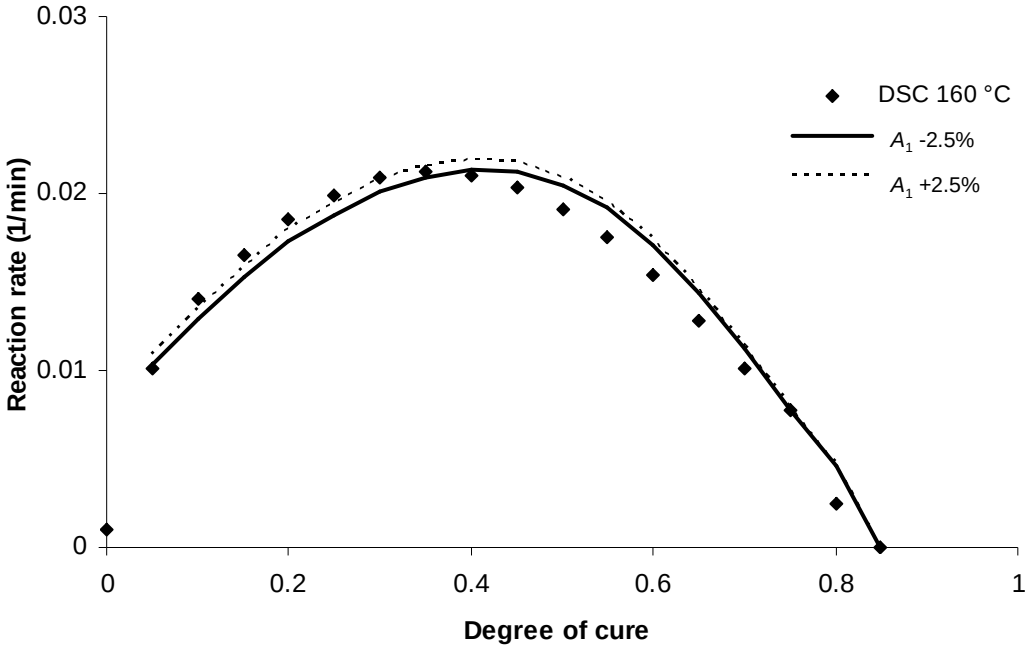

Figure 8.12: Reaction rate versus degree of cure for the isothermal cure of MTM 44-1 resin system at 160°C (estimated parameter A_1)

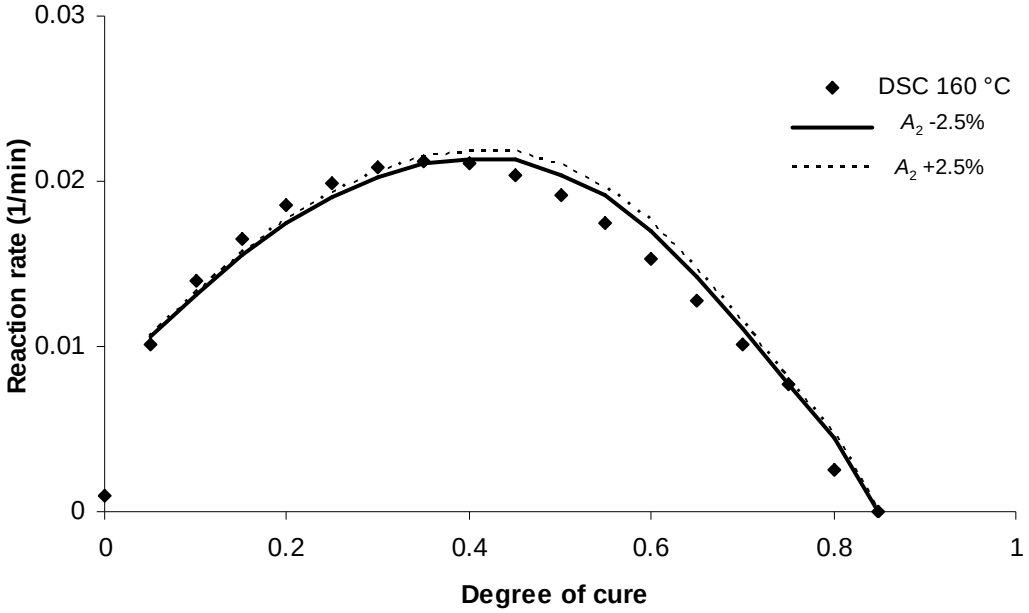

Figure 8.13: Reaction rate versus degree of cure for the isothermal cure of MTM 44-1 resin system at 160°C (estimated parameter A_2)

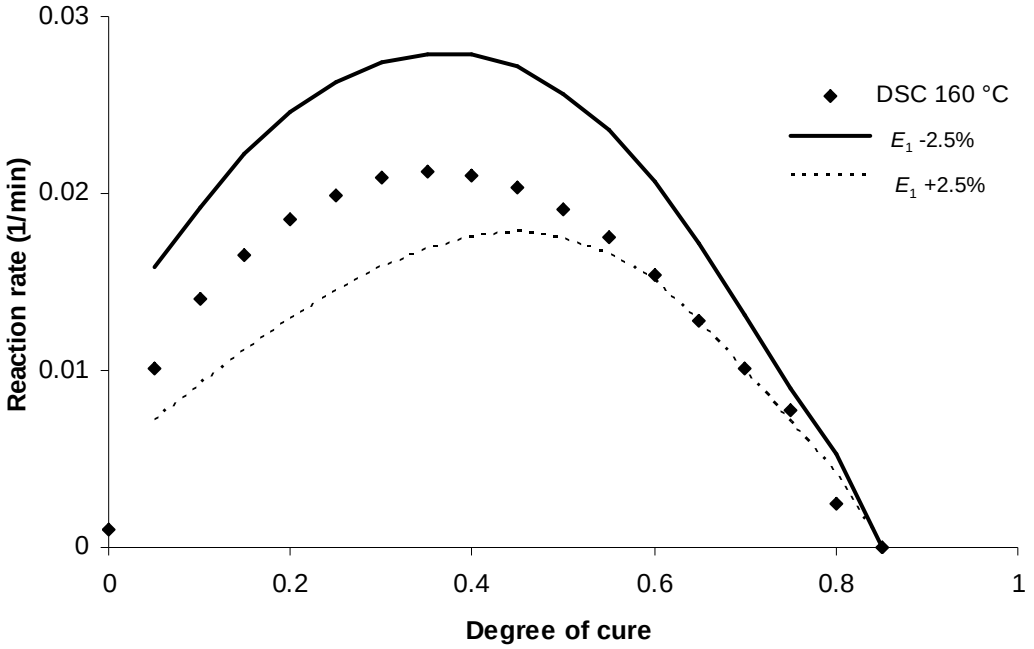

Figure 8.14: Reaction rate versus degree of cure for the isothermal cure of MTM 44-1 resin system at 160°C (estimated parameter E_1)

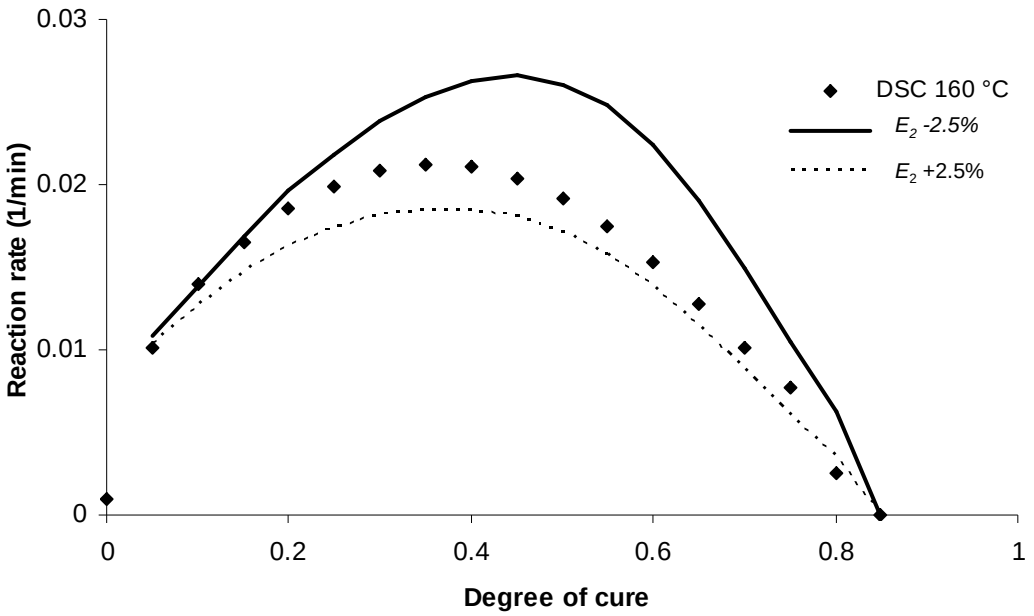

Figure 8.15: Reaction rate versus degree of cure for the isothermal cure of MTM 44-1 resin system at 160°C (estimated parameter E_2)

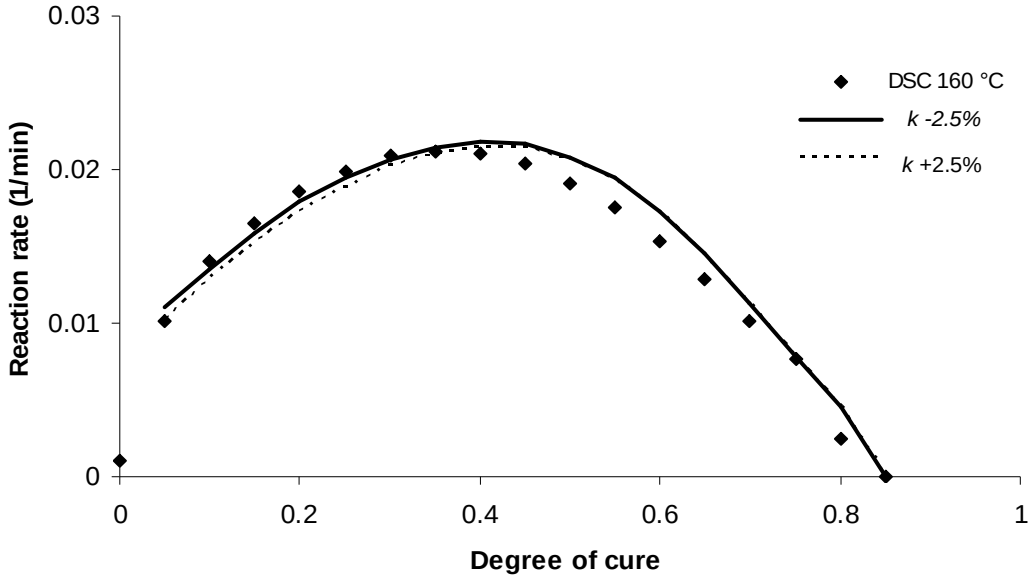

Figure 8.16: Reaction rate versus degree of cure for the isothermal cure of MTM 44-1 resin system at 160°C (estimated parameter *k*)

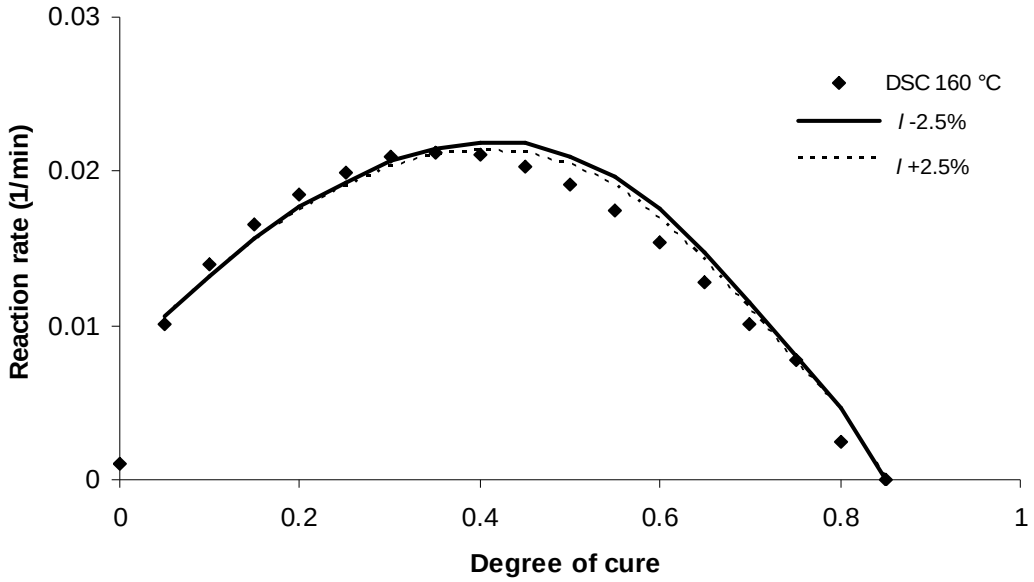

Figure 8.17: Reaction rate versus degree of cure for the isothermal cure of MTM 44-1 resin system at 160°C (estimated parameter *l*)

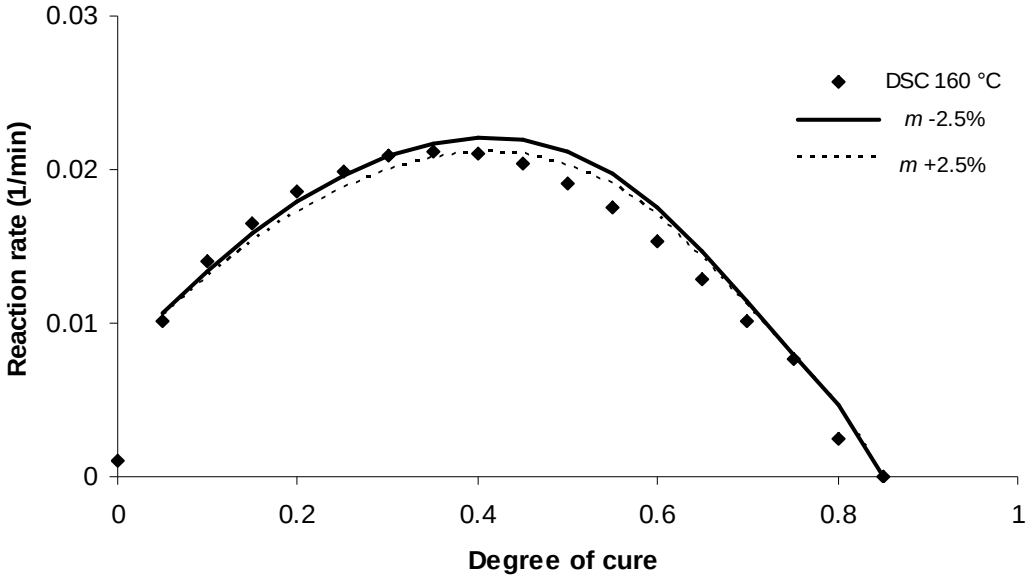

Figure 8.18: Reaction rate versus degree of cure for the isothermal cure of MTM 44-1 resin system at 160°C (estimated parameter m)

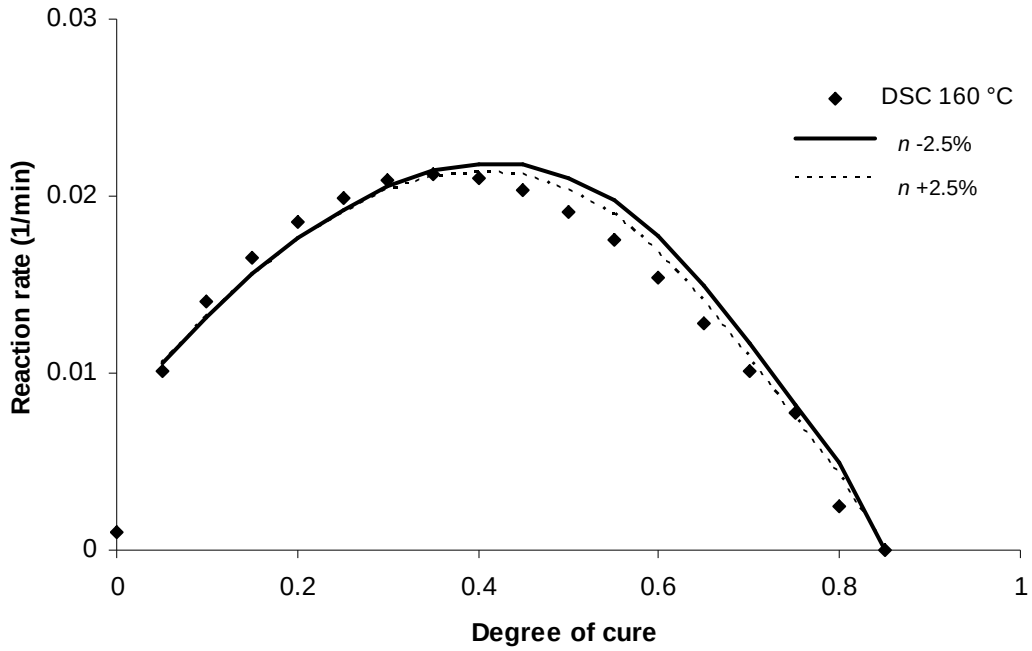

Figure 8.19: Reaction rate versus degree of cure for the isothermal cure of MTM 44-1 resin system at 160°C (estimated parameter n)

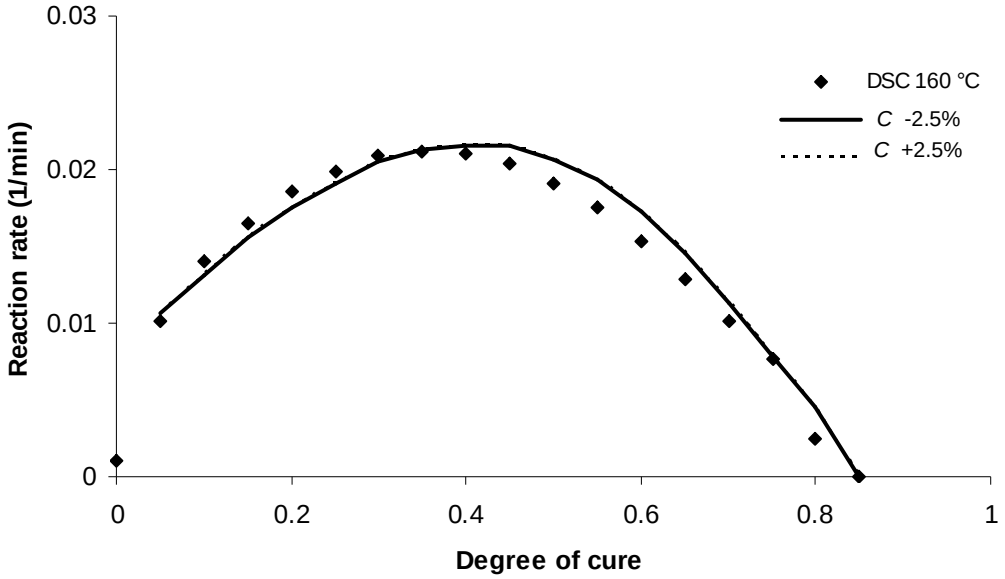

Figure 8.20: Reaction rate versus degree of cure for the isothermal cure of MTM 44-1 resin system at 160°C (estimated parameter C)

It can be concluded from the above figures that the model is insensitive to the changes in the parameters A_1, A_2, m, n, k, l and the diffusion factor C. On the other hand the fitting seems to be very sensitive to the changes of the activation energies E_1 and E_2. A ±2.5 % change in the values of the parameters has a significant effect on the fitting. This effect is the direct outcome of the fact that the nature of the reaction rates follows an exponential trend (Arrhenius relationship). An observation arises from figures 8.14 and 8.15. A 2.5 % decrease of the activation energies causes an increase of the reaction rate while an increase of 2.5 % has quite the opposite effect. Even a very small increase or decrease of the fitting parameters causes a significant divergence of the model fit.

The same analysis applies for the whole range of experiments (isothermal and dynamic DSC experiments) and the rest of the cure kinetics models utilised in this study. Based on the fact that these cure kinetics models are similar to the one used in this analysis, the same sensitivity to the parameters is expected, especially on the activation energies.

Chapter 9

9. Refractive Index Monitoring of Resin and Nanocomposite Cure

This deals with the refractive index cure monitoring of the three resin systems and their nanocomposites containing carbon nanotubes. Optical fibres were embedded into the materials and the change of the refractive index was monitored in the whole range of the curing reaction. The measurements were based on isothermal tests. A good correlation of the refractive index change and the degree of cure was established. An industrial application of the utilisation of optical fibres and dielectric sensors to measure the refractive index change during cure is presented in appendix A.

9.1 Instrumentation (Fresnel Refractometer)

The experimental configuration used in order to measure the refractive index change during the cure of the resin systems and their nanocomposites is shown in figure 9.1.

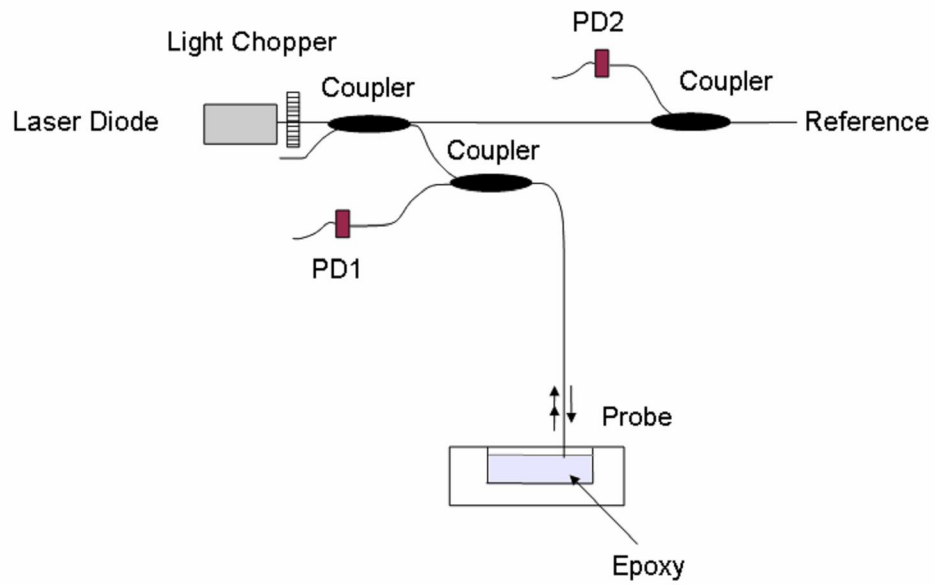

Figure 9.1: Experimental configuration used for the measurement of the refractive index change during cure [143,144]

The output from the laser diode operating at the appropriate wavelength is intensity modulated and coupled into a network of directional couplers. The Fresnel reflection from the fibre / resin system interface is monitored using photodiode PD_1. In the second arm, photodiode PD_2 monitors the reflection from the air / optical fibre interface, acting as an intensity reference to aid the normalisation of the signal and to account for any change in power coupled into the optical fibre from the laser diode. The outputs from the photodiodes are monitored using lock-in amplifiers. The refractive index determined using the refractometer is given by the following equations [145]:

$$n = n_{effco}\frac{1-\frac{\Delta}{\sqrt{R}}}{1+\frac{\Delta}{\sqrt{R}}} \qquad (9.1)$$

$$\Delta = \frac{n_{effco} - n_a}{n_{effco} + n_a} \qquad (9.2)$$

$$R = \frac{V_{air}}{V_{epoxy}} \qquad (9.3)$$

where, n_{effco} is the effective refractive index of the fibre mode, n_α is the refractive index of air given as 1.0002739 , V_{air} is the voltage produced by photodiode PD_2, obtained for the reflection from the fibre/air interface and V_{epoxy} is the voltage produced by photodiode PD_1, corresponding to the reflection from the fibre/resin interface.

For the correlation between the refractive index (RI) and the state of cure of the resin systems used, Cusano et al [14] proposed a relation that relates these two variables:

$$\alpha_n = \frac{n_t - n_o}{n_\infty - n_o} \qquad (9.4)$$

where n_t = RI at time t of the beginning of cure, n_0 = RI at the beginning of cure and n_∞ = RI at the end of cure. Equation 9.4 assumes a linear relationship between degree of cure and RI during the reaction. The relation follows the reaction up to the fully cured stage; this can be adapted to approach the maximum conversion (determined experimentally by DSC) by

$$\alpha(T) = a_n \alpha_{DSC}^{\max}(T) \qquad (9.5)$$

where $\alpha(T)$ is the conversion for the isothermal cure at temperature T and $\alpha_{DSC}^{\max}(T)$ is the maximum conversion obtained for an isothermal DSC experiment at temperature T.

9.2 Refractive index cure monitoring of the MY 750 / HY 5922 resin system and its nanocomposite containing 0.06 wt % of Hyperion carbon nanotubes (batch 1)

Optical fibres were embedded into the MY 750 / HY 5922 resin system and its nanocomposite in order to monitor the refractive index change during cure. For this purpose the Fresnel technique was utilised. Isothermal tests were conducted at 80^{o}C for about 6 hours. The aim of these measurements was to achieve a direct correlation between the refractive index and the degree of cure, but also to investigate how the refractive index changes when carbon nanotubes are incorporated into the resin system. Utilisation of equations 9.4 and 9.5 allows for the correlation of the measured refractive index with the degree of cure of the resin system and its nanocomposite containing 0.06 wt % Hyperion carbon nanotubes. This correlation is illustrated in figures 9.2 and 9.3. Furthermore, using the cure kinetics models developed for the resin systems (see chapter 7), a theoretical value for $\alpha_{DSC}^{\max}(T)$ was calculated based on the heating rates.

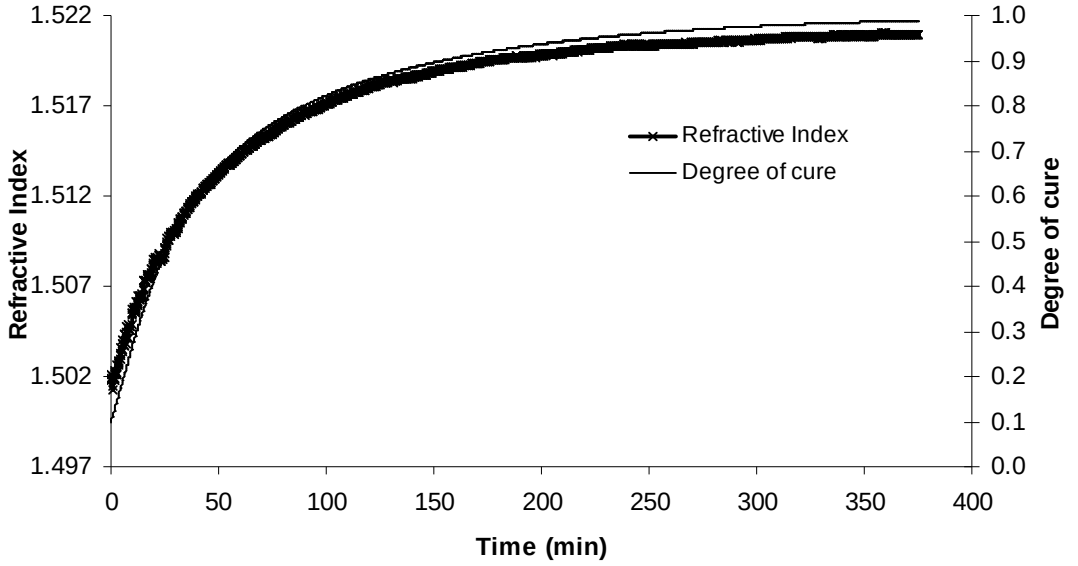

Figure 9.2: Refractive index and degree of cure (based on the cure kinetics model) comparison for the isothermal cure of the MY 750 / HY 5922 resin system at 80°C for 6 hours (1550 nm)

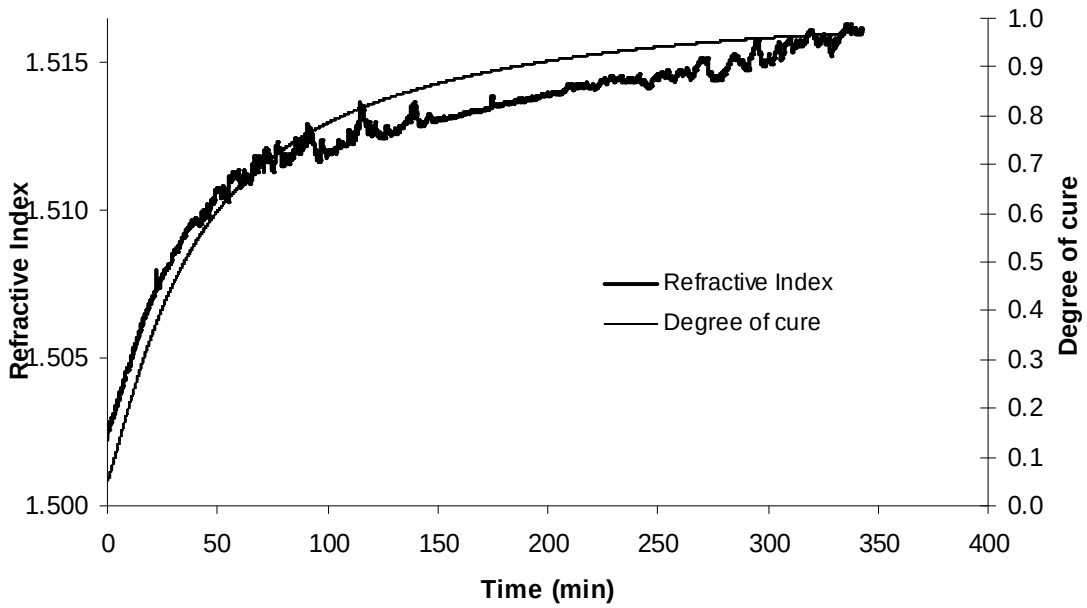

Figure 9.3: Refractive index and degree of cure (based on the cure kinetics model) comparison for the isothermal cure of the MY 750 / HY 5922 resin system containing 0.06 wt % Hyperion carbon nanotubes (batch 1) at 80°C for 6 hours (1550 nm)

The refractive index evolution of the neat resin presented in figure 9.2 is not as noisy as that of the nanocomposite presented in figure 9.3. In the case of the neat epoxy system, the refractive index starts at a value of 1.5019, corresponding to the uncured material and goes up to 1.5201 (corresponding to the fully cured), while for the nanocomposite the values are 1.5025 and 1.5152 for the uncured and the fully cured material, respectively. A potential explanation about this noisy signal, in the case of the nanocomposite, would be the mobility of carbon nanotubes up to the gelation point.

The resin system and its nanocomposite tests show a good correlation between the refractive index change and the degree of cure. It is important to note that the linear relationship between the degree of cure and the refractive index has not been proved to date. Lam and Afromowitz [146,147] propose that an epoxy resin's RI change is linear with respect to cure up until the gelation point, beyond which the formation of a giant macromolecule impedes shrinkage in volume of the sample and the linearity assumption is no longer valid. This correlation was observed for the MY 750 / HY 5922 resin system and its nanocomposite and is presented in figures 9.4 and 9.5.

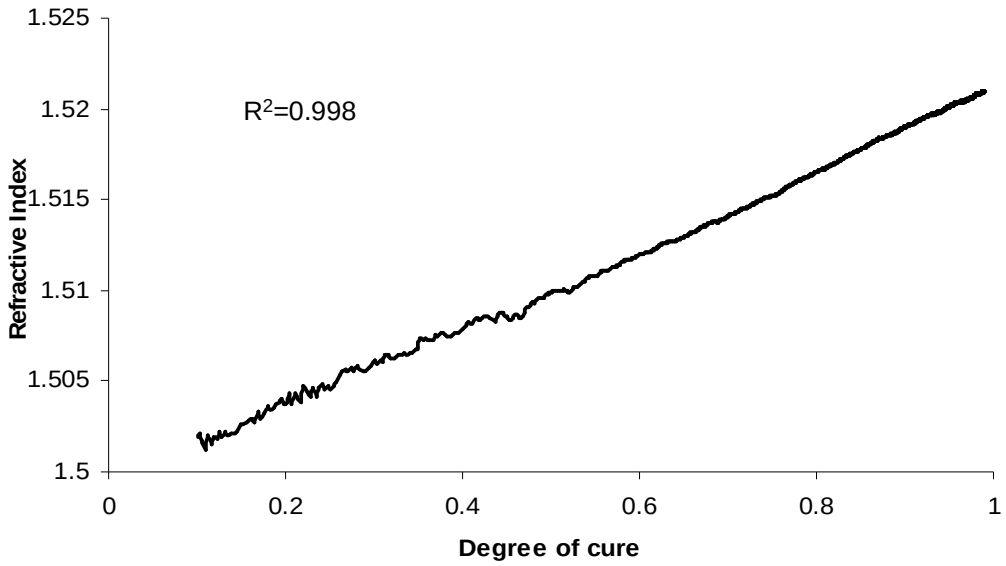

Figure 9.4: Correlation between the degree of cure and the refractive index for the isothermal cure of the MY 750 / HY 5922 resin system at 80°C for 6 hours (1550 nm)

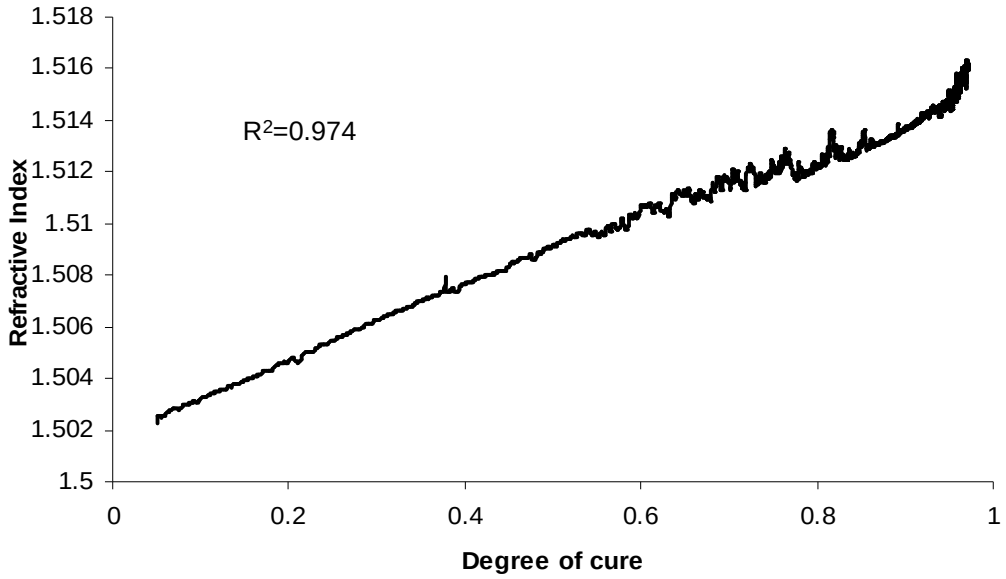

Figure 9.5: Correlation between the degree of cure and the refractive index for the isothermal cure of the MY 750 / HY 5922 resin system containing 0.06 wt % Hyperion carbon nanotubes (batch 1) at 80^{o}C for 6 hours (1550 nm)

The refractive index shows an almost linear trend, even at the later stages of the curing reaction. This is depicted from the r-coefficients of the linear correlation in figures 9.4 and 9.5.

9.3 Refractive index cure monitoring of the MTM 44-1 resin system and its nanocomposite containing 1 wt % of Thomas Swan carbon nanotubes (batch 6)

Isothermal curing tests were conducted at 180^{o}C for 2 hours for the MTM 44-1 resin system and its nanocomposite containing 1 wt % Thomas Swan carbon nanotubes (prepared with the utilisation of the ultrasonic bath and mixed by hand – see also chapter 3). The optical fibre was embedded after the following treatment: the resin system was heated up to 80^{o}C so that the viscosity decreased to a minimum. That allowed for the penetration of the fibre. The resin was allowed to cool down to room temperature. Figures 9.6 and 9.7 illustrate the refractive index evolution during the cure of the neat resin and its nanocomposite.

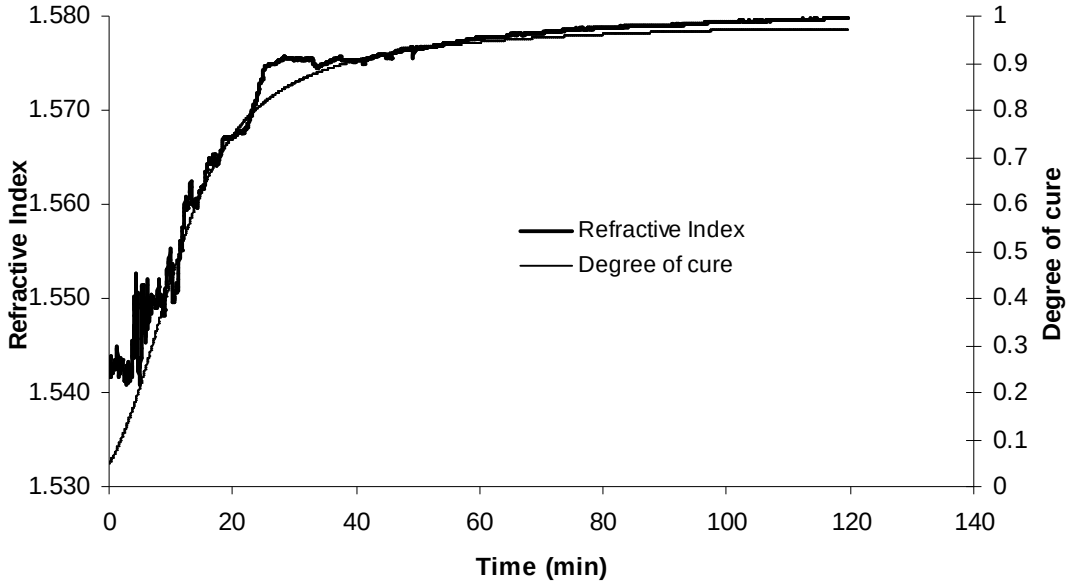

Figure 9.6: Refractive index and degree of cure (based on the cure kinetics model) comparison for the isothermal cure of the MTM 44-1 resin system at 180^{o}C for 2 hours (1550 nm)

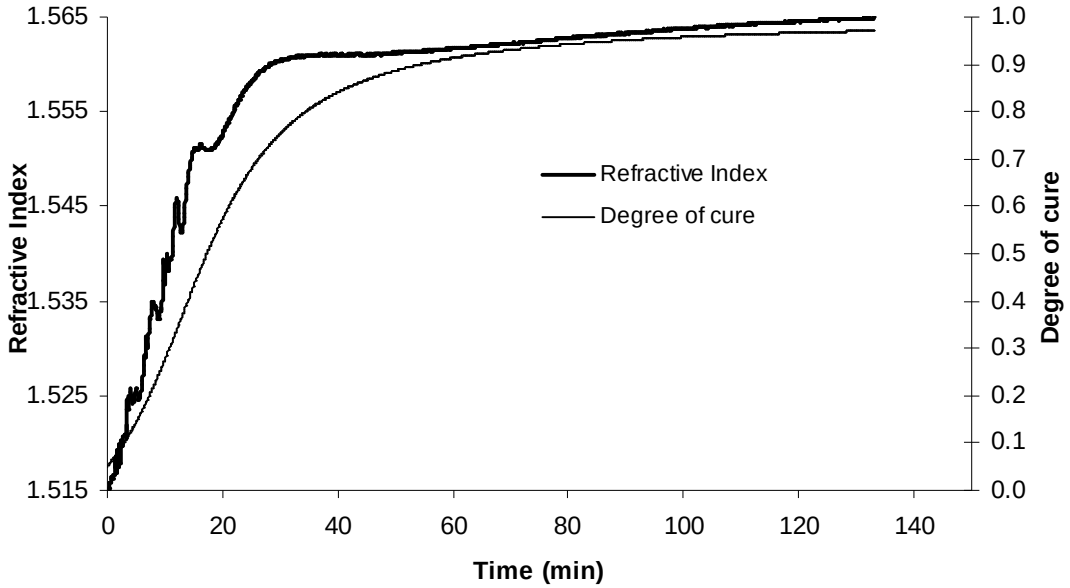

Figure 9.7: Refractive index and degree of cure (based on the cure kinetics model) comparison for the isothermal cure of the MTM 44-1 resin system containing 1 wt % Thomas Swan carbon nanotubes (batch 6) at 180^{o}C for 2 hours (1550 nm)

Both refractive index versus time curves indicate a noisy signal up to 30 minutes of the reaction. After that the signal seems to develop linearly. This trend occurs after gelation, which takes place at around 22 minutes for this resin system (see figure 5.39, chapter 5). A possible explanation for this noisy signal is the existence of air bubbles trapped into the resin. This was revealed from the SEM image of the fully cured sample presented in figure 9.8. The tip of the optical fibre is trapped between two air-bubbles. A possible scenario is that at the beginning of the reaction, the bubbles are moving, thus the signal that the optical fibre is sensing is noisy. After gelation, when the resin becomes solid the bubbles do not move and the noise vanishes.

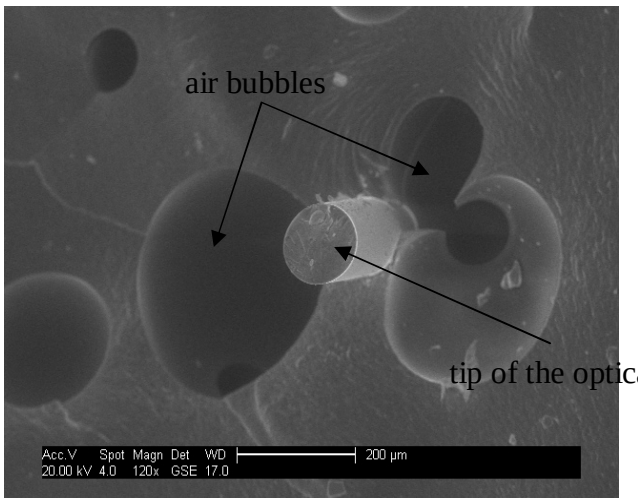

Figure 9.8: SEM image of the fracture surface of the MTM 44-1 resin system after curing at 180^{o}C for 2 hours

The refractive index of the uncured neat epoxy system was 1.5420 and after the end of the curing reaction it reached the value of 1.5798. Despite the fact that air-bubbles exist in the system, the correlation with the degree of cure is very good. The same observation applies for the nanocomposite containing 1 wt % carbon nanotubes, however, in this case a linear correlation could not be established before gelation. This difficulty in correlating the refractive index to the degree of cure before gelation is probably the synergistic effect of the existence of air-bubbles, and the mobility of carbon nanotubes. The same occurred in the case of the MY 750 / HY 5922 nanocomposite where a noisy signal was produced due to the incorporation of carbon nanotubes. The refractive index in this case had a value of 1.5153,

which corresponds to the uncured specimen and was raised up to 1.5650 at the end of the reaction. Another potential explanation of the resulted noisy signal is phase separation, which occurs at some point during the curing reaction, leading to a heterogeneous two-phase system. The optical fibre was not able to detect the two-phases, despite the fact that the epoxy-rich particles had a size ranging from 5 to 15 μm (mean diameter of the optical fibre 125 μm, mean diameter of the optical fibre core 8-10 μm). This is better seen on the SEM images of figure 9.9. The fully cured specimen of the neat MTM 44-1 resin system that contained two optical fibres was polished on one side. This caused the pull-out of the fibre. However, the imprint of the fibres was left on the resin surface (see figure 9.9a). Figures 9.9b to c illustrate the 'trough' of the optical fibre and the surface area of the fully cured specimen. In figure 9.9d it is observed that part of the optical fibre might still be remaining on the polished surface. Observation on SEM did not end up in managing to distinguish the two phases (optical observation). Nevertheless, the utilisation of the optical fibres led to a good correlation between the refractive index change and the degree of cure for the neat epoxy system after gelation. A possible explanation for this is that the measured refractive index is a function of the refractive indices of the thermoset-rich and the thermoplastic-rich phases.

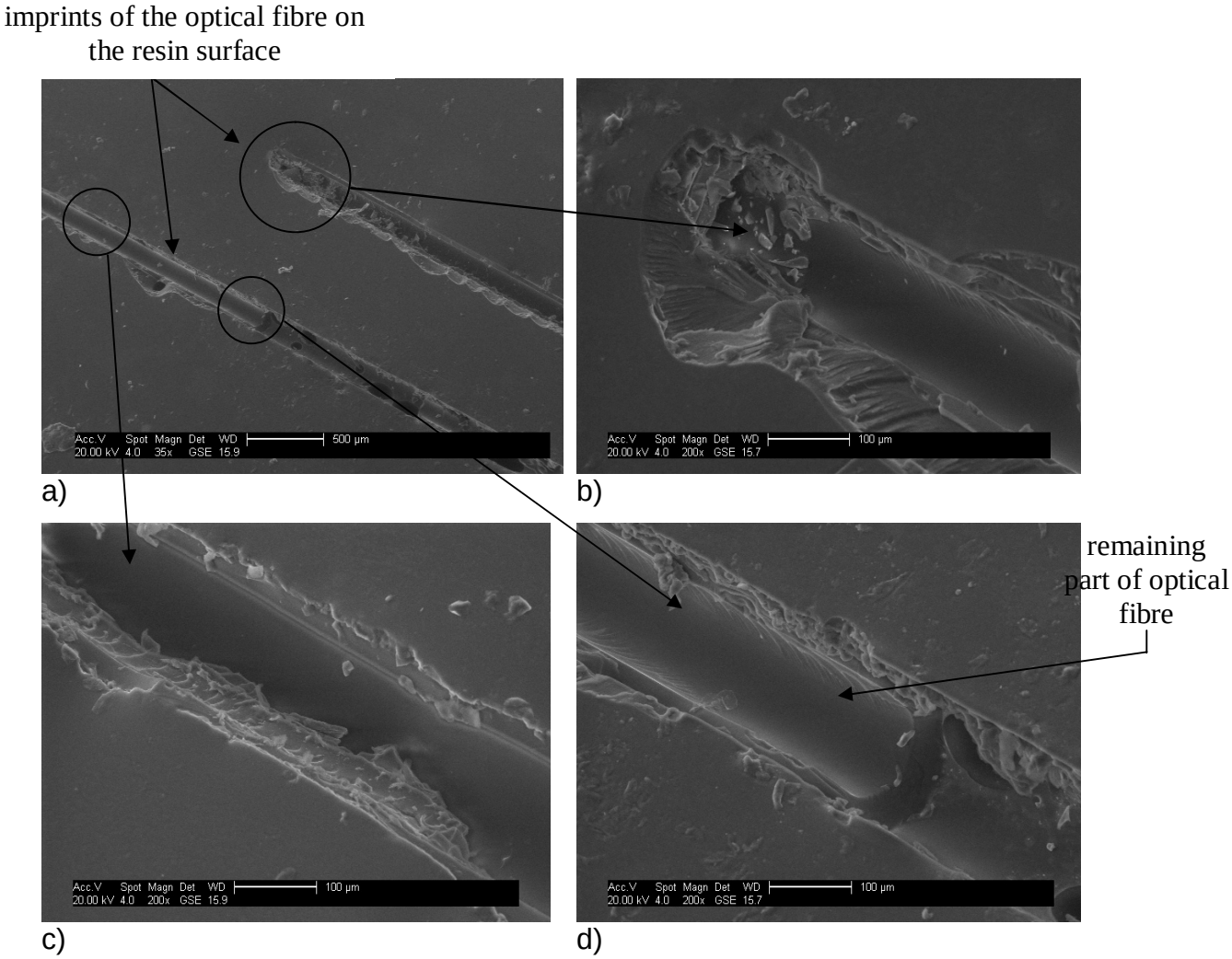

Figure 9.9: Environmental SEM images of the top surface of the fully cured MTM 44-1 resin system illustrating the 'trough' of the optical fibres a) low magnification and b-d) high magnifications of a)

Figure 9.10 illustrates a schematic of the embedded optical fibres in the epoxy resin system and its nanocomposite containing 1 wt % carbon nanotubes. The domains of the thermoset-rich phase particles are also depicted. It should be noted that if a certain percentage of the epoxy-rich phase particles is concentrated near the sensing are of the optical fibre, which has a sensing diameter similar to the size of the particles, it would be possible to distinguish the two phases (the continuous thermoplastic-rich phase and the particle thermoset-rich phase). However, as discussed in chapter 10, when carbon nanotubes were incorporated into the resin system that led to the formation of epoxy-rich phase particles of the size of 5-50 µm. This difference could lead to the assumption that particles having a diameter as big as 50 µm would be easily detected from the optical fibre.

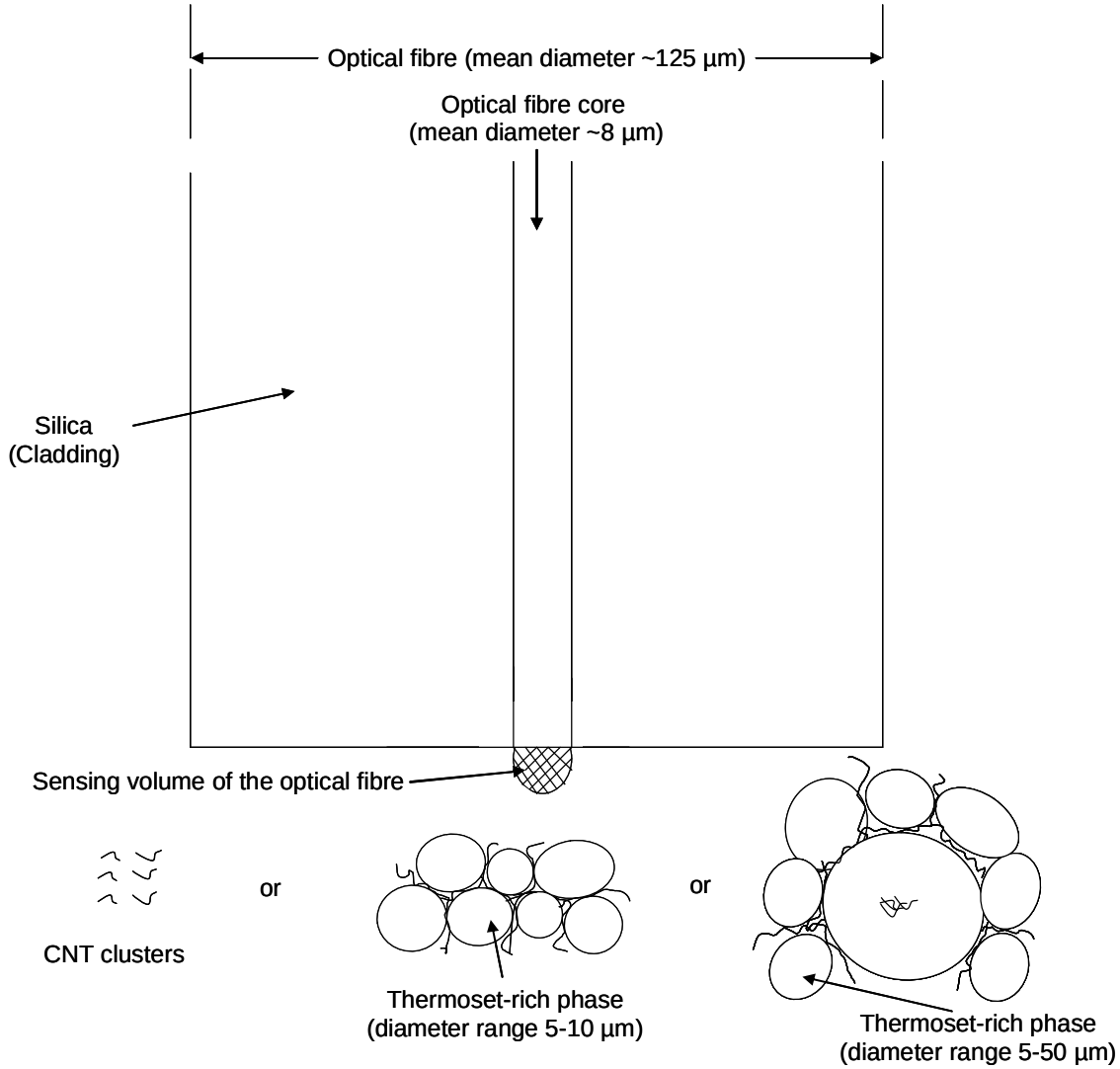

Figure 9.10: Schematic of the optical fibre embedded into the MTM 44-1 resin system and its nanocomposite containing 1 wt % Thomas Swan carbon nanotubes

9.4 Refractive index cure monitoring of the 8552 resin system

Isothermal curing experiments were conducted at 180^{o}C for about 135 minutes for the 8552 resin system. The resin was heated up to 80^{o}C and remained there for about ten minutes, a time interval that allowed for the penetration of the fibre. At that temperature the initial degree of cure was less than 5 %. Subsequently, the resin was allowed to cool down to room temperature and then heated to 180^{o}C at a rate of 8^{o}C/min. By the time that the isothermal temperature of 180^{o}C was reached the degree of cure did not

exceed 15 %. Figure 9.11 illustrates the refractive index measurement for this epoxy system.

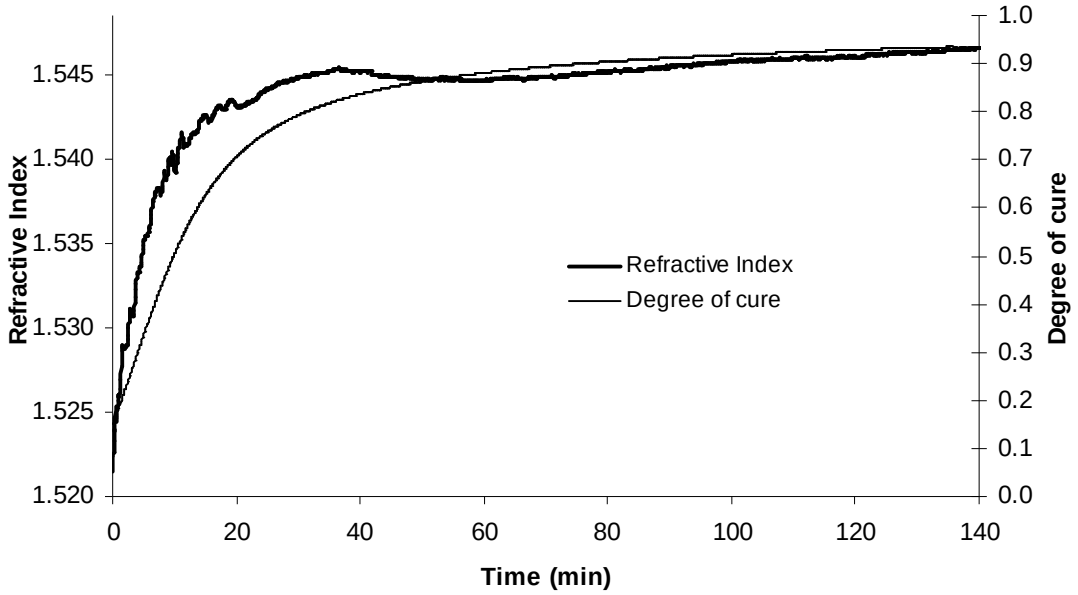

Figure 9.11: Refractive index and degree of cure (based on the cure kinetics model) comparison for the isothermal cure of the 8552 resin system at 180^{o}C for 135 minutes (1550 nm)

The value of the refractive index is 1.5215 at the beginning of each isothermal, and 1.5466 at the end of the test. The final degree of cure reached at that temperature is about 93 %. The refractive index seems to follow the same trend as the degree of cure curve but there is a deviation. This deviation is also followed after the occurrence of gelation. The reason for that is the existence of air bubbles, trapped in the epoxy system. This became evident when the fracture surface of a specimen after an isothermal cure test was analysed on SEM. The image is depicted in figure 9.12.

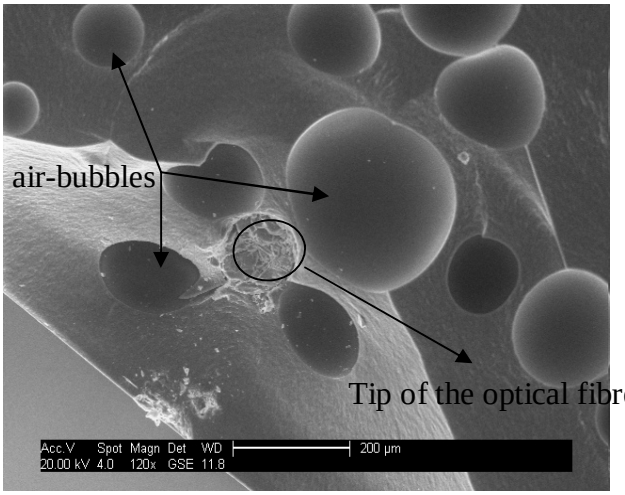

Figure 9.12: SEM image of the fracture surface of the 8552 resin system after curing at 180^{o}C for 135 minutes

The fractured optical fibre is surrounded by air bubbles that move during the initial stages of the reaction. This movement seems to stop after gelation, when the resin becomes solid, but still the wettability of the optical fibre is not adequate. It does not have enough contact with the surface of the resin, thus this deviation is observed. This is better seen in figure 9.11, where a decrease in the refractive index occurs during the isothermal test at around 40 minutes and then an increase again at around 100 minutes. However, it seems to follow the trend of the reaction.

9.5 Refractive index cure monitoring of the resin systems and their nanocomposites

In conclusion, the results of the refractive index measurements, based on isothermal curing tests, showed that the optical fibres seem to follow the curing reaction up to the end, although that some deviations occur. In the case of the MY 750 / HY 5922 that was liquid, the wettability of the optical fibre proved to be very good which resulted in a very good correlation between the refractive index change and the degree of cure. In addition, the incorporation of carbon nanotubes seems to be one of the reasons that the signal is not as smooth as in the case of the neat system. A potential explanation would be the mobility of the nanoparticles in the system.

A good correlation was found for the two commercial resin systems, but that occurred after gelation. One of the reasons that led to the deviation of the measured degree of cure was practically the trapped air in the resin. The disappearance of the air bubbles would allow for a less noisy signal, especially at the initial stages of the curing reaction (pre-gel state). However, the formation of the two-phase system after phase separation (MTM 44-1 resin system and its nanocomposite) together with the mobility of the nanoparticles was probably the main reason that led to a deviation on the correlation at the initial stages of the curing reaction. After gelation a good correlation was established.

Chapter 10

10. An Overall Discussion on the Effect of Carbon Nanoparticle Addition on the Epoxy Resin Systems and Suggestions for Future Work

In this part a general discussion of the effect of the carbon nanoparticle incorporation into the resin systems is presented. Suggestions for future work are also presented.

10.1 Overall Discussion

The study reported in this thesis aimed to give answers to questions arising from the incorporation of carbon nanoparticles into the resin systems utilised. These questions are based on the main argument of how the incorporation of carbon based nanofillers affects the cure of epoxy resins and how these effects depend upon the nature of the nanofiller, for a given resin system. The study has provided answers to these questions for the specific combinations of two very different epoxy resins, namely the liquid MY 750 / HY 5922 and the toughened epoxy MTM 44-1 when carbon nanotubes and carbon black particles were incorporated. Nevertheless, it is clear that these answers are unlikely to be generic or at least final. Recently presented work from the TUHH in Germany [148] has shown that quite different effects on the cure kinetics can be obtained. It is quite likely that further study is going to be required so that the effects of this kind of fillers on the cure kinetics of thermosets will be well understood in terms of producing commercial end-products.

Several ‘tools’ were developed in the course of this work, which allowed for the analysis of the experimental data and the conclusions drawn from this study. The ones which are specific to the study of uncured epoxy nanocomposites can be listed as mixing techniques and microstructural characterisation (Chapter 4), offline cure monitoring by following changes in

the rheological properties (chapter 5) and thermal analysis (chapter 5) and cure monitoring via optical fibre sensors (chapter 9 and Appendix A) (NB The optical fibre monitoring involved a collaboration with the Optics group of Prof. Tatam, Cranfield University). More generic tools which were required for the study and the development of cure kinetics modelling in thermosets include the methodology of thermal analysis for obtaining cure kinetics models and the utilisation of Genetic Algorithms (GAs) as a parameter fitting technique. The validation of the modelling methodology used in this study, being developed into a standard for epoxy systems, was carried out during the participation in an international Round-Robin programme (chapter 8 and appendix B). This participation concentrated on the utilisation of GAs for cure kinetics modelling and the comparison of the analysis with different methodologies developed by the individual participant groups.

Initially, the cure kinetics of three epoxy systems was studied in terms of rheology, cure kinetics modelling and glass transition temperature development. DSC and rheometry studies were conducted and techniques developed in this group such as the utilisation of GAs were used for the development of cure kinetics models. The incorporation of carbon nanotubes and carbon black particles into the two epoxy resins required the utilisation of new techniques in terms of dispersing the nanoparticles in the epoxy matrices and studying the properties of the formed nanocomposites.

The next paragraphs are going to be concentrated on the techniques utilised to study the properties of the formed nanocomposites and the comparison with the properties of the neat systems.

10.1.1 Preparing and handling uncured epoxy nanocomposites

There was no past expertise of working wih carbon nanoparticle containing treating thermoset nanocomposites in the group when this project started. The sourcing of the materials was to some extent dictated by the requirements of the project funding the work (utilisation of optical fibres as a cure monitoring technique on the base resin systems), but primarily by availability. There

were considerable problems in learning to handle the commercial CNT / epoxy Hyperion premix in a safe manner. Initially simple mechanical mixing techniques were utilised in order to achieve dispersion of the nanoparticles into the resin systems. The simple mixing was found to be inadequate. Later on the purchase of the Dispermat® CN F2 model shear mixer, which was tested on the MY 750 / HY 5922 resin with the incorporation of the Hyperion carbon nanotubes and the Monarch carbon black particles, gave the possibility of developing a mixing technique which allowed for a better state of dispersion to be achieved. Finally the purchase of the Branson S-450D ultrasonic horn gave us the possibility of achieving an acceptable level of carbon nanotube dispersion. Further optimisation of the ultrasonication process will allow the achievement of excellent dispersion results, at least for two-part epoxy resin systems. The utilisation of the ultrasonic horn on preformulated resin systems, such as the one-part MTM 44-1 resin system, is likely to be problematic due to the fact that the temperatures reached on the horn surface cause the 'onset' of the curing reaction. However, depending on the concentration of carbon nanoparticles incorporated into the resin system, an acceptable state of dispersion would be possible to be achieved with the optimisation of the mixing process.

10.1.2 Microstructural characterisation of the polymer nanocomposites

Initially TEM was utilised to characterise the structure of the formed nanocomposites. However, images from TEM are much more difficult to obtain when compared with the utilisation of other techniques, such as SEM. TEM images do not represent the general structure of the thermoset matrix, certainly less so than SEM images. SEM characterisation of cured nanocomposite samples is becoming a standard technique. It proved to be quite effective, especially in the latest stages of the study. The characterisation was based on images obtained from the cold fractured surface of cured specimens. The combination of SEM and TEM techniques is likely to prove very useful, especially in conjuction with other techniques, such as AFM / UFM and Nanoindentation [149].

The utilisation of SEM proved to be a particularly suitable tool in the case of the MTM 44-1 resin system. Initially TEM was utilised in order to characterise the microstructure of the base system. It revealed that the system phase separates (figure 4.7) and that the thermoset and the thermoplastic form two different phases: a thermoset-rich phase with particles size between 3 to 13 μm and a continuous thermoplastic phase. This was based on the characterisation of a relatively small area on the specimen surface. The utilisation of SEM gave an estimation of the epoxy-rich phase particles size ranging between 5-15 μm (figures 4.12a and b). Thus the particle size estimates from the two techniques are in approximate agreement.

It was mentioned in chapters 4 and 9 that the incorporation of carbon nanoparticles in this resin led to the formation of some 'superparticles' in the epoxy-rich phase. This very interesting observation was made especially with the incorporation of 1 wt % of Thomas Swan carbon nanotubes and it was independent of the dispersion technique utilised (see table 3.1). The formed particles had a size ranging from 5 to 50 μm. The 50 μm epoxy-rich particles initially seemed to be formed because of the fact that the smaller particles were united in a 'superparticle'. However, a further analysis by SEM suggests that these big particles are formed around large clusters of CNTs, while the smaller particles contained some or no CNTs. This suggests that the carbon nanotubes, when they form clusters in the epoxy-rich phase can affect the final size of the epoxy-rich particles. Figure 10.1 shows the SEM images of the neat MTM 44-1 resin and its nanocomposite incorporating carbon nanotubes.

In figure 10.1a it is shown that the neat system contains epoxy-rich particles of the size ranging from 5 to 15 μm. Figure 10.1b shows that the nanocomposite that contains the carbon nanotubes has a different topography of particles differing in the size (5 to 50 μm). It is observed that the bigger particles contain clusters of carbon nanotubes, while the smaller ones contain some or no carbon nanotubes. The existence of large globular domains,

formed around the aggregates of carbon nanotubes, indicate that the nanofillers might contribute to phase separation 'via nucleation and growth'.

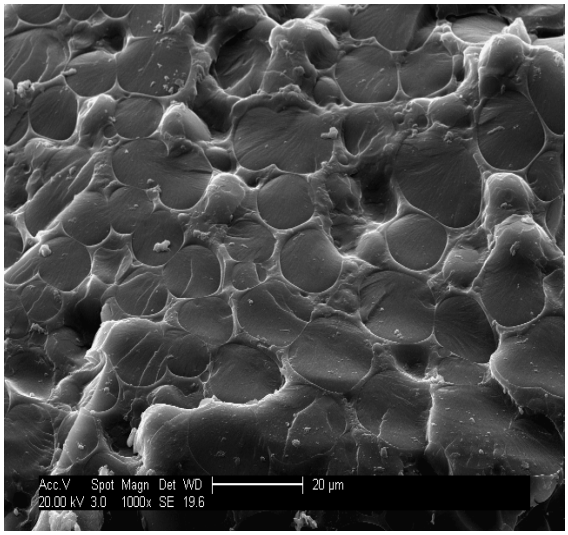

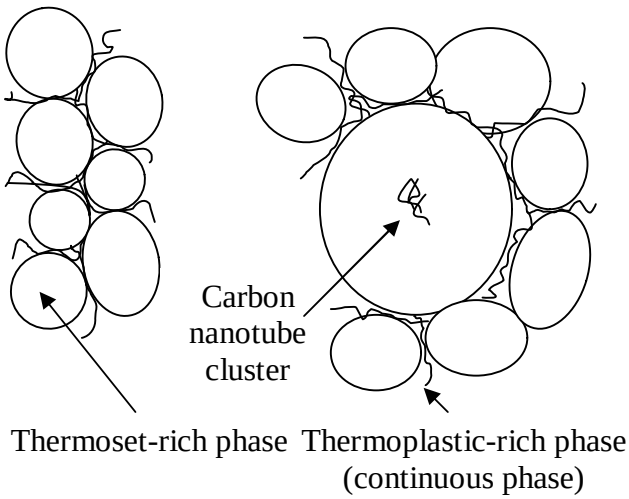

a)

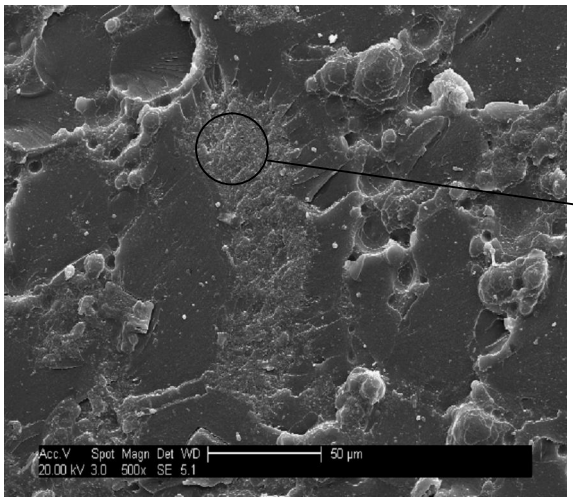

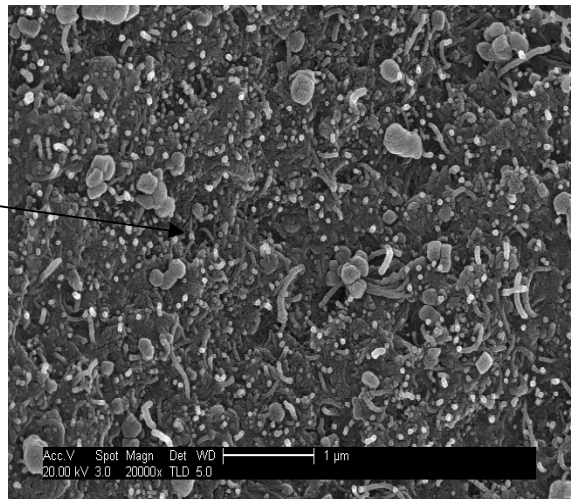

b) c)

Figure 10.1: MTM 44-1 resin system a) without the incorporation and b) and c) with the incorporation of 1 wt % Thomas Swan carbon nanotubes after curing at 190^{o}C for 2 hours (image c is a magnification of the nanotube cluster in image b – a schematic representation of the system with and without the incorporation of carbon nanotubes is also represented)

The images of figures 10.1b and c suggest that the fully cured material contains areas with different crosslink densities. It might be expected that the smaller epoxy-rich phase particles are the regions with the high-crosslink density, while the epoxy-rich phase particles that contain carbon nanotubes are the regions with low crosslink density. This assumption is illustrated in figure 10.2.

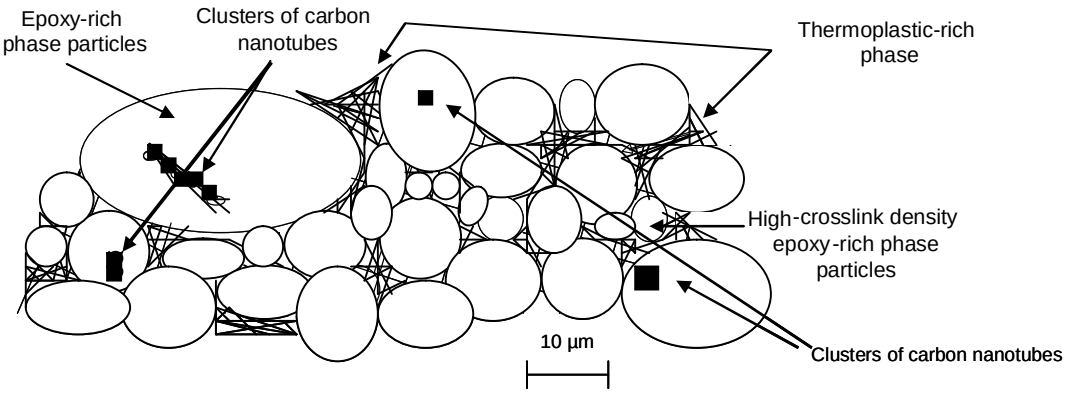

Figure 10.2: Schematic of the different crosslink density areas in the MTM 44-1 resin system containing 1 wt % Thomas Swan carbon nanotubes

SEM and TEM prove to be powerful tools used to characterise the microstructure of fully cured materials. Microstructural characterisation of the mixtures in the uncured state remains a difficult problem. Optical microscopy would be the obvious solution, but it does not offer sufficient resolution. For example Wang and Peijs [150] utilised optical microscopy to show the evolution of dispersion of CNTs in composite solutions. At the initial stages where big clusters of CNTs existed the imaging was very good, in contrast to the later stages of dispersion where it became difficult to distinguish the individual CNTs from the polymer matrix. There are only a few cases [151] where a combination of TEM and optical microscopy (nanodispersion and microdispersion characterisation respectively) was utilised. In most of the cases a combination of SEM and TEM seems to be the preferred way to characterise the structure of the nanocomposites.

10.1.3 Cure monitoring via optical fibre sensors

Initially the purpose of the project was to embed optical fibres into the three base resin systems, measure the refractive index change during cure and correlate it with the degree of cure. A good correlation was established for the three epoxy systems. The incorporation of carbon nanotubes into the resin systems was the next step. At this point an online cure monitoring technique was a prerequisite in order to check the status of the curing reaction. Dielectric spectroscopy would be the prefered technique for nanocomposites containing low concentrations of carbon nanoparticles or non-conductive particles. The main problem arises when higher concentrations of nanoparticles are incorporated into the resin systems due to the fact that the systems become electrically conductive.

The utilisation of optical fibres (Fresnel refractometers in particular) proved to be a very good alternative, used to overcome the problem of shorting out of dielectric sensors. The technique was initially utilised with the MY 750 / HY 5922 containing 0.06 wt % Hyperion carbon nanotubes (batch 1). The correlation was found to be good despite the fact that the signal was noisy (see figures 9.2 to 9.5). This was not the case for the base system, where a very smooth signal was shown. A possible scenario would be that during the curing reaction the nanoparticles are moving. However, after gelation where the mobility of carbon nanotubes is reduced to a minimum, the noisy signal was still noticed.

Later on the technique was utilised for the preformulated ACG MTM 44-1 resin system and its nanocomposite containing 1 wt % Thomas Swan carbon nanotubes (batch 6), and also for the Hexcel 8552 resin system. In the case of the nanocomposite, dielectric analysis was not possible to be utilised due to the appreciable electrical conductivity of the formed material. Instead, Fresnel refractometers were utilised. The signal was found to be noisy which suggested that the technique is sensitive to microstructure formation (phase separation phenomenon takes place – mobility of carbon nanotubes) in the pregel-region. It was attributed to the formation of the two-phase material and the mobility of carbon nanotubes between the two forming phases. The

correlation between the refractive index and the degree of cure at the pre-gel stage was less good than in the case of the MY 750 / HY 5922 resin system and its nanocomposite. However, after gelation had occurred the signal became smooth and a linear correlation could be established.

These tests showed that the technique gives promising results over the whole range of the curing reaction for two part resin systems and after gelation for the one-part pre-formatted materials. As was also shown in chapter 9, the optical fibre in the case of the MTM 44-1 resin system and its nanocomposite was not able to distinguish between the formed phases. This would be attributed to the fact that the particles had a size similar to the fibre core in the case of the neat system and larger in the case of the nanocomposite. As was shown in figure 10.2 the formed system contains phase separated areas. That means that the refractive index measured from the optical fibre is not the signal of one of the phases but it is probably a function of the refractive indices of the different areas.

The utilisation of optical fibres proved to be a very promising technique in terms of cure monitoring of nanocomposites. Optimisation of the technique so that the sensitivity could be improved and the signal becomes better would result in the next generation of online cure monitoring techniques, at least for two-part systems.

10.1.4 Cure kinetics modelling

Cure kinetics models were constructed for the base resins and their nanocomposites so that a direct comparison could be established. This comparison highlighted the effect of carbon nanotube addition on the resin systems tested. This comparison was also based on the raw data presented in chapter 5.

The comparison between the models of the MY 750 / HY 5922 resin system and its nanocomposites (batches 1 and 5) did not show any significant differences. The calculated parameter values (presented in table 7.1) showed a small variation as far as the pre-exponential factors A_1 *and* A_2 are

concerned when carbon nanotubes were incorporated into the epoxy system. The activation energies E_1 *and* E_2 showed a small decrease. The main difference was noticed for the pre-exponential factors A_d of the diffusion terms, where a decrease of their values took place. The fact that no significant differences were not observed was probably due to the fact that a very low concentration of carbon nanotubes was incorporated. This observation is also seen in the values of the total heats of reaction (presented in table 5.2) where a trend was not clear (suggested by the calculated errors - standard deviations).

The models used for the MTM 44-1 resin system and its nanocomposite containing carbon nanotubes (batch 6) showed some differences (see table 7.2). The pre-exponential factor A_1 showed a decrease for the nanocomposite when compared with the one of the neat resin. The activation energy E_1 showed an increase while E_2 decreased for the nanocomposite, respectively. The main difference was observed for the diffusion factor C of the nanocomposite, which showed an increase of an order of magnitude, when compared to the one of the neat system. This decrase together with the decrease of the total heats of the reaction (presented in table 5.4) suggested that the immobilisation effects are not too strong. This difference was mainly attributed to the high concentration of carbon nanotubes incorporated into the resin system.

The validation of the cure kinetics modelling methodology utilised in this study was applied to the 8552 resin system, where the same model as in the case of the MTM 44-1 resin system was used. Another model, which was suggested from the main participants in the Round Robin scheme was also utilised for the validation of the cure kinetics modelling methodology previously established in the group at Cranfield University (see equation 8.3). The results of the Round Robin study are summarised in appendix B.

10.1.5 Glass transition temperature advancements

The incorporation of nanofillers in a liquid polymer matrix results in a structure and properties differed than those of the unfilled resins. The effect of the filler can vary as a function of its type and specific surface, the concentration and conditions used [152,153]. The incorporation of carbon nanoparticles in a liquid epoxy matrix results in changes occurring in the glass transition temperature. It has been suggested by some authors that these changes are associated with the formation of boundary layers differing in their structure and properties from characteristics of the polymer situated outside the sphere of influence of the filler surface [154]. The incorporation of carbon nanotubes is assumed to lead to a free volume increase and a polymer density decrease in the boundary layers. In addition to that, the density of low molecular weight liquids increases in the boundary layers [152]. This results in the decrease of the initial glass transition temperature of the system.

The glass transition temperature advancements were studied by means of Temperature Modulated DSC. Initially, the Hyperion carbon nanotubes and the Monarch carbon black particles incorporated into the MY 750 / HY 5922 resin system were dispersed by shear mixing (batches 1 to 4). The effect on the measured properties was a function of the state of dispersion. The utilisation of shear mixing alone led to a poor state of dispersion. The glass transition temperatures either showed a decrease or remained almost the same, compared to that of the neat resin system (see figures 6.2-6.4). This was attributed to the main phenomena that take place:- reduction of the reaction rate due to the consumption of the hardener-resulting in a reduction of the T_g and mobility limitations that do not allow the polymer chains to move freely-resulting in an increase of the T_g. In this case where a poor dispersion was achieved, the first phenomenon prevails over the latter (decrease in the glass transition temperatures at the later stages of cure) or they counteract each other resulting in the same values of the final T_gs.

Later on, the ultrasonic horn (batch 5) was tested and a good state of dispersion was achieved. That led to an increase in the glass transition

temperature. In this case, the mobility limitations prevail over the effect of the reduction of the hardener.

Of special interest is the decrease of the glass transition temperatures observed, in the region of 0 to 80 % degree of cure, when the Hyperion carbon nanotubes were incorporated into the MY 750 / HY 5922 resin system. This decrease started from the uncured state of the materials. The only available theory that may apply to this is the 'free volume' theory that was mentioned at the beginning of this paragraph [152-154]. The incorporation of carbon black particles into the same resin system led to a small increase of the glass transition temperatures in the uncured state. That suggests a considerable decrease in the mobility or flexibility of the absorbed polymer [155]. This decrease in flexibility causes the properties of the absorbed polymer to be shifted towards the glassy state, and the glass transition temperature which is dependent on the mobility or flexibility of the polymer, to be shifted to higher temperatures.

A further analysis of the Hyperion carbon nanotube incorporation into the MY 750 / HY 5922 resin system was conducted. The premix that contains the predispersed Hyperion carbon nanotubes is a mixture of DGEBA based resin and a very high molecular weight solid epoxy derived from a liquid epoxy resin and bisphenol-A (EPON 1009 F). The average molecular weight of this solid epoxy is ~ 4000 g/mol [109,156]. When dispersed into the less viscous MY 750 resin (average molecular weight of DGEBA 386.4 g/mol [157]) its concentration did not exceed 2 wt % per batch produced. That means that at the molecular level 990 molecules of DGEBA resin are mixed with 2 molecules of EPON 1009F resin. This estimated ratio suggests that the EPON 1009F resin effect on the cure kinetics mechanism and the glass transition temperature advancement of the curing reaction is negligible. This was in evidence when a batch of the premix (Epon 828/1009F) without any carbon nanotubes was produced and characterised. Stoichiometric ratio of the HY 5922 curing agent was added to the batch. The T_g corresponding to the uncured and the fully cured material were found to be -35^{o}C and 54^{o}C respectively (-10^{o}C for the EPON 828/1009F system and -80^{o}C for the HY

5922 curing agent). The mixing of the premix with the amine hardener led to a T_g value which is almost the same with that of the MY 750 / HY 5922 resin system (T_{go}=-32^{o}C). This led to the assumption that the presence of EPON 1009F in the system did not produce any side reaction affecting the glass transition temperature. The results of this analysis are summarised in table 10.1.

Resin ratios	Average molecular weight (g/mole)	T_{go}(^{o}C)	$T_{g\infty}$(^{o}C)
MY 750	386.4 [157]	-16±1 (T_g)	-
HY 5922	380-420 [106]	-80±1 (T_g)	-
EPON 1009 F	4000 [156]	-	-
MY 750 / HY 5922	-	-32±1	45±1
MY 750/EPON 828/1009F / HY 5922	-	-33±1	45±1
EPON 828/1009F / HY 5922	-	-35±1	54±1
EPON 828/1009F / HY 5922 3.06 wt % Thomas Swan CNTs	-	-41±1	51±1
MY 750 / HY 5922 0.06 wt % Thomas Swan CNTs	-	-50±1	45±1

Table 10.1: Glass transition temperature values and average molecular weights corresponding to the MY 750 epoxy, HY 5922 amine hardener, EPON 1009 F resin, MY 750 / HY 5922 resin, the EPON 828 / 1009F / HY 5922 resin and their nanocomposites containing Thomas Swan carbon nanotubes

Further on, in order to prove that no side reaction took place during the incorporation of the Hyperion premix into the resin system, the ‘double system’ (containing no nanotubes) was mixed into the MY 750 resin and then

the curing agent was added. The produced system was characterised and it was found that the total heat of reaction measured under dynamic DSC tests was found to be 335 J/g (neat epoxy system: 344 J/g) and the T_g values corresponding to the uncured and the fully cured resin were -33^{o}C and 45^{o}C, respectively. That means that the addition of the 'double system' into the resin does not affect the cure kinetics mechanism and any difference observed is only the result of the incorporation of carbon nanotubes.

In order to support the above statement, a batch of EPON 828/1009F resin that contained 3.06 wt % of Thomas Swan carbon nanotubes was prepared (same concentration as the Hyperion carbon nanotubes into the premix). Stoichiometric ratio of the curing agent was added and the batch was characterised. It was found that the initial T_g was -41^{o}C (almost 10^{o}C lower that that of the neat resin) and the final T_g 51^{o}C. Further on, dry Thomas Swan carbon nanotubes were incorporated into the neat system and the characterisation showed that initial T_g was -50^{o}C (18^{o}C lower than that of the neat resin system) and the final one 45^{o}C. That proved that the decrease of the initial T_gs in the system was the result of the incorporation of carbon nanotubes.

The MTM 44-1 resin system when tested with the incorporation of Thomas Swan carbon nanotubes and Monarch carbon black particles (batches 6-10) showed decreased or similar values of the final glass transition temperatures compared to the neat system (see figures 6.2-6.4). The possible causes proposed for the MY 750 / HY 5922 resin system and its nanocomposites apply for this resin system as well. The glass transition temperatures of the uncured materials either showed a small decrease or remained the same.

The lower final glass transition temperatures of the nanocomposites when compared with that of the neat system, together with the lower heats of reaction measured may mean that the incorporation of nanoparticles leads to a material with a lower crosslink density compared with that of the neat system. As was also shown in figure 10.2, the formed nanocomposite

contains areas with different crosslink densities, and has also different refractive indices. That would also mean that the different areas exhibit different glass transition temperatures and that the signal of the Temperature Modulated DSC is a complicated function of the T_gs of these areas.

10.2 Suggestions for future work

The study of the three epoxy systems and their nanocomposites, incorporating carbon nanoparticles, provided valuable data about the cure kinetics mechanisms, but also of their glass transition temperature advancements. The utilisation of the available techniques allowed for the achievement of a good state of dispersion, especially in the case of the MY 750 / HY 5922 resin system when the Hyperion carbon nanotubes were incorporated (see table 3.1). The achievement of a good state of dispersion is a prerequisite for the optimisation of the properties of the produced nanocomposites. A nanocomposite that incorporates well disperserd nanofillers would be expected to show enhanced electrical (e.g. electrical conductivity), thermal (e.g. thermal conductivity) or mechanical properties (studied at elevated temperatures). The following areas of study seem likely to be rewarding:

- **Localisation phenomenon of carbon nanoparticles in toughened epoxies**

In the case of the MTM 44-1 resin system and its nanocomposites, due to the complexity of the system (contains a certain percentage of thermoplastic) it was not easy to obtain a good state of dispersion. This might be also the result of the phase separation phenomenon that occurs at a specific conversion. The study revealed that carbon black particles prefer to be localised at the interface between the epoxy-rich and the thermoplastic-rich phases, while carbon nanotubes prefer the thermoset-rich phase. However, this localisation phenomenon might be the effect of the utilisation of the ultrasonic bath and a function of the solvent used. A further study in other

systems would prove beneficial in terms of establishing some explanations of this phenomenon.

- **Phase separation phenomenon in toughened epoxies incorporating carbon nanoparticles**

The phase separation phenomenon would normally require techniques such as light scattering or light transmission in order to establish the so-called 'cloud point', as long as the percentage of the thermoplastic in the resin is known. Unfortunately, this was not the case here, because of the fact that the toughened epoxy used was a commercial one part resin system. The utilisation of dielectric spectroscopy as a cure monitoring technique might be a way to monitor the phase separation phenomenon, however, limitations would occur due to the electrical conductivity of the material. Some dielectric experiments would be beneficial when a low concentration of carbon nanoparticles is incorporated into the resin system and the conductivity is not too high to short out the electrodes. As an alternative technique, the utilisation of optical fibres seems to give promising results. Some extra experiments would also be very interesting in terms of monitoring the state of the dispersion of carbon nanoparticles in the resin systems. Especially in the case of toughened epoxy systems it would prove to be really useful if the optical fibres incorporation could distinguish between the two formed phases (thermoset-rich and modifier-rich phases). Further work would also prove to be beneficial in terms of establishing a technique which allows valid measurements of the separate refractive indices of the formed phases.

In addition, it was suggested that the incorporation of carbon nanotubes affects the formation of the particle size after the beginning of phase separation. Further work in this field is essential in order to understand how the nanoparticles affect the phase separation phenomenon and consequently the mechanical properties of the end product.

- **Cure kinetics modelling methodology of two-phase materials**

The cure kinetics models developed for the MTM 44-1 resin system and its nanocomposite were valid within a limited temperature-conversion window. That was the case because of the non-validity of the superposition principle between the dynamic and isothermal cure experiments. Development of a cure kinetics modelling methodology which would describe the two phase material (before and after the formation of the two phases) would be of great interest.

Chapter 11

11. Conclusions

- For the MY 750 / HY 5922 resin system, the incorporation of carbon nanoparticles does not affect the total heat of cure reaction, within experimental error. However, the maximum rate of cure under dynamic heating conditions occurs at 2-3 C higher than in unmodified resin. There are measurable changes in the glass transition temperature development during cure. At the low conversion end the T_g is depressed by nearly 10 C, regardless of the quality of the dispersion, while the final T_g appears increased in those samples in which good dispersion has been achieved.
- In the MTM 44-1 resin system, the phase separation in the presence of CB particles is accompanied by their localisation at the interphase between the epoxy-rich and the thermoplastic-rich phases. The carbon nanotubes, in contrast, cluster within the thermoset-rich phase.
- The addition of 1wt% of multiwalled carbon nanotubes to the MTM 44-1 system has been observed to cause a reduction in the rate of isothermal cure, the effect being more pronounced at higher cure temperatures.
- Model fits for the rate of cure dependence upon cure temperature/cure time, developed from DSC data using Genetic algorithms, have been validated by comparison of a specific model for 8552 resin within an international Round Robin exercise on cure kinetics modeling (to be published via University of British Columbia).
- For the resin systems investigated, the refractive index change during cure was found to be well correlated with the degree of cure determined independently by DSC. The fibre optics method is therefore a candidate for in-situ cure monitoring of resins containing carbon nanoparticles.

References

1. National Physical Laboratory, 'Good practice guide to cure monitoring', http://www.npl.co.uk/materials/cure/gpg/introduction.html, accessed 3rd October 2006
2. G.M. Maistros and I.K. Partridge, 'Monitoring autoclave cure in commercial carbon fibre / epoxy composites', Composites part B, **29 B**, 1998, p. 245 – 250
3. G.M. Maistros and I.K. Partridge, 'Dielectric monitoring of cure in a commercial carbon-fibre composite', Composites Science and Technology, **53**, 1995, p. 355-359
4. V. Antonucci, K-T. Hsiao and S.G. Advani, 'Review of polymer composites with carbon nanotubes', G.O. Shonaioke and S. Advani, Advanced Polymeric Materials-Structure Property Relationships, CRC Press, 2003, p. 397-437
5. D. Abraham and R. McIlhagger, 'Glass fibre epoxy composite cure monitoring using parallel plate dielectric analysis in comparison with thermal and mechanical testing techniques', Composites Part A, **29A**, 1998, p. 811-819
6. A. McIlhagger, D. Brown and B. Hill, 'The development of a dielectric system for the on-line cure monitoring of the resin transfer moulding process', Composites Part A, **31**, 2000, p. 1373-1381
7. C. Li, M. Wang, R. Wang, Z. Qiao, Y. Wan, L. Tian, Q. Liu, H. Zhang, D. Liang and C. Tang, 'Fiber-optic composite cure sensor: Monitoring the curing process of composite material based on intensity modulation', Composites Science and Technology, **63**, 2003, p. 1749-1758
8. M.A. Afromowitz and K-Y. Lam, 'The optical properties of curing epoxies and applications to the fiber-optic epoxy cure sensor', Sensors and Actuators, **A21-A23**, 1990, p. 1107-1110
9. A. Cusano, G. Breglio, M. Giordano, L. Nicolais, and A. Cutolo, 'Multifunction fiber optic sensing system for smart applications', IEEE/ASME Transactions on Mechatronics, **9**, 2004, p. 40-49

10. J.P. Dunkers, J.L. Lenhart, S.R. Kueh, J.H.V Zanten, S.G. Advani and R.S. Parnas, 'Fiber optic flow and cure sensing for liquid composite molding', Optics and Lasers in Engineering, **35**, 2001, p. 91-104
11. F.H. Chowdhury, M.V. Hosur and S. Jeelani, 'Studies on the flexural and thermomechanical properties of woven carbon / nanoclay-epoxy laminates', Materials Science and Engineering, **A 421**, 2006, p. 298-306
12. O. Decroly and M. Claes, 'Carbon nanotubes: reviewing their multifunctional properties for polymers', High Performance Fillers 2006, Cologne, Germany, 21-22 March 2006, p. 1-11
13. Z. Yao, N. Braidy, G. A. Botton and A. Andronov, 'Polymerisation from the surface of single-walled carbon nanotubes – Preparation and characterisation of nanocomposites', Journal of the American Chemical Society, **125**, 2003, p. 16015 – 16024
14. L. Valentini, I. Armentano, D. Puglia and J. M. Kenny, 'Dynamics of amine functionalized nanotubes / epoxy composites by dielectric relaxation spectroscopy', Carbon, **42**, 2004, p. 323 - 329
15. K. Lau, M. Lu, C. Lam, H. Cheung, F-L. Sheng and H-L. Li, 'Thermal and mechanical properties of single – walled carbon nanotube bundle – reinforced epoxy nanocomposites: the role of solvent for nanotube dispersion', Composites Science and Technology, **65**, 2005, p. 719 – 725
16. J-P. Pascault, H. Sautereau, J. Verdu and R.J.J. Williams, 'Thermosetting Polymers', Chapter 2: 'Chemistry of crosslinked polymer synthesis', p. 24-44
17. Z. Samaras, 'Modeling and monitoring the cure of thermosetting systems for industrial applications', PhD thesis, Cranfield University, United Kingdom, September 2005, p.14-16
18. G. van Assche, S. Swier and B. van Mele, 'Modelling and experimental verification of the kinetics of reacting polymer systems', Thermochimica Acta, **388**, 2002, p. 327 – 341
19. C.B. Bucknall and I.K. Partridge, 'Phase separation in crosslinked resins containing polymeric modifiers', Polymer Engineering and Science, **26**, 1986, p. 54-62

20. J.B. Enns and J.K. Gillham, 'The time-temperature-transformation (TTT) cure diagram: modeling the cure behavior of thermosets', Journal of Applied Polymer Science, **28**, 1983, p. 2567-2591
21. K. Hofmann and W. G. Glasser, 'Cure monitoring of an epoxy – amine system by dynamic mechanical thermal analysis (DMTA), Thermochimica Acta, **166**, 1990, p. 169 – 184
22. T. Frey, K.-H. Grobe-Brinkhaus and U. Rockrath, 'Cure monitoring of thermoset coatings', Progress in Organic Coatings, **27**, 1996, p. 59 – 66.
23. J .K. Gillham and J. B. Enns, 'On the cure properties of thermosetting polymers using torsional braid analysis', Trends in Polymer Science, **2**, 1994, p. 406-419
24. P.I. Karkanas and I.K. Partridge, 'Cure modelling and monitoring of epoxy / amine resin systems. II. network formation and chemoviscosity modelling', Journal of Applied Polymer Science, **77**, 2000, p. 2178-2188
25. H. H. Winter, 'Can the gel point of a cross-linking polymer be detected by the *G' - G''* crossover?', Polymer Engineering and Science, **27**, 1987, p. 1698-1702
26. M. K. Um, I. M. Daniel and B.S. Hwang, 'A study of cure kinetics by the use of dynamic differential scanning calorimetry', Composites Science and Technology, **62**, 2002, p. 29-40
27. P.J. Flory, 'Principles in polymer chemistry', Cornell University Press, Ithaca, New York, 1953
28. J.F. Stephenson, 'Free radical polymerization models for simulating reactive processing', Polymer Engineering and Science, **26**, p. 746-759
29. S. Sourour and M.R. Kamal, 'Differential Scanning Calorimetry of epoxy cure: isothermal cure kinetics', Thermochimica Acta, **14**, 1976, p. 41-59
30. V.M. Gonzalez-Romero, 'Studies of reactive polymer processing with fibre glass reinforcements', PhD thesis, University of Minnesota, 1983
31. G.L. Batch and C.W, Macosko, 'Kinetic model for crosslinking free radical polymerisation including diffusion limitations', Journal of Applied Polymer Science, **44**, 1992, p. 1711-1729
32. K. Horie, H. Hiura, M. Sawada, I. Mita and H. Kambe, 'Calorimetric investigation of polymerisation reactions.III. Curing reaction of epoxides

with amines', Journal of Polymer Science, Part A-1, **8**, 1970, p. 1357-1372

33. G. Wisanrakkit and J.K Gillham, 'The glass transition temperature (T_g) as an index of chemical conversion for a high-T_g amine/epoxy system: Chemical and diffusion-controlled reaction kinetics', Journal of Applied Polymer Science, **41**, 1990, p.2885-2929
34. M. Opalicki, J.M. Kenny and L. Nicolais, 'Cure kinetics of neat and carbon-fibre-reinforced TGDDM / DDS epoxy systems', Journal of Applied Polymer Science, **61**, 1996, p. 1025-1037
35. M. Blanco, M. A. Concuera, C.C Ricardi and I. Mondragon, 'Mechanistic kinetic model of an epoxy resin cured with a mixture of amines of different functionalities', Polymer, **46**, 2005, p.7989-8000
36. A. Yousefi, P.G. Lafleur and R. Gauvin, 'Kinetic studies of thermoset cure reactions: A review', Polymer Composites, **18**, 1997, p.157-168
37. R. Serra, J. Sempere and R. Nomen, 'A new method for the kinetic study of thermoanalytical data: The non-parametric kinetics method', Thermochimica Acta, **316**, 1998, p. 37-45
38. A.A. Skordos and I. K. Partridge, 'Cure kinetics modelling of epoxy resins using a non-parametric numerical procedure', Polymer Engineering and Science, **41**, 2001, p.793-805
39. V.M. Gonzalez-Romero and N. Casillas, 'Isothermal and temperature programmed kinetic studies of thermosets', Polymer Engineering and Science, **29**, 1989, p. 295-301
40. P.W.K. Lam, H.P. Plaumann and T. Tran, 'An improved kinetic model for the autocatalytic curing of styrene-based thermoset resins', Journal of Applied Polymer Science, **41**, 1990 p. 3043-3057
41. H. Teil, S.A. Page, V. Michaud and J-A.E. Manson, 'TTT-cure diagram of an anhydrite-cured epoxy system including gelation, vitrification, curing kinetics model, and monitoring of the glass transition temperature', Journal of Applied Polymer Science, **93**, 2004, p.1774-1787
42. C.S Chern and G.W. Poehlein, 'A kinetic model for curing reactions of epoxides and amines', Polymer Engineering and Science, **27**, 1987, p.788-795

43. U. Khanna and M. Chanda, **'**Kinetics of anhydride curing of isophthalic diglycidyl ester using differential scanning calorimetry', Journal of Applied Polymer Science, **49**, 1993, p. 319-329
44. M.L. Williams, R.F Landel and J.D Ferry, 'The temperature dependence of relaxation mechanisms in amorphous polymers and other glass-forming liquids', Journal of American Chemical Society, **77**, 1955, p. 3701-3707
45. P.I. Karkanas, I.K. Partridge and D. Attwood, 'Modeling the cure of a commercial epoxy resin for applications in resin transfer moulding', Polymer International, **41**, 1996, p. 183-191
46. P.I. Karkanas and I.K. Partridge, 'Cure modeling and monitoring of epoxy / amine resin systems. I. Cure kinetics modeling', Journal of Applied Polymer Science, **77**, 2000, p. 1419-1431
47. P.I. Karkanas, 'Cure modeling and monitoring of epoxy/amine resin systems', PhD thesis, Cranfield University, United Kingdom, March 1998
48. R.J. Varley, J.H. Hodgkin, D.G. Hawthorne, G.P. Simon and D. McCulloch, 'Toughening of a trifunctional epoxy system, Part III: Kinetic and morphological study of the thermoplastic modified cure process', Polymer, **41**, 2000, p. 3425-3436
49. B. Fernandez, M.A. Concuera, C. Marieta and I. Mondragon, 'Rheokinetic variations during curing of a tetrafunctional epoxy resin modified with two thermoplastics', European Polymer Journal, **37**, 2001, p. 1863-1869
50. S-G. Hong and C-K. Chan, 'The curing behaviors of the epoxy/dicyanamide system modified with epoxidized natural rubber', Thermochimica Acta, **417**, 2004, p. 99-106
51. N. Boyard, C. Sinturel, M. Vayer and R. Erre, 'Morphology and cure kinetics of unsaturated polyester resin/block copolymer blends', Journal of Applied Polymer Science, **102**, 2006, p. 149-165
52. S-J. Wu, 'Cure reaction and phase separation behavior of cyanate ester-cured epoxy/polyphenylene oxide blends', Journal of Applied Polymer Science, **112**, 2006, p. 1139-1145

53. E. Girard-Reylet, C.C. Riccardi, H. Sautereau and J.P. Pascault, 'Epoxy-aromatic diamine kinetics. 1. Modeling and influence of the diamine structure', Macromolecules, **28**, 1995, p. 7599-7607
54. A. Bonnet, J. P. Pascault, H. Sautereau, M. Taha and Y. Camberlin, 'Epoxy-diamine thermoset/thermoplastic blends. 1. Rates of reactions before and after phase separation', Macromolecules, **32**, 1999, p. 8517-8523
55. A. Bonnet, Y. Camberlin, J. P. Pascault and H. Sautereau, 'Epoxy-diamine thermoset / thermoplastic blends: thermoset reactions and rheological evolutions during curing', Macromolecular Symposia, **149**, 2000, p. 145-150
56. S. Swier and B. van Mele, 'Mechanistic modeling of the epoxy-amine reaction in the presence of polymeric modifiers by means of Modulated Temperature DSC', Macromolecules, **36**, 2003, p. 4424-4435
57. S. Iijima, 'Helical microtubules of graphitic carbon', Nature, **354**, 1991, p. 56-58
58. T.W. Ebessen and P.M. Ajaian, 'Large scale synthesis of carbon nanotubes ', Nature, **358**, 1992, p.220-222
59. D. Qian, E.C. Dickey, R. Andrews and T. Rantell, 'Load transfer and deformation mechanisms in carbon nanotube-polystyrene composites', Applied Physics Letters, **76**, 2000, p.2868-2870
60. M.A. Lopez-Manchado, L. Valentini, J. Biagiotti and J.M. Kenny, 'Thermal and mechanical properties of single-walled carbon nanotubes-polypropylene composites prepared by melt processing', Carbon, **43**, 2005, p. 1499-1505
61. Z. Zhang, J. Zhang, P. Chen, B. Zhang, J. He and G-H. Hu, 'Enhanced interactions between multi-walled carbon nanotubes and polystyrene induced by melt mixing', Carbon, **44**, 2006, p. 692-698
62. S. Ghose, K.A. Watson, D.M. Delozier, D.C. Working, E.J. Siochi and J.W. Connell, 'Incorporation of multi-walled carbon nanotubes into high temperature resin using dry mixing techniques', Composites: Part A, **37**, 2006, p. 465-475
63. S. Ghose, K.A. Watson, K.J. Sun, J.M. Criss, E.J. Siochi and J.W. Connell, 'High temperature resin / carbon nanotube composite

fabrication', Composites Science and Technology, **66**, 2006, p. 1995-2002

64. M. Moniruzzaman, F. Du, N. Romero and K. I. Winey, 'Increased flexural modulus and strength in SWNT/epoxy composites by a new fabrication method', Polymer, **47**, 2006, p. 293-298
65. X. Gong, J. Liu, S. Baskaran, R. D. Voise, and J. Young, 'Surfactant-assisted processing of carbon nanotube / polymer composites', Chemistry of Materials, **12**, 2000, p. 1049-1062
66. M. S. P. Shaffer, and A. H. Windle, 'Fabrication and characterisation of carbon nanotube / poly(vinyl alcohol) composites', Advanced Materials, **11**, 1999, p. 937-941
67. F. H. Gojny and K. Schulte, 'Functionalisation effect on the thermo-mechanical behavior of multi wall carbon nanotube / epoxy-composites', Composites Science and Technology, **64**, 2004, p. 2303-2308
68. H. Miyagawa, M. J. Rich, L. T. Drzal, 'Thermo-physical properties of epoxy nanocomposites reinforced by carbon nanotubes and vapor grown carbon fibers', Thermochimica Acta, **442**, 2006, p. 67-73.
69. B.H. Chang, Z.Q. Liu, L.F. Sun, D.S. Tang, W.Y. Zhou, G. Wang, L.X. Qian, S.S. Xie, J.H. Fen and M.X. Wan, 'Conductivity and magnetic succeptibility of nanotube / polypyrrole nanocomposites', Journal of Low Temperature Physics, **119**, 2000, p. 41-48
70. S. Cui, R. Canet, A. Derre, M. Couzi and P. Delhaes, 'Characterization of multiwall carbon nanotubes and influence of surfactant in the nanocomposite processing', Carbon, **41**, 2003, p. 797-809
71. F. H. Gojny, J. Nastalczyk, Z. Roslaniec and K. Schulte, 'Surface modified muti-walled carbon nanotubes in CNT/epoxy-composites', Chemical Physics Letters, **370**, 2003, p. 820-824.
72. Z. Yaping, Z. Aibo, C. Qinghua, Z. Jiaoxia and N. Rongchang, 'Functionalised effect on carbon nanotube / epoxy nanocomposites', Materials Science and Engineering A, **435-436**, 2006, p. 145-149
73. C. Stephan, T.P. Nguyen, M. Lamy de la Chapelle, S. Lefrant, C. Journet and P. Bernier, 'Characterization of single walled carbon nanotubes-PMMA composites', Synthetic Metals, **108**, 2000, p. 139-149

74. H. Miyagawa and L.T. Drzal, 'Thermophysical and impact properties of epoxy nanocomposites reinforced by single-wall carbon nanotubes', Polymer, **45**, 2004, p. 5163-5170
75. H. Miyagawa, A.K. Mohanty, L.T. Drzal and M. Misra, 'Nanocomposites from biobased epoxy and single-wall carbon nanotubes: synthesis, mechanical and thermophysical properties evaluation', Nanotechnology, **16**, 2005, p.118-124
76. L. Valentini, J. Macan, I. Armentano, F. Mengoni and J. M. Kenny, 'Modification of fluorinated single-walled carbon nanotubes with aminosilane molecules', Carbon, **44**, 2006, 2196-2201
77. J.D. Fidelus, E. Wiesel, F.H. Gojny, K. Schulte and H.D. Wagner, 'Thermo-mechanical properties of randomly oriented carbon / epoxy nanocomposites', Composites: Part A: **36**, 2005, p. 1555-1561
78. Y.S. Song and J.R. Youn, 'Influence of dispersion states of carbon nanotubes on physical properties of epoxy nanocomposites', Carbon, **43**, 2005, p. 1378-1385
79. Y. H. Liao, O.M. Tondin, Z. Liang, C. Zhang and B. Wang, 'Investigation of the dispersion process of SWNTs / SC-15 epoxy resin nanocomposites', Materials Science and Engineering A, **385**, 2004, p. 175-181
80. J.A. Kim, D. G. Seong, T.J. Kang and J. R. Youn, 'Effects of surface modification on rheological and mechanical properties of CNT / epoxy composites', Carbon, **44**, 2006, p. 1898-1905
81. E. T. Thostenson, C. Li, T. W. Chou, 'Nanocomposites in context-Review', Composites Science and Technology, **65**, 2005, p. 491-516
82. S. P. Wang, A. Garton and T.K. Stephenson, 'The effect of carbon surface functionality on tetrafunctional epoxy resin-diaminodiphenylsulfone cure reactions', Journal of Applied Polymer Science, **40**, 1990, p. 99-112
83. M. Grenier-Loustalot and P. Grenier, 'The mechanism of epoxy-resin curing in the presence of glass and carbon fibres', Polymer, **33**, No 6, 1992, p. 1187-1199
84. Y.H. Liao, Z. Liang, Y-B Park, B. Wang and C. Zhang. 'Fabrication and characterisation of carbon nanotube / glass fibre-reinforced multiscale

composites', 47th AIAA / ASME / ASCE / AHS / ASC Structures, Structural Dynamics, and Materials Conference, 1-4 May 2006, Newport, Rhode Island, USA, (1858), p. 1-6

85. J.C. Lucas, J. Borrajo and R.J.J. Williams, 'Cure of unsaturated polyester resins: 2. Influence of low-profile additives and fillers on the polymerisation reaction, mechanical properties and surface rugosities, Polymer, **34**,1993, p. 1886-1890
86. J. Mijovic, 'Cure Kinetics of neat versus reinforced epoxies', Journal of Applied Polymer Science, **31**, 1986, p. 1177-1187
87. J. Sandler, M. S. P. Shaffer, T. Prasse, W. Bauhofer, K. Schulte, and A. H. Windle, ' Development of a dispersion process for carbon nanotubes in an epoxy matrix and the resulting electrical properties' Polymer, **40**, 1999, p. 5967-5971
88. C.A. Martin, J.K.W. Sandler, M.S.P. Shaffer, M-K. Schwarz, W. Bauhofer, K. Schulte and A.H. Windle, 'Formation of percolating networks in multi-wall carbon-nanotube-epoxy composites', Composites Science and Technology, **64**, 2004, p. 2309-2316
89. F.H. Gojny, M.H.G. Wichmann, B. Fiedler, W. Bauhofer and K. Schulte, 'Influence of nano-modification on the mechanical and electrical properties of conventional fibre-reinforced composites', Composites Science and Technology, **65**, 2005, p. 2300-2313
90. M.H.G. Wichmann, J. Sumfleth, F.H. Gojny, M. Quaresimin, B. Fiedler and K. Schulte, 'Glass-fibre-reinforced composites with enhanced mechanical and electrical properties – Benefits and limitations of a nanoparticle modified matrix', Engineering Fracture Mechanics, **73**, 2006, p. 2346-2359
91. F.H. Gojny, M.H.G. Wichmann, B. Fiedler, I.A. Kinloch, W. Bauhofer, A.H. Windle and K. Schulte, 'Evaluation and identification of electrical and thermal conduction mechanisms in carbon nanotube / epoxy composites', Polymer, **47**, 2006, p. 2036-2045
92. A. Moisala, Q. Li, I.A. Kinloch and A.H. Windle, 'Thermal and electrical conductivity of single- and multi-walled carbon nanotube-epoxy composites', Composites Science and Technology, **66**, 2006, p. 1285-1288

93. G.D. Liang and S.C. Tjong, 'Electrical properties of low-density polyethylene / multiwalled carbon nanotube nanocomposites', Materials Chemistry and Physics, **100**, 2006, p. 132-137
94. D. Puglia, L. Valentini, I. Armentano and J.M. Kenny, 'Effects of single-walled carbon nanotube incorporation on the cure reaction of epoxy resin and its detection by Raman spectroscopy', Diamond and Related Materials, **12** (2003), p. 827-832
95. M.-T. Ton-That, T.-D. Ngo, P. Ding, G. Fang, K.C. Cole and S.V. Hoa, 'Epoxy nanocomposites: analysis and kinetics of cure', Polymer Engineering and Science, **44**, 2004, p. 1132-1141
96. M. Lu, M. Shim and S. Kim, 'Effect of filler on cure behaviour of an epoxy resin system: Cure modeling', Polymer Engineering and Science, **39**, 1999 , p. 274 – 285
97. T. Zhou, M. Gu, Y. Jin and J. Wang, 'Studying on the cure kinetics of a DGEBA / EMI-2,4 / nano-sized carborundum system with two curing kinetic methods', Polymer, **46**, 2005, p. 6174-6181
98. M. Ivankovic, I. Brnardic, H. Ivankovic and H. J. Mencer, 'DSC study of the cure kinetics during nanocomposite formation: epoxy / poly(oxypropylene)diamine / organically modified montmorillonite system', Journal of Applied Polymer Science, **99**, 2006, p. 550-557
99. Z. Shi, D. Yu, Y. Wang and R. Xu, 'Nonisothermal cure kinetics in the synthesis of polybenzoxazine-clay nanocomposites', Journal of Applied Polymer Science, **88,** 2003, p. 194-200
100. H. Xie, B. Liu, Z. Yuan, J. Shen and R. Cheng, 'Cure kinetics of carbon nanotube / tetrafunctional epoxy nanocomposites by isothermal Differential Scanning Calorimetry', Journal of Polymer Science: Part B: Polymer Physics, **42**, 2004, p. 3701-3712
101. H. Xie, B. Liu, Q. Sun, Z. Yuan, J. Shen and R. Cheng, 'Cure kinetics of carbon nanofibres / epoxy composites by isothermal DSC', Journal of Applied Polymer Science, **96**, 2005, p. 329-335
102. M. Paradise and T. Goswami, 'Carbon nanotubes – Production and industrial applications', Materials and Design, **28**, 2007, p. 1477-1489
103. R. Baugham, A. Zakhidov and W. Heer, 'Carbon nanotubes – the route toward applications', Science, **297**, 2002, p. 787-792

104. E. Thostenson, Z. Ren and T. Chou, 'Advances in the science and technology of carbon nanotubes and their composites: A review', Composites Science and Technology, **61**, 2001, p. 1899-1912
105. J. Smith, 'Slicing in extra thin', Tire review, 2005, http://www.smalltimes.com, accessed 17th November 2006
106. Araldite 'MY 750 + HY 5922' impregnating resin system, material safety datasheet, Vantico, 2000
107. ACG 'MTM 44-1' matrix resin, material safety datasheet, Advanced Composites, 2004
108. 'Hexply 8552' resin, material safety datasheet, Hexcel Composites, 2004
109. 'EPON resin 1009F', technical datasheet, Hexion Specialty Chemicals, Inc. 2005
110. Hyperion Catalysis International, material safety datasheet, September 2004
111. http://www.thomas-swan.co.uk, accessed 5th December 2006
112. Carbon Black – Monarch 570, Material safety datasheet, Cabot, June 2004
113. http://www.ptli.com/testlopedia/tests/DSC-d3417.asp, accessed 18th November 2006
114. C. Sandu and R.K. Singh, 'Modelling differential scanning calorimetry', Thermochimica Acta, **159**, 1990, p. 267-298
115. E. Verdonck, K. Schaap and L.C. Thomas, 'A discussion of the principles of Modulated Temperature DSC (MTDSC)', International Journal of Pharmaceutics, **192**, 1999, p. 3-20
116. G. van Assche, A. van Hemelrijck, H. Rahier and B. van Mele, 'Modulated Temperature Differential Scanning Calorimetry: cure, vitrification and devitrification of thermosetting systems', Thermochimica Acta, **304 / 305,** 1997, p 317 – 334
117. T. Liu and G.F. Fernando, 'Processing of polymer composites: an optical fibre-based sensor system for on-line amine monitoring, Composites: Part A, **32**, 2001, p. 1561-1572
118. V.M. Murukeshan, P.Y. Chan, L.S. Ong and L.K. Seah, 'Cure monitoring of smart composites using Fibre Bragg Grating based embedded sensors', Sensors and Actuators, **79**, 2000, p. 153-161

119. S.J. Buggy, Cranfield University, United Kingdom, unpublished work
120. A.J. Kinloch and A.C. Taylor, 'The mechanical properties and fracture behaviour of epoxy-inorganic micro- and nano-composites', Journal of Materials Science, **41**, 2006, p. 3271-3297
121. J. Shen, W. Huang, L. Wu, Y. Hu and M. Ye, 'Thermo-physical properties of epoxy nanocomposites reinforced with amino-functionalized multi-walled carbon nanotubes', Composites: Part A, **38**, 2007, p. 1331-1336
122. R.J.J. Williams, B.A. Rozenberg and J.-P. Pascault, 'Reaction induced phase separation in modified thermosetting polymers', Advances in Polymer Science, **128**, 1996, p. 95-156
123. G.M. Maistros, H. Block, C.B. Bucknall and I.K. Partridge, 'Dielectric monitoring of phase separation during cure of blends of epoxy resin with carboxyl-terminated poly(butadiene-co-acrylonitrile)', Polymer, **33**, 1992, p. 4470-4478
124. S. Swier and B. van Mele, 'The heat capacity signal from modulated temperature DSC in non-isothermal conditions as a tool to obtain morphological information during reaction-induced phase separation', Polymer, **44**, 2003, p. 6789-6806
125. F. Gubbels, R. Jerome, Ph. Teyssie, E. Vanlathem, R. Deltour, A. Calderone, V. Parente and J. L. Bredas, 'Selective localization of carbon black in immiscible polymer blends: a useful tool to design electrical conductive composites', Macromolecules, **27**, 1994, p. 1972-1974
126. F. Gubbels, R. Jerome, E. Vanlathem, R. Deltour, S. Blacher and F. Brouers, 'Kinetic and thermodynamic control of the selective localization of carbon black at the interface of immiscible polymer blends', Chemistry of Materials, **10**, 1998, p. 1227-1235
127. B.G. Soares, F. Gubbels, R. Jerome, P. Teyssle, E. Vanlathem and R. Deltour, 'Electrical conductivity in carbon black-loaded polystyrene-polyisoprene blends. Selective localization of carbon black at the interface', Polymer Bulletin, **35**, 1995, p. 223-228
128. A.E. Zaikin, R. Yu. Mindubaev and V.P. Arkhireev, 'A study of the localisation of carbon black particles at the interfaces in heterogeneous polymer blends', Colloid Journal, **61**, 1999, p. 459-466

129. M. Sumita, K. Sakata, Y. Hayakawa, S. Asai, K. Miyasaka and M. Tanemura, 'Double percolation effect on the electrical conductivity of conductive particles filled polymer blends', Colloid and Polymer Science, **270**, 1992, p. 134-139
130. L. Ci and J. Bai, 'The reinforcement role of carbon nanotubes in epoxy composites with different matrix stiffness', Composites Science and Technology, **66**, 2006, p. 599-603
131. J. Bai, 'Evidence of the reinforcement role of chemical vapour deposition multi-walled carbon nanotubes in a polymer matrix', Carbon, **41**, 2003, p. 1325-1328
132. J. P. Pascault and R. J. J. Williams, 'Glass transition temperature versus conversion relationships for thermosetting polymers', Journal of Polymer Science Part B: Polymer Physics, **28**, 1990, p. 85-95
133. M. R. Vanlandingham, R. F. Eduljee, J.W. Gillespie, 'Relationships between stoichiometry, microstructure, and properties for amine-cured epoxies', Journal of Applied Polymer Science, **71**, 1999, p. 699-712
134. M. Roylance, J. Player, W. Zukas and D. Roylance, 'Modeling of ultrasonic processing', Journal of Applied Polymer Science, **93**, 2004, p. 1609-1615
135. M. Mitchell, 'An introduction to genetic algorithms', MIT press, 5th edition, 1999
136. A.A. Skordos and I.K. Partridge, 'Inverse heat transfer for optimisation and online thermal properties estimation in composites curing', Inverse Problems in Science and Engineering, **12**, 2004, p.157-172
137. P. Hubert, A. Johnston, A. Poursatip and K. Nelson, 'Cure kinetics and viscosity models for Hexcel 8552 epoxy resin', 46th International SAMPE Symposium, 6-10 May , 2001, p. 2341-2354
138. L. Sun, S.-S. Pang, A.M. Sterling, I.I. Negulescu and M.A. Stubblefield, 'Thermal analysis of curing process of epoxy prepreg', Journal of Applied Polymer Science, **83**, 2002, p.1074-1083
139. L. Sun, S.-S. Pang, A.M. Sterling, I.I. Negulescu and M.A. Stubblefield, 'Dynamic modeling of curing process of epoxy prepreg', Journal of Applied Polymer Science, **86**, 2002, p. 1911-1923

140. J. Player, M. Roylance, W. Zukas and D.K. Roylance, 'UTL consolidation and out-of-autoclave curing of thick composite structures', 32nd International SAMPE Technical Conference, Boston, MA, USA, 5-9 November 2000, p. 757-767
141. D. Dykeman and A. Poursartip, 'Round Robin invitation: DSC measurement and model analysis for T800/3900-2 cure kinetics', UBC Composites Group, Department of Materials Engineering, The University of British Columbia, Update November 2004
142. K.C. Cole, J.-J. Hechler and D. Noel, 'A new approach to modeling the cure kinetics of epoxy-amine thermosetting resins. 2. Application to a typical system based on bis[4-(diglycidylamino)phenyl]methane and bis(4-aminophenyl) sulfone', Macromolecules, **24**, 1991, p. 3098-3110
143. S.J. Buggy, E. Chehura, S.W. James and R.P. Tatam, 'Optical fibre grating refractometers for resin cure monitoring', Journal of Optics A: Pure and Applied Optics, **9**, 2007, p. S60-S65
144. S.J. Buggy, E. Chehura, A.A. Skordos, A. Dimopoulos, S.W. James, I.K. Partridge and R.P. Tatam, 'Fibre grating refractometer sensors for composite process monitoring', Presented at the SPIE Europe Optical Metrology Conference, Munich, Germany, 17-21 June 2007
145. C.B. Kim and C.B. Su, 'Measurement of the refractive index of liquids at 1.3 and 1.5 micron using a fibre optic Fresnel radio meter', Measurement Science and Technology, **15**, 2004, p. 1683-1686
146. K.-Y. Lam and M.A. Afromovitz, 'Fibre-optic epoxy composite cure sensor. I. Dependence of refractive index of an autocatalytic reaction epoxy system at 850 nm on temperature and extent of reaction', Applied Optics, **34**, 1995, p. 5635-5638
147. K.-Y. Lam and M.A. Afromovitz, 'Fibre-optic epoxy composite cure sensor. II. Performance characteristics', Applied Optics, **34**, 1995, p. 5639-5644
148. A. de la Vega, K. Schulte, J. Kovacs and W. Bauhofer, TUHH, Germany, unpublished work
149. H. Lee, S. Mall, V. Nalladega, S. Sathish, A. Roy and K. Lafdi, 'Characterisation of carbon nanofibre reinforced epoxy composites using

nanoindentation and AFM / UFM techniques', Polymers & Polymer Composites, **14**, 2006, p. 549-562

150. Z. Wang and T. Peijs, Queen Mary, University of London, United Kingdom, unpublished work
151. M. Gullon, J. Vera-Agullo, H. Varela-Rizo, M. Weisenberger and R. Andrews, University of Alicante, Spain, unpublished work
152. Ye.B. Trostyanskaya, A.M. Poimanov and Ye.F. Nosov, 'The processes accompanying the curing of diglycidyl ethers in the presence of filler powders, and thei effects on the physico-mechanical properties of the cured binders', Polymer Science USSR, **15**, 1973, p. 692-701
153. Ye.B. Trostyanskaya, A.M. Poimanov and Ye.F. Nosov, 'The structure and the properties of epoxide resins cured by amines in the presence of fillers', Polyme Science USSR, **15**, 1973, p. 1212-1219
154. Ye.M. Filyanov, 'Effect of a filler on the glass transition temperature of an epoxy resin and its relation to the filled polymer properties', Polymer Science USSR, **20**, p. 2074-2078
155. A. Yim, R.S. Chahal and L.E.ST. Pierre, 'The effect of polymer-filler interaction energy on the T_g of filled polymers', Journal of Colloid and Interface Science, **43**, 1973, p. 583-590
156. 'EPIKOTE^{TM} RESIN 1009', Product datasheet, Resolution Performance Products, June 2004
157. 'Araldite MY 750', safety datasheet, Huntsman, January 2004

Appendix A

In this appendix some photos of the RTM demonstration and the infusion test of the MY 750 / HY 5922 resin system are presented. Optical fibres and dielectric sensors were utilised to study the curing reaction. The data were used to establish a correlation between the two techniques.

RTM demonstration test

The purpose of this test was to use simultaneously dielectric sensors and optical fibres, embedded in the resin system and measure the flow (time required for the resin to fill the RTM mould), conversion and refractive index change during the curing reaction. The dielectric equipment used and the steps in order to conduct this industrial experiment is illustrated in figure A:

a)

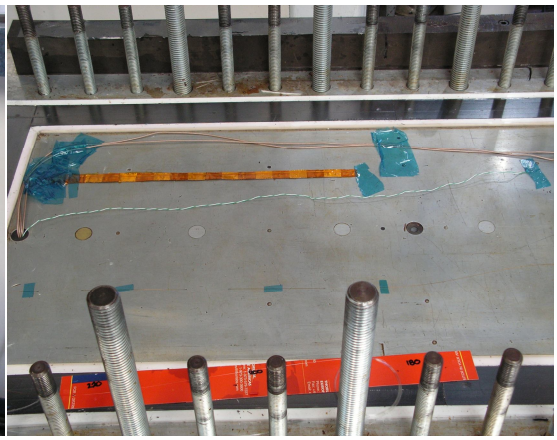

b)

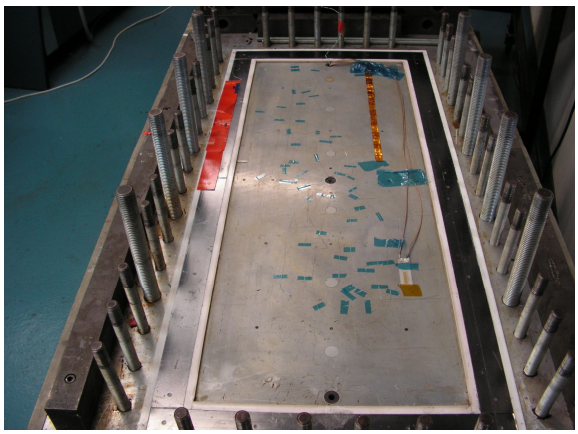

c)

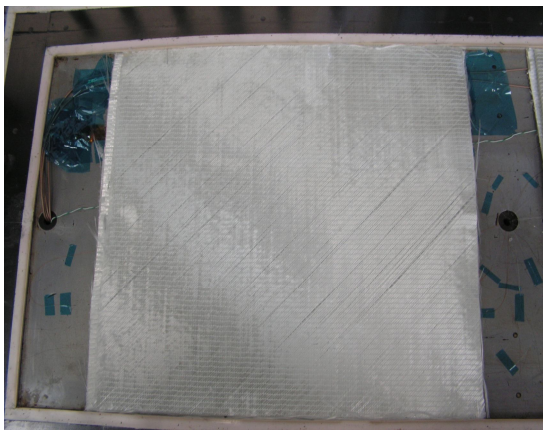

d)

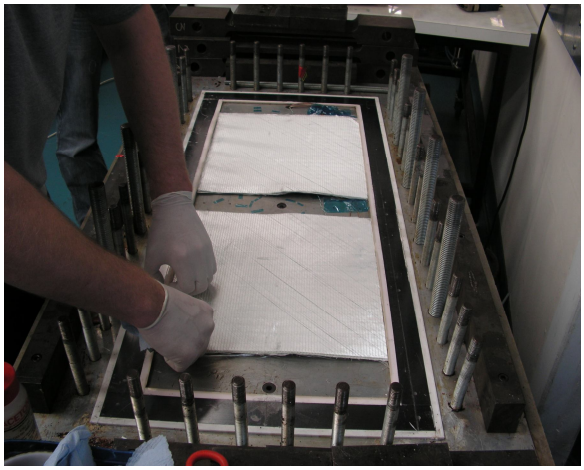

e)

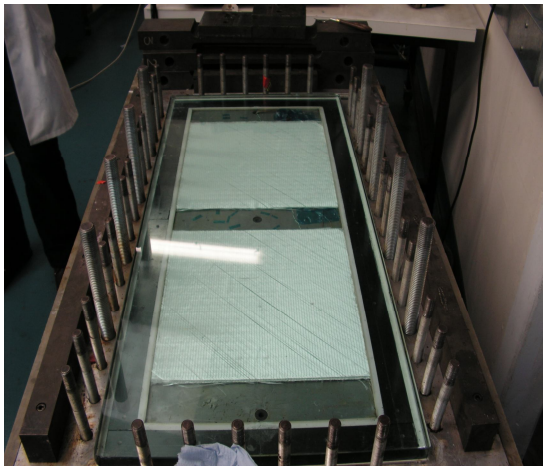

f)

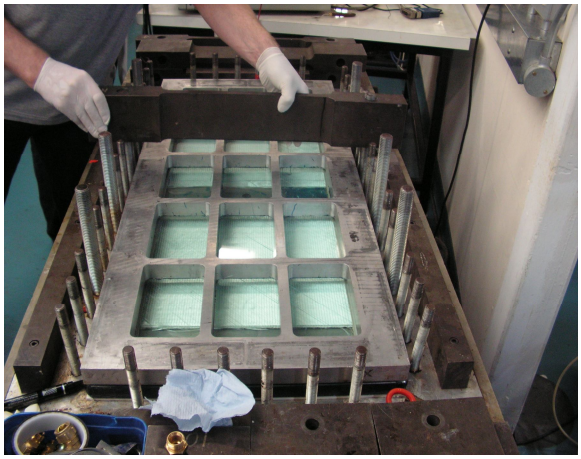

g)

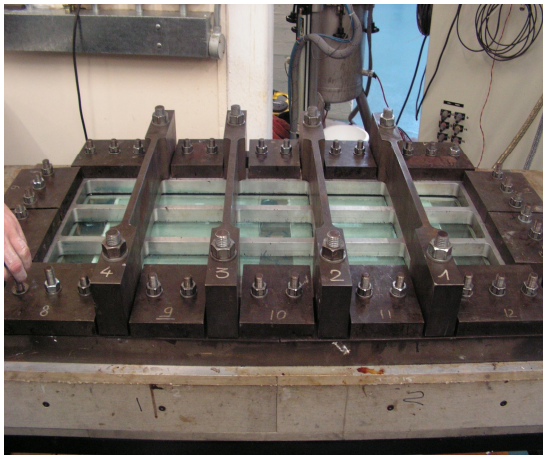

h)

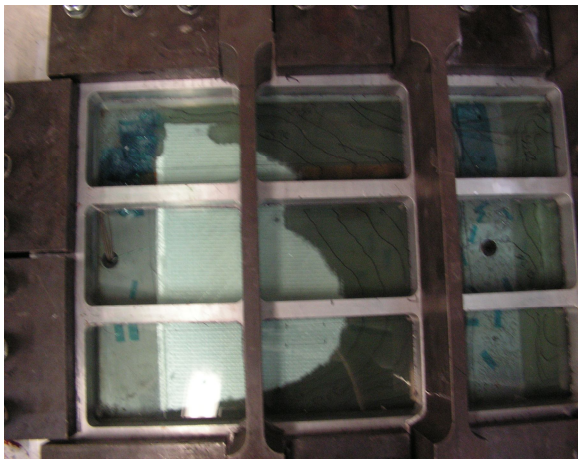

i)

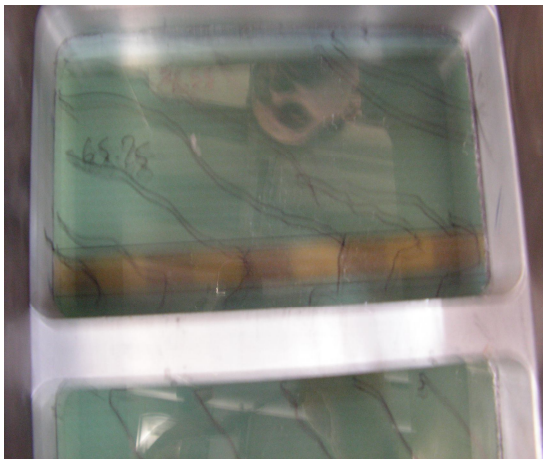

j)

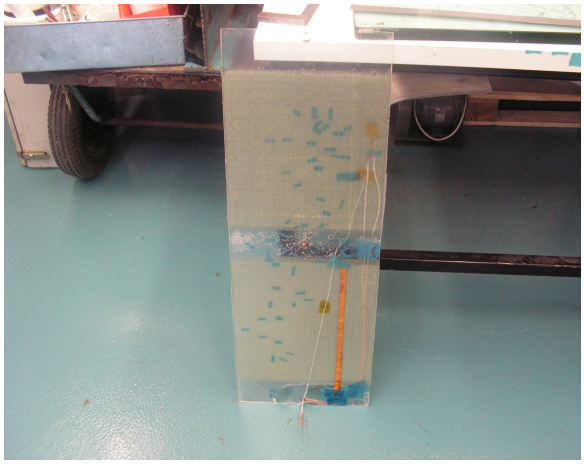

k)

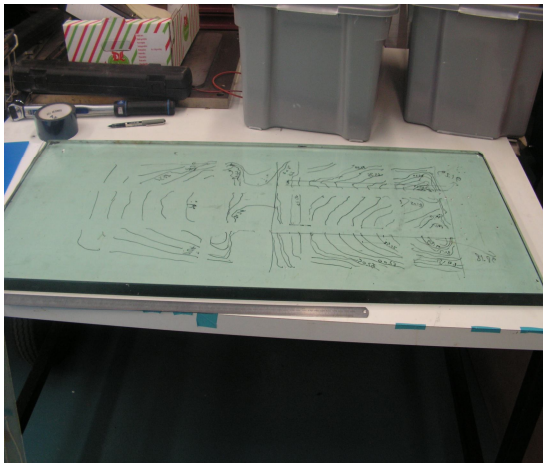

l)

Figure A: RTM test of the curing of the MY 750 / HY 5922 resin system and the subsequent steps: a) the dielectric bridges used to measure flow and degree of cure, b) the flow and dielectric sensors, c) the experimental setup comprising of the dielectric sensors and optical fibres embedded on the RTM surface, d) and e) the glass fabric layup used, f) the top glass plate used to seal the RTM, g) the pressure bars, h) schematic of the sealed mould, i) and j) monitoring and measuring the flow, k) and l) the panel produced after the end of the test (the optical fibres, the dielectric sensors and the designated areas used to measure flow time are well distinguished)

Infusion test

In this test, dielectric sensors and optical fibres were utilised in a smaller scale experiment (compared to the RTM test) in order to verify the correlation of the data established between the two online monitoring techniques. MY 750 / HY 5922 resin system was used for this purpose. The major steps followed to conduct this test are illustrated in figure B:

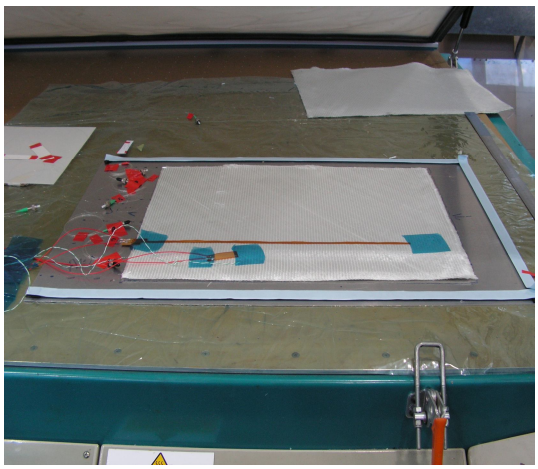

a)

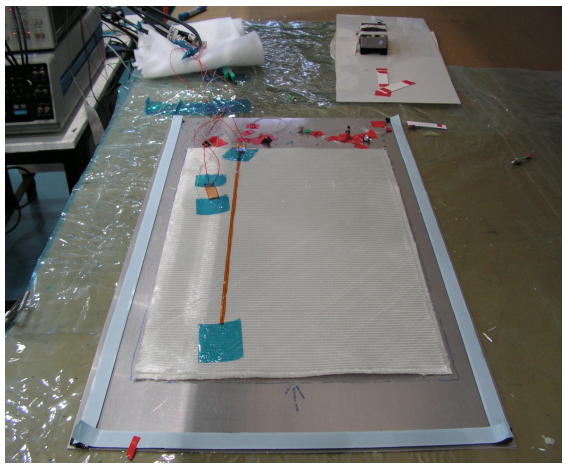

b)

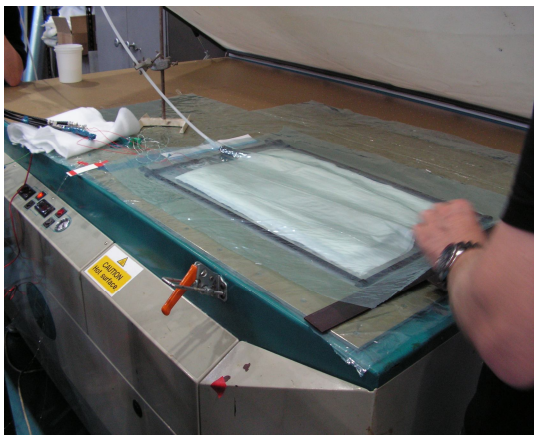

c)

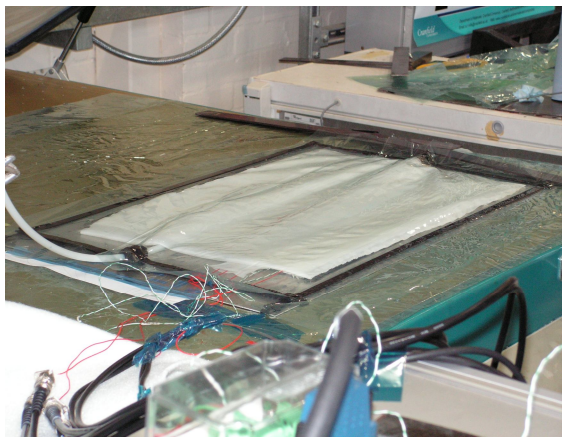

d)

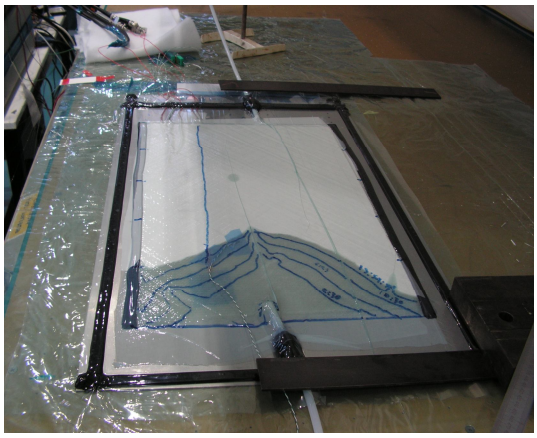

e)

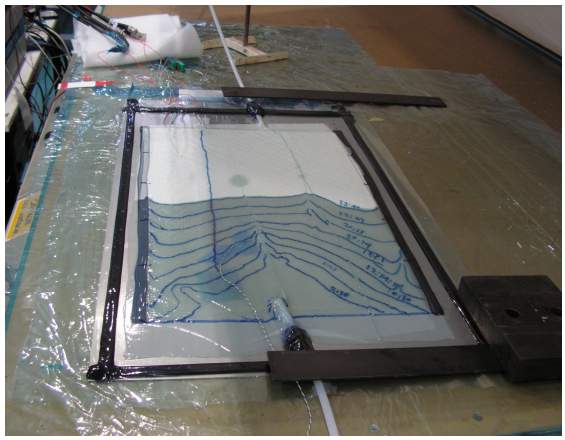

f)

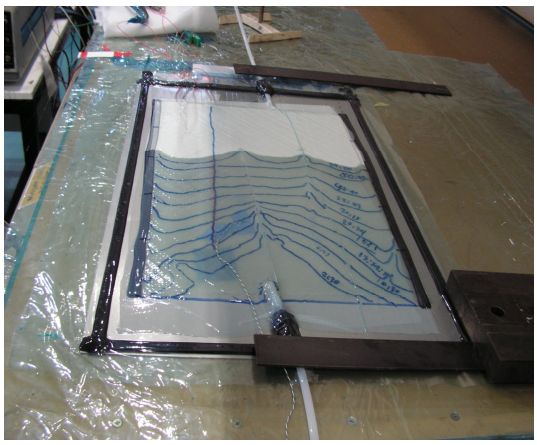

g)

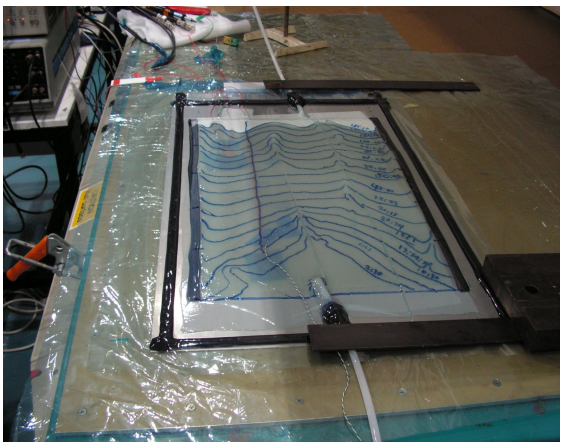

i)

Figure B: Infusion test of the curing of the MY 750 / HY 5922 resin system and the subsequent steps: a) the experimental setup comprising of the dielectric sensors and b) the optical fibres embedded on the testing surface (below and on the top of the glass fabric), c) and d) the vacuum bag used, e) and f) monitoring and measuring the flow, g) and i) the panel at the final stages of the filling process (the optical fibres, the dielectric sensors and the designated areas used to measure flow time are well distinguished)

Appendix B

In this appendix the final report of the Round Robin participation is contained. Our group is denoted as group E.

ROUND ROBIN RESULTS
FOR T800H/3900-2

FINAL REPORT

Prepared by

Donna Dykeman and Anoush Poursartip
Materials Engineering
The University of British Columbia

December 2007

Report Contents

1.0 EXECUTIVE SUMMARY

The goal of the Round Robin was to understand the sources of uncertainty in the measurement-to-modeling decision-making process for cure kinetics modeling based on DSC testing. The study consisted of a series of experimental and modeling stages, the strategy of which was to systematically reduce the sources of variability between laboratories from measurement to model-fitting stages, as outlined in Table 1.1. In stage 1, participants made all measurement and modeling decisions on the same material (T800H/3900-2 provided by The Boeing Company); in stage 2, participants were given a raw data set produced by UBC for T800H/3900-2 and were asked to perform their data reduction, analysis and model fitting preferences; and, in stage 3, participants were given the baselines to apply for area measurements and the Tg-α curve, and were asked to analyze the data and fit a cure model of their choice. The study did not pursue the analysis or model selection/fitting stages due to time constraints, and the difficulty for some participants to adjust their model fitting programs to fit the proposed model. At each stage, participants were asked to report their measurements, analysis decisions, model parameters, and their measure for the goodness of model fit to data. Measurements were also required to establish the quality of each DSC instrument, referred to as stage 0.

The results of the Round Robin study showed that the greatest variability in prediction of degree of cure for the limits of a standard cure cycle occurred for stage 1 (±22.5% maximum variability) followed by stages 2 and 3 (±10% maximum variability). In comparison, a literature review of models for Hexcel 8552 (updated since the UBC Round Robin Invitation document, 2004) showed variability between degree of cure predictions to be as high as ±80%. Table 1.2 records several measures of variability for the Round Robin and literature review model comparisons. The literature review provided a worst case scenario of uncertain batch-to-batch variability, a combination of resin and prepreg information, and a wide range of cure measurement and modelling decisions. The Round Robin study was able to reduce the variability by ensuring instrument quality and material consistency between laboratories (stage 1), and furthermore by sharing a common data set (stages 2 and 3). Therefore, at each stage of the decision-making process there are opportunities to evaluate sources of uncertainty.

The remainder of this report presents the results for each stage of the Round Robin, and offers a commentary on the differences between each laboratory's decision-making process. Table 1.3 summarizes the experimental, reduction, analysis and modeling decisions made by all participants throughout the three stages of the Round Robin. The final step of the study is to open the discussion reported herein to participants and partners (Table 1.4).

1.1. ROUND ROBIN RESULTS

1.1.1. Stage 0: Instrument quality and material quality control

All instruments used in this study were heat flux devices with disk-type sample and reference cells, a sample volume of at least 25 mm^3, and a nitrogen atmosphere with a temperature range of at least -60 to 550^oC (see Table 1.5 for a list of general instrument specifications for each laboratory). Three types of tests were performed by each laboratory to determine the quality of the heat flow signal in terms of noise, repeatability and reproducibility: 1) five dynamic zero-line tests (heat flow measurement without samples or sample containers), and two isothermal zero-lines, to determine noise and the repeatability of the instrument heat flow signal; 2) three dynamic tests on standard materials, tin and indium, to determine reproducibility and calibration accuracy; and, 3) three dynamic tests on the CFRP system T800H/3900-2 to determine reproducibility of the signal across a broad temperature range.

The peak-to-peak noise (pp) is the maximum variation of the measured signal in relation to the mean signal value for a given test [Hohne et al., 1996]. The 'short-time' noise was measured over a 1-minute period at the indicated temperatures for scanning rates of 2 and 5^oC/min, recorded in Table 1.6. The pp noise was reported to be less than 1 μW in most cases. Resolution at the beginning and end of reaction will be most affected by noise, as well as slow heating rates. The isothermal noise is also less than 1 μW, recorded in Table 1.6, measured during 100 and 250^oC holds after the signal had reached temperature equilibration.

The temperature-dependent range of the deviation from the 'mean' zero-line (absolute or in %) gives a measure of the repeatability [Hohne et al., 1996]. Table 1.7 reports the repeatability for five zero-lines from 5^oC/min scans between 50 and 275^oC. Repeatability for 2^oC/min scans was also collected, but was not significantly different from the 5^oC/min scans.

Accuracy of temperature and enthalpy measurements was compared by measuring the onset temperature and heat of melting for indium and tin (see Table 1.8 for test results from each laboratory and standard values). ASTM E967 for DSC temperature calibration states that for an interlaboratory comparison reproduced measurements for melting temperatures should be suspect if they are different by 1.5^oC (95% confidence interval). ASTM E793 for measurement of enthalpies of fusion recommends that reproduced measurements for the enthalpy of fusion should be considered suspect if they differ by more than 8.6% (95% confidence interval). Unlike the ASTM standards, duplicates were not performed, but given this guideline groups B and E measured melting temperatures beyond the deviation allowed by the standard

for both materials and group C for tin, and groups C and E measured enthalpies lower than the standard for both materials. The greatest cause for concern is the low heats of melting measured by groups C and E. It is advised that both laboratories perform their own calibration across a wide temperature range to assure that heat flows are accurate. All instruments used at least indium to calibrate temperature and enthalpy. Group B used cesium chloride, indium, tin, zinc and bismuth to calibrate for temperature and heatflow, and Group E used indium and tin to calibrate temperature.

Initial Tg and heat of reaction reproducibility for the CFRP T800H/3900-2 was compared from three 5°C/min dynamics submitted by each laboratory. The Tg of the prepreg before testing, Tg_0, ranged from -2.69 to 7.93°C with an average of 4.51 ± 3.75 °C (Table 1.9). Not all groups returned a piece of prepreg to the UBC lab for testing the Tg_0, nor was Tg_0 consistently tested for the remainder of the stages. Group F did note a change in their material Tg_0 during the study and requested new material be sent to continue the study.

Baselines for heat of reaction measurement were drawn as straight lines between the start and end temperatures of the reaction for all groups except D and E. Group D used a flat baseline up to the onset temperature of degradation (as measured by TGA), and then a straight line to a local minimum in heat flow. Group E used a sigmoidal baseline. The heat of reaction ranged from 115.09 to 159.89 J/g between 0.2 and 10°C/min test conditions with an average of 144.96 ± 16.39 J/g (±11.3%), as recorded in Table 1.9. Group D used modulated DSC to remove the effect of changes in Cp, but the findings still lie within the range of measurements found by the other groups. The high variability within laboratory F (Table 1.9) may be due to the variability in resin fraction for small sample sizes.

Figure 1.1 (a) shows the heat flow signal with temperature for the 5°C/min test measured by each laboratory; laboratory C did not submit their data. Figure 1.1 (b) shows the degree of cure plotted against temperature. Also shown in Figure (b) is the variability within a laboratory compared with the variability between laboratories (with and without group B). The reaction timing measured by instrument B is in advance of the others, and hence is the most significant contributor to variability between laboratories. By degree of cure of 0.2, the maximum variability between the other four laboratories is roughly 1%. Without knowledge of the zerolines and the subtraction process from the measured signal for CFRP, it is difficult to comment further on this discrepancy.

In general, the quality of the instruments is good. Instrument E has the most zeroline variability. Instruments C and E showed considerable variation from the standard heat of melting for tin. Instrument

C had the lowest value, which may also explain their low value for CFRP heat of reaction (Table 1.9). Yet the reduced data from these groups agreed well with others (Figure 1.1 (b)). Instrument B has a difference related to the reaction timing, which may be due to zero-line curvature, or a calibration effect due to using several standards.

1.1.2. Stage 1: Participants perform cure measurements and develop cure models for T800H/3900-2 prepreg system

This section summarizes the experimental-to-modeling decisions made by each laboratory to produce cure models for T800H/3900-2. Table 1.10 records the experimental decisions for each group. Group B used dynamic tests to fit a model, Group D used both isothermal and dynamic tests, and all other groups used only isothermals apart from one dynamic to determine the ultimate heat of reaction. The ranges of isothermal temperatures used for fitting varied from 20°C (groups C and E), to 40°C (group A), 70°C (group D) and 80°C (group F). The mean temperatures for groups A, C, D and E were between 160 and 170°C, whereas for group C it was 205°C. Group C only intended to measure the chemical reaction, not diffusion, and hence decided to test above their measured Tg_∞ of 193°C (measured during cooling from 320°C during a 5°C/min dynamic; according to UBC's TGA measurements, reaching 320°C would have caused degradation and hence lowered Tg_∞).

The following general data reduction decisions were made by all groups concerning baselines for heat of reaction calculations. The same dynamic baseline decisions were made as discussed for stage 0. All groups used a horizontal isothermal baseline. Figure 1.2 (a) shows the heats of reaction measured for all isothermal tests, and (b) for dynamic tests performed by groups B and D. Groups A and D back-calculated the magnitude of the isothermal baseline heat flow in order to equate $H_{Ultimate}$ and H_{Total}. All other groups set the isothermal baseline magnitude to match the heat flow at the end of the reaction (indicated by negligible change in heat flow), or when the test was stopped. The isothermals for group C were missing ~10J/g compared to their $H_{Ultimate}$, and were not adjusted to account for the difference. Group D reported up to 11% difference between isothermal and dynamic heats of reaction, and attributed some of the missing heat lost during the ramp to the isothermal hold, and the remaining was recovered by back-calculating the isothermal baseline. Group F reported missing ~20J/g from isothermal heat of reactions and attributed all heat lost to the ramp. In contrast, group A did not report any missing heat of reaction and did not account for heat lost during the ramp to the isothermal hold, but did start their initial degree of cure at 0.01. Dynamic heats of reaction for group B were lower than D due to the difference between using a straight-line baseline and flat baseline, respectively. Figure 1.3 shows the Tg-α curves

from data provided by the participants. This data was not required of participants, but provided a comparison as to the influence of analysis decisions. Figure 1.3 shows that when $H_{Total} = H_{Ultimate}$, no matter the exact value, the Tg-α relationships overlap.

Table 1.11 records the data analysis, model selection, and model fitting strategies reported by each group for stage 1. Secondary test methods were not employed to determine initial monomer content. Nor were measurements taken to track the consumption of reactants, and hence all models were applied on a phenomenological basis. The models and values for parameters are recorded in Table 1.12. Most groups followed the assumption that the total heat measured by the DSC was analogous to the heat evolved by the consumption of epoxide, and their models were based on the consumption of epoxide (α) described by either an autocatalytic reaction or some variation of the Horie model. Group B did not follow the above assumption and proposed a two-term sequential reaction with the following design: in the first term the depletion of epoxide (A or α) is coupled with the formation of some product (B or β), which in turn is consumed by an nth order reaction to produce C. The normalized concentrations of α and β start at 0.99995 and 0.00003, respectively, and the degree of cure was defined as (1 – α), and the rate of cure by dα/dt. This relationship implies that epoxide bonds are only participating in the first reaction, and hence their depletion will be faster than if they were also a part of the second reaction. Only groups B and D showed fits to dynamic data.

Figures 1.4 (a) and (b) compare the model predictions for a 5°C/min dynamic in terms of degree of cure versus temperature and cure rate. In Figure (a) the data from Figure 1.1 (b) is also included, indicated by black circles. At this heating rate diffusion was not a factor. The percent deviation in Figure (a) between the six models is greater than 10% until high degrees of cure. Given that degree of cure data for 5°C/min tests of at least five of the groups were under 10% after 170°C (Figure 1.1 (b)), differences have accrued during data analysis and model selection/fitting. Models B, E and F show the most deviation from the mean predictions (models A, C and D). Model F proposed a temperature dependent order of reaction, n over a (1-α) term, which increases with temperature and effectively delayed the reaction at higher temperatures and degrees of cure. Model E overestimated the progress of cure after 170°C, which perhaps is best explained by the limited isothermal temperature range used to fit the data and lack of diffusion control. The timing of model B is in advance of all other models, which may be traced back to the decision to treat the second reaction separate from any epoxide interaction, reflected in Figure (b) as well.

Figures 1.5 (a) and (b) compare the degree of cure with respect to temperature predictions for the MRCC heating rate limits of 0.56°C/min and 2.86°C/min, respectively, followed by a 140 minute hold at 180°C. For the low MRCC limit the degree of cure predictions at the end of the ramp varied between 0.72 and 0.99 in degree of cure (±12.7% deviation), and 0.89 to 1 at the end of the hold (±4.9%). Given the Tg-α curve of Figure 1.3, the range of Tg's at the end of the 0.56°C/min ramp would be 166 to 225°C. Models A, D and F have the similar cure profiles up to the point where diffusion becomes dominant, and then groups A and D continue to coincide in the diffusion zone. For the upper MRCC limit, models vary between 0.19 and 0.32 in degree of cure at the end of the ramp (±22.5%), and between 0.87 and 1 at the end of the hold (±6.1%). Similar comments can be made for Figure (b) as in (a). Also on these figures are three circles indicating the degree of cure calculated by interrupting the cure cycle and measuring the residual heat of reaction, performed by UBC.

1.1.3. Stage 2: Common data set, individual reduction-to-modeling decisions

In Stage 2, groups were given the same data set to analyze, provided by UBC. Most participants continued to perform area calculations to determine the degree of cure with time and temperature, and used the same baseline methodology as outlined for each group in Stage 1, as well as the same data reduction techniques. Group D also used a straight line between the onset and end of the dynamic reaction curves rather than a flat baseline. Group D and E used both isothermal and dynamic data to fit their models. Table 1.13 records the experiments used by each group to fit a model. Table 1.14 records the model and parameters chosen by each group. Groups A and F maintained the same model. Group B added diffusion to the second reaction (B→C), and group E added a second autocatalytic reaction and a diffusion factor to their entire equation. Group D opted for a simpler chemical and diffusion model. Figure 1.6 shows the Tg-α models proposed by groups B and D, which differ considerably below 0.55 degree of cure. Group B used Tg in their diffusion model, but group D did not.

Figures 1.7 (a) and (b) compare the degree of cure predictions with respect to temperature for the MRCC limits, 0.56°C/min and 2.8°C/min ramps respectively, to 180°C for a 140 minute hold. For the slower heating rate, degree of cure varied from 0.78 to 0.89 at the end of the ramp (±6.5%), and 0.93 to 1 at the end of the hold (±3.1%). Given Figure 1.6, the Tg range at the end of the ramp was roughly 173 to 203°C. For the upper limit, degree of cure varied from 0.11 to 0.34 at the end of the ramp (±33.5% difference), and 0.91 to 1 at the end of the hold (±3.6%). Again, the model for group B would better match the timing of the others at high heating rates if the assumption of heat flow analogous to epoxide reaction were used. Otherwise, the timing is fairly consistent between the groups until the different

diffusion definitions are active. The effect of group F's rules for reaction orders (before and after 170°C) are apparent during the slow heating rate. Worthy of note is the complexity of the chemical models and how this may relate to variability. Models A and F use a single reaction and overlap up to the point of diffusion dominance. Comparatively, models D and E use at least two reaction mechanisms, and their rate of cure matches well up to the diffusion dominated zone. The comparison to interrupted tests show that models D and E follow a similar cure profile up to the point of diffusion, after which model A predicts the most accurate final degree of cure.

1.1.4. Stage 3: Common data and reduction, individual model and fitting

In Stage 3, participants received data which had the areas and temperatures of interest (Tg's, peak temperatures) measured. Baselines were provided with the raw data, and were the same as those used in Stage 2 for dynamic and isothermal data, respectively, as decided by the majority of participants. A diagonal baseline between the start and end points of the cure reaction were used for dynamics, which resulted in excellent agreement between isothermal and dynamic total heats of reaction ($H_{ultimate}$ = 133 J/g). Unfortunately this decision is incorrect and leads to differences in dynamic and isothermal cure rates as shown in Figure 1.8. Participants chose the same data and models as in Stage 2. Groups D and E noted the differences in cure rates between isothermals and dynamics due to model fitting using data from both test modes. Group F changed their definition of final degree of cure to account for diffusion. Table 1.15 records the models and parameters proposed by each group. Figure 1.9 shows the Tg-α data and proposed models by groups B and D. Figures 1.10 (a) and (b) compare the model fits to the MRCC limits with degrees of cure calculated for interrupted tests throughout the cycle. For the lower heating rate, degree of cure varied between 0.77 and 0.92 at the end of the ramp (±6.7% deviation), and 0.88 to 1 at the end of the hold (±4.5%). For the higher heating ramp, degree of cure varied between 0.22 to 0.33 at the end of the ramp (±1.8%), and 0.88 to 1 at the end of the hold (±4.5%). The variability is roughly the same as that measured for stage 2, except for the decrease in variability at the end of the ramp during the highest heating rate by the MRCC standard, low degrees of cure and low temperatures. The same comment can be made for this stage regarding chemical model complexity: models A and F overlap and used a single reaction mechanism each, and models D and E overlap and used at least two reaction mechanisms each. According to the comparison to interrupted tests, for the slow heating rate all of the models (except B) perform very well up to the diffusion zone, and then model F predicts the most accurate final degree of cure. For the high heating rate, the best fit is for models D and E up to the diffusion zone, and thereafter group F.

1.1.5. Summary of measurement and modeling uncertainty

Variability within the Round Robin study was clearly better than that of the 8552 literature review. Furthermore, variability decreased between stage 1 and the latter two stages. Below is a summary of the major sources of uncertainties identified between the levels of this study:

Literature review:

i. Material quality control. Batch-to-batch variability and possible changes to the chemistry (the findings span a decade). Also, the state of the material before cure testing was not reported, and hence the history of the material may have been an important factor.
ii. Unknown instrument and measurement quality, and a wide variety of instruments used.
iii. Range of experimental parameters. Those using dynamic data produced higher cure rates than the isothermal tests. Dynamic and isothermal data was not cross-compared for improved model fitting.
iv. Data reduction decisions were not consistently reported.
v. Comparing both resin and prepreg. Opalicki et al. [1996] showed a change in timing between the two.
vi. Chemical model accuracy. Some models could only be applied to isothermal or dynamic conditions, but not both. The choice of reactions to model, and the complexity of the chemical model, also varied.

Round Robin, Stage 0:

i. Heat flow accuracy over a wide range of temperatures. This was evident for both standard materials and CFRP.

Round Robin, Stage 1:

i. Range of experimental parameters. The use of higher temperatures and dynamics (excluding diffusion dominated zones) lead to overestimated cure rates at low temperatures and degrees of cure.
ii. Baseline selection within a data set. Although groups A and D used different baselines for their dynamic experiments, their cure predictions overlap very well for the MRCC limits.
iii. $H_{Total} = H_{Ultimate}$. This proved necessary for Tg-α data to overlap between groups.
iv. Following the underlying assumption that heat flow is analogous to the reaction of epoxide. The underlying assumption may not be true, but it should be recognized that following it versus not will cause significant differences in the interpretation of degree and rate of cure of epoxide.
v. Diffusion model accuracy.

Round Robin, Stage 2:

i. Diffusion model accuracy.

ii. Chemical model accuracy

Round Robin, Stage 3:

i. Baseline selection. A linear baseline created an artificial difference between dynamic and isothermal cure rates. A method of checking for consistency between isothermal and dynamic data is needed.

ii. Diffusion model accuracy.

iii. Chemical model accuracy.

1.1.6. Future direction

In the near future we would like to publish a paper based on the findings of the Round Robin study, with all participants and partners as joint authors. We propose the following steps for accomplishing this:

1. Feedback from participants:
    a. Please check for consistency between your findings reported to us, and the presentation of your findings in the report.
    b. Add your comments regarding how we have compared the models and what we could do to provide more insight into the study of uncertainty.
    c. Please give us your evaluation of the Round Robin process. What would you do differently in a Round Robin of the same design? We left out the final model fitting stage to a common model due to complications for some to use their fitting methodologies for the model proposed. How could we have accommodated your methodology better?
    d. The above questions are not intended to be exclusive. Please feel free to address your individual concerns.
2. Publication: Results of the Round Robin
    a. UBC will start drafting a paper for publication while you review the findings, and will review/include your comments as we receive them.
    b. Participants will be invited to review the paper before submission.

Table 1.1 Outline of Round Robin stages

Uncertainty Parameter	Stage 1	Stage 2	Stage 3
Experimental Set-up (sample preparation, test parameters, test schedule)	Individual Laboratory Decision	Common	Common
Data Reduction (e.g. area measurement, peak temperature, Tg)	Individual	Individual	Common
Data Set Analysis / Model Fitting	Individual	Individual	Individual

Table 1.2 Comparison of variability between 8852 literature survey and T800H/3900-2 Round Robin results

Material	8552, AS4/8552[1]	T800H/3900-2	T800H/3900-2	T800H/3900-2
Stage	N/A	1	2	3
Time to gel (min) 177°C/180°C	18.29 ± 6.97 (±38.1 %)	18.5 ± 3.57 (±19.3%)	19.4 ± 1.7 (±8.8%)	19.0 ± 2.0 (±10.3%)
DOC end of ramp, LMRCC[2]	0.50 ± 0.24 (±46.7%)	0.83 ± 0.11 (±12.7%)	0.80 ± 0.06 (±7.1%)	0.81 ± 0.06 (±7.4%)
DOC end of hold, LMRCC	0.89 ± 0.08 (±8.8%)	0.96 ± 0.05 (±4.9%)	0.97 ± 0.03 (±3.0%)	0.94 ± 0.03 (±3.3%)
DOC end of ramp, HMRCC[3]	0.35 ± 0.28 (±81.8%)	0.24 ± 0.05 (±22.5%)	0.23 ± 0.02 (±8.4%)	0.23 ± 0.02 (±10.1%)
DOC end of hold, HMRCC	0.89 ± 0.07 (±8.4%)	0.95 ± 0.06 (±6.1%)	0.96 ± 0.03 (±3.3%)	0.93 ± 0.03 (±3.1%)
$H_{Ultimate}$ (J/g)	189.11 ± 12.27 (±6.5%)	144.96 ± 16.39 (±11.3%)	133.55 ± 1.26 (±0.9%)	134.54 ± 0.61 (±0.5%)
Max CR end of ramp (/sec), HMRCC	9.00E-4 ± 7.78E-4 (±86.4%)	4.90E-4 ± 5.03E-5 (±10.3%)	5.00E-4 ± 3.9E-5 (±7.9%)	5.00E-4 ± 3.8E-5 (±7.6%)

[1] Excluding models by Ng et al. for all measurements, and Costa et al. and Sun et al. (b) for measurements involving isothermal holds

[2] LMRCC refers to the lowest heating rate limit of the MRCC, 1.8°C/min for 8852 and 0.56°C/min for 3900-2

[3] HMRCC refers to the highest heating rate limit of the MRCC, 3°C/min for 8852 and 2.86°C/min for 3900-2

Table 1.3 Conglomeration of choices made throughout the Round Robin study between all participants to demonstrate the variation in the decision-making process

Stage	Decision process	Choices made by participants in this study
0: Instrument quality	Zero-line repeatability	Repeat dynamic tests without sample or pans
	Signal noise	Dynamic and isothermal tests
	Calibration check	Enthalpy and onset temperature of melting for standard materials across a wide temperature range
	Initial material state	Measured Tg_0
	Repeatability and reproducibility of reaction heat flow	Repeat dynamic tests on CFRP, analyzed for degree and rate of cure and heat of reaction
1: All decisions made by individual laboratories	Process conditions to test	Isothermal temperatures and hold times, dynamic heating rates, combinations
	Test methods	Programmed ramp to isothermal holds; modulation amplitude and period; heating rate to measure Tg_i's, maximum temperatures, etc.
	Data reduction	All used area calculations to measure degree and rate of cure. Decisions pertained to baseline selection and balancing $H_{Total} = H_{Ultimate}$. Tg_i measured by heat flow and heat capacity signals.
	Data analysis	Activation energy was calculated by 1. traditional isothermal kinetic method; 2. cure rate isoconversionals; 3. multivariable nonlinear regression programs.
	Model selection	Phenomenological models with parameters based on the Horie model, versus a sequential model fit. Other behaviour and reactions modeled included diffusion and etherification.
	Model fitting	a. Least squares; b. linear regression; c. multivariable nonlinear regression
	Goodness of fit	Visual inspection of model fit to cure rate or heat flow
2: Raw data provided by UBC, individual laboratories reduce, analyze and model. Laboratories chose the same data reduction decisions as Stage 1 and only changed the model and parameter values.		
3: Raw data and data reduction provided by UBC, individual laboratories analyzed the data, selected and fit a model. Participants chose the same analysis method and model, and only changed the parameter values.		

Table 1.4 Participants and partners

Participants/Partners	Affiliation
Dr. Pascal Hubert, Dr. Martine Dubé	McGill University, Dept. of Mechanical Engineering, Montreal, Quebec, Canada
Dr. Nuri Ersoy[1], Dr. Nihan Ugay[1] Dr. Melih Papila[2]	[1]Bogazici University, Polymer Research Centre, Istanbul, Turkey [2]Sabanci University, Turkey
Dr. Michele Giordano, Dr. Vincenza Antonucci	National Research Council Italy, Institute of Composite Materials Technology, Napoli, Italy
Dr. Karl Nelson	Boeing Phantom Works, Seattle, Washington, United States
Professor Ivanna Partridge, Thanos Dimopoulos	Cranfield University, School of Industrial and Manufacturing Science, Advanced Materials Department, Polymer Composites Group, Bedford, United Kingdom
Dr. Andrew Johnston[3], Dr. Mehdi Hojjati[4], Dr. Jihua (Alex) Chen[4], Ghislain Chouinard[4]	[3]National Research Council Canada, Institute for Aerospace Research, Ottawa, Ontario, Canada [4]Aerospace Manufacturing Technology Centre, Montreal, Quebec, Canada
Dr. Kenneth Cole[5], Ngo Tri Dung[6]	[5]National Research Council Canada, Industrial Materials Institute, Boucherville, Quebec, Canada [6]Concordia University, Dept. of Mechanical & Industrial Engineering, Montreal, Quebec, Canada
Dr. Anoush Poursartip, Donna Dykeman	University of British Columbia, Dept. of Materials Engieering, Composites Group, Vancouver, British Columbia, Canada

Table 1.5 General instrument information

Group	Manufacturer	Model	Type	Sample Volume (mm^3)	Atmosphere	Scanning Range (^oC/min)
A	TA Instruments	Q100	Heat flux disk-type	133	Nitrogen	-90 to 750
B	Netzsch	204 Phoenix	Heat flux disk-type	25	Nitrogen	-170 to 700
C	TA Instruments	Q1000 MDSC	Heat flux disk-type	40	Nitrogen	-150 to 550
D	TA Instruments	Q1000 MDSC	Heat flux disk-type	40	Nitrogen	-90 to 550
E	TA Instruments	2920 MDSC	Heat flux disk-type	40	Nitrogen	-60 to 600
F	TA Instruments	Q1000 MDSC	Heat flux disk-type	40	Nitrogen	-180 to 725

Table 1.6 Scanning and Isothermal Noise

Group	2^oC/min at 100 °C (± µW)	2^oC/min at 250 °C (± µW)	5^oC/min at 100 °C (± µW)	5^oC/min at 250 °C (± µW)	100^oC (± µW)	250^oC (± µW)
A	<0.001	<0.001	<0.001	<0.001	<0.001	<0.001
B	<1	<1	<1	<1	<1	<1
C	2.18	0.49	0.345	0.08	0.185	0.251
D	<0.001	<0.001	<0.001	<0.001	<0.001	<0.001
E	0.333	0.429	0.57	0.372	0.851	0.963
F	<0.001	<0.001	<0.001	<0.001	0.19	0.15

Table 1.7 5^oC/min Zero-line Repeatability Determined by Five Tests

Group	at 50 °C (± µW)	at 125 °C (± µW)	at 200 °C (± µW)	at 275 °C (± µW)
A	1.344	1.329	1.062	2.181
B	<0.2	<0.2	<0.2	<0.2
C	3.86	0.74	7.03	
D	37.18	23.307	13.36	8.33
E	12000	11000	12000	12500
F	9.4	6.73	6.09	5.06

Table 1.8 Calibration check

Group	10°C/min scan on indium[1] sample			10°C/min scan on tin[2] sample		
	Mass (mg)	T_m onset (°C)	H_m (J/g)	Mass (mg)	T_m onset (°C)	H_m (J/g)
A	19.04	156.44	27.35	8.40	230.76	58.43
B	14.85	160.30	29.90	15.05	236.9	57.41
C	5.33	157.38	25.56	4.09	234.53	32.27[3]
D	19.17	158.00	27.57	14.8	231.07	58.49
E	12.03	160.00	23.782	7.82	236.12	47.85
F	11.10	157.31	26.99	9.10	233.10	56.78
Average		157.53 ± 2.43 (±1.5%)	27.46 ± 2.72 (±9.9%)		233.01 ± 4.22 (±1.8%)	57.32 ± 6.49 (±11.3%)
Standard		156.6[4]	28.43[4]		232.01[4]	59.07[4]

[1]Purity of indium 99.9999%
[2]Purity of tin 99.99%
[3]Considered an outlier observation and not used in subsequent calculations
[4]Perkin Elmer Periodic Table, Version 2.02g

Table 1.9 Tests for material quality upon arrival at each laboratory, and reproducibility of heat of reaction

Group	Temperature Scan Range (°C)	Time out of Freezer[2] (hours)	Three Scans at 5°C/min		
			Mass (mg)	$H_{Ultimate}$ (J/g)	Tg received, Tg_0 (°C)
A	30 to 320	28	7.90 ± 0.84	147.37 ± 1.66	7.93[1]
B	-40 to 320	90	19.47 ± 1.76	138.67 ± 5.98	5.97 ± 2.87
C	-20 to 320	68	5.24 ± 1.17	115.09 ± 1.18	6.63 ± 0.10
D	-30 to 320	6	16.11 ± 0.98	159.89 ± 7.38	4.85 ± 0.44
E	-30 to 320	48	5.63 ± 3.30	155.94 ± 8.49	-2.69 ± 1.32
F	-30 to 321	48	5.97 ± 0.06	152.80 ± 14.73	4.38 ± 0.76
Average				144.96 ± 16.39 (±11.3%)	4.51 ± 3.75 (±83%)

[1]Group A did not start their tests for Stage 0 at low enough temperatures to measure Tg_0. Rather, the Stage 1 value is reported here for a 5°C/min test.
[2]Storage temperature requested of participants, and their reported temperature, was -18°C

Table 1.10 Experimental decisions for stage 1

Group	Dynamic dT/dt (°C/min)	Modulation (± °C / seconds)	Isothermal temperature and time [°C (hours)]	Residual dT/dt (°C/min ± °C / seconds)	No. of repeat tests
A	5		140 (6), 160 (6), 180 (6)		2
B	2, 5, 10			5	3
C			195 (2), 200 (1), 205 (1.3), 210 (1.3), 215 (1.3)		1
D	1 to 10	1 / 60	130 to 200 in 10°C intervals	4 ± 1 °C / 60	1
E	5		150 (2), 170 (2)		3
F	5		130 (7.7hr), 150 (6.7hr), 170 (6hr), 190 (5hrs), 210(4.7hrs)	2	

Table 1.11 Data reduction and analysis decisions for stage 1

Group	Model	Analysis to find Arrhenius constants	Model fitting strategy
A	E-A: Autocatalytic Diffusion: Chen and Poehlein [1987], modified by Cole et al. [1990]	Cure rate isoconversional at 0.1 degree of cure	Weighted least squares fit to isothermal data. Visual goodness of fit to isothermals
B	E-A: Autocatalytic E-OH: nth order	Multivariable nonlinear analysis program to determine all model parameters. Visual goodness of fit to dynamic heat flow profiles.	
C	E-A: Sourour & Kamal [1976]	Multivariable nonlinear analysis program, [Berkley-Madonna]	
D	E-A: decoupled Horie model [1970] with autocatalytic etherification expression Diffusion: Macedo & Litovitz [1965] modified by Simon [2000]	Cure rate isoconversionals at 0.02 to 0.95 degree of cure	Least squares fit to isothermal and dynamic data
E	E-A: Autocatalytic	1) Plotted ln[dα/dt] vs ln[1-α], linear regression to find n; 2) ln[(dα/dt)/(1-α)n] vs ln[α] calculate m and ln[K]	
F			

Table 1.12 Models and parameters for stage 1

Group	Model	Parameters and values
A	$$\frac{d\alpha}{dt} = \frac{K\alpha^m(1-\alpha)^n}{1+e^{C\{\alpha-(\alpha_{C0}+\alpha_{CT}T)\}}}$$	A = 49571 /sec E = 65933 J/mol m = 0.40 n = 1.62 C = 17.60 a_{C0} = -1.22, a_{CT} = 0.0044 α_0 = 0.01
B	$$A \rightarrow B \rightarrow C$$ $$\frac{d\alpha_1}{dt} = \frac{d(A \rightarrow B)}{dt} = K_1\alpha^{m_1}\beta^{n_1}$$ $$\frac{d\alpha_2}{dt} = \frac{d(B \rightarrow C)}{dt} = K_2\beta^{m_2}$$ $$\frac{d\alpha}{dt} = fK_1\alpha^{m_1}\beta^{n_1} + (1-f)K_2\beta^{m_2}$$	log A_1 = 4.49 /sec E_1 = 63290 J/mol m_1 = 0.36 n_1 = 0.87 log A_2 = 7.64 /sec E_2 = 98269 J/mol m_2 = 0.58 f = 0.65 α_0 = 0.00005 β_0 = 0.00003
C	$$\frac{d\alpha}{dt} = \left(K_1 + K_2\alpha^m\right)(1-\alpha)^n$$	A_1 = 55599 /sec E_1 = 58383 J/mol A_2 = 72908 /sec E_2 = 51341 J/mol m = 0.58 n = 1.43
D	$$\frac{d\alpha}{dt} = k_1\alpha^{m_1}(1-\alpha)^{n_1} + k_2\alpha^{m_2}(1-\alpha)^{n_2} + k_3\alpha^{m_3}(1-\alpha)^{n_3}$$ $$Tg = \frac{\alpha\lambda(Tg_\infty - Tg_0)}{1-(1-\lambda)\alpha} + Tg_0 + \frac{D}{1+\exp(-F(\alpha-\alpha_C))}$$ $$k_d = A_d \exp\left(-\frac{E_d}{RT}\right)\exp\left(-\frac{b}{fv}\right)$$ $$fv = 0.00008(T-Tg) + 0.025$$	If T < 124°C and α < 0.035, Then A_1 = 34378*Ln(α) + 229563 /sec and E_1 = 73300 J/mol; If A_1 < 50000 /sec, then A_1 = 50000 /sec. Else, If T < 124°C and α > 0.035, then A_1 = 113881 /sec and E_1 = 73300 J/mol; Else, If T > 124°C, Then A_1 = 14240 /sec and E_1 = 66435 J/mol. A_2 = 473684 /sec, E_2 = 73063 J/mol A_3 = 1.5E9 /sec, E_3 = 115624 J/mol Tg_0 = 8.8 °C, Tg_∞ = 200 °C, λ = 0.8 D = 35, F = -25, notes on α_c to follow $A_{d,1\text{-}2}$ = 4E12 /sec, $E_{d,1\text{-}2}$ = 60000 J/mol, $b_{1\text{-}2}$ = 0.52, $A_{d,3}$ = 1.5E9 /sec, b_3 = 0.7
E	$$\frac{d\alpha}{dt} = K\alpha^m(1-\alpha)^n$$	A = 144879 /sec E = 71130 J/mol m = 0.19 n = 0.98
F	$$\frac{d\alpha}{dt} = K\alpha^m(1-\alpha)^n$$	A = 71167 /sec E = 66800 J/mol m = 0.42 n = 0.015/K*T-5.53

Table 1.13 Experimental decisions for stages 2 and 3

Group	Dynamic dT/dt (^{o}C/min)	Isothermal temperature and time [^{o}C (hours)]
A	1, 2, 4, 5	140, 160, 180
B	0.5 to 0.5	120 to 190
D	1 to 10	130 to 200
E	5	120 to 200
F	5	120 to 250

Table 1.14 Models and parameters for stage 2

Group	Model	Parameters and Values
A	$$\frac{d\alpha}{dt} = \frac{K\alpha^m(1-\alpha)^n}{1+e^{C\{\alpha-(\alpha_{C0}+\alpha_{CT}T)\}}}$$	A = 1.60E5 /sec E = 71177 J/mol m = 0.26, n = 1.01 C = 21.57 a_{C0} = -1.22, a_{CT} = 0.0046
B	$$\frac{d\alpha}{dt} = fK_1\alpha^{m_1}\beta^{n_1} + (1-f)K_2\beta^{m_2}$$ $$\frac{1}{K_2} = \frac{1}{K_{Chemical}} + \frac{1}{K_{Diffusion}}$$ $$K_{Diffusion} = k_d \exp\left\{\frac{C_1(T-Tg)}{C_2+(T-Tg)}\right\}$$ $$Tg(\alpha) = Tg_0 \exp\left\{\frac{g_1\alpha}{g_2-\alpha}\right\}$$	log A_1 = 3.95 /sec E_1 = 59537 J/mol m_1 = 0.33, n_1 = 0.68 log A_2 = 9.11 /sec E_2 = 99549 J/mol m_2 = 0.93 f = 0.89 log k_D = -1.92 C_1 = 0.14, C_2 = 1.70 K Tg_0 = 322.26 K, g_1 = 3.19 g_2 = 8.30
D	$$\frac{d\alpha}{dt} = \frac{K(1-\alpha)(B-\alpha)(b+\alpha)}{1+\exp[C(\alpha-(\alpha_{C0}+\alpha_{CT}T))]} + K_3\alpha^m(1-\alpha)^n$$	A = 59938 /sec E = 65000 J/mol b = 0.17, B = 1 A_3 = 3E9 /sec, E_3 = 115000 J/mol m = 3, n = 1 C = 20, a_{C0} = -1.88, a_{CT} = 0.0061 Tg_0 = 8.8 °C, Tg_∞= 228 °C, λ = 1 Tg = 214.45α + 12.55 °C
E	$$\frac{d\alpha}{dt} = \frac{K_1\alpha^k(1-\alpha)^l + K_2\alpha^m(1-\alpha)^n}{1+\exp[C(\alpha-(a_{C0}+a_{CT}*T))]}$$	A_1 = 165497 /sec E_1 = 82183 J/mol A_2 = 31633 /sec E_2 = 64626 J/mol k = 0.84, l = 0.29 m = 0.36, n = 1.49 C = 9.92, a_{C0} = -1.32, a_{CT} = 0.0048 /K
F	$$\frac{d\alpha}{dt} = K\alpha^m(1-\alpha)^n$$	A = 18450 /sec E = 61300 J/mol m = 0.42 n = 2.48 T<=170°C 1.63 T>170°C

Table 1.15 Models and parameters for stage 3

Group	Model	Parameters
A	$$\frac{d\alpha}{dt} = \frac{K\alpha^m(1-\alpha)^n}{1+e^{C\{\alpha-(\alpha_{C0}+\alpha_{CT}T)\}}}$$	A = 1.47E5 /sec E = 70919J/mol m = 0.26, n = 0.94 C = 17.19 a_{C0} = -1.26, a_{CT} = 0.00452
B	$$\frac{d\alpha}{dt} = fK_1\alpha^{m_1}\beta^{n_1} + (1-f)K_2\beta^{m_2}$$ $$K_2 = K_{Chemical} + K_{Diffusion}$$ $$K_{Diffusion} = k_d \exp\left\{\frac{C_1(T-Tg)}{C_2+(T-Tg)}\right\}$$ $$Tg(\alpha) = Tg_0 \exp\left\{\frac{g_1\alpha}{g_2-\alpha}\right\}$$	log A_1 = 4.16 /sec E_1 = 59970 J/mol m_1 = 0.28 n_1 = 0.13 log A_2 = 4.49 /sec E_2 = 62113 J/mol m_2 = 0.33 f = 0.54 log k_D = -1.16 C_1 = 0.86, C_2 = 28.77 K, Tg_0 = 310.04 K, g_1 = 58.35, g_2 = 122.15
D	$$\frac{d\alpha}{dt} = \frac{K(1-\alpha)(B-\alpha)(b+\alpha)}{1+\exp[C(\alpha-(\alpha_{C0}+\alpha_{CT}T))]} + K_3\alpha^m(1-\alpha)^n$$	A = 59938 /sec, E = 65000 J/mol b = 0.17, B = 1 A_3 = 3E9 /sec, E_3 = 115000 J/mol m = 3, n = 1 C = 20, a_{C0} = -1.88, a_{CT} = 0.0061 Tg_0 = 8.8 °C, Tg_∞= 228 °C, λ = 1 Tg = 214.45α + 12.55 °C
E	$$\frac{d\alpha}{dt} = \frac{K_1\alpha^k(1-\alpha)^l + K_2\alpha^m(1-\alpha)^n}{1+\exp[C(\alpha-(a_{C0}+a_{CT}*T))]}$$	A_1 = 47833 /sec E_1 = 65140 J/mol A_2 = 330523 /sec E_2 = 82184 J/mol k = 0.45, l = 1.77 m = 2.06, n = 0.39 C = 15.58, a_{C0} = -1.32, a_{CT} = 0.0048 /K
F	$$\frac{d\alpha}{dt} = K\alpha^m(\alpha_f-\alpha)^n$$	A_1 = 3.60E5 /sec E_1 = 79600 J/mol A_2 = 8.28E3 /sec E_2 = 59200 J/mol m = 0.47 n = 0.79 T≤160°C 0.015*T-1.67 T>170°C a_f = 0.0047*T+0.04 T≤210°C 1 T > 210°C

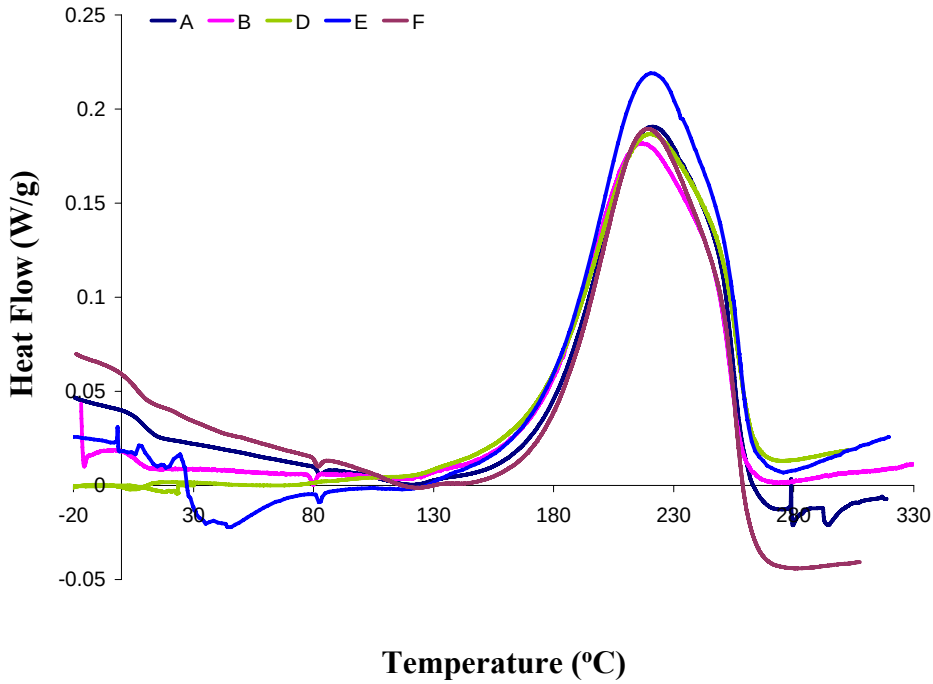

Figure 1.1 (a) Stage 0: Heat flow for 5°C/min dynamic scans on T800H/3900-2

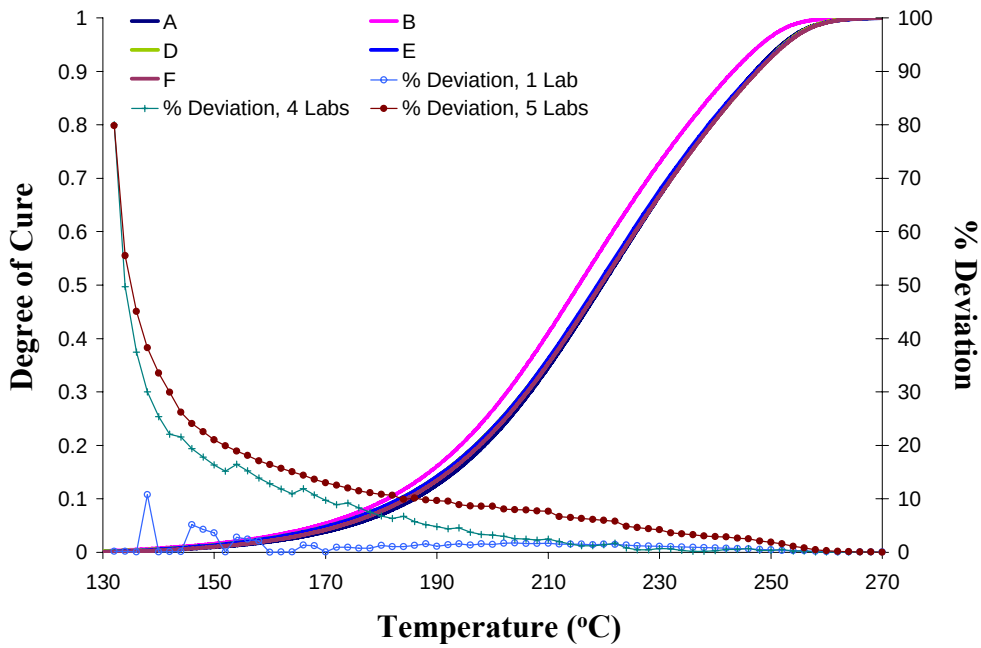

Figure 1.1 (b) Stage 0: Degree of cure for 5°C/min dynamic scans on T800H/3900-2 with a comparison of % deviation for various data groups

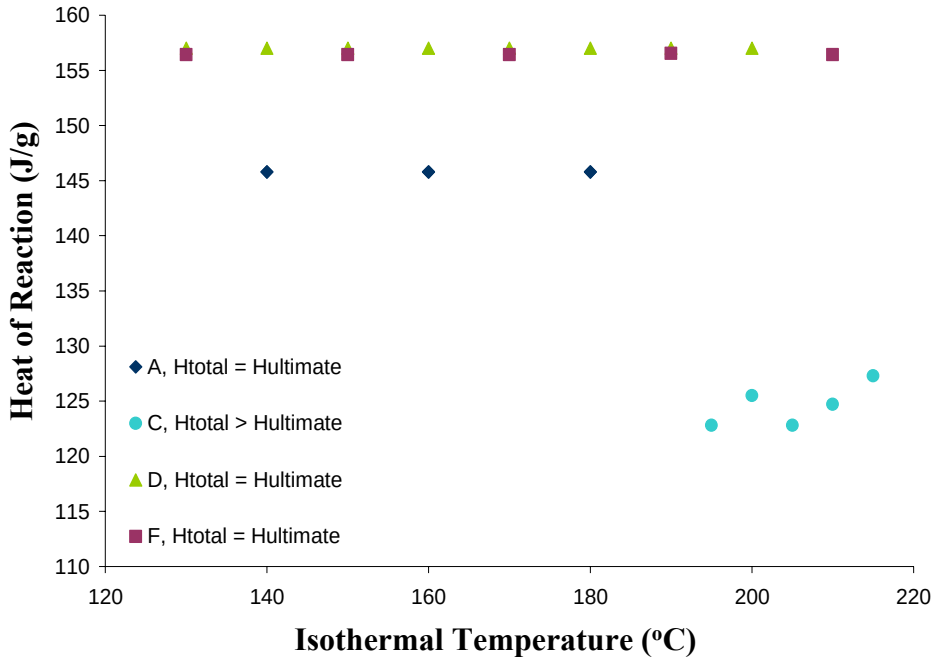

Figure 1.2 (a) Stage 1: Isothermal heats of reaction

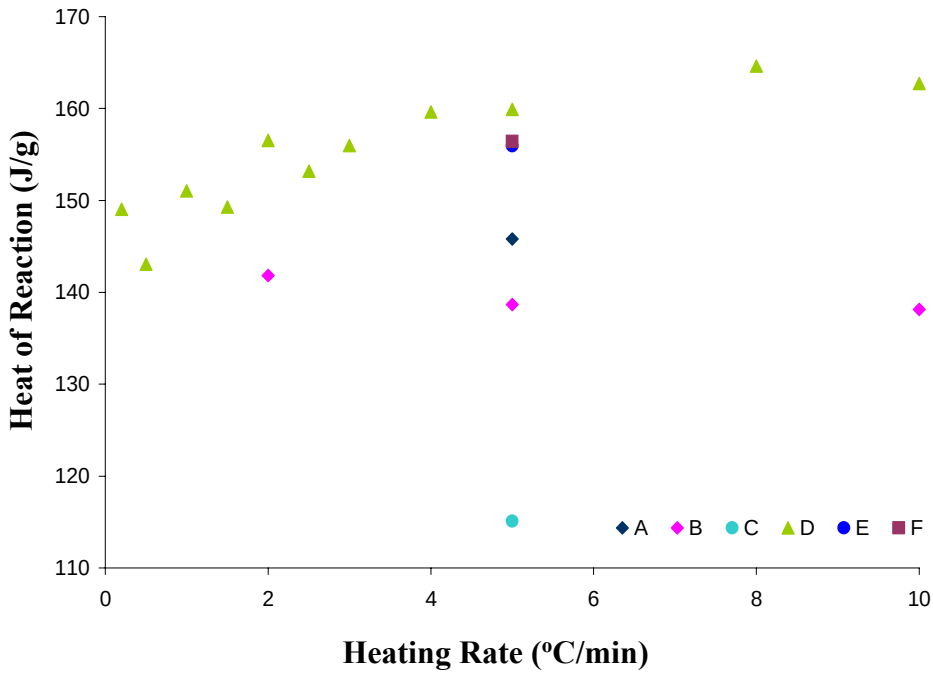

Figure 1.2 (b) Stage 1: Dynamic heats of reaction

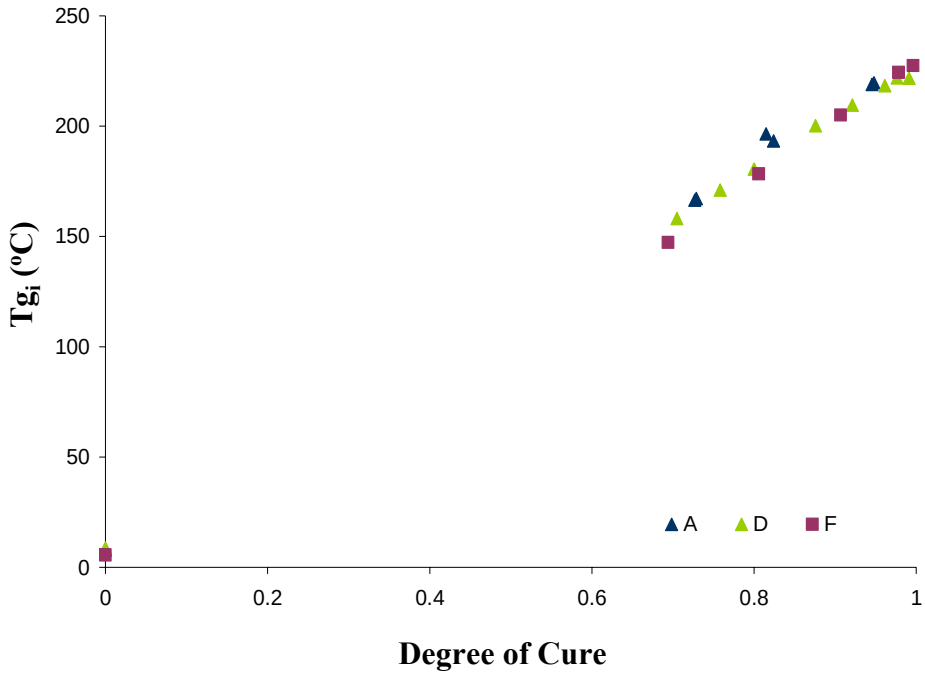

Figure 1.3 Stage 1: Tg-α relationships

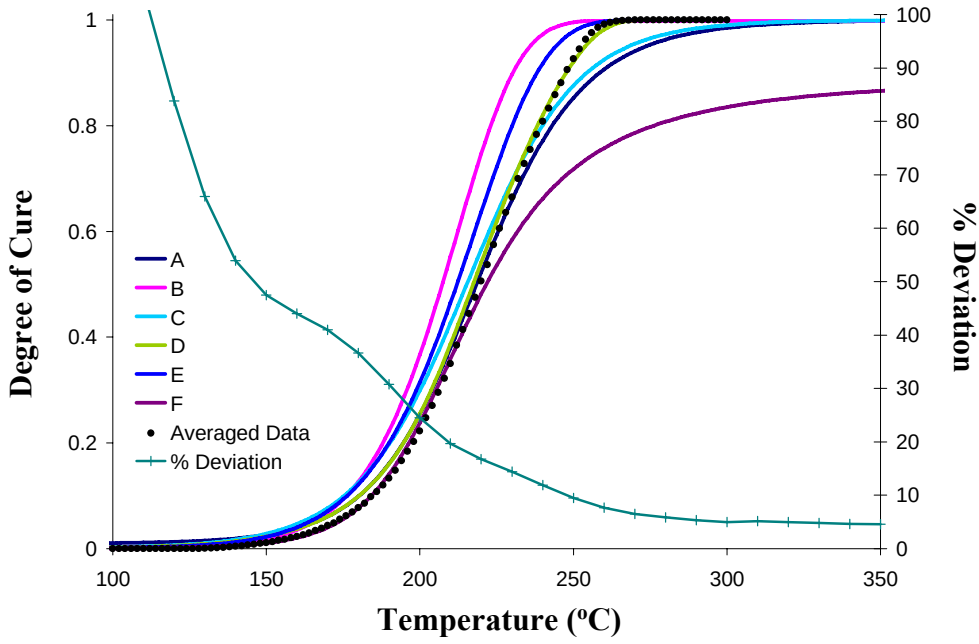

Figure 1.4 (a) Stage 1: Model prediction of degree of cure for a 5°C/min dynamic

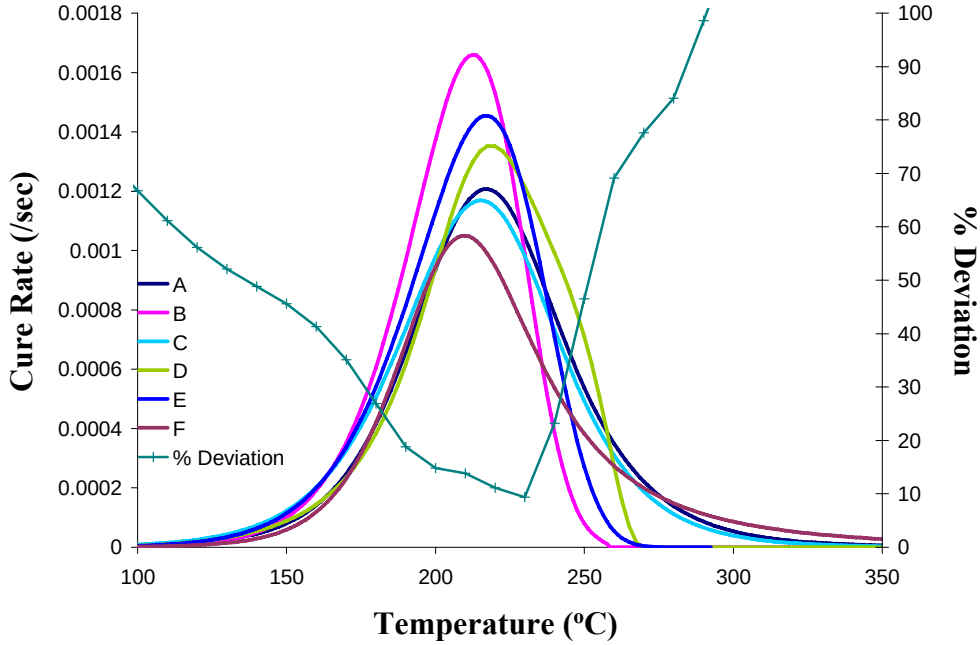

Figure 1.4 (b) Stage 1: Model prediction of cure rate for a 5ºC/min dynamic

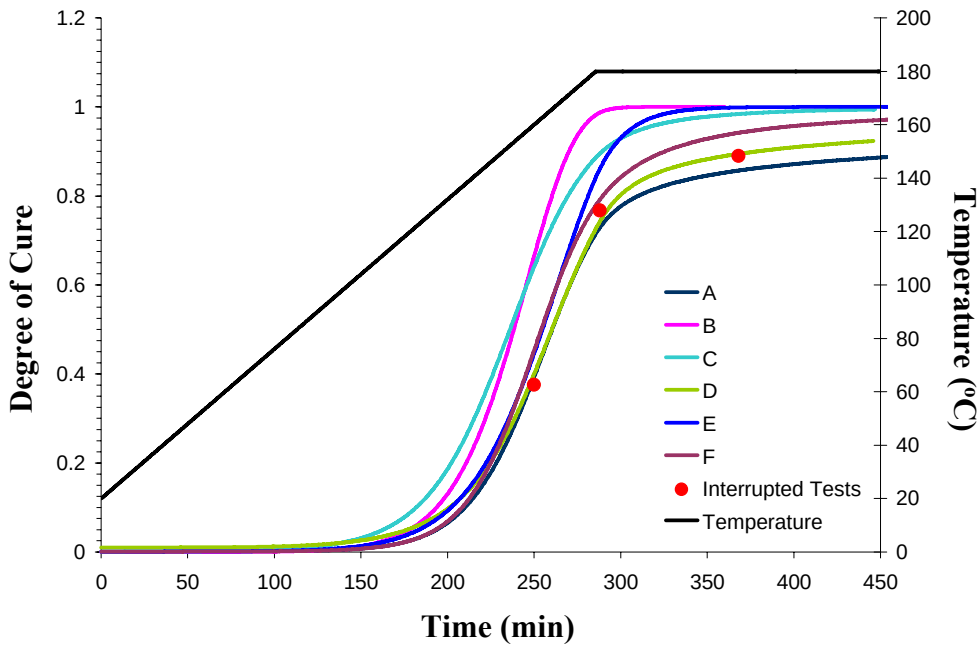

Figure 1.5 (a) Stage 1: Model predictions for MRCC lower limit of 0.56ºC/min ramp to 180ºC

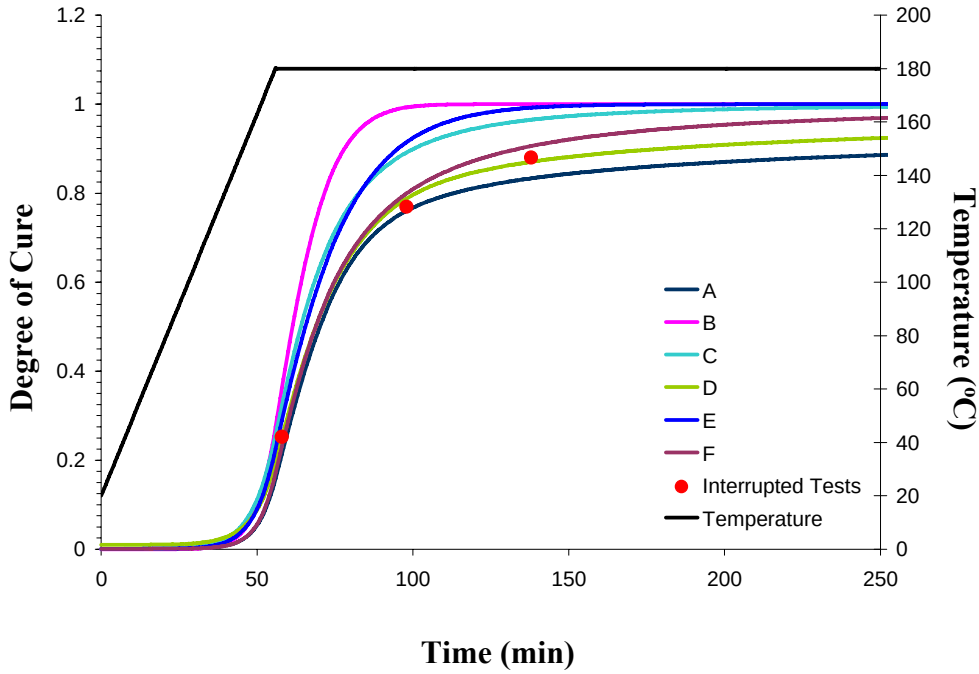

Figure 1.5 (b) Stage 1: Model predictions for MRCC upper limit of 2.86°C/min ramp to 180°C

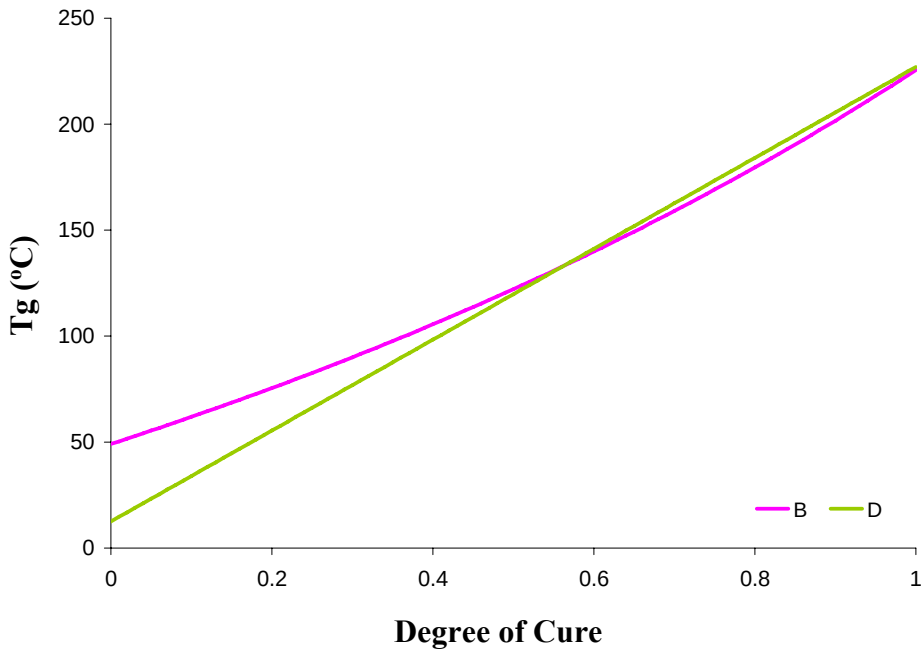

Figure 1.6 Stage 2: Tg-α models proposed

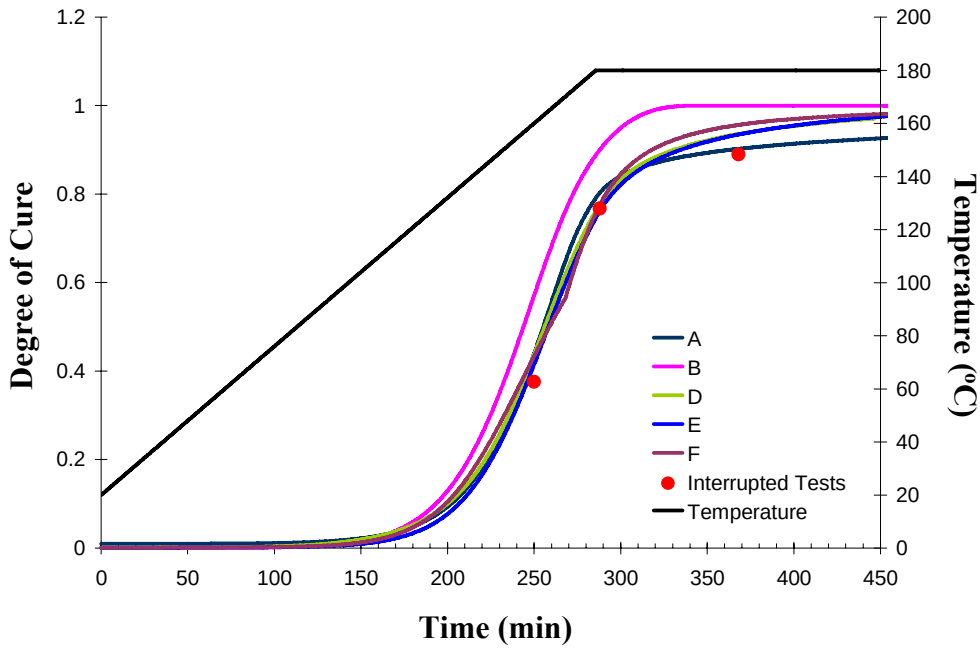

Figure 1.7 (a) Stage 2: Model predictions for MRCC lower limit of 0.56°C/min ramp to 180°C

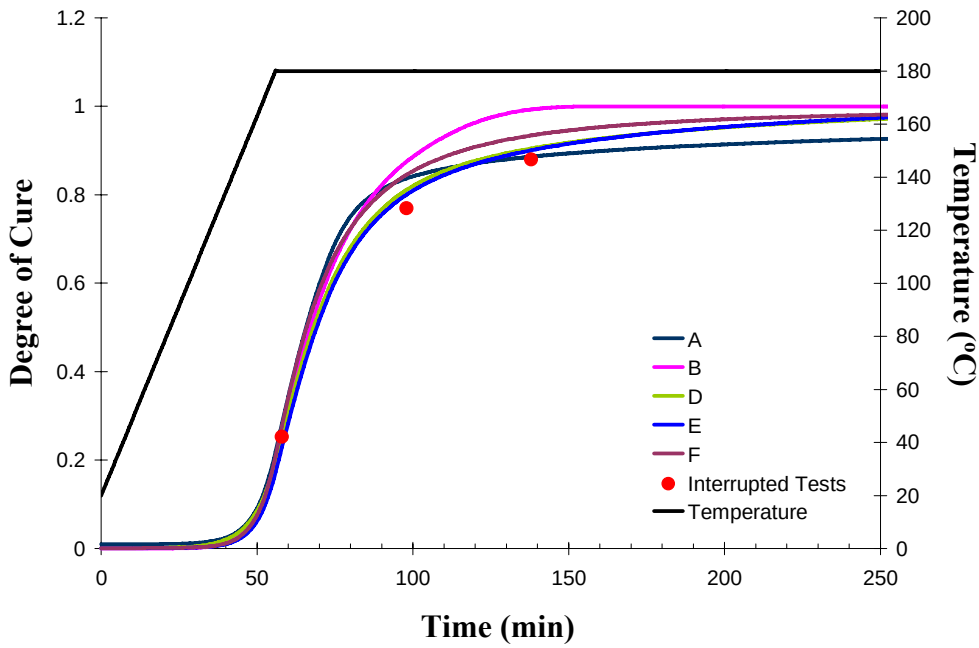

Figure 1.7 (b) Stage 2: Model predictions for MRCC upper limit of 2.8°C/min ramp to 180°C

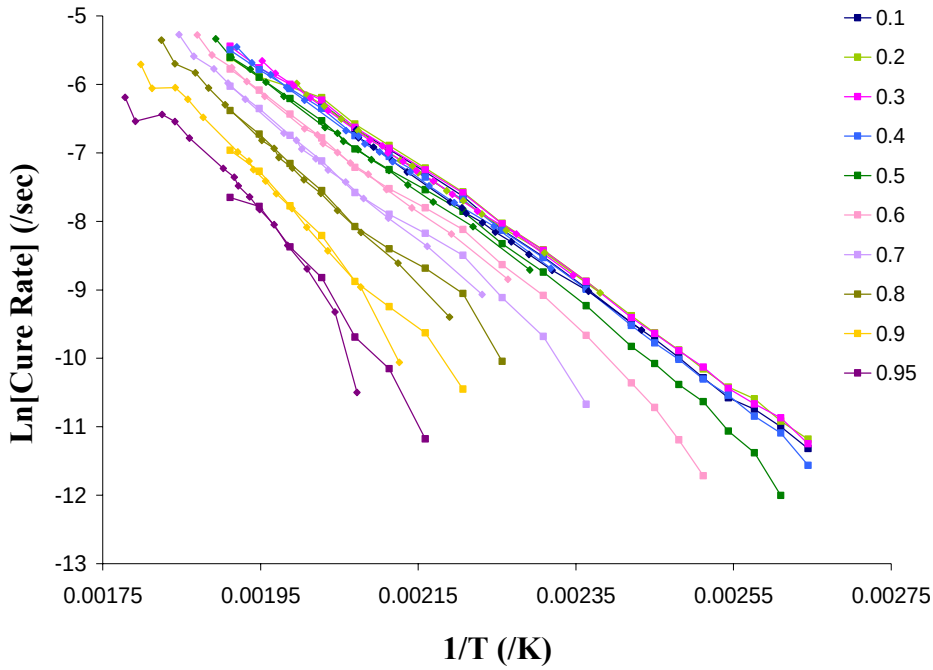

Figure 1.8 Stage 3: Cure rate isoconversional data supplied to all participants

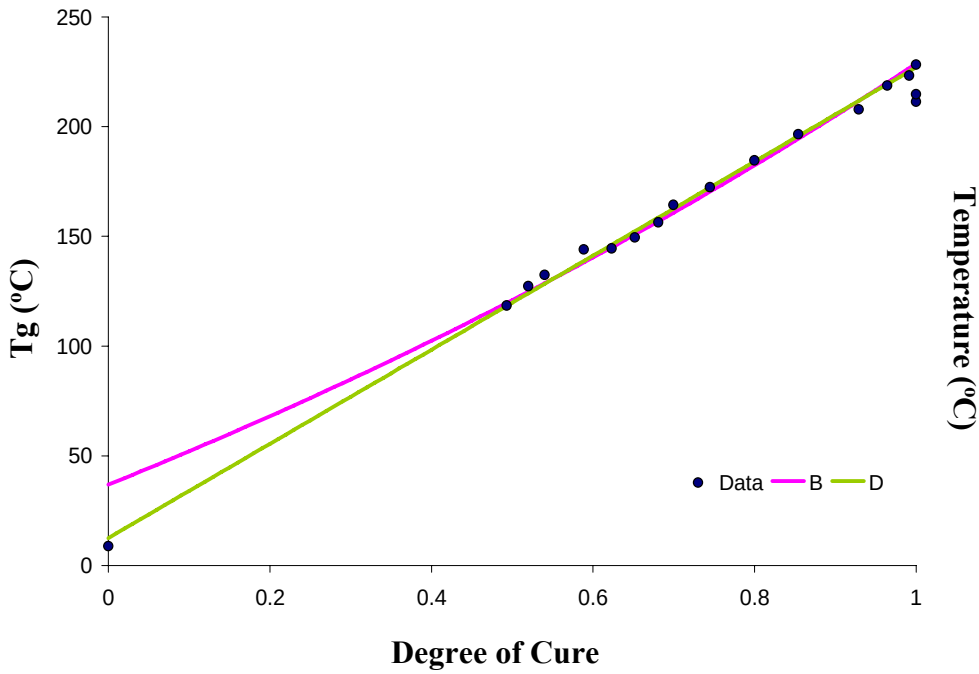

Figure 1.9 Stage 3: Tg-α data and models proposed

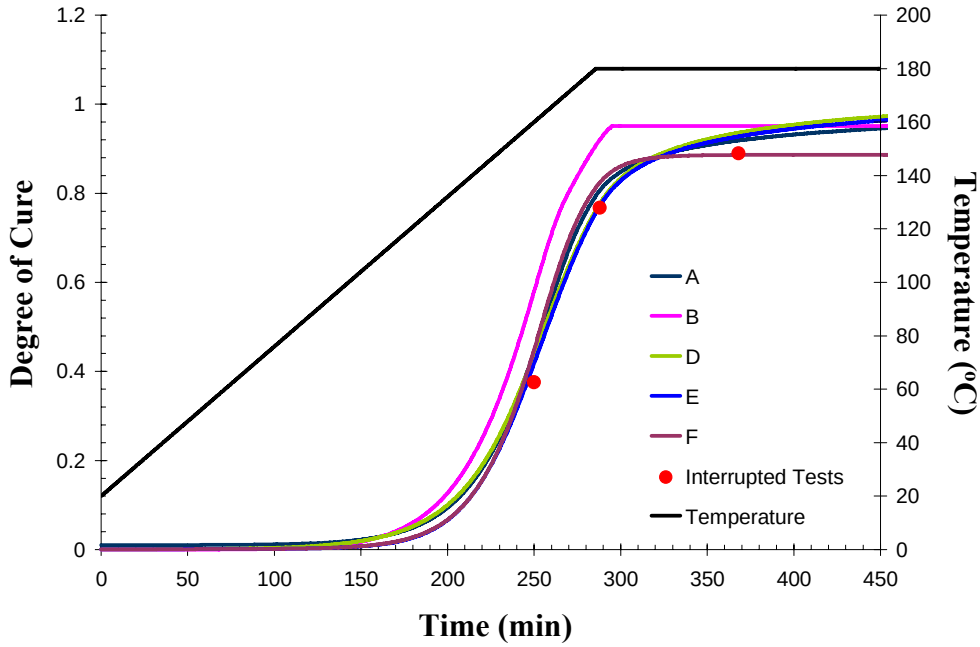

Figure 1.10 (a) Stage 3: Model predictions for MRCC lower limit of 0.56°C/min ramp to 180°C

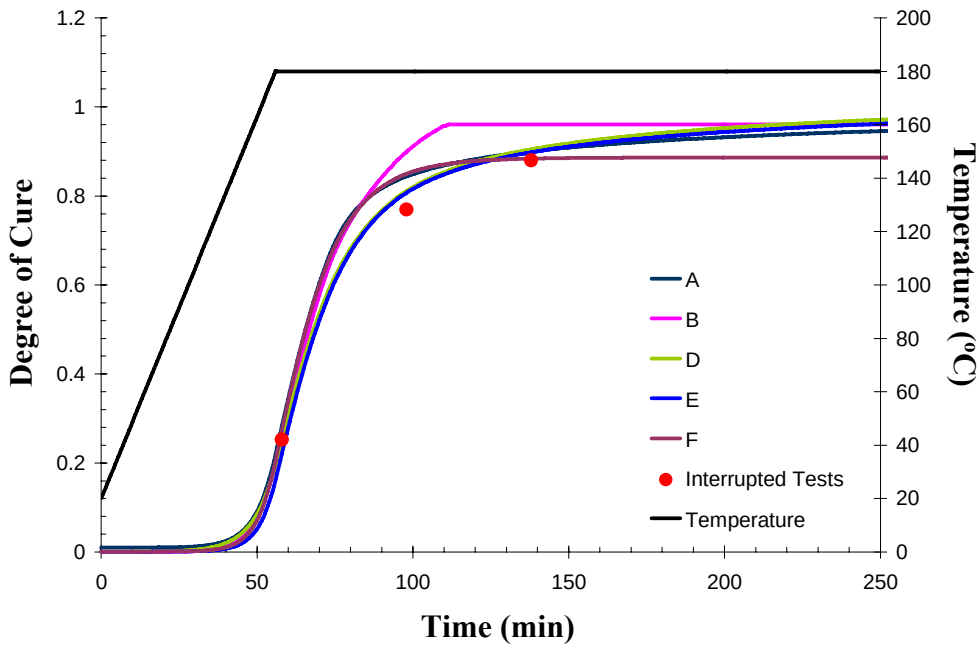

Figure 1.10 (b) Stage 3: Model predictions for MRCC upper limit of 2.8°C/min ramp to 180°C